TESE DE DOUTORAMENTO

STRUCTURAL CONTROL OF MEMBRANE-TARGETED PEPTIDES FOR DELIVERY OF FUNCTIONAL PROTEINS

Marta Pazo Pascual

ESCOLA DE DOUTORAMENTO INTERNACIONAL DA UNIVERSIDADE DE SANTIAGO DE COMPOSTELA

PROGRAMA DE DOUTORAMENTO EN CIENCIA E TECNOLOXÍA QUÍMICA

SANTIAGO DE COMPOSTELA

2021

USC
UNIVERSIDADE
DE SANTIAGO
DE COMPOSTELA

AUTORIZACIÓN DO DIRECTOR

STRUCTURAL CONTROL OF MEMBRANE-TARGETED PEPTIDES FOR DELIVERY OF FUNCTIONAL PROTEINS

D. Javier Montenegro García.....

INFORMA/N:

Que a presente tese, correspóndese co traballo realizado por Dna Marta Pazo Pascual, baixo a miña dirección, e autorizo a súa presentación, considerando que reúne os requisitos esixidos no Regulamento de Estudos de Doutoramento da USC, e que como director desta non incorre nas causas de abstención establecidas na Lei 40/2015.

De acordo co indicado no Regulamento de Estudos de Doutoramento, declara tamén que a presente tese de doutoramento é idónea para ser defendida en base á modalidade de COMPENDIO DE PUBLICACIÓNS, nos que a participación do/a doutorando/a foi decisiva para a súa elaboración e as publicacións se axustan ao Plan de Investigación.

En Santiago de Compostela, de de 2021

USC
UNIVERSIDADE
DE SANTIAGO
DE COMPOSTELA

AUTORIZACIÓN DO TITOR DA TESE

STRUCTURAL CONTROL OF MEMBRANE-TARGETED PEPTIDES FOR DELIVERY OF FUNCTIONAL PROTEINS

D. Juan R. Granja Guillán.....

INFORMA/N:

Que a presente tese, correspóndese co traballo realizado por Dna Marta Pazo Pascual, baixo a miña dirección, e autorizo a súa presentación, considerando que reúne os requisitos esixidos no Regulamento de Estudos de Doutoramento da USC, e que como director desta non incorre nas causas de abstención establecidas na Lei 40/2015.

De acordo co indicado no Regulamento de Estudos de Doutoramento, declara tamén que a presente tese de doutoramento é idónea para ser defendida en base á modalidade de COMPENDIO DE PUBLICACIÓNS, nos que a participación do/a doutorando/a foi decisiva para a súa elaboración e as publicacións se axustan ao Plan de Investigación.

En Santiago de Compostela, de de 2021

USC
UNIVERSIDADE
DE SANTIAGO
DE COMPOSTELA

DECLARACIÓN DA AUTORA DA TESE

Structural control of membrane-Targeted Peptides for delivery of Funcional Proteins

Dna. Marta Pazo Pascual..

Presento a miña tese seguindo o procedemento axeitado ao Regulamento, e declaro que:

1) A tese abarca os resultados da elaboración do meu traballo.

2) De ser o caso, na tese faise referencia ás colaboracións que tivo este traballo.

3) Confirmo que a tese non incorre en ningún tipo de plaxio doutros autores nin de traballos presentados por min para a obtención doutros títulos.

4) A tese é a versión definitiva presentada para a súa defensa e coincide a versión impresa coa presentada en formato electrónico

E comprométome a presentar o Compromiso Documental de Supervisión no caso de que o orixinal non estea na Escola.

En Santiago de Compostela, de de 2021

Fdo. Marta Pazo Pascual

USC
UNIVERSIDADE
DE SANTIAGO
DE COMPOSTELA

A mis padres

USC
UNIVERSIDADE
DE SANTIAGO
DE COMPOSTELA

AGRADECIMIENTOS

En primer lugar, me gustaría dar las gracias a mi director de la tesis, Javier Montenegro, por darme su confianza para emprender el camino de la tesis doctoral. Gracias por todos los consejos y por tu trato tan cercano, pero sobre todo gracias por la motivación y por no ponerle límites a la imaginación. Gracias a ti he aprendido una de las grandes lecciones de la tesis, que siempre se puede materializar una idea.

También tengo que agradecerle a mi tutor, Juan Granja, haberme dado la primera oportunidad para iniciarme en la investigación durante las prácticas del grado, y confió en mi para que siguiera mi carrera investigadora. Gracias por tus sabios consejos y tu ayuda.

A los doctores Manuel Amorín, Rebeca Fandiño y el Profesor Luis Castedo gracias por los consejos en los seminarios de grupo, los ánimos y los buenos momentos compartidos en las celebraciones, cenas y excursiones. Junto a Juan y Javier hacéis posible que continúe el compañerismo y el buen royo que caracteriza al grupo de investigación. Os doy las gracias porque hacer la tesis en vuestro grupo es formar parte de la familia que habéis ido construyendo estos años.

Agradecer a todos los organismos e instituciones nacionales e internacionales que han financiado esta tesis doctoral y todos los proyectos de investigación en los que he podido participar. Especialmente a la Xunta de Galicia por haberme concedido una beca predoctoral (ED481A-2017/142) y haberme dado la posibilidad de irme de estancia.

Gracias al Prof. Mark Nitz y a la universidad de Toronto por haberme acogido durante tres meses en el Lash Miller Centre. Muchas gracias por haberme dado la oportunidad de crecer como investigadora y como persona. A todos los compañeros del laboratorio que me acogieron como una más: Adam, Alexander, Benjamin, Jay, Lisa y Rahul y en especial a Ehsen, Daniel, Jose, Nesrin, Rahul y Zach por tantas conversaciones y por estar tan pendientes de mi. A mi compañera de residencia Farah, que me enseñó la versión nocturna de la ciudad. Por último, a Raquel por haberme acompañado en tantas aventuras y viajes en la estancia, por ser la última pieza que hizo de la estancia una de las mejores experiencias de mi vida.

Me gustaría agradecerles todo el apoyo a mis compañeros del Laboratorio que después de tantos años se han convertido en amigos.

Los que ya estaban cuando yo empecé Lionel, Nuria, Arcadio y Jorge por acogerme tan bien y hacerme sentir integrada en el grupo desde el primer momento. A Juanillo por enseñarme todo lo que sé del laboratorio, por toda la paciencia que tuvo conmigo durante mis TFG y TFM, por confiar siempre en mi y por ser tan buen amigo. Muchas gracias, sin tu ayuda no habría podido empezar. A Marisa por cuidarme tanto, por todos los buenos consejos, el gran optimismo y por tantos bailes de canciones interminables. A Alberto por ser mi primer maestro, por los vídeos chorra, los chistes y por ser tan buen compañero. A Evita por apoyarme tanto, por animarme y por esperarme tantas veces a que acabase en el comedor. Gracias a los cuatro por haber compartido tanto tiempo conmigo en el laboratorio, por toda la paciencia, pero sobre todo por los buenos momentos.

A Irene y a Iria que siempre confiaron en mi y me animaron a seguir. A Ale por ser tan buen compañero, por ayudar de más y por animarme y aconsejarme en los momentos flojos. A Ángel por ser tan bueno, por facilitarme la vida, por tener siempre buenas palabras y ánimos para seguir. A Jose por tener ese buen humor y animarnos a todos en el laboratorio. A Fede gracias por preocuparte tanto por mi, por darme tanta seguridad y por convertirte en mi amiga. A Nacho por ese positivismo que le caracteriza y por prestarse siempre a echarme un cable. A Julián por ser tan sonriente y entusiasta, también por todos los buenos consejos. A Richard,

Ghibom y Sahnawaz por llegar con tantas ganas y por tantos buenos momentos. Geert y Mariette por acogernos siempre en su casa y ser tan amables.

A Giulia gracias por ser mi amiga y mi consejera, por todos los paseos y charlas, por ser mi compañera de congresos. Por tantos cotilleos, meriendas, noches, copas y vinos de chicas. Gracias por estar siempre. A Viqui por ser la persona más positiva del laboratorio, la que siempre tiene buena cara y la que te hace reír en cada momento. Gracias por tantas horas en baile y por ser mi vecina de vitrina. A Iván por ser tan animado, por ser el organizador de eventos sociales y por convertirte en un buen amigo.

A Hectoriño, el mago, por dejarme conocer la buena persona que eres, por preocuparte tanto por todos y sobre todo por animarnos tantos mediodías y tardes. Gracias por hacerme crecer como persona. A Alfonsiño por animarme y apoyarme tanto en los peores momentos, por tener la capacidad de sacarme una sonrisa en todo momento. Gracias por ser tan buen amigo. A Lamiñas por amenizarnos siempre el tiempo de laboratorio y por haber compartido tan de cerca conmigo nuestros inicios en la investigación. Gracias por tantos cafés calientes pero templados para llevar. A Martín por ser el la persona más animada y sociable del mundo. El hecho de que todos te tengamos tanto cariño sin compartir laboratorio es muestra de lo buena persona que eres.

A Alicia por sus fuertes convicciones y perseverancia que nos animan al resto a seguir nuestro camino. A Rebeca por ser una persona tan maravillosa, por tu espíritu de superación y por ser siempre tan amable y amigable. A Jose Mari (Chemita) gracias por tener siempre una sonrisa, por alegrarme el día a día y por la paciencia que tienes cuando me meto contigo. Gracias por ser hijo del fuego. A Patri, la última doctoranda en incorporarse, gracias por las charlas en los ratitos de descanso y por ser tan positiva, te deseo mucha suerte y paciencia en la tesis.

A Patri (Lago) gracias por dejarme conocer a una persona excelente en mis últimos años de carrera, por inspirar siempre tanta calma y por solucionar todos los problemas y dudas administrativas.

A Sandra por ser tan buena pupila y a los otros dos pollitos Marcos (Marcolino) y Ezequiel (Zeko). A los tres tuve la oportunidad y la gran suerte de conocerlos a fondo durante el desconfinamiento. Gracias por ayudarme en esta última etapa, por las conversaciones de comida, las bromas y la compañía. Sin duda alguna el laboratorio se queda en buenas manos con vosotros.

A la gente que pasó por el laboratorio estos años como Leti, gracias por cuidarme, apoyarme y por no perder el contacto conmigo todos estos años. A Charlene por tantas comidas en el Numaru, por las risas y por el espíritu de supervivencia que tienes. A los chicos de Máster del curso pasado Borja, Cayetana y Dema les agradezco todos los buenos momentos que me han dado en el laboratorio y les deseo mucho éxito en sus proyectos futuros.

Gracias al personal Técnico del CiQUS, Laura, Pablo y Arcadio por haberme tratado siempre tan bien. A Rebeca por ponerme las mejores placas células y por los ánimos.

Muchas gracias a todos los compañeros de los grupos de Jose Luis Mascareñas, Eugenio Vázquez y Miguel Vázquez y al grupo de Jose Costas. A David y Jacobo por ser compañeros dentro y fuera del CiQUS, gracias por los buenos momentos, los ánimos y las charlas en los instrumentales. A Soraya gracias por ser una excelente compañera, por ser tan positiva, tener una sonrisa y por ayudarme siempre que lo necesité. A David Fer por tener siempre buenas palabras y ganas de ayudar. Gracias a Bea por todos los buenos momentos y por tener siempre una sonrisa. A Jesús, Eva y Lamas por compartir conmigo los primeros momentos de la tesis, las fiestas, los juegos de mesa, los maratones de pelis y tantas risas.

A Ángela muchas gracias por haberte convertido en una persona indispensable en mi vida, la primera persona con la que hablé el primer día de universidad. Gracias por todo el ánimo y por todos los grandes momentos que hemos pasado todos estos años.

Gracias a Nuria e Iago por todas las quedadas, todas las risas, por aumentar mi vicio a los juegos de mesa y por todo el ánimo que me disteis en mi última etapa de tesis. A Beni por ser la zona no ciqus en las quedadas, por el apoyo y por todos los buenos momentos. Gracias a Roi y a Cris por haber sido mis amigos y compañeros de piso en mis comienzos de la tesis y por haberme dado el positivismo y la confianza para seguir.

Muchas gracias a todos los miembros de la Sociedad Xuvenil Galega de Química, que me enseñaron lo bonita que puede ser la divulgación científica. En especial a Álvaro, Nuria, Roi y Sergio por compartir conmigo la dirección de la asociación.

A mis amig@s de Tui tengo mucho que agradecerles porque siempre tienen un rato que dedicarme, un plan para disfrutar y toda la paciencia para escucharme.

Mis amigas de toda la vida (regas) Adriana, Ángela B., Ángela C., Olalla y Sandra. Gracias por estar y apoyarme en cada etapa de mi vida. Cualquier momento con vosotras se siente como volver a casa. Gracias por seguir creciendo y madurando juntas.

A Andrea por acogerme desde el primer momento por todas las experiencias. Gracias por toda la confianza que me das y por estar siempre cuando hace falta y por ser tan buena amiga. A Sara Presa por apoyarme en cada paso de mi vida, por encontrar siempre un momento para mi y por el apoyo incondicional. Pero sobre todo por ser una excelente compañera de aventuras nocturnas y diurnas.

L@s que llegaron durante mis años de bachillerato Ángela, Alba, Berna, Brais, Carla, Celia, Clara P. Clara V., Judi, Iago, Lily, Lucas, Maikel, Sara S., Sofi, Xavi, Lucas. Muchas gracias por todos los buenos momentos, las risas, las fiestas, las aventuras y por dejarme formar parte de las mejores anécdotas vividas.

A mis Carliñas por tan buenos momentos que compartimos juntas, los conciertos, las quedadas y por enseñarme a relativizar los problemas.

También tengo muchísimo que agradecerle a la persona que me ha acompañado durante toda esta aventura de la tesis, a Álvaro. Sin duda es la persona que ha compartido más de cerca todas mis preocupaciones, problemas y las alegrías. Gracias por compartir conmigo la pasión por la química y no dejar que las decepciones pesaran más que las alegrías. Gracias por cuidarme.

Me gustaría agradecerle a mi familia todo el apoyo y los ánimos que me han dado durante toda la tesis. A mis padres por estar siempre cuando los necesito, animarme en los peores momentos y hacerme ver que todos los problemas se superan. A mis abuelas, Julia y Concha, que siempre me transmitieron una filosofía para vivir con tranquilidad y un espíritu de superación. A mi hermano Santi, mi otra mitad, por darme todo el apoyo, buenos consejos y mucha paciencia a todas mis quejas. A María mi cuñada por ser tan alegre y por su espíritu de independencia tan inspirador También me gustaría mostrar mi agradecimiento a todos mis tíos y mis primos, Pascualines y Pacitos. Por último, como pequeño homenaje familiar, decir la gran satisfacción que tengo de poder convertirme en la segunda doctora de la familia después de mi Bisabuelo el Dr. Alejo Diz Jurado.

USC
UNIVERSIDADE
DE SANTIAGO
DE COMPOSTELA

Index

Index *15*

Abbreviations and Acronyms *17*

Abstract *21*

Resumen *23*

Resumo *25*

General Objectives *31*

General Introduction *35*

1. Therapeutic interest of Proteins and Antibodies **37**
1.1 Applications 38
1.2 Limitations 39
1.2.1 Stability limitations 39
1.2.2 Transport (size) limitations 40

CHAPTER 1: DYNAMIC CPPS *41*

1. Introduction **43**
1.1 History of CPPs 45
1.1.1 Classification of CPPs 46
1.1.1.1 Cationic CPPs 46
1.1.1.2 Amphipathic CPPs 46
1.1.1.3 Hydrophobic CPPs 48
1.2 Artificial Assays for Membrane Transport Characterization 48
1.2.1 Large Unilamellar Vesicles (LUVs) measures 49
1.2.2 BLM measures 50
1.3 Dynamic covalent transport systems 53
1.3.1 Dynamic covalent bonds 53
1.3.2 Hydrazones and oximes bonds 54
1.3.3 Peptide libraries 54

2. Objectives **57**

3. Results: Tuning the Properties of Penetrating Peptides by Oxime Conjugation **61**

4. Conclusions **69**

CHAPTER 2: PEPTIDE DESIGN FOR HELICAL CONTROL *73*

1. Introduction **75**
1.1 Peptide design for membrane perturbation 77
1.1.1 Stabilization of peptide helical structures 78
1.1.2 Circular dichroism of peptides 81
1.2 Peptide interactions for Cell internalization 82
1.2.1 Peptide self-assembly in membranes 82
1.2.2 Cellular uptake of CPPs 85
1.2.3 Cell toxicity 88
1.2.4 Clinical trials with CPPs 88

2. Objectives **89**

3. Results: Oligoalanine helical callipers for cell penetration 93

4. Conclusions 99

CHAPTER 3: ASSEMBLY OF PEPTIDE NANOPORES AND DELIVERY OF FUNCTIONAL PROTEINS 103

1. Introduction 105

1.1 Intracellular transport of Proteins and Antibodies 107

1.1.1 Direct delivery through plasma membrane 108

1.1.1.1 Physical methods 109

1.1.1.2 Chemical methods 111

1.1.2 Endocytic uptake 115

1.1.2.1 Endosomal routes 115

1.1.2.2 Endosome characteristics 117

1.1.2.3 Delivery strategies 117

1.2 Intracellular targeting 125

2. Objectives 129

3. Results: Short oligoalanine helical peptides for supramolecular nanopore assembly and protein cytosolic delivery 133

4. Conclusions 145

General discussion 149

General Conclusions 171

SUPPORTING INFORMATION 175

1. Tuning the Properties of Penetrating Peptides by Oxime Conjugation 177

2. Oligoalanine Helical Callipers for Cell Penetration 199

3. Short oligoalanines helical peptides for supramolecular nanopore assembly and protein cytosolic delivery 227

Abbreviations and Acronyms

α-HL	α-hemolysin
βGBA	β-glucocerebrosidase
aa	Amino acid
Ac	*N*-terminal acetylated
Acm	Acetamidomethyl
$AcP(Ox)_2$	Parent peptide
Ag	Antigen
Anti-LAMP1	Lysosome Associated Membrane Protein
anti-NPC	Anti-nuclear pore complex
ANTS	8-aminonaphthalene-1,3,6-trisulfonic acid
APCs	Antigen presenting cells
AZT	Azidothymidine
BBB	Blood-Brain Barrier
BGTC	Bis (guanidinium)-tren-cholesterol
BLM	Black Lipid Membrane
BMP	Bis(monoacylglycero) phosphate
BNCT	Boron Neutral Capture Therapy
bPEI	Phenylbiguanide polyethylenimine
BPs	Benzopolysulfanes
BSA	Bovine serum albumin
CAMP	Cell-penetrating artificial mitochondria-targeting peptide
CB	Coomassie blue
CD	Circular dichroism
CDCs	Cholesterol dependent cytolysins
CF	Carboxyfluorescein
CFR8	Octaarginine labelled with CF
CG-MD	Coarse-grained Molecular Dynamics
CLQ	Chloroquine
cmc	critical micellar concentration
CPDs	Cell Penetrating Poly(disulfide)s
CPP	Cell penetrating peptides
CPZ	Chloropromazine
CRISPR	Clustered Regularly Interspaced Short Palindromic Repeats
CTB	cholera toxin B
CXCR4	chemokine receptor
Cyt c	cytochrome C
DCLs	Dynamic combinatorial libraries
dNMPs	Deoxyribonucleotides monophosphate

DOPE	Dioleoyl phosphatidylethanolamine
DOSP	Dioleyl succinyl paromomycin
DPA	2,2'-Dipicolylamine
DPX	p-xylene-bis-pyridinium bromide
DYN	Dynasore
EC_{50}	Concentration at half activity
EGF	Epidermal growth factor
EIPA	5-(N-Ethyl-N-isopropyl)amiloride
EPR	Enhanced permeability and retention effect
Fab	Antigen binding fragment
FD	Fabry's disease
FGF12	Fibroblast Growth Factor-12
FRET	Fluorescence resonance energy transfer
FTags	Fluorinated tag
g	Conductance
GAG	GlucosAminoGlycan
GBA	4-guanidinobenzene
GFP	Green fluorescent protein
GLA	α-galactosidase A
GUVs	Giant Unilamellar Vesicles
Hep	Heparin
hMSC	Human mesenchymal stem cells
HPLC	High Performance Liquid Chromatography
HPTS	8-Hydroxy-1,3,6-pyrenetrisulfonate
I	Current
iCP-Parkin	Cell permeable Parkin protein
IgG	Immunoglobulin-G
IMT-P8	Institute of Microbial Technology-Peptide 8
iTOP	Induced transduction by osmocytosis and propanebetaine
K8	Anticytokeratin 8 antibody
LLO	Lysteriolysin O
LTM	Lysosomal targeting moiety
LSDs	Lysosomal diseases
LUVs	Large Unilamellar Vesicles
MACPF	Membrane attack complexes/perforin-like
MbCD	Methyl-β-cyclodextrine
MM27	Imidazole-based helper lipid
MN	Microneedle
MTD	Macromolecule transduction domain
MTS	Mitochondrial targeting sequence
mtt	4-Methyltrityl

MTT	3-(4,5-dimethylthiazol-2-yl)-2,5-diphenyltetrazolium bromide
MP1	Minimal peptide 1
MP2	Minimal peptide 2
MSNs	Mesoporous silica nanoparticles
n	Hill coefficient
NLS	Nuclear localization sequence
NOLS	Nucleolar location sequence
NP	Nanoparticles
NPC	*p*-nitrophenylcarbonate
NPSCs	Nanoparticle stabilized nanocapsules
OVA	Egg ovalbumin
P3	Peptide 3
PAMAM	Poly(aminoamine) dendrimer
pAkt	Anti phospho-Akt antibody
PAsp(DET)	Poly(N-(N-(2-aminoethyl)-2-aminoethyl) aspartamide)
PCC	Propionyl coenzyme-A carboxylase
PD	Parkinson's disease
PDS	Pyridyldisulfide
PEG	Polyethylene glycol
PEI	Polyethylenimine
PFO	Perfringolysin O
pI	Isoelectric point
PI	Propidium iodide
PNAs	Peptide nucleic acids
PNP	Polymer nanoparticle
PONI	Poly(oxanorborneneimide)
PPI	Polyproline I helix
PPII	Polyproline II helix
PPIs	Protein-Protein interactions
PSs	Polymersomes
PTDMs	Protein transduction domain mimics
PTDs	Protein transduction domains
r	Pore radius
R8	Octaarginine
RGD	Arg-Gly-Asp
RIP	Ribosome-inactivating protein
RNase A	Ribonuclease A
RSN	Rough silica nanoparticles
SAP	Sweet arrow peptide
SLO	Streptolysin O
SNARE	N-ethylmaleimide-sensitive factor attachment protein receptor

USC UNIVERSIDADE DE SANTIAGO DE COMPOSTELA

SPPS	Solid phase peptide synthesis
SPQ	6 methoxy-N-(3-sulfopropyl) quinolinium
SUVs	Small Unilamellar Vesicles
SV40	Simian Virus 40
T3SS	Type 3 Secretion System
TALE	transcription activator-like effector
TAMRA	5-Carboxytetramethylrhodamine
T_{Acet}	Acetone Tail
T_{Gly}	Glyceraldehyde tail
T_{Gua}	Guanidinium tail
TFE	Trifluoroethanol
TPP1	Tripeptidyl peptidase-1
TTP	Triphenylphosphonium
V	Voltage
V-ATPase	Vacuolar ATPase
VSVG	Vesicular stomatitis virus glycoprotein
W	Wortmannin
Y	Fractional activity
Y_{MAX}	Maximum activity

USC UNIVERSIDADE DE SANTIAGO DE COMPOSTELA

Abstract

Plasma membrane plays a key role controlling the influx and efflux of bioactive molecules in the cell. As only small molecules can cross the cell membrane, traditional drugs have small sizes and follow the Lipinski's rules. Thus, therapies based on biomacromolecules such as proteins or antibodies were less employed. The large size of these protein molecules also represents an obstacle for crossing the plasma membrane and to interact with their target within the cell. As a consequence, many intracellular targets of protein therapeutics still remain as "*undruggable*" targets. The main objective of this thesis is to design and synthesize carriers that will allow a better understanding of the transport and release proteins and antibodies into living cells.

In chapter 1, we have designed a new α-helix-forming peptide bearing reactive groups. The reactive moieties allowed us to build up small libraries with "clickable" reactions between the peptide and aldehyde pendants without further purification steps. The cationic and hydrophobic pendants modulate the peptide ability to interact with cells. The evaluation of the peptides in artificial delivery models and later *in vitro* assays allowed us to identify the best characteristics for cellular penetration and cellular viability. In this case, the increment of cationic residues improves the penetration as well as the cell viability. The most relevant data extracted was that a balance between the hydrophobic and the cationic part was required.

During the chapter 2, we decided to focus on the secondary structure of oligoalanine peptide scaffolds to identify selective helical folding in membranes that would allow a supramolecular self-assembly in membranes. This helical folding could control the release of cargos from endosomes into the cytosol. We started to build up a library of amphipathic peptides based on alanine. Alanine was chosen as scaffold because of its strong α-helical stabilizing character (0.77 kcal per mol). A balanced ratio between cationic and hydrophobic residues (arginines and leucines) was also chosen. A small library of peptides was developed by permutation of these arginine and leucine amino acids along the oligoalanine scaffold. The final peptides were evaluated by circular dichroism in three different environments (lipid, aqueous buffer, and TFE media) in order to know the degree of folding, and relate it with *in vitro* delivery and cytotoxicity. The results showed correlation between helical folding in membranes and good penetration abilities. On the other hand, the structures with more helical folding in aqueous buffer than membranes showed an increase in cytotoxicity. The best peptide candidate in cellular uptake and viability (helical content of 13% in buffer and 50% in membranes) had a radial distribution of leucines and aligned distribution of arginines. Its penetration and cytotoxicity were evaluated in different cell lines and its endosomal internalization route was studied and characterized by inhibition uptake experiments.

In chapter 3, the best peptide candidate studied in the chapter 2 was tested for the cytosolic delivery of biomacromolecular cargos such as dextran (a polymer well known for its internalization by endocytosis). We characterized the transport mechanism using artificial lipid bilayer models. A selective interaction for anionic lipids (present in endosomes) was observed in artificial release models based on large unilamellar vesicles (LUVs). These artificial vesicles displayed a leakage or release of small fluorophores such as ANTS in LUVs⊂ANTS/DPX or of large fluorescent polymers such as in LUVs⊂dextran in dose-response kinetic experiments. In addition, the LUVs system showed a greater self-assembly of peptide in the presence of anionic lipids by FRET efficiency assays. The stability of these LUVs was tested in the presence of peptide, and it was found that the peptide could release molecules from the vesicles without showing lytic behavior, even at high peptide concentrations. Molecular dynamics

computational studies pointed to a transient pore formation. Therefore, we proposed that the mechanism of action was through the formation of a supramolecular pore, which was confirmed by planar membrane assays (BLM). This technique also allowed us to estimate a diameter pore size of approximately 4-5 nm. Finally, we decided to explore the scope of biomacromolecules delivered into cells by the peptide. The molecules of biological interest tested were proteins (saporin, Cre recombinase and GST-NLS-GFP) and antibodies (such as IgG and Mab414). Moreover, different cell lines such as HeLa, Vero, A549 and ARPE-19 were tested. We also studied the potential delivery of antibodies in tissue of murine cornea, ex vivo. As conclusion of the good delivery results, the pore-forming peptide MP1 was confirmed as an excellent candidate for the intracellular delivery and release of proteins and antibodies..

USC UNIVERSIDADE DE SANTIAGO DE COMPOSTELA

Resumen

La membrana plasmática desempeña un papel clave en el control del flujo de moléculas bioactivas en la célula. Como sólo las moléculas pequeñas pueden atravesar la membrana celular, los fármacos tradicionales tienen tamaños pequeños y siguen las reglas de Lipinski. Así, las terapias basadas en biomacromoléculas, como las proteínas o los anticuerpos, han sido menos empleadas. El gran tamaño de estas moléculas proteicas también representa un obstáculo para atravesar la membrana plasmática e interactuar con su objetivo dentro de la célula. En consecuencia, muchas dianas intracelulares de las terapias proteicas siguen siendo inaccesibles. El objetivo principal de esta tesis fue diseñar y sintetizar transportadores que permitieran comprender mejor el transporte y la liberación de proteínas y anticuerpos en las células vivas.

En el capítulo 1 hemos diseñado un nuevo péptido formador de α-hélices con grupos reactivos. Los grupos reactivos nos permitieron construir pequeñas bibliotecas con reacciones "clicables" entre el péptido y las colas de aldehído sin necesidad de otros pasos de purificación. Las colas catiónicas e hidrofóbicas modularon la capacidad del péptido para interactuar con las células. La evaluación de los péptidos en modelos de transporte artificiales y los posteriores ensayos *in vitro* nos permitieron identificar las mejores características para penetración y viabilidad celular. En este caso, el incremento de residuos catiónicos mejoraba tanto la penetración como la viabilidad celular. El dato más relevante extraído fue que es necesario un equilibrio entre la parte hidrofóbica y la catiónica.

Durante el capítulo 2, decidimos centrarnos en la estructura secundaria de los andamios peptídicos de oligoalanina para identificar un plegamiento helicoidal selectivo en las membranas que permitiera un autoensamblaje supramolecular en las mismas. Este plegamiento helicoidal podría controlar la liberación de cargas de los endosomas al citosol. Creamos una biblioteca de péptidos anfipáticos basados en alaninas. La razón por la que se escogió la alanina como esqueleto fue por su fuerte carácter estabilizador α-helicoidal (0,77 kcal por mol). También se eligió una relación de equilibrio entre residuos catiónicos e hidrofóbicos (argininas y leucinas). La pequeña biblioteca de péptidos que desarrollamos fue mediante la permutación de estos aminoácidos de arginina y leucina a lo largo de la secuencia de alaninas. Los péptidos finales se evaluaron mediante dicroísmo circular, en tres entornos diferentes (lípidos, tampón acuoso y medio TFE) para conocer el grado de plegamiento, y relacionarlo con la internalización *in vitro* y la citotoxicidad. Los resultados mostraron una correlación entre el plegamiento helicoidal en las membranas y una buena capacidad de penetración. Por otro lado, las estructuras con mayor plegamiento helicoidal en tampón acuoso que en membranas mostraron un aumento de la citotoxicidad. El mejor candidato a péptido en cuanto a internalización y viabilidad celular (contenido helicoidal del 13% en tampón y del 50% en membranas) tenía una distribución radial de leucinas y alineada de argininas. Se evaluó su penetración y citotoxicidad en diferentes líneas celulares y se estudió su ruta de internalización endosomal, caracterizándola mediante experimentos de inhibición de la endocitosis.

En el capítulo 3, el mejor candidato (en penetración y viabilidad) identificado en el capítulo 2 se probó para la entrega citosólica de cargas de biomacromoléculas como el dextrano (un polímero bien conocido por su internalización por endocitosis). También se caracterizó su mecanismo de transporte utilizando modelos de bicapa lipídica artificial, y se observó una interacción selectiva para los lípidos aniónicos (presentes en los endosomas) en modelos artificiales de liberación basados en vesículas unilamelares grandes (LUVs). Estas vesículas

artificiales mostraron una fuga o liberación de pequeños fluoróforos como ANTS en LUVs⊂ANTS/DPX o de grandes polímeros fluorescentes como en LUVs⊂dextrano en experimentos cinéticos de dosis-respuesta. Además, el sistema de LUVs mostró un mayor autoensamblaje del péptido en presencia de lípidos aniónicos mediante ensayos de eficiencia FRET. La estabilidad de las LUVs en presencia de péptido se comprobó, y se observó que el péptido podía liberar moléculas de las vesículas sin mostrar un comportamiento lítico, incluso a altas concentraciones de péptido. Por otro lado, los estudios computacionales de dinámica molecular apuntaron a una formación transitoria de poros. Por lo tanto, propusimos un mecanismo de acción a través de la formación de un poro supramolecular, lo que se confirmó por ensayos de membrana plana (BLM). Esta técnica también nos permitió estimar un tamaño de diámetro de poro de aproximadamente 4-5 nm. Por último, decidimos explorar la variedadde biomacromoléculas que podían ser introducidas en las células por el péptido. Las moléculas de interés biológico que se probaron fueron proteínas (saporina, recombinasa Cre y GST-NLS-GFP) y anticuerpos (como IgG y Mab414). Además, se testó en diferentes líneas celulares como HeLa, Vero, A549 y ARPE-19. También se estudió el potencial de entrega de anticuerpos en el tejido de la córnea murina, *ex vivo*. Como conclusión de los buenos resultados de transporte,el péptido formador de poros MP1 se confirmó como un excelente candidato para la entrega y liberación intracelular de proteínas y anticuerpos.

.

USC UNIVERSIDADE DE SANTIAGO DE COMPOSTELA

Resumo

A membrana plasmática xoga un papel crave no control do fluxo de moléculas bioactivas que entran na célula. Existen diversos mecanismos de entrada na célula para as moléculas, algunhas internalizan mediante procesos naturais (activación de proteínas de membrana, canles ou endocitosis) mentres que outras internalizan por simple difusión a través da membrana. Este adoita a ser o caso das moléculas de pequenas dimensións. Por esta razón, a gran maioría das terapias con dianas intracelulares que se desenvolveron ata o momento seguían as regras de Lipinski (tamaños reducidos, alta solubilidade, capacidade para cruzar a membrana…). Sen embargo, co paso do tempo foise incrementando o número de dianas terapéuticas para inducir ou restaurar novas funcións. Moitas destas dianas téñense que abordar mediante macromoléculas de interese biolóxico que abarcan o espazo terapéutico que os fármacos de pequenas dimensións non poden cubrir. Unha das grandes limitacións que ten o transporte intracelular de biomacromoleculas é que está limitada por diversas barreiras (membrana plasmática, endocitose, proteasas, etc.), e por iso moitas veces é necesario que a entrada estea mediada ou facilitada por un transportador. Na natureza atópanse exemplos de microorganimos que poden acceder ao espazo intracelular. Por exemplo os virus, que penetran nas células para introducir o seu material xenético. Cando se estaba investigando a actuación dunha das proteínas do virus do VIH descubriuse que era capaz de internalizar nas células por si soa. Máis tarde descubriuse a secuencia peptídica mínima para a internalización, que se chamou Tat, e seguiuse investigando sobre outras secuencias peptídicas con capacidade de penetración celular. Desta maneira iniciouse o campo de investigación dos péptidos penetrantes de células ou CPP e o estudo do seu potencial como transportadores celulares. O desenvolvemento de novos péptidos transportadores de moléculas de interese biolóxico foi o obxectivo principal que se desenvolveu no traballo desta tese doutoral.

Estes péptidos penetrantes pódense clasificar de distintas maneiras pero, atendendo ás súas propiedades físico químicas, atopámonos con péptidos catiónicos, anfifílicos e hidrofóbicos. No primeiro caso, os péptidos catiónicos conteñen residuos de arxinina ou lisina, que están cargados a pH fisiolóxico. A súa vantaxe principal é a capacidade de interaccionar coas partes aniónicas que compoñen as membranas. É reseñable o comportamento dos grupos guanidinio das arxininas. Trátase dun grupo que sempre está protonado a pH fisiolóxico e que a única maneira que ten de reducir a repulsión electrónica entre cargas lindeiras é mediante complexación de contraións. Estes contraións son os que lle confiren capacidades especiais ás arxininas, como por exemplo, variar o grao de anfifilicidade ou hidrofobicidade. Por esta razón, moitas das estruturas dos péptidos penetrantes conteñen arxinina na súa secuencia peptídica. Os péptidos anfifílicos adoitan estar compostos por un dominio catiónico e por outro hidrofóbico separados no espazo. Neste caso a vantaxe principal é que poden interaccionar coa parte aniónica das membranas polo lado catiónico do péptido e coa parte hidrofóbica das bicapas co dominio hidrofóbico do péptido. Finalmente, o último tipo de péptidos penetrantes reportados son os hidrofóbicos, que son ricos en aminoácidos de tipo alanina, leucina, fenilalanina, triptófano, etc. A súa vantaxe é a gran afinidade e interacción que teñen pola rexión interna e hidrofóbica das membranas.

Durante o desenvolvemento de novas secuencias peptídicas penetrantes fíxose necesariaa creación de novas técnicas para caracterizar as súas propiedades. Por exemplo, introducíronse modelos de bicapas lipídicas como son as vesículas ou as membranas planas. Os modelos vesiculares adoitan a conter moléculas fluoresencentes no seo da estrutura nun estado

de repouso. Por tanto, calquera acción sobre a membrana que varíe a fluorescencia interprétase como actividade transmembrana, tanto por medio de transporte como por liberación do contido intravesicular. Doutra banda, os modelos de membranas planas miden experimentalmente os cambios na intensidade de corrente que se recollen despois de aplicar unha diferenza de potencial. Unha membrana na posición intermedia entre dúas cámaras que conteñen tampón acuoso conectadas a unha diferenza de voltaxe actúa como condensador e non dará cambios de corrente. Con todo, a introdución dun poro ou canle que comunique as dúas cámaras de tampón resultará nunha variación na intensidade de corrente. Por tanto, estes modelos de membranas artificiais permíten medir comportamentos de afinidade con membranas, penetración, transporte, estabilidade lipídica, tipos de ensamblaxe en membranas e, por conseguinte, serven para a súa caracterización (número de monómeros, tamaño do poro, etc). Os datos así obtidos axudan a entender, correlacionar e extrapolar as características e habilidades destes péptidos penetrantes dende sistemas artificiais a sistemas celulares vivos.

Unha estratexia para crear bibliotecas de péptidos penetrantes de forma rápida e eficiente é mediante o uso de enlaces dinámicos. Algúns destes tipos de enlaces dinámicos son as hidrazonas, as oximas ou os disulfuros. As principais características que presentan este tipo de enlaces é que se poden levar a cabo en medios acuosos, fórmanse os compostos finais sen reaccións secundarias, e non necesitan pasos de purificación adicionais. As ligazóns dinámicas tamén son capaces de responder a estímulos externos, é dicir, hidrolízanse e fórmanse en función das condicións nas que se atopan.

No primeiro capítulo da tese creouse unha pequena biblioteca peptídica que incorporaba dous motivos reactivos para a formación de enlaces dinámicos. Isto permitiunos caracterizar que modificacións sobre unha mesma secuencia base melloraban a súa capacidade como péptidos penetrantes de células. O deseño do péptido base foi capaz de adoptar unha estrutura secundaria formadora de hélices alfa. A principal vantaxe desta estrutura secundaria foi que permitía separar dúas rexións ben diferenciadas, unha catiónica e outra hidrofóbica, o que lle confiriu á estrutura un carácter anfifílico. Ademais, na interfase de ambas rexións introducíronse dous grupos reactivos alcoxiamina. Desta maneira non se distorsionou o carácter anfifílico do péptido independentemente da natureza do aldehido. Estas alcoxiaminas introducíronse durante a síntese en fase sólida, mediante un método desenvolvido no noso laboratorio, que se basea na desprotección ortogonal das lisinas nun medio ácido suave.

Unha vez que se desanclou o péptido da resina (na forma acetilada no extremo N-terminal) caracterízouse a súa estrutura secundaria, mediante a técnica de dicroísmo circular, que indicou unha estrutura con certo carácter helicoidal. Esta estrutura derivatizouse con distintos aldehidos que tiñan dende unha natureza hidrofóbica a unha catiónica, o que deu lugar aos anfifilos finais. Neste caso seleccionamos o isovaleraldehido e un aldehido de guanidinio sintético como colas reactivas. Para avaliar a capacidade de transporte de ADN e penetración leváronse a cabo ensaios en sistemas lipídicos artificiais como as vesículas unilamelares grandes (LUVs) descritos anteriormente. De entre os anfifilos testados, obtívose transporte unicamente no caso do péptido co aldehido de guanidinio sintético. Para comprobar se o comportamento destes anfifilos era equiparable ao comportamento en cultivos celulares foi necesario marcar o péptido cunha sonda fluorescente, a carboxifluoresceína. A carboxifluoresceína ancorada ao péptido permitiunos observar a súa capacidade de penetración por técnicas de microscopía. Os anfifilos empregados no caso do péptido fluorescente contiñan colas de guanidinio, colas de acetona, colas de isovaleraldehido, ou colas de gliceraldehido. As micrografías das células co péptido e a cuantificación da internalización confirmaron que o anfifilo coa cola de guanidinio internalizou máis que os outros dous anfifilos. A secuencia que presentou menor grao de internalización era a que contiña o gliceraldehido. Estes experimentos

de microscopía tamén amosaron un patrón de internalización punteado que colocalizaba cos lisosomas, o que nos indicou unha posible internalización mediada por un proceso de endocitosis. Con todo, o anfifilo que contiña a acetona non mostrou nin un patrón punteado nin colocalización cos lisosomas, dando a entender que a estrutura podería ter internalizado mediante un mecanismo de translocación directa. A viabilidade destes compostos volveu sinalar como mellor candidato ao anfifilo que contiña a cola de guanidinio, mentres que a viabilidade máis baixa atopouse para o péptido coa cola de acetona. Este comportamento fixo que nos plantexáramos unha posible distorsión da membrana por interaccións hidrofóbicas e un mecanismo de internalización de translocación directa. O dato máis relevante que extraímos desta pequena librería peptídica foi a necesidade dun equilibrio entre os elementos que compoñen a parte hidrofóbica e a parte catiónica.

Outro tipo de bibliotecas peptídicas abordáronse durante o capítulo 2 mediante o deseño racional de péptidos, que é fundamental para a produción de novas xeracións de CPPs. As estratexias de deseño de péptidos foron evolucionado ao longo do tempo para abarcar e xerar novas estruturas cun amplo abanico de funcionalidades. Con todo, o deseño racional das secuencias peptídicas é un reto, porque mesmo as secuencias curtas limitadas aos aminoácidos naturais poden dar lugar a innumerables variacións posibles. Isto supón unha limitación á hora de extraer conclusións sobre o comportamento e a actividade dos péptidos. Mediante o estudo tanto das secuencias naturais de péptidos penetrantes como as dalgunhas toxinas ou rexións transmembrana das proteínas, pódense coñecer que aminoácidos favorecen unha conformación fronte a outra. Por exemplo, os aminoácidos de alanina son coñecidos polo seu carácter estabilizador de alfa hélices, mentres que por exemplo a glicina ou a prolina son desestabilizadoras. Durante o desenvolvemento do capítulo 2 propuxemos a hipótese de que controlando o pregamento da estrutura secundaria dos péptidos poderíase obter unha autoensamblaxe supramolecular selectiva nas membranas, e desta maneira poderíase manexar a liberación de fármacos de forma controlada dende os endosomas ao citosol. Por iso, durante o avance deste capítulo levouse a cabo o desenvolvemento doutra biblioteca de peptídica usando deseños racionais. Escolleuse á alanina coma o aminoácido central para construír a biblioteca peptídica. As secuencias de péptidos que propuxemos tiñan certo carácter anfifílico e contaban con leucinas como motivos hidrofóbicos (para mellorar as interaccións hidrofóbicas coa membrana), e residuos catiónicos de arxinina que inducen a interacción coas superficies aniónicas das membranas. Ademais, a arxinina ten un carácter estabilizador helicoidal e unha cadea lateral o suficientemente longa como para incrustarse na membrana e facilitar a ensamblaxe en entornos lipídicos.

Os deseños iniciais estaban inspirados nas secuencias peptídicas propostas polo Prof. Baldwin, que empregaba oligoalaninas de 16 aminoácidos das que tomamos a lonxitude final dos nosos péptidos. Tamén nos inspiramos nos deseños do Prof. Dowdy, coas variacións do péptido Tat, que contiñan tres arxininas aliñadas, como requisito para conservar a capacidade penetrante. Da mesma forma que no capítulo anterior, mantívose unha relación de equilibrio entre residuos catiónicos e hidrófobos 3/3, arxininas e leucinas. A biblioteca de péptidos que se deseñou é o resultado da permutación na posición dos aminoácidos arxinina e leucina ao longo da secuencia de alaninas. A estrutura secundaria dos péptidos finais estudouse mediante dicroísmo circular, en tres ambientes diferentes (medio lipídico, acuoso e TFE) coa fin de coñecer o grao de pregamento e a porcentaxe de contido helicoidal de cada estrutura. Así mesmo, tamén se avaliou a internalización en cultivo celular de cada composto tanto por microscopía como por citometría de fluxo. Os resultados mostraron que era necesaria a presenza de tres leucinas na secuencia para obter un pregamento en hélice e para incrementar a internalización. Ademais, tamén atopamos que para obter un pregamento axeitado era necesario

a aliñación das arxininas. A posición das leucinas próximas ás arxininas melloraba o pregamento helicoidal no medio acuoso, mentres que unha disposición oposta incrementaba o contido helicoidal en liposomas. O mellor resultado mostrou que a disposición radial destas leucinas maximizaba o pregamento helicoidal en liposomas e provocaba a maior diferenza entre os medios acuosos e lipídicos. Os resultados correlacionaron a maximización deste pregamento helicoidal cos mellores datos de internalización, obtendo maior internalización canto maior era o pregamento en liposomas. Os estudos de viabilidade celular mostraron un patrón distinto, no que a toxicidade aumentaba co aumento do carácter helicoidal no medio acuoso. A tendencia citotóxica maximizábase cando a helicidade no medio acuoso era maior que en liposomas. Da mesma forma que no capítulo anterior, as micrografías de microscopía revelaron un patrón de internalización por puntos (nas estruturas con suficiente capacidade de penetración, denominadas **P6**, **P7** e **P8)**. Debido á internalización moderada dos compostos, só caracterizamos o mellor candidato peptídico, o que tiña unha distribución radial de leucinas e unha distribución aliñada das arxininas, **P8**. Estudouse en profundidade o mecanismo de entrada deste péptido por colocalización con lisosomas e por ensaios de internalización en presenza de inhibidores da endocitose. Tanto a colocalización positiva como a reducción da internalización con inhibidores demostraron que o péptido **P8** seguía unha vía de internalización endosomal, e principalmente un mecanismo de endocitose mediada por caveolina. O comportamento de P8 tamén se estudou noutras liñas celulares confirmando a súa boa capacidade de penetración e viabilidade, concluíndose que o deseño racional permitía controlar o pregamento helicoidal e, en consecuencia, a internalización e a viabilidade.

Durante o capítulo 3 profundouse na caracterización do pregamento de péptidos en membranas para o tranporte e liberación de fármacos. O gran interese que existe en liberar fármacos de natureza proteica no espazo intracelular reside na gran versatilidade e a innumerable cantidade de dianas ás que se poden dirixir. Aínda que tradicionalmente os fármacos proteicos estaban dirixidos ás dianas das membranas na superficie celular, actualmente estanse desenvolvendo multitude de transportadores para facilitar a tarefa da entrega citosólica. Con todo, este tipo de terapias presentan algunhas limitacións, como a estabilidade, a preservación da integridade da proteína a nivel celular, e sobrepasar as barreiras celulares. As limitacións relacionadas cos tamaños macromoleculares e o transporte débense a que o tamaño limita a entrada a través das membranas. Esta adoita estar mediada por procesos endocíticos, onde se non se produce a liberación destes fármacos acábanse degrandando ou exocitando. Por iso, algúns dos transportadores que se deseñaron tentan evitar estas vías de internalización e abordan a entrada directa ao citosol cruzando a membrana plasmática. Por exemplo, todos os métodos físicos que inducen distorsións transitorias na membrana plasmática, as nanopartículas transportadoras deseñadas polo Prof. Rotello que inducen unha fusión de membrana, ou as esterificacións da propia proteína propostas polo Prof. Raines. Os péptidos penetrantes tamén abordan a entrada celular de fármacos proteicos, como Pep-1 (ou o seu nome comercial Chariot®) desenvolto polo Prof. Divita, ou máis recentemente publicados as decargininas desenvolvidas polo Prof. Hackenberger. Outros transportadores están deseñados para destruír os endosomas ou provocar distorsións na membrana endosomal suficientes como para liberar de forma eficiente estas cargas proteicas. Algúns aproveitanse das características específicas que teñen estes compartimentos, como o enriquecemento en lípidos aniónicos, o descenso do pH no interior endosomal, ou a diferenza de voltaxe con respecto ao citosol. Na liberación endosomal existen exemplos de transportadores de moi diversa natureza como polímeros que aproveitan o efecto de esponxa de protóns que xera presión osmótica e acaba rompendo os endosomas. Algúns exemplos son o polímero PEI ou o dendrímero PAMAM e as modificacións de ambos. No caso dos péptidos penetrantes que liberan cargas

dos endosomas ao citosol, coñécense varios exemplos, tales como as modificións do péptido Tat onde destaca o péptido dfTAT desenvolvido polo Prof. Pellois, as modificacións de toxinas peptídicas desenvolvidas polo Prof. Futaki, entre das cales sobresae o péptido L17E, ou as achegas feitas polo noso grupo de investigación con lipopéptidos ou glicopeptidos para o transporte de proteínas como Cas9 ou concanavalina A.

Sobre os antecedentes descritos no capítulo 2, decidimos explorar se estes sistemas de helicidad modulable serían capaces de actuar como transportadores eficientes de macromoléculas. Polo tanto, propuxemos a avaliación desta proba de concepto sobre a ensamblaxe selectiva nas membranas dos endosomas para distorsionarlas e liberar biomacromoléculas no citosol. Os tranportadores peptídicos que desenvolvemos tiñan unha estrutura peptídica baseada nos conceptos desenvolvidos no capítulo 2. A estrutura caracterizouse en modelos de membrana artificiais e mediante simulacións computacionais. Tal e como observamos no capítulo anterior, 4 voltas helicoidais son suficientes para cuantificar a helicidade. Tamén se seleccionou de novo unha lonxitude de 16 aminoácidos cun esqueleto de alaninas, tres leucinas e tres arxininas. Durante o desenvolvemento deste capítulo 3 deseñamos e sintetizamos tres novas estruturas que chamaremos péptido mínimo 1 (**MP1**), péptido mínimo 2 (**MP2**) e péptido 3 (**P3**). **MP1**, **MP2** e **P3** están acetilados nos extremos N-terminais. Como estruturas de control, eliximos o péptido **GALA** e o péptido de octaarxinina **R8**. Nun estudo inicial de helicidade, de transporte de proteína e citotoxicidade, atopamos tanto unha boa ensamblaxe helicoidal como unha boa actividade de transporte e viabilidade para **MP1** en comparación coas outras dúas estruturas e os controis propostos. Por este motivo decidimos caracterizar en profundidade o comportamento deste péptido **MP1** en modelos de membranas artificiais. En primeiro lugar, usamos vesículas unilamelares grandes ou LUVs e comprobamos a tendencia que tiña **MP1** a pregarse en forma de alfa hélice ao aumentar a cantidade de vesículas e máis fortemente en presenza de vesículas aniónicas (que simulan a contorna endosomal). Esta afinidade por ensamblarse en membranas aniónicas tamén a atopamos durante os experimentos de FRET, mostrando unha forte asociación péptido-péptido en presenza de vesículas e unha afinidade péptido-membrana coas leucinas orientadas cara á cara interna da bicapa lipídica. Outros estudos de vesículas que se levaron a cabo foron os ensaios dose-resposta de liberación de pequenos fluoróforos como ANTS (LUVs ⊂ ANTS / DPX) ou de moléculas grandes como dextrano (LUVs ⊂ dextrano). Nestes ensaios observamos unha clara capacidade de **MP1** para liberar sondas fluorescentes pequenas e dextranos de 10 kDa (cun radio hidrodinámico de 2,5 nm). Unha das observacións que tamén se fixeron nestes experimentos é que **MP1** non comprometía a integridade vesicular, mesmo cando se someteu ás vesículas a altas concentracións de péptido. A continuación, leváronse a cabo unhas simulacións computacionais para poder predicir baixo que condicións ou como se establecían as ensamblaxes supramoleculares do péptido nas membranas. Curiosamente, ao someter ao sistema a un campo eléctrico, observouse a formación dunha ensamblaxe fibrilar do péptido que inducía unha invaxinación e despois a formación dun poro. Debido a este resultado e ás observacións anteriores, propuxemos a hipotésis da formación dun poro como mecanismo de liberación en membranas. A existencia deste poro supramolecular confirmouse mediante ensaios en membranas planas (BLM). Esta última técnica tamén nos permitiu facer unha estimación do tamaño de poro cun diámetro aproximado de 4-5 nm. Finalmente, para coñecer o alcance de **MP1** na aplicación como transportador en medios biolóxicos levamos a cabo diferentes ensaios con proteínas (saporina, recombinasa Cre, e GST- NLS-GFP) e anticorpos (como IgG e Mab414) en distintas liñas celulares. Nestes ensaios observamos que a cantidade de **MP1** que facía falta para transportar unha proteína ou outra variaba, e ademais tamén observamos que é necesario optimizar a cantidade de péptido para cada tipo de

biomacromolécula. Con todo, a cantidade optimizada para cada proteína non variaba dunha liña celular a outra excepto no caso dos experimentos realizados *ex vivo* en tecido de córnea de rato.

Finalmente, puidemos concluír que o poro peptídico que se propuxo como mecanismo de liberación para todas as cargas nas probas biolóxicas eran compatibles coas estimacións do tamaño do poro proposto, convertendo ao composto estudado, **MP1,** nun bo candidato para o transportee liberación citosólica de proteínas e anticorpos.

.

USC UNIVERSIDADE DE SANTIAGO DE COMPOSTELA

General Objectives

USC UNIVERSIDADE DE SANTIAGO DE COMPOSTELA

USC
UNIVERSIDADE
DE SANTIAGO
DE COMPOSTELA

General Objectives

Research in chemical sciences is aimed to understand new concepts and develop new tools that can help solving problems across different disciplines such as Biology, Medicine and Materials Sciences. One of these challenges, where new molecules are required is the drug delivery in different genetic, autoimmune, infectious, or metabolic diseases. New biomolecular scaffolds, such as proteins or nucleic acids are emerging as a new class of potential therapeutic agents. However, limitations in the transport of these macromolecules into the cell are strongly hindering the development of new therapies. One of the basic problems in the cellular delivery of these macromolecular hydrophilic drugs is the entrapment in small vesicular compartments called endosomes, which prevent the release of their content to the cytosol. In addition, the endosomes expose the therapeutics to extreme conditions that will eventually degrade the cargo. In this Thesis, we have tried to address the problem of the drug delivery and endosomal release of functional proteins into the cells. We have focused on the development and design of new synthetic vehicles based on control helical folding of cell penetrating peptides. In the first chapter, we developed techniques to characterize and evaluate the different cell penetrating peptides. We designed a small dynamic library of helical peptides bearing dynamic covalent bonds that were further functionalized with different pendants to extract structure/activity conclusions about cationic and hydrophobic residues balance. In the second chapter, we designed a second helical peptide library based in other synthetic strategy: the permutation in the positions of the amino acids of short oligoalanine scaffolds. We could evaluate the influence of helicity in cellular activity, internalization as well as viability. Finally, in the third chapter of this Thesis, we decided to test the ability of the peptides designed in chapter 2 for the delivery of macromolecular cargoes with potential therapeutic activity. We also characterized the physicochemical properties in membranes of CPPs to hypothesis the mechanism of action.

USC
UNIVERSIDADE
DE SANTIAGO
DE COMPOSTELA

General Introduction

USC UNIVERSIDADE DE SANTIAGO DE COMPOSTELA

USC
UNIVERSIDADE
DE SANTIAGO
DE COMPOSTELA

1. Therapeutic interest of Proteins and Antibodies

Proteins are the key players that control structure and functional processes in living matter. Many of these processes are involved in metabolic regulation, specific catalysis or structural cell support. Therefore, proteins are macromolecules with great therapeutic potential. The first functional therapeutic protein was insulin, which was purified from animal pancreases and administered to patients with diabetes mellitus in 1922.[1] Antibodies are glycoproteins produced by the immune system against pathogens and other foreign antigens, and whose high specificity towards their targets convert them into powerful therapeutic tools. Antibody-based therapies had already been used prior to insulin in the form of serum-based therapies, but at the time, these products contained poorly defined mixtures of antibodies and other blood proteins. The earliest serum therapy was an antitoxin against diphtheria that was awarded the first Nobel Prize in Medicine in 1901.[2] The main drawback of protein-based therapies was their initial unavailability in a pure form, a major constraint until new production methodologies were developed to reach affordable quantities of proteins and antibodies. For instance, the recombinant DNA technology for the production of proteins was not developed until 1973,[3] while the method for the production of well-defined, monoclonal antibodies in cell culture was described by Köhler and Milstein in 1975.[4] It was only then when protein treatments could start to expand.

Initial protein therapeutics focused on the interaction and recognition of membrane targets. These protein targets became popular due to their accessibility and because these surface proteins can be used to distinguish among cell types.[5] For example, some of the originally approved protein-based therapeutics that targeted the cell surface were developed against cancer, because tumor cells overexpress a variety of membrane receptors.[6] This specific recognition can be used for the selective delivery of chemotherapeutics and toxins, as well as for the stimulation of the immune response against the tumor cells. These therapies based on the recognition of surface receptors by antibodies and related proteins, such as antibody-drug conjugates, have been widely reviewed.[7,8,9] On the other hand, there are many potential targets and pathways in the intracellular space that are involved in disease processes, and that have been underexplored due to the delivery limitations. Currently, intracellular delivery of proteins and antibodies is emerging as a new class of potential therapeutics.[10,11,12,13]

[1] D. S. Dimitrov, in *Methods Mol. Biol.*, NIH Public Access, **2012**, pp. 1–26.
[2] V. Irani, A. J. Guy, D. Andrew, J. G. Beeson, P. A. Ramsland, J. S. Richards, *Mol. Immunol.* **2015**, *67*, 171–182.
[3] I. S. Johnson, in *Biotechnol. Biol. Front.*, Routledge, **2019**, pp. 46–56.
[4] G. KÖHLER, C. MILSTEIN, *Nature* **1975**, *256*, 495–497.
[5] N. J. Yang, M. J. Hinner, *Methods Mol. Biol.* **2015**, *1266*, 29–53.
[6] L. M. Nadler, P. Stashenko, R. Hardy, W. D. Kaplan, L. N. Button, D. W. Kufe, K. H. Antman, S. F. Schlossman, *Cancer Res.* **1980**, *40*, 3147–3154.
[7] P. V. Escribá, J. M. González-Ros, F. M. Goñi, P. K. J. Kinnunen, L. Vigh, L. Sánchez-Magraner, A. M. Fernández, X. Busquets, I. Horváth, G. Barceló-Coblijn, *J. Cell. Mol. Med.* **2008**, *12*, 829–875.
[8] H. Yin, A. D. Flynn, *Annu. Rev. Biomed. Eng.* **2016**, *18*, 51–76.
[9] A. Beck, L. Goetsch, C. Dumontet, N. Corvaïa, *Nat. Rev. Drug Discov.* **2017**, *16*, 315–337.
[10] T. A. Slastnikova, A. V. Ulasov, A. A. Rosenkranz, A. S. Sobolev, *Front. Pharmacol.* **2018**, *9*, 1208.
[11] K. Singh, W. Ejaz, K. Dutta, S. Thayumanavan, *Bioconjug. Chem.* **2019**, *30*, 1028–1041.
[12] Y. W. Lee, D. C. Luther, J. A. Kretzmann, A. Burden, T. Jeon, S. Zhai, V. M. Rotello, *Theranostics* **2019**, *9*, 3280–3292.
[13] M. Chiper, K. Niederreither, G. Zuber, *Adv. Healthc. Mater.* **2018**, *7*, 1701040.

1.1 Applications

One of the most important advantages of protein therapy is the potential unlimited number of new biological targets.[1,14] Traditionally, **small molecules** following Lipinski's rules[15] have been dominating pharmaceutical industry, as they present optimal bioavailability due to their solubility and permeability properties.[16] In comparison, bioavailability of macromolecules such as proteins is much lower, but they have a greater surface area to establish intermolecular interactions and, therefore, can be directed towards previously undruggable targets. An example of an emerging novel therapeutic strategy, which takes advantage of the interaction area of large molecules, is the modulation of Protein-Protein interactions (PPIs), because there are many aberrant PPIs involved in diseases.[17] Therefore, proteins or antibodies are excellent PPIs modulators due to their well-defined three-dimensional conformation that can control affinity and selectivity. Accordingly, protein therapeutics can target simultaneously multiple binding pockets or hotspots.[18,19]

Therapeutic proteins can be classified, according to their application, into proteins for inhibition or activation effect, proteins that have enzymatic activity and fluorescent proteins for cellular imaging as a proof-of-concept for delivery. One example of a therapeutical application of protein activation is the restoration of p53 tumor suppression protein activity. The activation of p53 could be restored by different antibodies,[20] protein mutants such as 53BP2,[21] or a mutant peptide of a fraction of p53.[22] Protein inhibitors or inactivators include, among others, ribosome-targeted immunotoxins that belong to the ribosome-inactivating protein (RIP) family, such as Gelonin[23] or Saporin-S6.[24] Proteins with enzymatic activity can be used to correct metabolic deficiencies, such as those that occur in lysosomal storage disorders (LSD). A special category within this group include endonucleases such as FokI or Cas9, with applications in gene editing, for the treatment of genetic diseases.[25,26,27] Finally, proteins that only have the function of cellular imaging agents such as GFP protein or labelled IgG antibody, are usually employed for location-specific labeling[28] or as proof-of-concept cargo for delivery studies.[29]

[14] A. J. Carter, O. Kraemer, M. Zwick, A. Mueller-Fahrnow, C. H. Arrowsmith, A. M. Edwards, *Drug Discov. Today* **2019**, *24*, 2111–2115.
[15] C. A. Lipinski, F. Lombardo, B. W. Dominy, P. J. Feeney, *Adv. Drug Deliv. Rev.* **2001**, *46*, 3–26.
[16] T. L. Nero, C. J. Morton, J. K. Holien, J. Wielens, M. W. Parker, *Nat. Rev. Cancer* **2014**, *14*, 248–262.
[17] H. Lu, Q. Zhou, J. He, Z. Jiang, C. Peng, R. Tong, J. Shi, *Signal Transduct. Target. Ther.* **2020**, *5*, 213.
[18] B. Leader, Q. J. Baca, D. E. Golan, *Nat. Rev. Drug Discov.* **2008**, *7*, 21–39.
[19] D. E. Scott, A. R. Bayly, C. Abell, J. Skidmore, *Nat. Rev. Drug Discov.* **2016**, *15*, 533–550.
[20] K. Sabapathy, D. P. Lane, *J. Mol. Cell Biol.* **2019**, *11*, 317–329.
[21] A. Friedler, L. O. Hansson, D. B. Veprintsev, S. M. V. Freund, T. M. Rippin, P. V. Nikolova, M. R. Proctor, S. Rüdiger, A. R. Fersht, *Proc. Natl. Acad. Sci. U. S. A.* **2002**, *99*, 937–942.
[22] G. Selivanova, V. Iotsova, I. Okan, M. Fritsche, M. Ström, B. Groner, R. C. Grafström, K. G. Wiman, *Nat. Med.* **1997**, *3*, 632–638.
[23] C. M. Pirie, D. V. Liu, K. Dane Wittrup, *Mol. Cancer Ther.* **2013**, *12*, 1774–1782.
[24] M. Akishiba, T. Takeuchi, Y. Kawaguchi, K. Sakamoto, H.-H. Yu, I. Nakase, T. Takatani-Nakase, F. Madani, A. Gräslund, S. Futaki, *Nat. Chem.* **2017**, *9*, 751–761.
[25] D. Carroll, *Genetics* **2011**, *188*, 773–782.
[26] J. K. Joung, J. D. Sander, *Nat. Rev. Mol. Cell Biol.* **2013**, *14*, 49–55.
[27] R. Jansen, J. D. A. van Embden, W. Gaastra, L. M. Schouls, *Mol. Microbiol.* **2002**, *43*, 1565–1575.
[28] M. Pazo, G. Salluce, I. Lostalé-Seijo, M. Juanes, F. Gonzalez, R. Garcia-Fandiño, J. Montenegro, *RSC Chem. Biol.* **2021**, *2*, 503–512.
[29] K. A. Mix, J. E. Lomax, R. T. Raines, *J. Am. Chem. Soc.* **2017**, *139*, 14396–14398.

1.2 Limitations

Protein and antibody-based therapies present challenges associated to the nature of these macromolecules, such as cargo stability and transport.

1.2.1 Stability limitations

Most proteins have short *in vivo* half-lives, suffering from physical and chemical instability and low oral bioavailability.[30] Protein activity is affected by immunogenicity,[31] which can depend on therapy duration, dose and route of administration.[32] In addition, proteolysis, mediated by proteases present in serum, extracellular matrix, lysosomes, and oxidation can also destroy protein activity.[33]

Immunogenicity is usually modulated by protein engineering, introducing masking moieties by PEGylation or glycosylation, or through sequence modifications, to remove T-cell epitopes or humanize the protein.[31] In addition, PEG extents its properties such as water solubility and flexibility to carriers and cargos in order to prolong their plasma half-life, by reducing kidney clearance or phagocytosis.[34,35] In protein cargos, PEGylation sites are placed in nucleophilic groups, such as amines or thiols in the lateral side chains of lysines or cysteines.[36] PEG polymers can also be used to improve carrier properties, for instance, being part of the surface of inorganic nanoparticles (NP) in order to avoid aggregation, increase the solubility or modify the size.[37] Stability limitations can be addressed by the development of new delivery strategies in order to improve the therapeutic impact of proteins. However, these strategies can also expose cargoes to undesirable conditions during the delivery process. For instance, during encapsulation the proteins can be exposed to high temperature, chemicals or organic solvents, which can affect protein stability and/or function.[38] Therefore, taking these problems into account, drug encapsulation methods must maintain the integrity and stability of the protein during encapsulation, administration and storage.[30,39] Examples of drug encapsulation and complexation approaches are hydrogels, which simplify a slow and non-interrupted administration with excellent biocompatibility on *in vivo* experiments.[40] Furthermore, hydrogels can also mitigate denaturation[41] and increase the thermal stability of encapsulated proteins.[42] The evolution of injectable hydrogels based on polymers and nanoparticles has achieved the release of large therapeutic agents such as proteins or human mesenchymal stem cells (hMSC).[43,44]

---

[30] S. D. Putney, P. A. Burke, *Nat. Biotechnol.* **1998**, *16*, 153–157.
[31] A. S. De Groot, D. W. Scott, *Trends Immunol.* **2007**, *28*, 482–490.
[32] Z. E. Sauna, D. Lagassé, J. Pedras-Vasconcelos, B. Golding, A. S. Rosenberg, *Trends Biotechnol.* **2018**, *36*, 1068–1084.
[33] N. Varkhede, R. Bommana, C. Schöneich, M. L. Forrest, *J. Pharm. Sci.* **2020**, *109*, 191–205.
[34] I. Ekladious, Y. L. Colson, M. W. Grinstaff, *Nat. Rev. Drug Discov.* **2019**, *18*, 273–294.
[35] J. Milton Harris, R. B. Chess, *Nat. Rev. Drug Discov.* **2003**, *2*, 214–221.
[36] N. Nischan, C. P. R. Hackenberger, *J. Org. Chem.* **2014**, *79*, 10727–10733.
[37] A. S. Karakoti, S. Das, S. Thevuthasan, S. Seal, *Angew. Chemie - Int. Ed.* **2011**, *50*, 1980–1994.
[38] A. Fu, R. Tang, J. Hardie, M. E. Farkas, V. M. Rotello, *Bioconjug. Chem.* **2014**, *25*, 1602–1608.
[39] F. Scaletti, J. Hardie, Y. W. Lee, D. C. Luther, M. Ray, V. M. Rotello, *Chem. Soc. Rev.* **2018**, *47*, 3421–3432.
[40] E. A. Appel, M. W. Tibbitt, M. J. Webber, B. A. Mattix, O. Veiseh, R. Langer, *Nat. Commun.* **2015**, *6*, 6295.
[41] S. E. Miller, Y. Yamada, N. Patel, E. Suárez, C. Andrews, S. Tau, B. T. Luke, R. E. Cachau, J. P. Schneider, *ACS Cent. Sci.* **2019**, *5*, 1750–1759.
[42] C. M. Meis, E. E. Salzman, C. L. Maikawa, A. A. A. Smith, J. L. Mann, A. K. Grosskopf, E. A. Appel, *ACS Biomater. Sci. Eng.* **2020**, acsbiomaterials.0c01306.
[43] G. A. Roth, E. C. Gale, M. Alcantara-Hernandez, W. Luo, E. Axpe, R. Verma, Q. Yin, A. C. Yu, H. L. Hernandez, C. L. Maikawa, et al., *ACS Cent. Sci.* **2020**, *6*, 1800–1812.
[44] A. K. Grosskopf, G. A. Roth, A. A. A. Smith, E. C. Gale, H. L. Hernandez, E. A. Appel, *Bioeng. Transl. Med.* **2020**, *5*, e10147.

For proteins that are active inside the cytosol, additional obstacles can appear. If the protein is internalized following an endocytic pathway, the limited release capacity decreases the therapeutic efficacy.[45] Moreover, in endosomes, carriers should preserve the active folding of proteins and protect them from acidic pH and enzymatic degradation.[46] In addition, once the protein cargo reaches the cytosol they could undergo either exocytosis or be digested under physiological conditions, which prevents the execution of its function.[47]

1.2.2 Transport (size) limitations

The size, shape and charge of macromolecules control their diffusion rates (Fick's law).[48] The large size of proteins reduces their diffusion rate and limits their extravasation, or circulation in tissues, which complicates the accumulation of the bioactive drug in their sites of action. For example, it has been proved that in some cases only the 20% of a specific mAbs could reach its corresponding membrane target, while the remaining amount was retained in blood.[49]

The large size of these protein molecules also represents an obstacle for crossing the plasma membrane and to interact with their target within the cell. As a consequence, many intracellular targets of protein therapeutics still remain as "*undruggable*" targets. Therefore, the interest in protein-based therapies has prompted the development of new delivery methods to expand the catalogue of "druggable" targets and fill the existing gap between extracellular and intracellular targets.[50]

USC UNIVERSIDADE DE SANTIAGO DE COMPOSTELA

[45] M. P. Stewart, A. Sharei, X. Ding, G. Sahay, R. Langer, K. F. Jensen, *Nature* **2016**, *538*, 183–192.
[46] D. W. Grainger, *Expert Opin. Biol. Ther.* **2004**, *4*, 1029–1044.
[47] A. El-Sayed, I. A. Khalil, K. Kogure, S. Futaki, H. Harashima, *J. Biol. Chem.* **2008**, *283*, 23450–23461.
[48] D. S. Banks, C. Fradin, *Biophys. J.* **2005**, *89*, 2960–2971.
[49] R. A. Beckman, L. M. Weiner, H. M. Davis, *Cancer* **2007**, *109*, 170–179.
[50] L. Mabonga, A. P. Kappo, *Biophys. Rev.* **2019**, *11*, 559–581.

CHAPTER 1: DYNAMIC CPPS

USC
UNIVERSIDADE
DE SANTIAGO
DE COMPOSTELA

1. Introduction

USC
UNIVERSIDADE
DE SANTIAGO
DE COMPOSTELA

1.1 History of CPPs

The first articles describing spontaneous protein cellular uptake were reported in 1988 by Green and Loewenstein,[51] and Frankel and Pabo,[52] when they were working with the transactivator of transcription protein (Tat) from HIV virus. They observed that Tat protein was taken up by cells and translocated into the nucleus. Years later, in 1991 when the research group of Prof. Prochiantz was studying the Antennapedia homeobox or homeodomain of *Drosophila* (DNA binding protein), they discovered a similar uptake of this protein into the nuclei of neuronal cells.[53] Modifications of this protein allowed the identification of the mutations that inhibited the translocation effect and determined that the third domain in the protein retained the penetrating ability. The translocating sequence of 16 amino acids isolated from Antennapedia was named penetratin43-58 (QIKIYFQNRRMKWKK).[54] At this moment, the terms of cell penetrating peptides (CPP) and protein transmembrane domain (PTD) are adopted and many new different sequences were identified.[55] For example, VP22 fusion protein from HSV-1 virus showed the same penetration capabilities, as described by Elliot and O'Hare in 1997.[56] In 1998, the minimal peptide sequence from the Tat protein was isolated by the group of Prof. Lebleu $Tat_{48\text{-}60}$ (C(Acm)GRKKRRQRRRPPQC).[57] The two previous cases highlighted the essential activity of basic residues, which controlled the interaction with the anionic components of the cell membrane.[53,57]

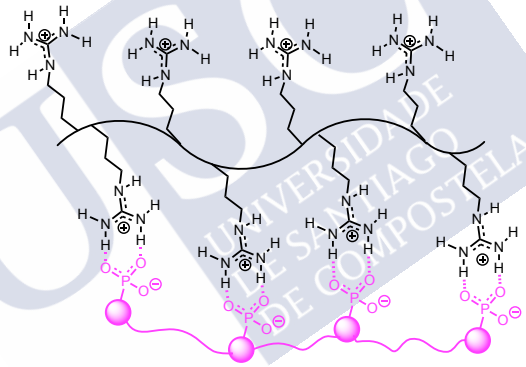

Figure 1. Hydrogen bonding between a phosphate counterion and protonated arginines.

This new transport process was deeply studied by Prof. Wender,[58] Prof. Futaki[59] and Prof. Matile,[60] who demonstrated that the cationic residues were responsible for the uptake, and was enhanced by the presence of arginine residues. They also could establish a minimal number of 4-5 arginines for translocation and an optimal number in 8-9 arginines to trigger membrane translocation. Prof. Futaki proposed a hydrogen bonding of the guanidinium groups with the lipidic phosphates as was previously reported by Frankel with the RNAs (Figure 1).[61]

[51] M. Green, P. M. Loewenstein, *Cell* **1988**, *55*, 1179–1188.
[52] A. D. Frankel, C. O. Pabo, *Cell* **1988**, *55*, 1189–1193.
[53] A. Joliot, C. Pernelle, H. Deagostini-Bazin, A. Prochiantz, *Proc. Natl. Acad. Sci. U. S. A.* **1991**, *88*, 1864–1868.
[54] D. Derossi, A. H. Joliot, G. Chassaing, A. Prochiantz, *J. Biol. Chem.* **1994**, *269*, 10444–10450.
[55] F. Heitz, M. C. Morris, G. Divita, *Br. J. Pharmacol.* **2009**, *157*, 195–206.
[56] G. Elliott, P. O'Hare, *Cell* **1997**, *88*, 223–233.
[57] E. Vivès, P. Brodin, B. Lebleu, *J. Biol. Chem.* **1997**, *272*, 16010–16017.
[58] P. A. Wender, D. J. Mitchell, K. Pattabiraman, E. T. Pelkey, L. Steinman, J. B. Rothbard, *Proc. Natl. Acad. Sci.* **2000**, *97*, 13003–13008.
[59] S. Futaki, T. Suzuki, W. Ohashi, T. Yagami, S. Tanaka, K. Ueda, Y. Sugiura, *J. Biol. Chem.* **2001**, *276*, 5836–5840.
[60] N. Sakai, S. Matile, *J. Am. Chem. Soc.* **2003**, *125*, 14348–14356.
[61] B. Calnan, B. Tidor, S. Biancalana, D. Hudson, A. Frankel, *Science.* **1991**, *252*, 1167–1171.

CPPs emerged as a new biological tool that was able to deliver different cargos such as nucleic acids, proteins, therapeutic molecules or probes.[62] Initial examples of *in vivo* applications of CPPs constituted a proof-of-concept of the real possibilities for these new family of peptide carriers. For example, transportan is a synthetic CPP developed by Prof. Langel in 1998, by combination of the aminoterminal sequence of the neuropeptide galanin and the wasp venom toxin mastoparan. A conjugate of this CPP and an antisense peptide nucleic acid (PNA) was able to internalize into cells to suppress the expression of galanin receptors.[63]

1.1.1 Classification of CPPs

There are a handful of criteria to classify CPPs based on their origin, sequence, function, or mechanism of cell internalization. According to their physical-chemical properties, all penetrating peptides can be classified in three different main classes:[64,65]

1.1.1.1 Cationic CPPs

Most known CPPs and the first to be discovered, as it was previously reported, are positively charged sequences of amino acids at physiological pH (arginine and lysine). This CPPs include Tat,[57] penetratin,[53] polyarginines[58,59] or Vectocell.[66] Arginine rich peptides have the strongest cell penetration capacity because of the guanidine head group, which has a pKa of 12.5 and it will be always protonated under physiological conditions.[67] On the other hand, guanidine has capacity to form bidentate hydrogen bonds with the negatively charged carboxylate, sulfate or phosphate groups of cell membrane (Figure 1). Prof. Wender highlighted the importance of hydrogen bonding of the guanidinium group. He performed a study with the monomethyl and dimethylguanidinium of arginines, which provided a compound 80% less effective to penetrate cells in the first case and 95 % less in the second.[68] Additionally, the enhancement of the backbone flexibility between guanidiniums groups also improved cell membrane association and cellular uptake.[69]

1.1.1.2 Amphipathic CPPs

These peptides are formed by two regions: a hydrophobic domain and hydrophilic domain. They can be subclassified into primary amphipathic CPP, secondary amphipathic CPP and proline rich sequences. **Primary amphipathic CPPs** were mainly described as chimeric structures where the two domains are separated from each other in the primary sequence. They usually include a hydrophobic domain bound to a nuclear localization signal (NLS), (SV40 T antigen: KKKRKV). The MPG[70] and the Pep-1[71] (first commercial carrier, Chariot™ Protein Delivery Reagent, Acitive Motif, USA) are two representative examples of this family. Other examples of amphiphilic CPPs were inspired by natural proteins like pVEC[72] (murine sequence

[62] K. M. Stewart, K. L. Horton, S. O. Kelley, *Org. Biomol. Chem.* **2008**, *6*, 2242–2255.
[63] M. Pooga, U. Soomets, M. Hallbrink, A. Valkna, K. Saar, K. Rezaei, U. Kahl, J.-X. Hao, X.-J. Xu, Z. Wisenfeld-Hallin, et al., *Nat. Biotechnol.* **1998**, *16*, 857–861.
[64] E. Koren, V. P. Torchilin, *Trends Mol. Med.* **2012**, *18*, 385–393.
[65] G. Guidotti, L. Brambilla, D. Rossi, *Trends Pharmacol. Sci.* **2017**, *38*, 406–424.
[66] C. De Coupade, A. Fittipaldi, V. Chagnas, M. Michel, S. Carlier, E. Tasciotti, A. Darmon, D. Ravel, J. Kearsey, M. Giacca, et al., *Biochem. J.* **2005**, *390*, 407–418.
[67] P. A. Wender, W. C. Galliher, E. A. Goun, L. R. Jones, T. H. Pillow, *Adv. Drug Deliv. Rev.* **2008**, *60*, 452–472.
[68] J. B. Rothbard, T. C. Jessop, P. A. Wender, *Adv. Drug Deliv. Rev.* **2005**, *57*, 495–504.
[69] J. B. Rothbard, E. Kreider, C. L. VanDeusen, L. Wright, B. L. Wylie, P. A. Wender, *J. Med. Chem.* **2002**, *45*, 3612–3618.
[70] G. D. M. C. Morris, P. Vidal, L. Chaloin, F. Heitz, *Nucleic Acids Res.* **1997**, *25*, 2730–2736.
[71] M. C. Morris, J. Depollier, J. Mery, F. Heitz, G. Divita, *Nat. Biotechnol.* **2001**, *19*, 1173–1176.
[72] A. Elmquist, M. Lindgren, T. Bartfai, Ü. Langel, *Exp. Cell Res.* **2001**, *269*, 237–244.

of the cell adhesion molecule vascular endothelial cadherin), the ARF_{1-22}[73] (fragment from tumor suppressor p14ARF, the p14 alternative reading frame) or the $BPrPR_{1-28}$[74] (peptide from unprocessed bovine prion protein).

Secondary amphipathic CPPs have a well-defined secondary structure like β-sheets or α-helixes. An example of amphipathic β-sheet CPP is VT5.[75] Amphipathic α-helix peptides are more frequent, where hydrophobic and hydrophilic residues are in opposite sides of the helix. They can derive from natural sources such as melittin, mastoparan or M-lycotoxin, from chimeric structures (e.g., MAP and transportan) or from completely artificial designs such as the synthetic protein transduction domains (PTDs) proposed by Prof. Dowdy.[76] Our research group has also contributed to the designs of secondary amphipathic peptides for different purposes such as gene delivery (Figure 2),[77] CRISPR/Cas9 delivery[78] or for selective protein recognition and delivery.[79]

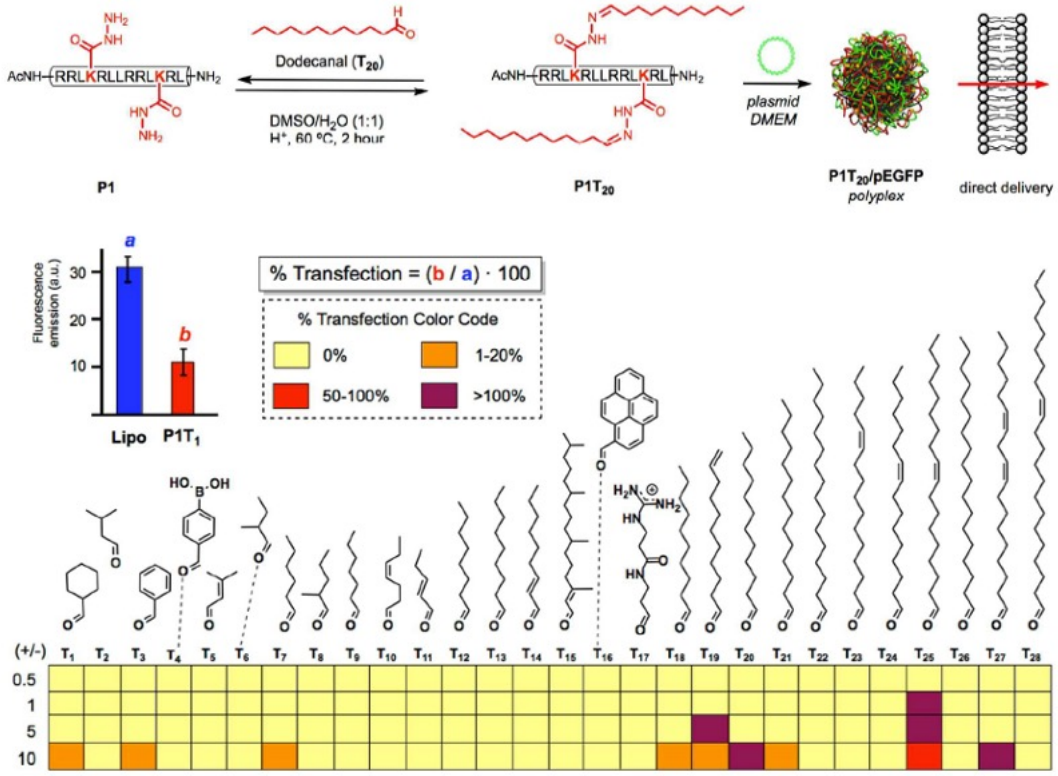

Figure 2. Reaction scheme to form amphiphiles from peptides and aldehydes for plasmid complexation and delivery (top). Heatmap for the transfection efficiency of the peptide P1 with different aldehydes and at different charge (+/-) ratios (bottom). Adapted with permission from ref[77] of Copyright (2017), The Royal society of chemistry.

[73] H. J. Johansson, S. El-Andaloussi, T. Holm, M. Mäe, J. Jänes, T. Maimets, Ü. Langel, *Mol. Ther.* **2008**, *16*, 115–123.
[74] M. Magzoub, S. Sandgren, P. Lundberg, K. Oglęcka, J. Lilja, A. Wittrup, L. E. Göran Eriksson, Ü. Langel, M. Belting, A. Gräslund, *Biochem. Biophys. Res. Commun.* **2006**, *348*, 379–385.
[75] J. Oehlke, E. Krause, B. Wiesner, M. Beyermann, M. Bienert, *FEBS Lett.* **1997**, *415*, 196–199.
[76] A. Ho, S. R. Schwarze, S. J. Mermelstein, G. Waksman, S. F. Dowdy, *Cancer Res.* **2001**, *61*, 474–7.
[77] I. Louzao, R. García-Fandiño, J. Montenegro, *J. Mater. Chem. B* **2017**, *5*, 4426–4434.
[78] I. Lostalé-Seijo, I. Louzao, M. Juanes, J. Montenegro, *Chem. Sci.* **2017**, *8*, 7923–7931.
[79] M. Juanes, I. Lostalé-Seijo, J. R. Granja, J. Montenegro, *Chem. - A Eur. J.* **2018**, *24*, 10689–10698.

Finally, **proline-rich peptides** can adopt a secondary structure named as polyproline I (PPI) and polyproline II (PPII) helixes. These secondary structures are responsible for the amphiphilicity of the polyproline peptides. In order to be folded they only have to contain 50% of proline in the sequence. One of the best-known proteins is γ-zein, which is the storage protein of maize.[80] This protein contains a proline rich domain (γ-ZNPRD) with repetitions of the sequence (VHLPPP).[81] This amphipathic region composed by $(VHLPPP)_8$ derived into other modifications such as $(VRLPPP)_3$ called sweet arrow peptide (SAP) or SAP containing fatty acids (like myristic acid or caproic acid).[82] Other typical proline-rich peptide is Bac7,[83] which is an antimicrobial peptide and adopts a hybrid form between α-helix and PPII.

1.1.1.3 Hydrophobic CPPs

Nonpolar and anionic residues are the main amino acid components of hydrophobic CPPs, which will have a strong affinity for the hydrophobic domains of cellular membranes. The uptake mechanism of hydrophobic peptides has been poorly studied compared with the other two classes of CPPs. Nevertheless, energy-independent uptake has been proposed to disrupt membranes by hydrophobic interactions.[84] Examples of hydrophobic CPPs include: PFVYLI C-terminal (a fragment from the peptide C105Y of α1-antitrypsin, which enhances gene expression from DNA particles)[85], pep-7 (a peptide identified by phage display),[86] SG3 peptide[87] and Fibroblast Growth Factor-12 (FGF12).[88] Moreover, these peptides can include chemical modifications[84] such as peptide stapling (to enhance the helicity),[89] prenylation (peptides with isoprenoid moiety, like farnesyl or geranyl)[90] or pepducin (cell penetrating lipidated peptides).[91,92]

1.2 Artificial Assays for Membrane Transport Characterization

The development of new CPPs structures requires transport assays that can be used to characterize their activity. The most employed transport assays are based on vesicles, which can be of different sizes such as Giant Unilamellar Vesicles (GUVs, 1-200 μm), Large Unilamellar Vesicles (LUVs, 100-1000 μm) and Small Unilamellar Vesicles (SUVs, 20-100μm).[93] In this thesis, we will only describe LUVs systems because of their simplicity to quantify and to compare peptide transport. Furthermore, the penetration and transport characterization by LUVs can give insights on the potential formation of channels or pores. However, the definitive proofs of the assembly of a transmembrane channel should be provided by planar membrane transport or Black Lipid Membrane (BLM) systems.

[80] J. Fernández-Carneado, M. J. Kogan, S. Castel, E. Giralt, *Angew. Chemie Int. Ed.* **2004**, *43*, 1811–1814.
[81] S. Pujals, E. Giralt, *Adv. Drug Deliv. Rev.* **2008**, *60*, 473–484.
[82] J. Fernández-Carneado, M. J. Kogan, N. Van Mau, S. Pujals, C. López-Iglesias, F. Heitz, E. Giralt, *J. Pept. Res.* **2005**, *65*, 580–590.
[83] K. Sadler, K. D. Eom, J.-L. Yang, Y. Dimitrova, J. P. Tam, *Biochemistry* **2002**, *41*, 14150–14157.
[84] F. Milletti, *Drug Discov. Today* **2012**, *17*, 850–860.
[85] M. Rhee, P. Davis, *J. Biol. Chem.* **2006**, *281*, 1233–1240.
[86] C. Gao, S. Mao, H. J. Ditzel, L. Farnaes, P. Wirsching, R. A. Lerner, K. D. Janda, *Bioorg. Med. Chem.* **2002**, *10*, 4057–4065.
[87] S. Gao, M. J. Simon, C. D. Hue, B. Morrison, S. Banta, *ACS Chem. Biol.* **2011**, *6*, 484–491.
[88] F. Nakayama, T. Yasuda, S. Umeda, M. Asada, T. Imamura, V. Meineke, M. Akashi, *J. Biol. Chem.* **2011**, *286*, 25823–25834.
[89] C. E. Schafmeister, J. Po, G. L. Verdine, *J. Am. Chem. Soc.* **2000**, *122*, 5891–5892.
[90] J. D. Ochocki, D. G. Mullen, E. V. Wattenberg, M. D. Distefano, *Bioorg. Med. Chem. Lett.* **2011**, *21*, 4998–5001.
[91] L. Covic, A. L. Gresser, J. Talavera, S. Swift, A. Kuliopulos, *Proc. Natl. Acad. Sci.* **2002**, *99*, 643–648.
[92] K. O'Callaghan, A. Kuliopulos, L. Covic, *J. Biol. Chem.* **2012**, *287*, 12787–12796.
[93] S. Matile, N. Sakai, A. Hennig, in *Supramol. Chem.*, John Wiley & Sons, Ltd, Chichester, UK, **2012**.

1.2.1 Large Unilamellar Vesicles (LUVs) measures

A standard assay to characterize transmembrane transport consists on the use of large unilamellar vesicles (LUVs). In these assays, LUVs are loaded with one or more fluorescent probes, and changes in fluorescence emission from internal dyes are used to measure transport activity (Figure 3A). In the initial state of the measurements, LUVs are in a resting state. When a channel or carrier that interacts with the lipid membrane is added, the intravesicular content changes. Therefore, time-dependent changes in fluorescence emission can be measured. Finally, a detergent is added to release all the vesicular content and normalize the kinetic fluorescent traces. These concentration-dependent transport fluorescence traces can be fitted to the Hill equation, from which the transport parameters are obtained such as the maximum activity (Y_{MAX}), the concentration at half activity (EC_{50}) and the Hill coefficient (n).[94,95] Some of the most common LUVs assays are:

Fluorescent transport assays. For example, carboxyfluorescein (CF) assays, where the probe is self-quenched by its high concentration and dilution causes an increase in fluorescence signals.[94] However, an important characteristic that should be taken into account with this probe is the sensitivity to pH. Another pH sensitive probe is 8-hydroxy-1,3,6-pyrenetrisulfonate (HPTS). HPTS assays can detect transport by efflux of the fluoresecent molecule itself, or the transport of H^+ or OH^- by changes in pH. HPTS can also be quenched in an HPTS / DPX system.[95] To avoid pH sensitivity problems, LUVs can also be loaded with a combination of anionic fluorophores like 8-aminonaphthalene-1,3,6-trisulfonic acid (ANTS) and cationic quenchers as p-xylene-bis-pyridinium bromide (DPX).[94] There are other tests to detect ion transport selectivity such as calcein for calcium transport, 6 methoxy-N-(3-sulfopropyl) quinolinium (SPQ) for chlorine transport or lucigenin for halide anions transport. The evaluation of the channel internal diameter can be achieved depending on the assay. For example, the efflux of HPTS / ANTS or DPX requires diameters close to 5Å and that of CF greater than 10Å. Probes of larger size are used to estimate sizes of greater diameter range, like fluorescent polymers such as dextran-FITC[96] or other efflux assays coupled to enzymes.[95]

DNA Transport Assays. To provide direct evidence on the specific transport of polyions such as DNA or CPPs with synthetic carriers, *U*-tube experiments are often used.[97,98] A hydrophobic or "bulk membrane" phase is placed at the bottom of a *U*-tube and two aqueous phases, *cis* and *trans*, are added on top of both sides (Figure 3B). To test the transport, carrier and cargo are added to the *cis* buffer and observed if they appeard in the *trans* buffer. In this case, Prof. Matile found that DPX as a cargo was complexed and transported by DNA, in the presence of the amphiphilic counterion activator dodecylguanidinium. Additionally, Prof. Matile exported the DNA/DPX transport to LUVs assays, where LUVs⊃HPTS/DPX increase the fluorescence when a carrier transports DNA across the lipid bilayer.[97] The system was employed for the evaluation of DNA transport abilities of CPPs, polymersomes, and

[94] S. Matile, N. Sakai, in *Anal. Methods Supramol. Chem.*, Wiley-VCH Verlag GmbH & Co. KGaA, Weinheim, Germany, **2012**, pp. 711–742.
[95] S. Matile, N. Sakai, A. Hennig, in *Supramol. Chem.*, John Wiley & Sons, Ltd, Chichester, UK, **2012**.
[96] M.-A. Sani, T. C. Whitwell, J. D. Gehman, R. M. Robins-Browne, N. Pantarat, T. J. Attard, E. C. Reynolds, N. M. O'Brien-Simpson, F. Separovic, *Antimicrob. Agents Chemother.* **2013**, *57*, 3593–3600.
[97] T. Takeuchi, V. Bagnacani, F. Sansone, S. Matile, *ChemBioChem* **2009**, *10*, 2793–2799.
[98] H. Fernández-Caro, I. Lostalé-Seijo, M. Martínez-Calvo, J. Mosquera, J. L. Mascareñas, J. Montenegro, *Chem. Sci.* **2019**, *10*, 8930–8938.

polymers.[99,100,101] Moreover, this LUVs⊃HPTS/DPX assay also allowed the generation of transport patterns for the differentiation of DNA sequences (Figure 3C).[101,102]

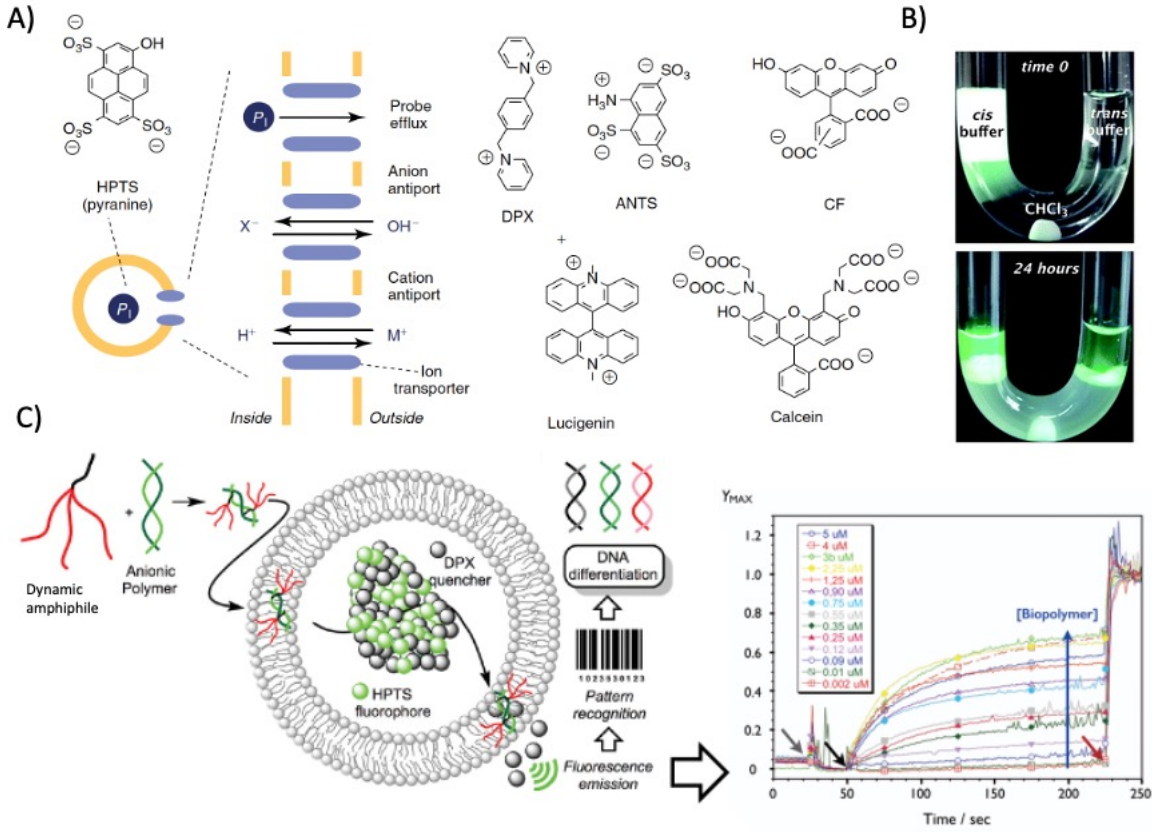

Figure 3. A) Different types of transport that can be studied in LUVs and structure of the encapsulated probes. Reproduced with permission from ref[95]. Copyright (2012), John Wiley and Sons. B) *U*-Tube transport at time 0 and after 24h. Reproduced with permission from ref[98]. Copyright (2019), Royal Society of Chemistry. C) DPX transport mediated by DNA-dynamic amphiphile complex and fluorescent kinetic measurements. Adapted with permission from ref[102]. Copyright (2014), John Wiley and Sons.

1.2.2 BLM measures

Black Lipid Membrane or BLM is a technique to characterize membrane pores. In BLM assays, voltage is applied through a thin barrier of a planar lipid membrane, with two annexed compartments containing aqueous electrolyte (chamber *cis* or *trans*) (Figure 4A). When a nanopore is inserted and opened in the membrane, the electrical potential induces the flow of ions through a pore and an ionic current is recorded.[103,94] Single current events appear and disappear in a stochastic manner (Figure 4B). Nonetheless, asymmetric repetition of different current levels could demonstrate different transition states[104] or different active structures

[99] J. Montenegro, J. Braun, O. Fischer-Onaca, W. Meier, S. Matile, *Org. Biomol. Chem.* **2011**, *9*, 6623–6628.
[100] J. M. Priegue, D. N. Crisan, J. Martínez-Costas, J. R. Granja, F. Fernandez-Trillo, J. Montenegro, *Angew. Chemie Int. Ed.* **2016**, *55*, 7492–7495.
[101] T. Takeuchi, S. Matile, *Chem. Commun.* **2013**, *49*, 19–29.
[102] J. M. Priegue, J. Montenegro, J. R. Granja, *Small* **2014**, *10*, 3613–3618.
[103] G. Maglia, A. J. Heron, D. Stoddart, D. Japrung, H. Bayley, **2010**, pp. 591–623.
[104] R. García-Fandiño, M. Amorín, L. Castedo, J. R. Granja, *Chem. Sci.* **2012**, *3*, 3280–3285.

(Figure 4C). These transition states are more frequent in systems composed by supramolecular interactions.[94]

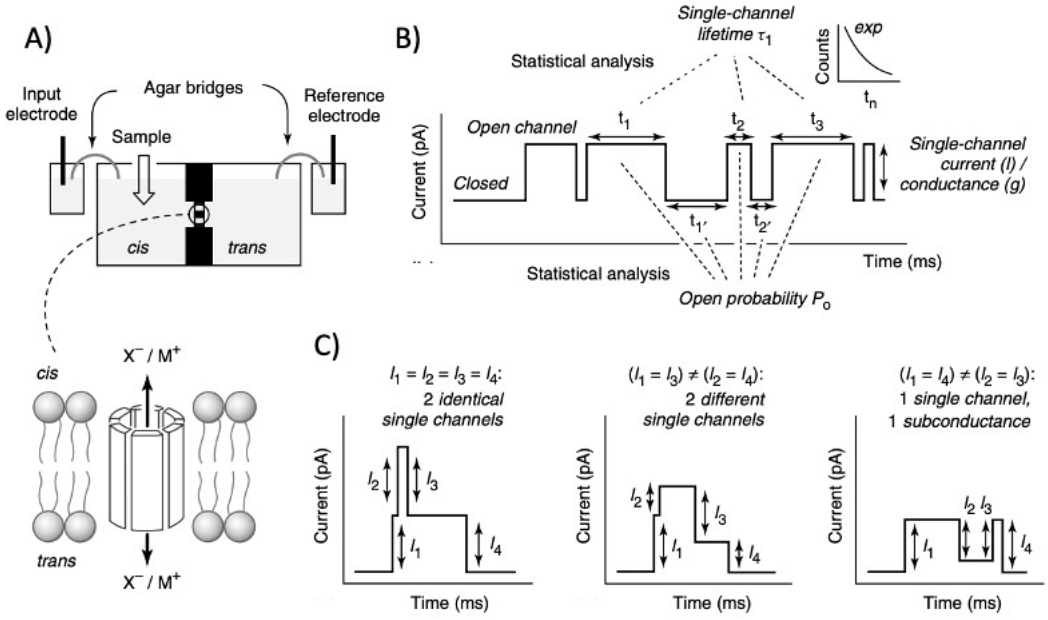

Figure 4. Standard configuration of a BLM experiment and data analysis. A) Set-up of a BLM measuring chamber. B) Interpretation of the current traces recorded in BLM experiments. C) Scheme of different current patterns that can identify different type of channels in the measurements. Reproduced with permission from ref[94]. Copyright (2012), John Wiley and Sons.

The activity of the synthetic channels depends on Ohm's law, which is determined by the linear relationship of the voltage applied to the BLM and the intensity of the recovered current. Ohm's Law link current (I), conductance (g) and voltage (V) (Equation 1). The development of Ohm's Law to relate the inner radio of the pore (r) to the conductance (g) results in Hille's equation[105] (Equation 2).

$$I = gV \qquad \text{(E1)}$$

Equation 1. Ohm's Law. I is the current, g is conductance and V is voltage.

$$\frac{1}{g} = \left(l + \frac{\pi r}{2}\right) \cdot \left(\frac{\rho}{\pi r^2}\right) \qquad \text{(E2)}$$

Equation 2. Hille equation. *g* is the pore conductance; *l* the length of the pore, *ρ* the resistivity of the recording solution and *r* the inner radius of the pore.

The group of Prof. Bayley has characterized in detail the α-hemolysin (α-HL), a staphylococcal toxin that inserts into membranes. In a BLM experiment, α-HL is a heptameric protein composed by a stem domain and a cap domain. The lumen of α-HL (2 nm) allows the pass of ions and produces changes in the open-closed current states (determined by BLM technique).[103] A wide range of mutations were applied to α-HL, such as 4 histidines in the lumen, which allows the detection of metal ions such Mn(II) or Zn(II).[106] One interesting

[105] B. Hille, *Ionic Channels of Excitable Membranes*, Sinauer Associates, Sunderland, MA, **1992**.
[106] H. Bayley, P. S. Cremer, *Nature* **2001**, *413*, 226–230.

modifications that Prof. Bayley made to α-HL was the inclusion of a cyclodextrin to constrict the lumen of the prore.[107,108] This lumen narrowing resulted improved resolution for the detection of small molecules such as nucleotides.[109] These designs established the basis for Oxford Nanopore Technologies (Oxford UK sequencing technology) (Figure 5A). Later, the group of Prof. Bayley developed a truncated hemolysin for nucleobase detection (Figure 5B).[110] Other α-HL variants could detect single states of catalytic mechanisms,[111] determine kinetics of growth and degradation of cell-penetrating poly(disulfides)s[112] and observe the phosphorylation or dephosphorylation of single molecules.[113]

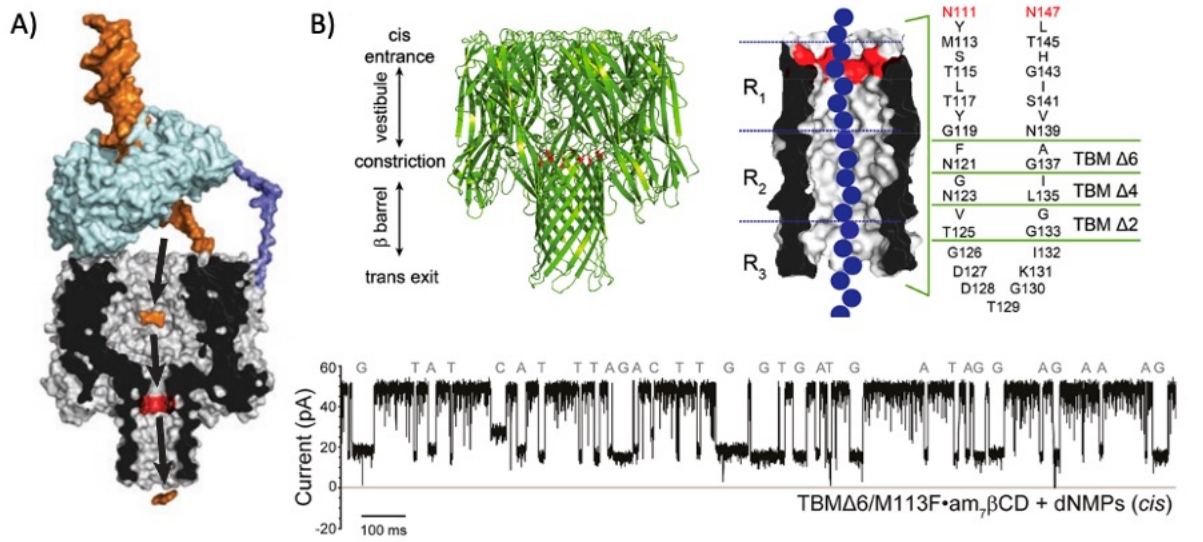

Figure 5. A) 3D structure of α-HL (grey and black) with an exonuclease (pale blue), DNA strand and deoxyribonucleotides (dNMPs) (gold), cyclodextrin (red). Reproduced with permission from ref[109]. Copyright (2008), Springer Nature. B) Complete structure (left) and a clipping structure (right) of α-HL and BLM recording with the passage of nucleotides. Adapted with permission from ref[110]. Copyright (2015), American Chemical Society.

There are other channels formed by single peptides that also were characterize by this technique. This is the case for mellitin and its variant MelP5, which displayed a larger pore diameter, a greater number of monomers per pore, a better defined and more stable channel in comparison with the wild-type mellitin.[114] Another example was the characterization of the structural hexameric assembly of the porinACj, demonstrating a uniform assembly instead of multiple oligomers.[115]

[107] Y. Astier, O. Braha, H. Bayley, *J. Am. Chem. Soc.* **2006**, *128*, 1705–1710.
[108] H. C. Wu, Y. Astier, G. Maglia, E. Mikhailova, H. Bayley, *J. Am. Chem. Soc.* **2007**, *129*, 16142–16148.
[109] D. Branton, D. W. Deamer, A. Marziali, H. Bayley, S. A. Benner, T. Butler, M. Di Ventra, S. Garaj, A. Hibbs, X. Huang, et al., *Nat. Biotechnol.* **2008**, *26*, 1146–1153.
[110] M. Ayub, D. Stoddart, H. Bayley, *ACS Nano* **2015**, *9*, 7895–7903.
[111] W. J. Ramsay, N. A. W. Bell, Y. Qing, H. Bayley, *J. Am. Chem. Soc.* **2018**, *140*, 17538–17546.
[112] G. S. Pulcu, N. S. Galenkamp, Y. Qing, G. Gasparini, E. Mikhailova, S. Matile, H. Bayley, *J. Am. Chem. Soc.* **2019**, *141*, 12444–12447.
[113] L. Harrington, L. T. Alexander, S. Knapp, H. Bayley, *ACS Nano* **2019**, *13*, 633–641.
[114] A. Fennouri, S. Finn, T. B. H. Schroeder, M. Mayer, *BBA - Biomembr.* **2017**, *1859*, 2051–2057.
[115] S. Krishnan R, R. Satheesan, N. Puthumadathil, K. S. Kumar, P. Jayasree, K. R. Mahendran, *J. Am. Chem. Soc.* **2019**, *141*, 2949–2959.

1.3 Dynamic covalent transport systems

1.3.1 Dynamic covalent bonds

Dynamic covalent chemistry combines properties of covalent and non-covalent bonds (Figure 6).[116] Under specific conditions, dynamic chemical bonds are formed and broken, allowing the reversibility of connectors with the corresponding molecular fragments. Imines, hydrazones and oximes, for example, can be hydrolyzed by acidic pH. However, disulfide dynamic bonds are less sensitive to pH and more dependent of redox chemistry.[117]

non-covalent	dynamic covalent	covalent
hydrogen bonds	disulfides	C-C
ion pairs	hydrazones	C-H
hydrophobic	boronic esters	C-O
π-π	imines	C-N
cation-π	thioesters	C-S
		C-P
		C-B
anion-π	hemi-/acetals	O-H
halogen bonds	hemiaminals	O-N
dipole-dipole	hemithioacetals	O-S
ion-dipole	dithianes	O-P
...	α-aminonitriles	O-B
	nitrones	...
	alkenes	
	enones	
	nitroolefins	
	...	

Figure 6. Most popular members of non-covalent, dynamic covalent and covalent bonds. Reproduced with permission from ref[116].C opyright (2014) Royal Society of Chemistry.

The switchable and exchangeable nature of dynamic bonds can lead to dynamic combinatorial libraries (DCLs). This term was first introduced by Professors Sanders and Otto.[117] DCLs are composed of networks of building blocks, whose main characteristic is dynamism, i.e. the interchangeable nature of its components. Dynamic covalent bonds can be also found in nature, such as disulfides for controlling protein folding. Additionally, these bonds are also found in artificial systems that exploit self-recognition, self-sorting or self-replicators.[118] These dynamic bonds have been related to prebiotic chemistry and the origin of life in the simplest organisms. Therefore, the study of these DCLs, such as self-replicators, can help to understand how these organisms have been developed. For example, through self-replicating peptide-derived macrocycles that assemble into fiber nanostructures[119] or host-induced diastereoselective amplification.[120]

[116] A. Wilson, G. Gasparini, S. Matile, *Chem. Soc. Rev.* **2014**, *43*, 1948–1962.
[117] P. T. Corbett, J. Leclaire, L. Vial, K. R. West, J. L. Wietor, J. K. M. Sanders, S. Otto, *Chem Rev* **2006**, *106*, 3652–3711.
[118] J. Li, P. Nowak, S. Otto, *J. Am. Chem. Soc.* **2013**, *135*, 9222–9239.
[119] J. M. A. Carnall, C. A. Waudby, A. M. Belenguer, M. C. A. Stuart, J. J. P. Peyralans, S. Otto, *Science.* **2010**, *327*, 1502–1506.
[120] P. T. Corbett, L. H. Tong, J. K. M. Sanders, S. Otto, *J. Am. Chem. Soc.* **2005**, *127*, 8902–8903.

1.3.2 Hydrazones and oximes bonds

Hydrazones and oximes are chosen frequently for biological applications. Its versatility was applied in the development of new polymers (containing hydrazides) for the transport of genetic material.[100,121,122] The reaction between hydrazides or alkoxyamines with aldehydes are considered "clickable", as occurs in good yields, without side reactions and lead to the corresponding hydrazones and oximes. Moreover, these reactions are compatible with aqueous media and make them suitable for biological applications. For instance, in chemical ligation[123] or in tagged proteins[124] reported by Prof. Dawson. The hydrolytic stability of these bonds has been studied by Prof. Raines, who demonstrated a decreasing stability as follows: oximes > hydrazones > acyl hydrazones.[125] However, the final stability also depends on macromolecule and the microenvironment of the bond.

1.3.3 Peptide libraries

Dynamic bonds such as oximes or hydrazones can be used to develop dendron-peptide amphiphiles. Prof. Matile developed a pattern recognition method based on peptide libraries as transporters in lipidic membranes of LUVs. These libraries were obtained by condensation of hydrazide reactive peptides and hydrophobic volatile aldehydes. When the cationic[126] or anionic[127] amphiphiles are assembled, a transport pattern for the corresponding polyions in vesicles can be generated. The counterion of these carriers are DNA for the cationic amphiphiles or polyarginine in the anionic amphiphiles (Figure 7A). Prof. Montenegro extended this methodology for the differentiation of nucleic acids with single nucleotide recognition.[102]

In a more biological context, the evolution of this small peptide libraries was tested for the transfection of siRNA *in vitro*.[128] Reactive peptides containing aliphatic hydrazides were analyzed in order to reach gene or protein delivery properties. These amphiphiles showed good transport properties for plasmids *in vitro* assays[77] and Cas9[78] showing satisfactory *in vitro* transport efficiency (Figure 7B).

In addition to amphiphilic peptide libraries, dynamic bond technology also allowed the evaluation of glycopeptide libraries. The possibility to include different chains by using an alkoxyamine connectors allowed the selective recognition of proteins and subsequent membrane transport of the resulting peptide/protein complexes. Selective protein discrimination between concanavalin A or streptavidin was achieved by α-mannose or biotin recognition moieties.[79] A small set of glycopeptides was also evaluated in order to study cell internalization of glycosyl penetrating peptides. The oxime dynamic bond allowed the study of the best glycans in internalization/toxicity balance.[129]

---

[121] J. M. Priegue, I. Lostalé-Seijo, D. Crisan, J. R. Granja, F. Fernández-Trillo, J. Montenegro, *Biomacromolecules* **2018**, *19*, 2638–2649.
[122] M. Juanes, O. Creese, P. Fernández-Trillo, J. Montenegro, *Medchemcomm* **2019**, *10*, 1138–1144.
[123] A. Dirksen, S. Dirksen, T. M. Hackeng, P. E. Dawson, *J. Am. Chem. Soc.* **2006**, *128*, 15602–15603.
[124] A. Dirksen, S. Yegneswaran, P. E. Dawson, *Angew. Chemie Int. Ed.* **2010**, *49*, 2023–2027.
[125] J. Kalia, R. T. Raines, *Angew. Chemie - Int. Ed.* **2008**, *47*, 7523–7526.
[126] T. Takeuchi, J. Montenegro, A. Hennig, M. Stefan, *Chem. Sci.* **2011**, *2*, 303–307.
[127] J. Montenegro, S. Matile, *Chem. - An Asian J.* **2011**, *6*, 681–689.
[128] C. Gehin, J. Montenegro, E.-K. Bang, A. Cajaraville, S. Takayama, H. Hirose, S. Futaki, S. Matile, H. Riezman, *J. Am. Chem. Soc.* **2013**, *135*, 9295–9298.
[129] I. Gallego, A. Rioboo, J. J. Reina, B. Díaz, Á. Canales, F. J. Cañada, J. Guerra-Varela, L. Sánchez, J. Montenegro, *ChemBioChem* **2019**, *20*, 1400–1409.

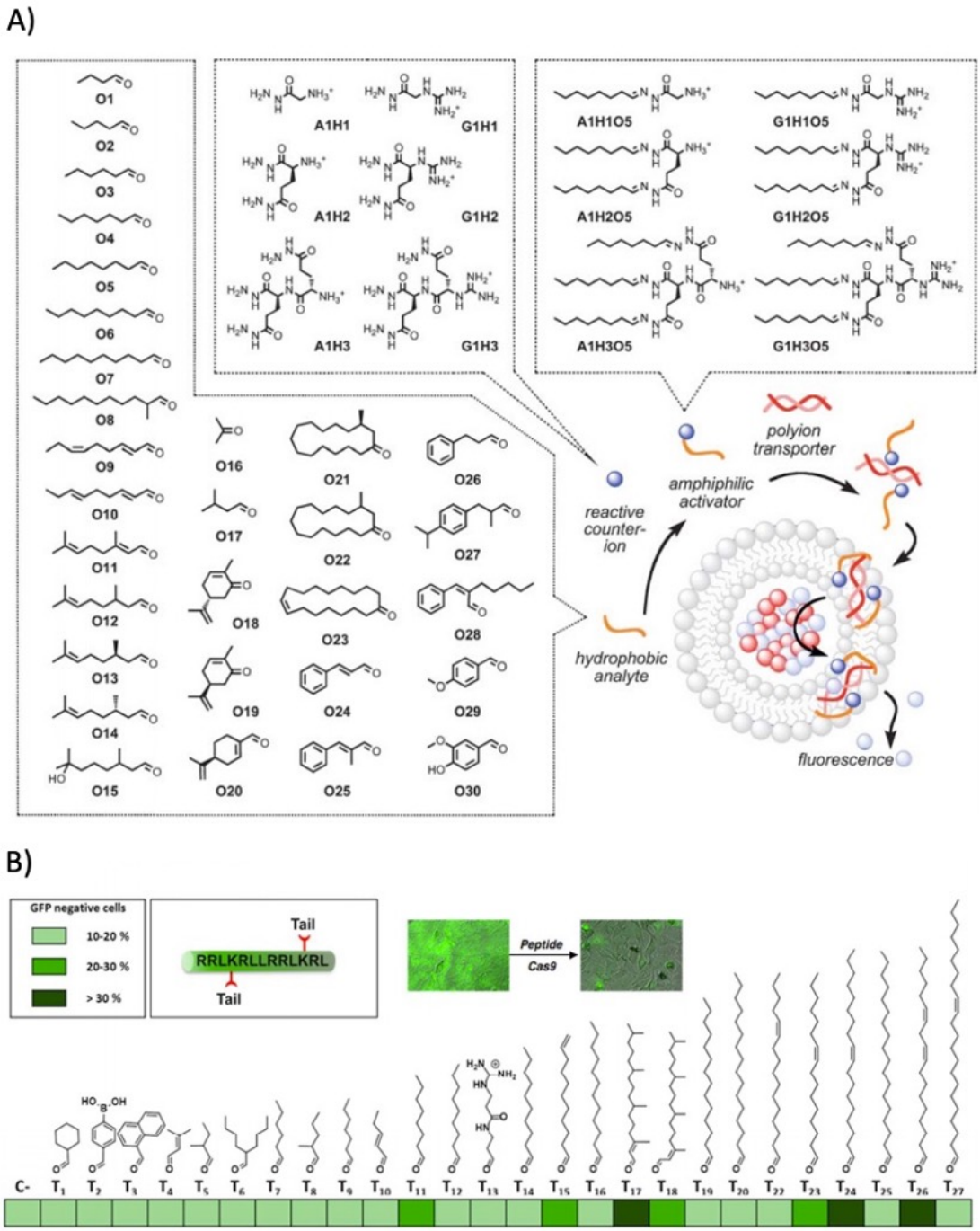

Figure 7. A) Small amphiphiles for DNA trasport in LUVs. Reproduced with permission from ref[126]. Copyright (2011) Royal Society of Chemistry. B) Lipopeptide for Cas9 delivery. Reproduced with permission from ref[78].Copyright (2017) Royal Society of Chemistry.

USC
UNIVERSIDADE
DE SANTIAGO
DE COMPOSTELA

2. Objectives

USC UNIVERSIDADE DE SANTIAGO DE COMPOSTELA

USC
UNIVERSIDADE
DE SANTIAGO
DE COMPOSTELA

The possibility to make peptide libraries through "clickable" reactions without further purification steps has critical importance.[77,78] Peptides have structural characteristics such as conformation of secondary structure, grade of hydrophobicity, hydrophilicity, amphiphilicity and net charge. The organization of these structural variables allows us to associate them with other properties of peptides like solubility, cell penetration capacity or toxicity and thus improve peptide designs to obtain particular capabilities (Figure 8). Dynamic bonds constitute an excellent synthetic methodology to modify and study different cell penetrating peptides.[102,]**¡Error! Marcador no definido.**

The principal objectives on this first chapter are:

1. The design of an amphipathic peptide structure, which would contain arginines, leucines and alanines to promote α-helical structures and assist cell uptake. The sequence will additionally incorporate two lysine residues, which will be functionalized with alkoxyamine reactive moieties. The selective lysine modification will be achieved by orthogonal protecting groups in solid phase peptide synthesis (SPPS).

2. Explore the reactivity of the peptide containing the reactive alkoxyamines with aldehyde tails to obtain, without further purification, a small library of oxime-modulated peptides.

3. Study the new peptides, after the reaction with aldehyde pendants, for the transport of biopolymers in artificial vesicles assays.

4. Study the transport properties in cellular assays. A fluorescent probe will be incorporated into the peptide structure in order to track the peptide in the intracellular space by microscopy.

5. Quantify the internalization and the cytotoxicity of all structures derived from the initial parent peptide and correlate the structure of the aldehyde pendants with these functional properties.

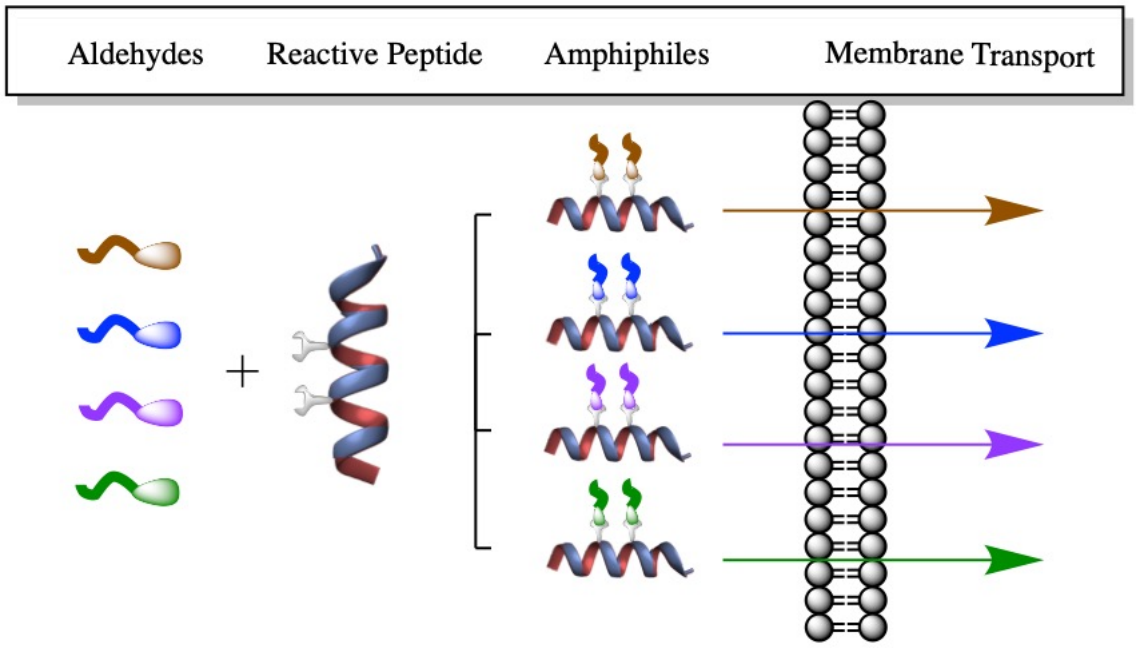

Figure 8. Scheme of reaction between aldehydes and the reactive helical peptide for membrane penetration.

USC
UNIVERSIDADE
DE SANTIAGO
DE COMPOSTELA

3. Results: Tuning the Properties of Penetrating Peptides by Oxime Conjugation

*The results of this chapter were originally published published as a contribution to the 8th EuCheMs Organic Division Young Investigators Workshop special issue in Synlett as:

M. Pazo, H. Fernández-Caro, J. M. Priegue, I. Lostalé-Seijo, and J. Montenegro, "Tuning the Properties of Penetrating Peptides by Oxime Conjugation" *Synlett*, **28**, 08, 924–928, Jan. 2017, doi: 10.1055/s-0036-1588689
https://www.thieme-connect.de/products/ejournals/pdf/10.1055/s-0036-1588689.pdf
Synlett 2017 Impact factor 2.369, Quartile 2 in Organic Chemistry

Affiliations:

Singular Research Centre in Chemical Biology and Molecular Materials, (CIQUS), Organic Chemistry Department, University of Santiago de Compostela (USC), Santiago de Compostela, Spain.

Email: javier.montenegro@usc.es

Copyrights:

This article was published with Thieme under a Gold Open Acccess license. Copyright © 2017, Rights Managed by Georg Thieme Verlag KG Stuttgart • New York. This article may be used for non-commercial purposes in accordance with Georg Thieme Verlag KG Terms and Conditions for self-archiving

Contributions:

Synthesis and characterization of the compounds and vesicle experiments.

USC
UNIVERSIDADE
DE SANTIAGO
DE COMPOSTELA

4. Conclusions

USC
UNIVERSIDADE
DE SANTIAGO
DE COMPOSTELA

USC
UNIVERSIDADE
DE SANTIAGO
DE COMPOSTELA

In this chapter, we have prepared a small peptide library using a "clikable" reaction that modulate the behavior of a parent peptide **AcP(Ox)$_2$**. Moreover, the importance of peptide hydrophilicity/hydrophobicity balance for cell uptake and cytotoxicity has been also studied.

1. An amphipathic peptide was designed and synthesized to give rise to a helical conformation, which segregates the hydrophobic and the hydrophilic domains.

2. The structure includes two reactive alkoxyamine functionalities located at the interphase of both domains, which could be incorporated during the solid phase peptide synthesis (SPPS) using orthogonal protecting groups.

3. The acetylated peptide with free alkoxyamines was purified by HPLC and was sufficiently stable for spectroscopic characterization. The circular dichroism (CD) spectra showed certain helical folding of the peptide that was enhanced in the presence of TFE and weaker in aqueous media.

4. The transport evaluation in vesicle assays confirmed that both the parent peptide and every generated amphiphile do not induce efflux of the fluorogenic content until DNA was added. This indicates that the observed DPX efflux was triggered by the exclusive action of the DNA counterion.

5. The parent peptide **AcP(Ox)$_2$** did not show activity, as well as the peptide with a hydrophobic isovaleraldehyde tail. Good transport activity was identified for the cationic tail **T$_{Gua}$**.

6. The parent peptide was labelled with a carboxyfluorescein probe. This peptide with free alkoxyamines was not fully stable over time, and it was necessary to trap the alkoxyamines with the corresponding aldehydes immediately after peptide cleavage.

7. Fluorophore conjugated peptides with three different aldehydes internalized into cells with higher efficiency than the octaarginine labelled with carboxyfluorescein **R8** control. The corresponding micrographs showed a cytosolic distribution pattern for **CFP(T$_{Gua}$)$_2$** and **CFP(T$_{Aceto}$)$_2$** and a punctate pattern for **CFP($_{Gly}$)$_2$**.

8. The punctate distribution pointed to an endosomal entrapment. A dose response concentration internalization experiment in cells was carried out to evaluate the importance of the concentration. At lower concentration we could avoid the saturation of cytosolic fluorescence. At this concentration, 2μM, the punctate internalization pattern was revealed for **CFP (T$_{Gua}$)$_2$** but not for **CFP (T$_{Aceto}$)$_2$**.

9. A punctate pattern colocalized with lysotracker indicated the potential endosomal peptide distribution. It was demonstrated the uptake by endosomal internalization for every structure with the exception of the **CFP(T$_{Aceto}$)$_2$**, which possess a strong hydrophobic character.

10. A good viability was found for all cases, except in the case of **CFP(T$_{Aceto}$)$_2$**, the peptide with acetone tails, which presented a cytotoxic character. The hydrophobicity of this compound could imply a greater interaction with membranes that is related to the disruptive character indicated above.

11. This strategy confirmed the applicability of the oxime bond to prepare a library of amphiphilic peptides and to evaluate hydrophobic/hydrophilic ratios.

12. For this peptide, an optimal ratio of 5/5 cationic/hydrophobic character was found, which increased the cell internalization while mantaining good cell viability.

USC
UNIVERSIDADE
DE SANTIAGO
DE COMPOSTELA

CHAPTER 2: PEPTIDE DESIGN FOR HELICAL CONTROL

USC
UNIVERSIDADE
DE SANTIAGO
DE COMPOSTELA

1. Introduction

USC
UNIVERSIDADE
DE SANTIAGO
DE COMPOSTELA

USC
UNIVERSIDADE
DE SANTIAGO
DE COMPOSTELA

1.1 Peptide design for membrane perturbation

Since Merrifield developed solid phase synthesis,[130] the design and synthesis of new artificial peptide sequences has become a routine method for chemists. However, careful planning of the synthetic strategy is critical to obtain peptide sequences with specific folding capabilities such as peptides that self-assemble into supramolecular structures. This thesis' chapter is focused on the biological applications of peptide designs with folding control and cell penetrating properties.

As mentioned in the previous chapter, CPPs can be classified according to their nature, as natural sequences, modifications of the wildtype sequences or chimeras or artificial peptides. Modifications of wildtypes are perfect examples of peptide engineering because they allow for improvements in the functional properties of the original sequences. For instance, modifications to get sensitivity to changes in pH, lipid environment or membrane potential. Many changes are directed to the responsiveness to pH changes and to switch from a toxic to a non-toxic behavior. This is the case for melittin[131] (bee venom) and the corresponding artificial analogue, MelP5,[132] which is more hydrophobic and less charged, but that retains pore-forming capacity.[114] This derivative opened the possibilities of redesigning melittin peptide in order to regulate membrane activity upon external stimuli such as pH.[133,134,135]

Inspired by these variations, other authors have proposed artificial substitutions in peptides derived from poisons or toxins. Prof. Futaki proposed in 2017 a CPP derived from a M-Lycotoxin (spider venom) that was capable of releasing proteins and antibodies into the intracellular space.[136] The modification consisted of the incorporation of glutamic acids in the hydrophobic part of an amphiphilic helical peptide. Glutamic acid (Glu) is protonated at acidic pH, which will change net charge of the molecule from anionic to neutral. Prof. Futaki and coworkers also discovered a preference pattern for including Glu residues in α-helixes. The best CPPs sequences had Glu following the i, i+4 positions at the interface between hydrophobic and hydrophilic sides of the helix (Figure 9). The Glu substitution pattern for improved membrane penetration with a reduction of toxicity was confirmed by its application to hemolytic peptides, melittin and ponericin-W3.[137]

In the case of chimeric peptides, a multitude of variants have emerged. These peptides include fragments of other natural or known sequences. One important example of chimeric peptide is transportan, which is a chimera between mastoparan peptide and a fragment of human neuropeptide galanine. Other chimera sequences such as MPG or Pep-1 also contain nuclear localization sequences (NLS) to help the carrier delivery its cargo.[138]

Completely artificial sequences with several designs have also been prepared and characterized as cell penetrating peptides.[139] As we discussed in the history of CPPs, the first sequences were derived from viral proteins that are enriched in cationic residues. However,

[130] R. B. Merrifield, *Science* **1965**, *150*, 178–185.
[131] A. J. Krauson, J. He, W. C. Wimley, *J. Am. Chem. Soc.* **2012**, *134*, 12732–12741.
[132] G. Wiedman, T. Fuselier, J. He, P. C. Searson, K. Hristova, W. C. Wimley, *J. Am. Chem. Soc.* **2014**, *136*, 4724–4731.
[114] A. Fennouri, S. Finn, T. B. H. Schroeder, M. Mayer, *BBA - Biomembr.* **2017**, *1859*, 2051–2057.
[133] G. Wiedman, W. C. Wimley, K. Hristova, *Biochim. Biophys. Acta - Biomembr.* **2015**, *1848*, 951–957.
[134] S. Li, S. Y. Kim, A. E. Pittman, G. M. King, W. C. Wimley, K. Hristova, *J. Am. Chem. Soc.* **2018**, *140*, 6441–6447.
[135] S. Y. Kim, A. E. Pittman, E. Zapata-Mercado, G. M. King, W. C. Wimley, K. Hristova, *J. Am. Chem. Soc.* **2019**, *141*, 6706–6718.
[136] M. Akishiba, T. Takeuchi, Y. Kawaguchi, K. Sakamoto, H. Yu, I. Nakase, T. Takatani-Nakase, F. Madani, A. Gräslund, S. Futaki, *Nat. Chem.* **2017**, *9*, 751–761.
[137] N. Tamemoto, M. Akishiba, K. Sakamoto, K. Kawano, H. Noguchi, S. Futaki, *Mol. Pharm.* **2020**, *17*, 2175–2185.
[138] Ü. Langel, *CPP, Cell-Penetrating Peptides*, Springer Singapore, Singapore, **2019**.
[139] D. M. Copolovici, K. Langel, E. Eriste, Ü. Langel, *ACS Nano* **2014**, *8*, 1972–1994.

hydrophobicity is a key parameter to consider in the design of artificial peptides, because the disposition of the residues can control the interaction with the membranes. Precisely, two aromatic amino acids were identified in different penetrating peptides as responsible of endosomolytic behavior such as tryptophan and phenylalanine.[140] These two amino acids bury and destabilize the lipid bilayer.[141,142] Other amino acids such as leucine increase cellular uptake and enter the cytoplasm directly across the plasma membrane.[143,144] The combination of these two factors (cationic and hydrophobic residues) affords amphipathic sequences, which have also proved their penetration potential.[145] These amphipathic structures can be originated from a secondary structure like the α-helix, where the hydrophobic and hydrophilic parts are segregated in space (Figure 9).

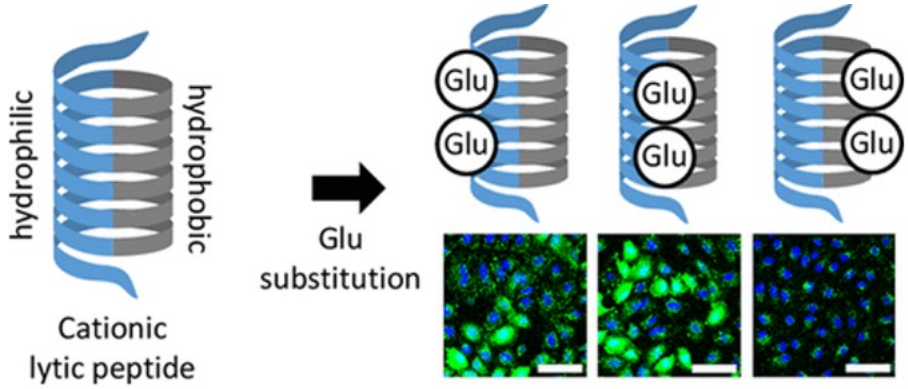

Figure 9. Representation of an amphipathic helical peptide the positions for glutamic acid substitutions to improve the cell penetrating properties. Microscope images show the delivery of dextran (green) by these peptide variants. Reproduced with permission from ref[137]. Copyright (2020) American Chemical Society.

1.1.1 Stabilization of peptide helical structures

Peptides adopt different secondary conformations and tridimensional arrangements, the α-helix and the β-strand are the most commons. Alpha helix has a hydrogen bonding pattern (i, i+4) between the oxygen of a carbonyl with the preceding fourth hydrogen of the amide (Figure 10).

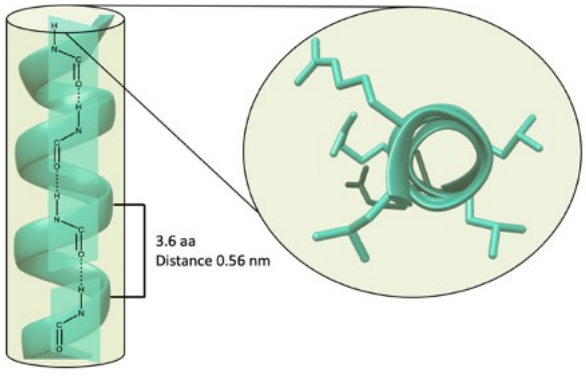

Figure 10. Lateral view of a helical peptide (left) and zenital view (right).

[140] P. Lönn, A. D. Kacsinta, X. S. Cui, A. S. Hamil, M. Kaulich, K. Gogoi, S. F. Dowdy, *Sci. Rep.* **2016**, *6*, 32301.
[141] L. Chen, L. Gan, M. Liu, R. Fan, Z. Xu, Z. Hao, L. Chen, *Appl. Surf. Sci.* **2011**, *257*, 5070–5076.
[142] A. V. Popova, A. G. Heyer, D. K. Hincha, *Biochim. Biophys. Acta - Biomembr.* **2002**, *1561*, 109–118.
[143] T. Fuselier, W. C. Wimley, *Biophys. J.* **2017**, *113*, 835–846.
[144] S. Schmidt, M. J. W. Adjobo-Hermans, R. Kohze, T. Enderle, R. Brock, F. Milletti, *Bioconjug. Chem.* **2017**, *28*, 382–389.
[145] P. M. Fischer, *Med. Res. Rev.* **2007**, *27*, 755–795.

The *de novo* design of helical peptides in aqueous conditions can be challenging because water competes for the hydrogen bonds. Therefore, to design new biocompatible helical peptides it is necessary to take into account the energetic contributions of each amino acid to the stabilization of the helix in the aqueous media. There are amino acids with a strong tendency to form helical structures and the highest propensity is found for Ala (Figure 11), followed by long side chain residues (Arg, Leu, Lys, Gln, Glu, Met). The rest of the amino acids have a lower helical propensity, while Gly or Pro have the lowest.[146,147] The great stabilizing character of Ala is due to the hydrophobic interaction between the carbon (lateral chain) of residue i and the β carbon of residue i+3 (with a 0.77 kcal·mol-1 enthalpic contribution) (Figure 11A).[148,149]

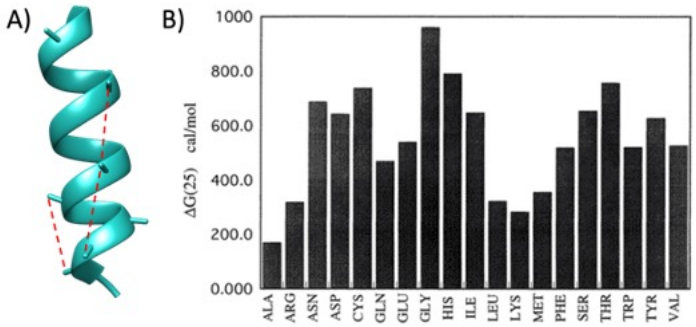

Figure 11. A) Alanine interactions involved in helical stabilization. B) Helix propensities of 19 amino acids depending on their ΔG at 25 °C. Reproduced with permission from ref[148]. Copyright (1996) American Chemical Society.

Each peptide sequence has their own contributions, for instance, Prof. Baldwin demonstrated the helical destabilization of oligoalanines with more than three lysine.[150] However, the alpha helix can also be stabilized by taking advantage of lateral interactions of side chains such as the ion pairing stablished between cationic and anionic residues.[150] Other lateral interactions that stabilize helical structures are peptide staples,[151] which have been obtained by covalent bonds or metal coordination[152,153] stabilized between two lateral side chains of amino acids of the sequence (Figure 12).

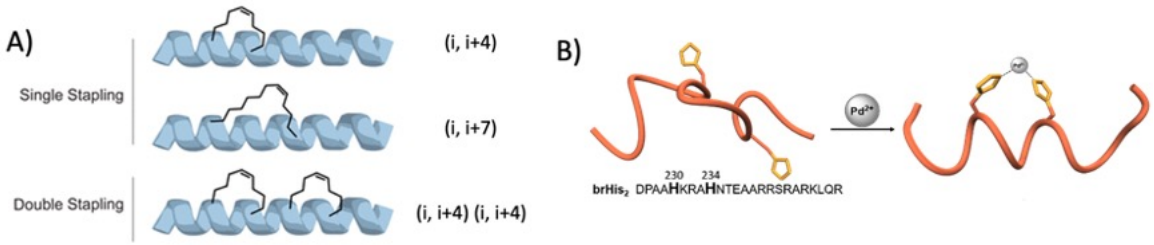

Figure 12. A) Patterns to form stapled peptides. Adapted with permission from ref[151]. Copyright (2014) American Chemical Society B) Metal stapling by Pd^{2+} histidine coordination. Adapted with permission from ref[152]. Copyright (2020) John Wiley and Sons.

[146] A. Chakrabartty, R. L. Baldwin, *Adv. Protein Chem.* **1995**, *46*, 141–176.
[147] A. Chakrabartty, T. Kortemme, R. L. Baldwin, *Protein Sci.* **1994**, *3*, 843–852.
[148] I. Luque, O. L. Mayorga, E. Freire, *Biochemistry* **1996**, *35*, 13681–13688.
[149] J. López-Llano, L. A. Campos, J. Sancho, *Proteins Struct. Funct. Bioinforma.* **2006**, *64*, 769–778.
[150] S. Marqusee, V. H. Robbins, R. L. Baldwin, *Proc. Natl. Acad. Sci. U. S. A.* **1989**, *86*, 5286–5290.
[151] L. D. Walensky, G. H. Bird, *J. Med. Chem.* **2014**, *57*, 6275–6288.
[152] S. Learte-Aymamí, C. Vidal, A. Gutiérrez-González, J. L. Mascareñas, *Angew. Chemie Int. Ed.* **2020**, *59*, 9149–9154.
[153] S. J. Smith, K. Du, R. J. Radford, F. A. Tezcan, *Chem. Sci.* **2013**, *4*, 3740–3747.

Prof. Dowdy developed Tat analogues that were optimized to enhance alpha-helical content and to identify the optimum disposition of the arginine residues. The best model included glutamine, tyrosine, three aligned arginines as the cationic part and alanines as hydrophobic residues. This Tat analogue also showed the best transduction activity and opened the design for *de novo* synthetic oligoalanines peptides.[76] Another notable example of the design and synthesis of an amphiphilic peptide is the GALA peptide. GALA is a synthetic peptide with 30 aa and the ability to switch from a random coil at neutral pH to a helical conformation by partial protonation of glutamic acids. Furthermore, in this helical conformation the GALA peptide has increased affinity for lipid membranes, mimicking viral fusion proteins.[154,155] Our research group has also developed *de novo* amphipathic helical peptides that segregate two surfaces and incorporate a reactive moiety to include lateral chains either hydrophilic[79,129] or hydrophobic[77,78] (Figure 13).

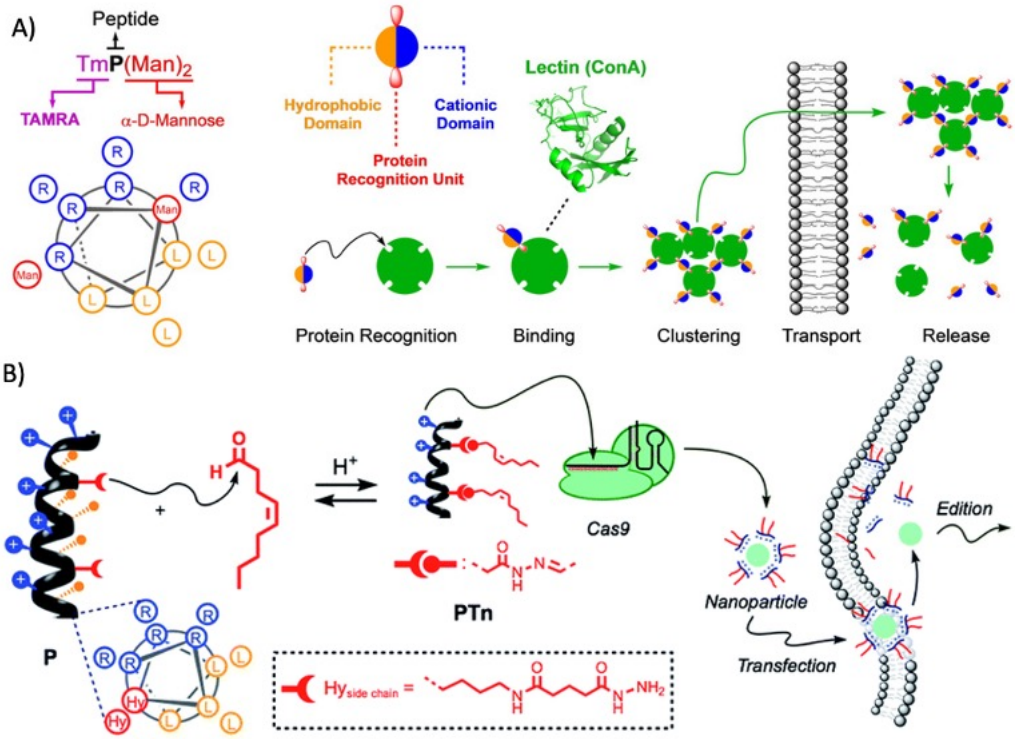

Figure 13. A) Glycan conjugation with reactive peptide for specifical Concanavalin A protein transport. Reproduced with permission from ref[79]. Copyright (2018) John Wiley and Sons. B) Aliphatic aldehyde conjugation with reactive hydrazide peptide for Cas9 complex and cytosolic delivery. Reproduced with permission from ref[78]. Copyright (2017) The Royal Society of Chemistry.

[76] A. Ho, S. R. Schwarze, S. J. Mermelstein, G. Waksman, S. F. Dowdy, *Cancer Res.* **2001**, *61*, 474–7.
[154] N. K. Subbarao, R. A. Parente, F. C. Szoka, L. Nadasdi, K. Pongracz, *Biochemistry* **1987**, *26*, 2964–2972.
[155] W. Li, *Adv. Drug Deliv. Rev.* **2004**, *56*, 967–985.
[79] M. Juanes, I. Lostalé-Seijo, J. R. Granja, J. Montenegro, *Chem. - A Eur. J.* **2018**, *24*, 10689–10698.
[129] I. Gallego, A. Rioboo, J. J. Reina, B. Díaz, Á. Canales, F. J. Cañada, J. Guerra-Varela, L. Sánchez, J. Montenegro, *ChemBioChem* **2019**, *20*, 1400–1409.
[77] I. Louzao, R. García-Fandiño, J. Montenegro, *J. Mater. Chem. B* **2017**, *5*, 4426–4434.
[78] I. Lostalé-Seijo, I. Louzao, M. Juanes, J. Montenegro, *Chem. Sci.* **2017**, *8*, 7923–7931.

1.1.2 Circular dichroism of peptides

Circular dichroism (CD) is a chiroptical method that provides information of the three-dimensional conformation of peptides and proteins. Circular dichroism is defined as the difference between the absorption of left-handed (A_L) and right-handed (A_R) circularly polarized light after passing through an asymmetric sample.[156] CD is a useful tool to classify peptides in the three most common secondary structure, i.e., α-helix, β-strand, and random coil, and also for the detection of some tertiary structures, such as coiled coil..[157] The chromophore in the skeleton of a peptide is the amide group (240 nm and below) and the asymmetry comes from Ψ (psi) and ϕ (phi) angles, which define the folded structure of a peptide (Figure 14A). In α-helixes, a weak but broad $n \rightarrow \pi^*$ electron transition appear around 220 nm and a more intense $\pi \rightarrow \pi^*$ electron transition around 190 nm. The characteristic bands of helical structures are two negative minimums at 222 nm and 208 nm and one positive maximum at 190 nm.[157,158] The band at 208 nm is a weak negative contribution of transition $n \rightarrow \pi^*$ (Figure 14B).[159,160]

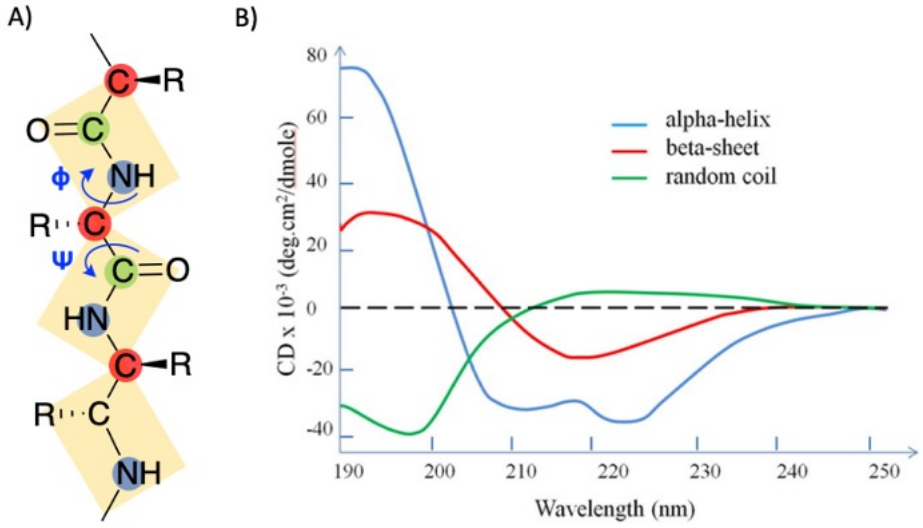

Figure 14. A) Ψ and ϕ angles in a peptide sequence. B) CD spectra of each of the three basic secondary structures of peptides (α-helix, β-sheet and random coil) Reproduced with permission from ref[161] Copyright (2014) Elsevier.

There are solvents that promote the helical folding such as trifluoroethanol (TFE), which does not compete for hydrogen bonding and thereby enhances single helix stability.[159,160] On the other hand, the ellipticity obtained from these measurements can be transformed into average molar ellipticity of the residues by applying Equation E3, which is an adaptation of Beer-Lambert law. [162] Moreover, it is widely accepted that molar ellipticity at 222 nm and 208 nm is proportional to the helical content in a peptide. For that reason, an equation taking that

[156] N. J. Greenfield, *Nat. Protoc.* **2006**, *1*, 2527–2535.
[157] S. M. Kelly, T. J. Jess, N. C. Price, *Biochim. Biophys. Acta - Proteins Proteomics* **2005**, *1751*, 119–139.
[158] R. W. Woody, *Monatshefte fur Chemie* **2005**, *136*, 347–366.
[159] N. E. Zhou, C. M. Kay, R. S. Hodges, *J. Biol. Chem.* **1992**, *267*, 2664–2670.
[160] T. M. Cooper, R. W. Woody, *Biopolymers* **1990**, *30*, 657–676.
[161] Y. Wei, A. A. Thyparambil, R. A. Latour, *Biochim. Biophys. Acta - Proteins Proteomics* **2014**, *1844*, 2331–2337.
[162] D. Corrêa, C. Henrique, I. Ramos, D. H. A. Corrêa, C. H. I. Ramos, *African J. Biochem. Res.* **2009**, *3*, 164–173.

value at 222 nm[163] or 208 nm[164] allows the calculation of the percentage of α-helix in a particular peptide sequence (Equation E4A and E4B).

$$[\Theta]_{MRt} = \frac{0.1 \text{ x } \Theta}{C \cdot l \cdot \text{number of residues}} \quad (\text{deg} \cdot \text{cm}^2 \cdot \text{dmol}^{-1}) \qquad \text{(E3)}$$

Equation E3. Formula to calculate the molar ellipticity. Θ is the ellipticity (mdeg), C is the peptide concentration (M) and l is the cell path length (cm).

$$[\Theta]\% = \frac{|\Theta MRt_{222}| - 2340}{30300} \text{ x } 100 \qquad \text{(E4A)}$$

$$[\Theta]\% = \frac{|\Theta MRt_{208}| - 4000}{33000-4000} \text{ x } 100 \qquad \text{(E4B)}$$

Equation E4A and E4B. Formula to calculate the percent of helicity in which the molar ellipticity at 222 nm (E4A) or 208 nm (E4B) is an absolute value.

1.2 Peptide interactions for Cell internalization

1.2.1 Peptide self-assembly in membranes

Peptide-membrane interactions are fundamental in cell as about 20-30% of genes encode transmembrane proteins.[165] Many of these proteins are channels that regulate the influx of different molecules, such as aquaporins[166] or sodium-potassium pumps.[167] Transmembrane proteins are composed by membrane spanning domain or transmembrane domain (TMD) that usually appear in the form of an α-helix.[168] Additionally, integral membrane proteins may have "soluble" domains on the surface regions.[169] Considering the peptide sequences of transmembrane domains, peptide channels and other peptides with membrane affinity, some amino acids have been found to show a preferential orientation in the membrane. For example, Trp often appears near the membrane interface close to the lipid carbonyls as in gramicidin. Arg and Lys have a hydrophobic backbone, which can "snorkel" inside the apolar part of membranes from the polar surface (phosphate groups).[170] Hydrophobic residues like Phe, Leu, Ile, Val residues have same probability to face lipids or protein surfaces, whereas Ala has a clear preference for the interior of α-helical membrane proteins (Figure 15).[171]

[163] Y.-H. Chen, J. T. Yang, *Biochem. Biophys. Res. Commun.* **1971**, *44*, 1285–1291.
[164] N. Greenfield, G. D. Fasman, *Biochemistry* **1969**, *8*, 4108–4116.
[165] M. S. Almén, K. J. V. Nordström, R. Fredriksson, H. B. Schiöth, *BMC Biol.* **2009**, *7*, 50.
[166] P. Agre, *Angew. Chemie Int. Ed.* **2004**, *43*, 4278–4290.
[167] J. C. Skou, *BBA - Biochim. Biophys. Acta* **1957**, *23*, 394–401.
[168] H. J. Sharpe, T. J. Stevens, S. Munro, *Cell* **2010**, *142*, 158–169.
[169] R. R. W. Wayne Albers, in *Basic Neurochem.*, Elsevier, **2012**, pp. 26–39.
[170] J. A. Killian, G. Von Heijne, *Trends Biochem. Sci.* **2000**, *25*, 429–434.
[171] M. B. Ulmschneider, M. S. P. Sansom, *Biochim. Biophys. Acta - Biomembr.* **2001**, *1512*, 1–14.

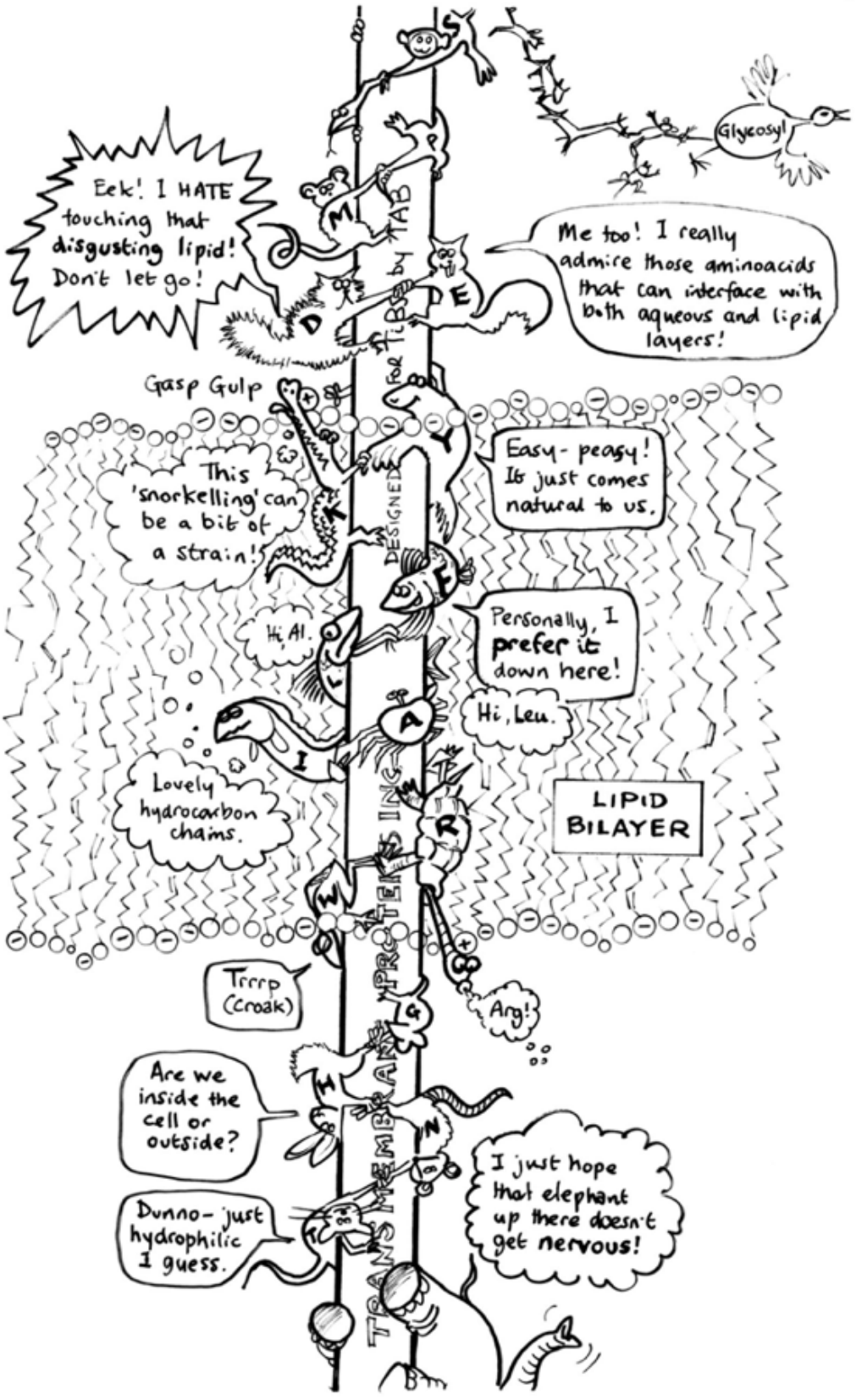

Figure 15. Illustration of the preferred amino acid localization in a transmembrane protein. Reproduced with permission from ref[170] copyright (2000) Elsevier.

Synthetic modifications in cell-penetrating peptides should increase the interaction with lipids and thus, facilitate transport. However, if a cell-penetrating peptide has a too strong affinity with the plasma membrane the uptake might be hindered.[139] Some of the examples that enhance membrane interaction by hydrophobic modifications are MelP5 (melittin modification), or pHD108 (MelP5 modification). Specifically, these structures include more acidic residues and hydrophobic residues, to enhance the response to acidic pH (i.e. by hydrophobicity enhanced by acid protonation), increasing the helical character and maximizing transport (i.e., as detected by leakage measurements in artificial membrane systems such as LUVs).[134,135] The same strategy of glutamic acids incorporation was also shown in L17E, despite that in this case the mutation was translated in transport activity (leakage in LUVs) at acidic pH and anionic vesicles but not in a enhancement of the helical behavior.[136]

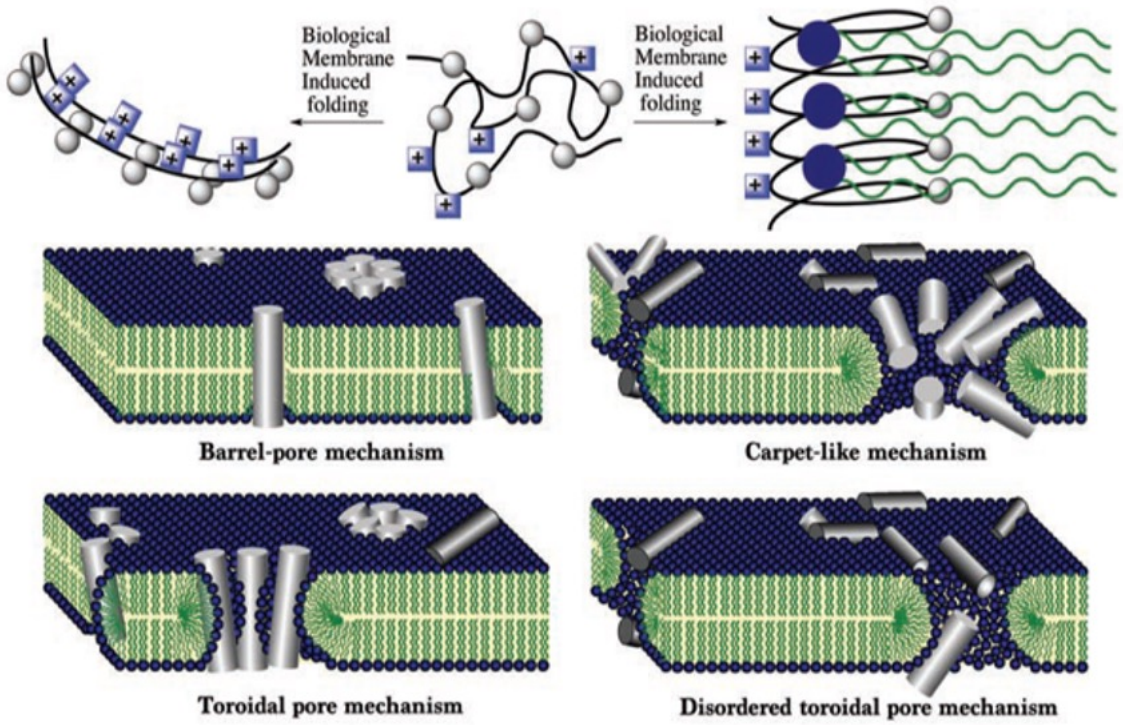

Figure 16. Mechanisms for membrane insertion of peptides. Reproduced with permission from ref[172] copyright (2015) EUREKA SCIENCE (FZC).

The interaction of peptides with the membrane can lead to the assembly of ordered supramolecular structures such as channels or dynamic transient pores. The mechanism of supramolecular self-assembly of peptides to form pores in membranes has been studied in depth, especially in the case of antimicrobial peptides, since they exert their activity on bacterial membranes. However, the conclusions of these antimicrobial peptides can be extended to different peptide assemblies in membranes such as CPPs. The proposed mechanisms are based on three elemental prototypes: the barrel pore, the carpet-like, and the toroidal mechanism (Figure 16). In the barrel-stave, peptides are transmembrane oriented, while in carpet-like mechanism peptides are positioned parallel in the membrane. In the toroidal mechanism, peptides are associated with the polar head of lipids oriented towards the inner side of the membranes. Finally, the disordered toroidal pore mechanism is an intermediate between barrel-stave and carpet-like models. Physical damage of peptides to membranes includes pore

formation, thinning, curvature alteration, electrostatic modification and localized perturbations. Furthermore, regardless of the supramolecular assembly mechanism, there is a concentration threshold above which membrane disruption occurs.[172,173,174]

1.2.2 Cellular uptake of CPPs

The mechanism of uptake of CPPs into cells has been a subject of controversy, as several options have been postulated. However, all of them share the same principle, namely the initial interaction of the cationic CPPs with the anionic part of the membrane,[145,64] as biological membranes can be enriched with negatively charged constituents such as lipids, glycans and proteins. The membrane potential (~ -70 mV in a resting cell with cytoplasmic-side negative[175]) works as the driving force for movements of positively charged species into cells (Figure 17A).[67] The point of agreement on the importance of electrostatic interaction with the membrane, is due to the fact that the most abundant CPPs are cationic or contain a cationic part. For this reason, we will discuss the importance of these cationic residues and their role in internalization. Afterwards, we will continue with a description of the most common mechanisms of internalization.

CPPs with an excess of cationic charges in close proximity exhibit strong electrostatic repulsion. To minimize this effect, lysine residues can be deprotonated, as its pK_a~10.2 can be reduced at physiological pH (7.4). However, the higher pk_a ~12.5 of the guanidinium of the arginine amino acid does not allow charge repulsion minimization by deprotonation (Figure 17B). Instead, nearby arginines minimize intramolecular charged repulsion by counterion scavenging.[60,176] The complexation of counterions is due to the ability of protonated guanidiniums to establish bidentate hydrogen bonds with lipid phosphates and other negatively charged membrane components[67] (Figure 17C). Therefore, guanidium-rich polymers are hydrophilic or lipophilic depending on their counterion.[60] Consequently, arginines show a higher uptake level compared to other basic amino acids such as lysine or histidine.[47]

[172] N. Rodriguez-Vazquez, H. Ozores, A. Guerra, E. Gonzalez-Freire, A. Fuertes, M. Panciera, J. Priegue, J. Outeiral, J. Montenegro, R. Garcia-Fandino, et al., *Curr. Top. Med. Chem.* **2015**, *14*, 2647–2661.
[173] A. Giuliani, G. Pirri, A. Bozzi, A. Di Giulio, M. Aschi, A. C. Rinaldi, *Cell. Mol. Life Sci.* **2008**, *65*, 2450–2460.
[174] E. Böhmová, D. Machová, M. Pechar, R. Pola, K. Venclíková, O. Janoušková, T. Etrych, *Physiol. Res* **2018**, *67*, 267–279.
[64] E. Koren, V. P. Torchilin, *Trends Mol. Med.* **2012**, *18*, 385–393.
[175] X. P. Dong, X. Wang, H. Xu, *J. Neurochem.* **2010**, *113*, 313–328.
[67] P. A. Wender, W. C. Galliher, E. A. Goun, L. R. Jones, T. H. Pillow, *Adv. Drug Deliv. Rev.* **2008**, *60*, 452–472.
[176] M. Nishihara, F. Perret, T. Takeuchi, S. Futaki, A. N. Lazar, A. W. Coleman, N. Sakai, S. Matile, *Org. Biomol. Chem.* **2005**, *3*, 1659–1669.
[60] N. Sakai, S. Matile, *J. Am. Chem. Soc.* **2003**, *125*, 14348–14356.
[47] A. El-Sayed, I. A. Khalil, K. Kogure, S. Futaki, H. Harashima, *J. Biol. Chem.* **2008**, *283*, 23450–23461.

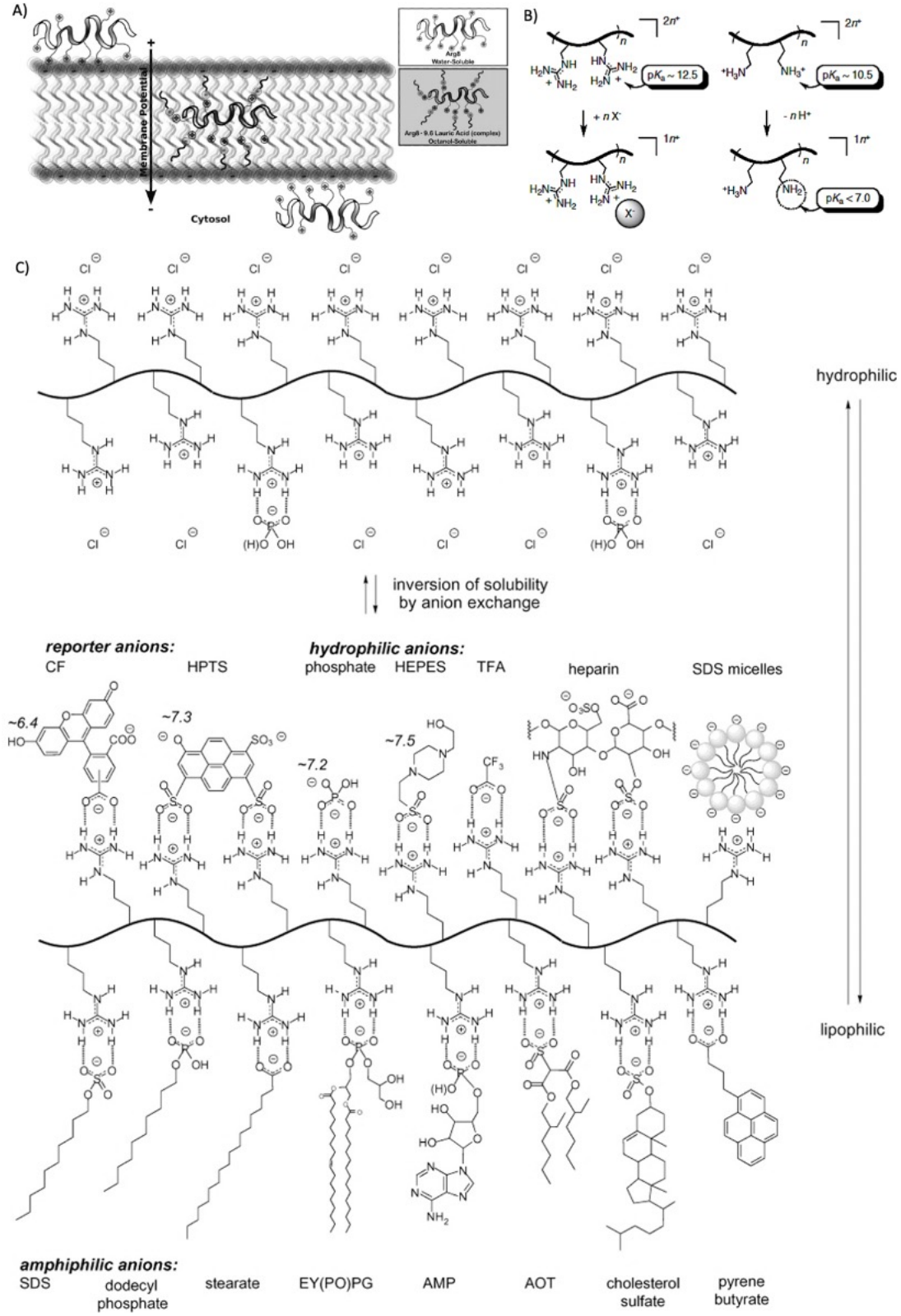

Figure 17. A) Interaction and membrane penetration of oligoaarginines. Reproduced with permission from ref[67] copyright (2008) Elsevier. B) pKa of arginines and lysines. Reproduced with permission from ref[176] copyright (2005) Royal society of chemistry. C) Guanidium interactions with counterions. Reproduced with permission from ref[60] copyright (2003) American Chemical Society.

The original hypothesis of CPPs uptake was based on direct penetration through the lipid bilayer. As we have discussed, highly cationic peptides are electrostatically attracted to the membrane due to the anionic charge of anionic components such as glucosaminoglycan (GAG) proteoglycans.[55] Peptide-membrane interactions, such as GAG clustering, can lead to GTPase activation and actin network remodeling. Next, modifications in membrane fluidity and reorganization of the lipids trigger the transbilayer exchange (i.e., flip-flop). The result is translated into lipid density fluctuation, disruptions by pores or inverted micelles (Figure 18-i-ii).[177]

Further investigations demonstrated that endocytic uptake was also present. Energy-dependent internalization mechanisms begin when a concentration threshold is exceeded, which is unique for each CPP or CPP-cargo complex (Figure 18-iii). For example, a macropinocytosis mechanism was reported for peptides such as R8 or Tat. However, there are other internalization routes like caveolin-dependent as well as clathrin dependent internalization for other peptides.[55] The endocytic pathway often depends not only on the peptide, but also on the concentration, cell type and the peptide-cargo complex. Furthermore, the mechanism may also vary depending on the type of cargo (DNA, RNA, plasmid, protein, antibody, small drugs, quantum dots).[62] The endosome escape is critical to achieve cytosolic delivery of th cargo (Figure 18-iv-v). However, if this do not happen, peptide and cargo will remain trapped in the endosomes and will be degraded ~1-2 h after the endocytic uptake (Figure 18-vi).[177] However, a different internalization mechanism was also described for poliaarginines called nucleation zones, which is triggered at high concentrations of the peptide. Nucleation zones disrupt plasma membrane and allowed direct internalization.[178]

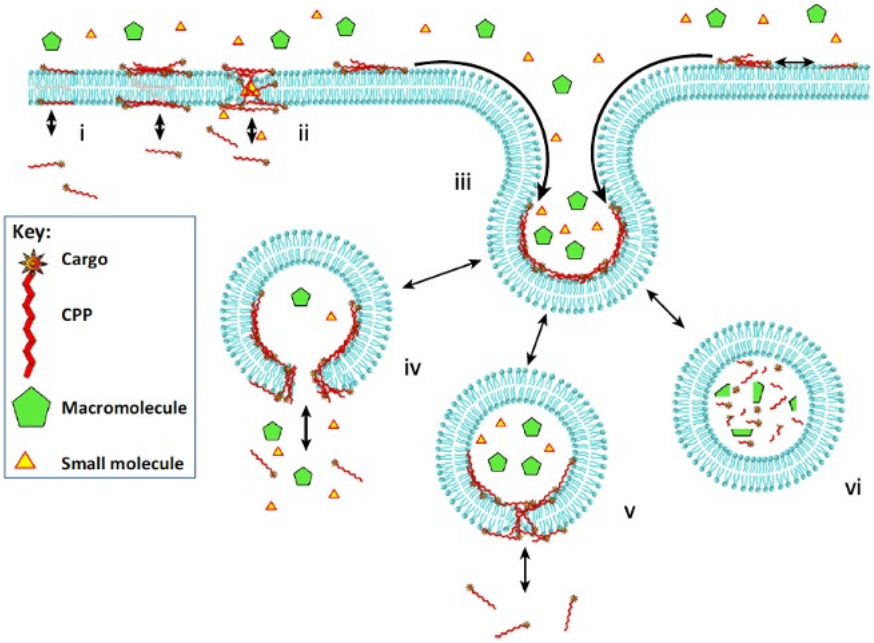

Figure 18. A) Uptake mechanism of CPPs. Reprinted with permission from ref[177] Copyright (2015) Elsevier.

[55] F. Heitz, M. C. Morris, G. Divita, *Br. J. Pharmacol.* **2009**, *157*, 195–206.
[177] W. B. Kauffman, T. Fuselier, J. He, W. C. Wimley, *Trends Biochem. Sci.* **2015**, *40*, 749–764.
[62] K. M. Stewart, K. L. Horton, S. O. Kelley, *Org. Biomol. Chem.* **2008**, *6*, 2242–2255.
[178] S. A. Bode, R. Wallbrecher, R. Brock, J. C. M. van Hest, D. W. P. M. Löwik, *Chem. Commun.* **2013**, *50*, 415–417.

1.2.3 Cell toxicity

The interaction of CPPs with cell membranes can induce perturbations that might provoke irreversible damage and cytotoxicity, which can be related to the amphipathic character of CPPs. It has also been demonstrated that cytotoxicity can be dependent on the type of cargo-peptide complex.[179] The most common assays to measure cytotoxicity are 3-(4,5-dimethylthiazol-2-yl)-2,5-diphenyltetrazolium bromide (MTT) and the propidium iodide (PI) assays. The MTT assay measures the metabolic activity as tetrazolium salts are converted to formazan by activity of the mitochondrial dehydrogenases. The amount of formazan is correlated with cell viability and quantified by absorbance (λ_{abs} = 570 nm). On the other hand, PI is a red nuclear dye not permeable in living cells, which can be used to quantify the number of death cells by fluorescence (λ_{abs} = 535 nm and λ_{em} =617 nm).

1.2.4 Clinical trials with CPPs

Since the discovery of the first sequences of CPPs, numerous peptides have been developed in recent years, some of which have already reached clinical trials.[138] The first CPP to reach a clinical trial was a cyclosporine-polyarginine conjugate (Psorban from Cell Gate Inc.) for the treatment of psoriasis.[180] The drug was able to penetrate the dermis and epidermis of human skin. However, complete functional release was not fast enough, and its development was abandoned after phase II. Revance Therapeutics (USA) is testing a botulinum toxin transdermal delivery system (150kDa) by complexation with two Tat sequences separated by a polylysine (RTP004).[181] KAI Pharmaceuticals developed and evaluated a δ-PKC peptide inhibitor conjugated with Tat (KAI-9803)[182] that prevents damage after acute myocardial infarction and completed the phase II clinical study in 2011. The cationic peptide DPV1047, Vectocell, was linked to a novel prodrug for antitumor activity, the final complex DTS-108 is ended at phase I clinical trials by Diatos and Drais pharmaceuticals in 2016.[183]

[179] S. El-Andaloussi, P. Järver, H. J. Johansson, Ü. Langel, *Biochem. J.* **2007**, *407*, 285–292.
[180] J. B. Rothbard, S. Garlington, Q. Lin, T. Kirschberg, E. Kreider, P. L. McGrane, P. A. Wender, P. A. Khavari, *Nat. Med.* **2000**, *6*, 1253–1257.
[181] J. Lee, P. Kennedy, J. M. Waugh, *Methods Mol. Biol.* **2015**, *1324*, 397–415.
[182] E. Bates, C. Bode, M. Costa, C. M. Gibson, C. Granger, C. Green, K. Grimes, R. Harrington, K. Huber, N. Kleiman, et al., *Circulation* **2008**, *117*, 886–896.
[183] R. Coriat, S. Faivre, O. Mir, C. Dreyer, S. Ropert, M. Bouattour, R. Desjardins, F. Goldwasser, E. Raymond, *Int. J. Nanomedicine* **2016**, *11*, 6207–6216.

2. Objectives

USC
UNIVERSIDADE
DE SANTIAGO
DE COMPOSTELA

Positively charged molecules and macromolecules with a certain degree of hydrophobicity can interact with anionic membranes and be taken up by cells.[¡Error! Marcador no definido.] Cell penetrating peptides are good vectors that translocate the cell membrane and introduce inside cells a wide variety of different cargoes. Membrane disruption is good for releasing cargo, but it can be toxic and therefore methodologies have to be developed that allow us to rationally design CPPs as we proposed in this chapter. We plan to achieve folding control of a peptide scaffold in different environments in order to extract structure/activity relationships about the activity and toxicity of these penetrating peptides (Figure 19).

The specific objectives of this chapter would be:

1. Design and synthesize peptide sequences with an α-helix structural control. For this purpose, an alanine-based peptide scaffold will be used with selected substitutions that include leucine as a stronger hydrophobic moiety and three arginine as cationic residues.

2. Optimize the position of the amino acid residues by permutations of 2-3 leucines and 3 arginines along the peptide backbone to build up a rational library of peptides.

3. Determine and characterize the predominant secondary structure by circular dichroism in different environments such as aqueous buffer and the lipid bilayer.

4. Determine the influence of the amino acid positions to promote folding in the aqueous buffer compared to the lipid environment.

5. Study the penetrating capacity of the peptide collection by cellular internalization studies in order to quantify the uptake and cytotoxicity of peptides *in vitro.*

6. Correlate folding structural properties with biological activity, both internalization and cytotoxicity.

7. Select the best peptide candidate from the above screening experiments to thoroughly investigate its uptake mechanism and test its activity in other cell lines.

8. Use this study in a follow up work for therapeutic protein delivery.

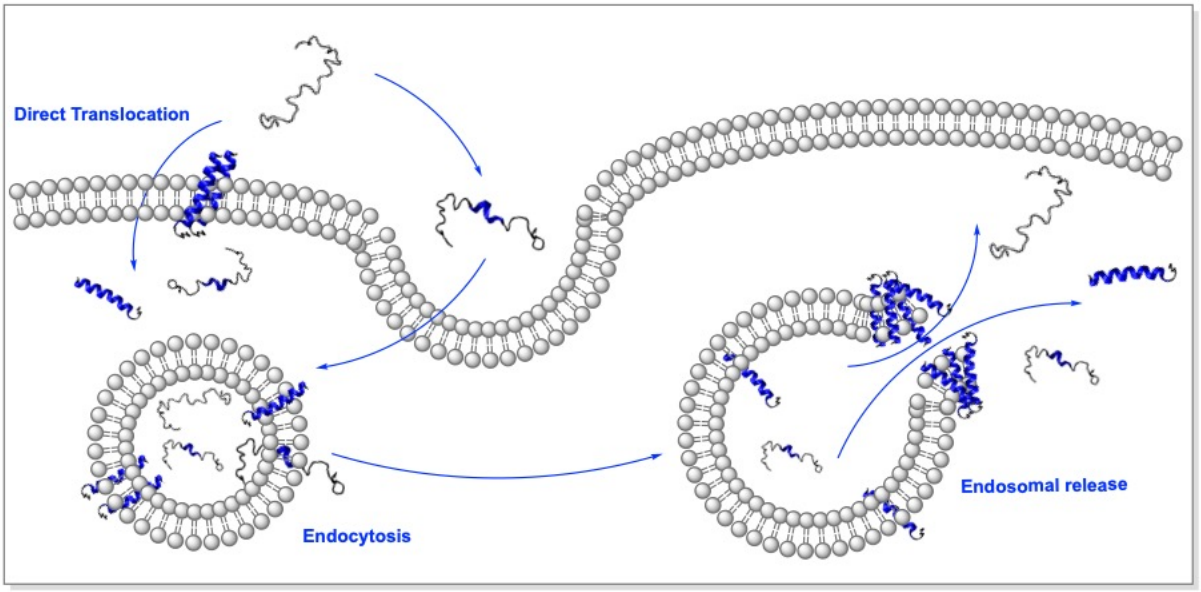

Figure 19. Behavior of peptide helical folding from aqueous to membrane environment for penetration.

USC
UNIVERSIDADE
DE SANTIAGO
DE COMPOSTELA

3. Results: Oligoalanine helical callipers for cell penetration

*The results of this chapter were originally published as part of the themed collection "2018 Emerging Investigators" in *Chemical Communication* as:

M. Pazo, M. Juanes, I. Lostalé-Seijo, and J. Montenegro, "Oligoalanine helical callipers for cell penetration" *Chem. Commun.*, **54**, 50, 6919–6922, 2018, doi: 10.1039/C8CC02304B.

https://pubs.rsc.org/en/content/articlelanding/2018/CC/C8CC02304B

Chemical Communications 2018 Impact Factor 6.164, Quartile 1 in multidisciplinar chemistry

Affiliations:

Centro Singular de Investigación en Química Biolóxica e Materiais Moleculares (CIQUS), Departamento de Química Orgánica, Universidade de Santiago de Compostela, 15782 Santiago de Compostela, Spain Email: javier.montenegro@usc.es

Copyrights:

Copyright © 2018, Rights managed by Royal Society of Chemistry. This article may be used for non-commercial purposes in accordance with RSC Terms and Conditions for self-archiving

Contributions:

Design and synthesis of the compounds, microscopy and cytometry of internalization experiments, viability assays.

USC
UNIVERSIDADE
DE SANTIAGO
DE COMPOSTELA

4. Conclusions

USC
UNIVERSIDADE
DE SANTIAGO
DE COMPOSTELA

USC
UNIVERSIDADE
DE SANTIAGO
DE COMPOSTELA

During this chapter we have studied the folding properties of a simple peptide structure. We have observed how amino acid substitutions along an oligoalanine peptide scaffold can modulate the biological properties such as uptake and toxicity. Basic structure/activity information was extracted to establish guidelines or standards to follow and achieve optimal peptide designs.

Specifically, in this chapter we have achieved:

1. The design and synthesis of a set of 8 oligoalanine peptide sequences. Each sequence has two heptad or 4.5 helical turns and also contains a fluorophore at the *N*-terminus.

2. All peptide structures exhibited the helical bands in CD and the helical folding for each peptide was maximized in the presence of the TFE solvent. The presence of the hydrophobic spacer, between the peptide and the fluorophore, only showed an increase in the helical folding in aqueous media.

3. Three Leu residues in the peptide sequence promote a better helical arrangement in membranes (**P1**-**P8**).

4. A radial arrangement of these leucine residues maximized the helical folding of the peptides in membranes (**P5*** and **P8**).

5. Alignment of 3 arginine residues enhanced the helicity in lipophilic and aqueous media compared to radial distribution (**P4 and P8**).

6. The proximity of leucine residues to cationic residues leads to helical stabilization in aqueous media (**P3*** and **P5***).

7. Retention of the helical configuration at high temperatures in liposomes for **P7** and **P8** demonstrated the existence of a strong peptide-membrane interaction.

8. Cellular uptake increased with the increment of helicity in membranes. In addition, during the internalization experiments, a punctated pattern of internalization was also observed in the microscopy images.

9. The correlation of peptide with viability showed, in the case of increased folding in membranes, an improvement in peptide uptake while not affecting viability. In contrast, structures with increased folding in aqueous medium showed worse internalization and higher toxicity, probably because these peptides have a surfactant or detergent effect.

10. The best candidate from this library of peptides was **P8**, which was studied in detail.

11. A punctate internalization pattern and colocalization of **P8** with lysosomes indicated an uptake mechanism mediated by endocytosis.

12. The uptake inhibition assays indicated that there were different uptake mechanisms oparatin at the same time but the principal mechanism mechanism was caveolin dependent endocytosis.

13. **P8** was also characterized in other cell lines (A549, SF9) showing good viability, good uptake and a dotted internalization pattern with diffuse fluorescence in the case of SF9 cells.

14. The partial fluorescence diffusion in this cell line (SF9) suggests the presence of cell-specific uptake mechanisms.

USC
UNIVERSIDADE
DE SANTIAGO
DE COMPOSTELA

CHAPTER 3: ASSEMBLY OF PEPTIDE NANOPORES AND DELIVERY OF FUNCTIONAL PROTEINS

USC
UNIVERSIDADE
DE SANTIAGO
DE COMPOSTELA

1. Introduction

USC
UNIVERSIDADE
DE SANTIAGO
DE COMPOSTELA

1.1 Intracellular transport of Proteins and Antibodies

The plasma membrane has a width around 4-10 nm and is the responsible of regulating the traffic of compounds.[5] Some small hydrophobic molecules can cross plasma membrane by passive diffusion across the lipid bilayer. The transport of polar or charged molecules, such as ions, water or glucose, requires specific channels or transporters like ionophores, aquaporins or glucose transporter.[5] However, plasma membrane is impermeable to hydrophilic macromolecules. Therefore, overcoming the cell membrane to reach the intracellular space is challenging for proteins or antibodies. During the last years, a variety of different approaches have been developed for delivering proteins inside cells. There are two major approaches for cell uptake: **crossing directly the plasma membrane** or **entering through an endosomal pathway**. The first method, direct intracellular delivery of proteins to cytosol, is a challenge because each protein has exclusive characteristics and properties such as size, surface charge, function and fragility. The second approach, the endocytic pathway, is the most common for intracellular protein delivery.[45] The entrapment of cargos in these compartments has to be overcome by carriers, so that the cargo can reach the cytosol and exert its biological activity (Figure 20).

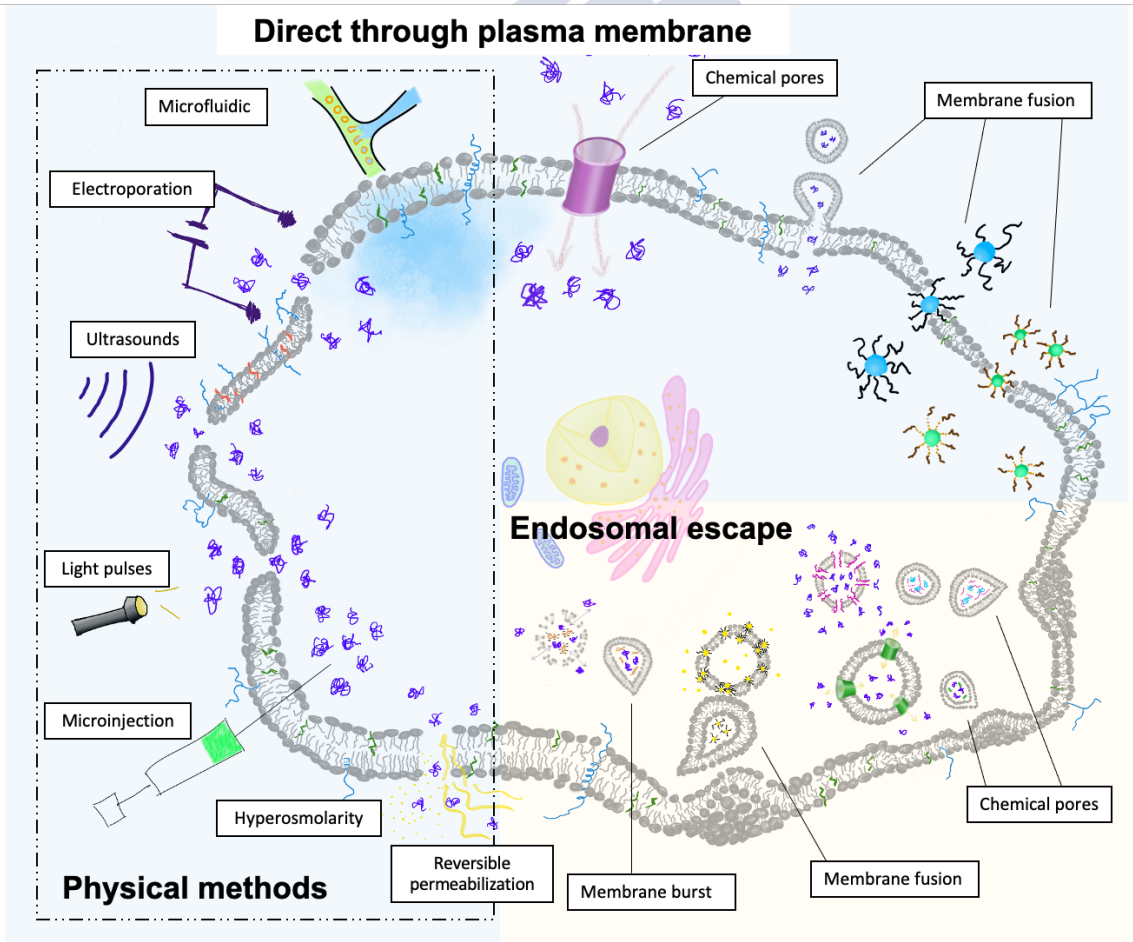

Figure 20. Mechanisms of cellular uptake of macromolecules. On the blue background, the methods that allow direct delivery across the plasma membrane; inside the dotted area the physical techniques. On the yellow background, the endosomal escape mechanisms.

Delivery methods can be classified in two groups: **physical methods** or **chemical agents**.

Physical methods consist in transient deformations of membranes mediated by mechanical forces, electrical fields, light pulses or other physical means, that allow the free trafficking of macromolecules. These techniques are considered the most straightforward approach to cross the plasma membrane to get into the cytosol. However, physical methods have low applicability *in vivo*, specially when targeting deep tissue, and can cause irreparable damage of cell membranes.

Chemical methods require the use of a molecular agent for the delivery. These agents may not need to interact with the cargo to facilitate delivery, such as in the case of protein pores. Chemical carriers bind the cargo and can be classified according to their natural composition into cell penetrating peptides (CPPs), lipids, polymers, dendrimers or nanoparticles, among others.[12,13] In addition, the association between carrier and cargo can be classified into supramolecular or covalent interactions. The supramolecular method is based on non-covalent interactions such as electrostatic interaction, host-guest complexation, or the hydrophobic effect. On the other hand, the covalent approach is based on covalent bonds *via* direct conjugation between cargo and carrier.[184] Nevertheless, the great diversity of proteins, in terms of size, shape, or charge, has prevented the elaboration of a universal method for the complexation of every protein with each carrier, especially when using supramolecular approaches. This is an important difference if we compar protein-based therapies with nucleic acid therapeutics, which have phosphate groups to establish electrostatic interactions or hydrogen bonds with the carrier. Although most of the examples of protein delivery are mediated by carriers, there are also examples of chemical or biological modification of the protein cargo for triggering cell uptake. This is the case of reversible esterification of charged residues,[29] the supercharging of the protein surface[185] or the engineering of endosomal disruption domains into the sequence.[186]

1.1.1 Direct delivery through plasma membrane

Direct delivery through plasma membrane requires a transient perturbation that generates pores, which provide direct connection with the cytosol for biomacromolecular transport. **Physical** methods and **chemical carriers** can afford these plasma membrane perturbations allowing the protein delivery into cytosol. **Chemical carriers** can operate following two main different mechanisms. In the first mechanism, the carrier forms a **channel** inserted into the plasma membrane allowing the diffusion of the cargo molecule into the cytosol. A second mechanism involves **membrane fusion** process, which is present in all living organisms and plays an important role in many fundamental cellular processes such as endocytosis, exocytosis, fertilization or synaptic neurotransmission.[187] In many cases, the fusion takes place between two lipid bilayers, from carrier and cell, that merge into one[188], but it can also be triggered by the lipophilic interaction of the carrier and the supramolecular assembly in the membrane (Figure 21).[39]

[184] X. Liu, F. Wu, Y. Ji, L. Yin, *Bioconjug. Chem.* **2019**, *30*, 305–324.
[185] D. B. Thompson, J. J. Cronican, D. R. Liu, *Methods Enzymol.* **2012**, *503*, 293–319.
[186] J. S. Kim, D. K. Choi, J. Y. Shin, S. M. Shin, S. W. Park, H. S. Cho, Y. S. Kim, *J. Control. Release* **2016**, *235*, 165–175.
[187] R. Jahn, T. Lang, T. C. Südhof, *Cell* **2003**, *112*, 519–533.
[188] H. R. Marsden, I. Tomatsu, A. Kros, *Chem. Soc. Rev.* **2011**, *40*, 1572–1585.
[39] F. Scaletti, J. Hardie, Y. W. Lee, D. C. Luther, M. Ray, V. M. Rotello, *Chem. Soc. Rev.* **2018**, *47*, 3421–3432.

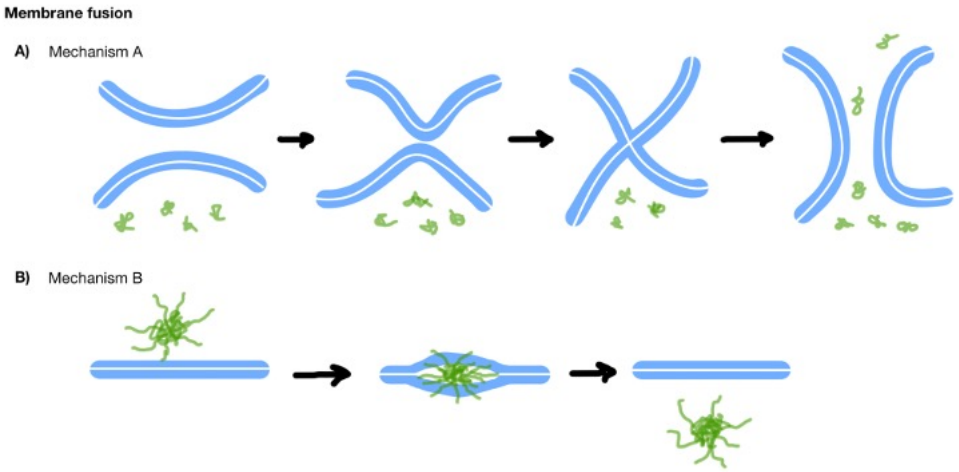

Figure 21. Scheme of membrane fusion mechanisms. A) Two lipid bilayers merging into one. B) Lipophilic interaction for transmembrane crossing.

1.1.1.1 Physical methods

One of the first methods used for the delivery of proteins inside the cell was **microinjection**, which can be use to deliver protein or antibody[189] solutions across the cell membrane or even the nuclear membrane with a glass capillary. This method is desirable when a precise control of timing and amount delivered is essential, but it is not adequate for the delivery of proteins into a large number of cells or in living systems. A potential high-troughput alternative to this technique is the **microneedle (MN) injection,** which is based on the design of surfaces with a microneedle pattern loaded with the protein to be delivered.[190] The microneedle injection is suitable for the delivery of proteins *in vitro*, such as in the case of Cas9-sgRNA ribonucleoprotein,[191] and they are also a promising strategy for intradermal delivery of antigens for vaccines.[190]

Electroporation consists in the application of voltage pulses creating transient pores in the membrane that can be crossed by proteins and antibodies.[192] The principal advantage is that this technique can be applied to all cell types. The major limitations is that sensitive cells cannot survive the treatment and the fact that, as electrodes are an invasive method, they have a limited use on in vivo applications.[193] One example is the delivery of fluorescent protein biosensors to primary cells with high efficiency, requiring a limited number of cells to monitor signaling pathways by Föster resonance energy transfer (FRET).[194] Other example of transport of recombinant proteins by electroporation has been recently applied for the characterization of kinetochore.[195]

Reversible membrane permeabilization can also be achieved by incubation with a buffered solution containing 25% ethanol. This method allowed a rapid intracellular delivery of a wide

[189] Y. Zhang, L.-C. Yu, *BioEssays* **2008**, *30*, 606–610.
[190] R. Jamaledin, C. Di Natale, V. Onesto, Z. Taraghdari, E. Zare, P. Makvandi, R. Vecchione, P. Netti, *J. Clin. Med.* **2020**, *9*, 542.
[191] A. Yamagishi, D. Matsumoto, Y. Kato, Y. Honda, M. Morikawa, F. Iwata, T. Kobayashi, C. Nakamura, *Appl. Sci.* **2019**, *9*, 965.
[192] J. Shi, Y. Ma, J. Zhu, Y. Chen, Y. Sun, Y. Yao, Z. Yang, J. Xie, *Molecules* **2018**, *23*, 3044.
[193] V. Torchilin, *Drug Discov. Today Technol.* **2008**, *5*, e95–e103.
[194] C. Sun, M. Ouyang, Z. Cao, S. Ma, H. Alqublan, N. Sriranganathan, Y. Wang, C. Lu, *Chem. Commun.* **2014**, *50*, 11536–11539.
[195] A. Alex, V. Piano, S. Polley, M. Stuiver, S. Voss, G. Ciossani, K. Overlack, B. Voss, S. Wohlgemuth, A. Petrovic, et al., *Elife* **2019**, *8*, e48287.

variety of cargoes including proteins.[196] Membrane permeabilization is also possible using a **hyperosmolar NaCl** solution combined with propanebetaine, a transduction compound. This method called **iTOP** (induced transduction by osmocytosis and propanebetaine) triggers macropinocytotic uptake and intracellular release of therapeutic proteins. The technique has very high efficiency even in difficult to manipulate primary cells.[197]

In **microfluidics,** cells are forced to pass through a hole smaller than cell diameter inducing fast deformation of cell membranes and facilitating passive diffusion. This technique is high throughput, being able to process 20,000 cells/s, and was able to deliver different cargos into immune cells and stem cells. This technique has been proved for antibody delivery or transcription factors.[198]

In **optoporation,** light pulses are used to permeabilize plasma membrane.[199] *In vivo* assays are limited by thermal damage threshold using millions of low-energy pulses at the tissue surface. A demonstration of protein delivery using light pulses and a BLAST platform (a silicon chip covered by porous silica membrane) was perfomed with β-lactamase.[200] Other codelivery example mediated by optoporation and assisted by gold nanorods was applied for antibody delivery.[201]

Ultrasound techniques have also been employed to complement other delivery approaches. In this regard, taking advantage of the particular properties of fluorinated molecules, it was possible to induce vaporization of fluorinated nanoemulsions that incorporate the biological cargo and consequently, the formation of a microbubble, which permeabilizes the membrane forming a transient pore. Proteins or antibodies can be masked by a fluorinated tag (FTags) for their solubilization into perfluorohexane and the resulting nanoemulsion can act as a delivery and contrast agent. The system was successfully proved *in vivo* for IgG delivery (Figure 22).[202]

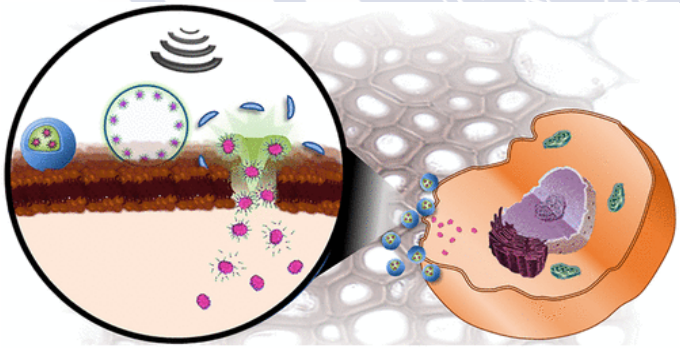

Figure 22. Delivery of proteins by a system of nanoemulsions containing fluorinated tags. The system is sensitive to activation by ultrasound forming microbubbles that cause transient disruptions in the membrane. Reproduced with permission from refs[202]. Copyright (2020), American Chemical Society.

[196] S. O'Dea, V. Annibaldi, L. Gallagher, J. Mulholland, E. L. Molloy, C. J. Breen, J. L. Gilbert, D. S. Martin, M. Maguire, F.-R. Curry, *PLoS One* **2017**, *12*, e0174779.
[197] D. S. D'Astolfo, R. J. Pagliero, A. Pras, W. R. Karthaus, H. Clevers, V. Prasad, R. J. Lebbink, H. Rehmann, N. Geijsen, *Cell* **2015**, *161*, 674–690.
[198] A. Sharei, J. Zoldan, A. Adamo, W. Y. Sim, N. Cho, E. Jackson, S. Mao, S. Schneider, M. J. Han, A. Lytton-Jean, et al., *Proc. Natl. Acad. Sci. U. S. A.* **2013**, *110*, 2082–2087.
[199] A. Vogel, J. Noack, G. Hüttman, G. Paltauf, *Appl. Phys. B Lasers Opt.* **2005**, *81*, 1015–1047.
[200] Y.-C. Wu, T.-H. Wu, D. L. Clemens, B.-Y. Lee, X. Wen, M. A. Horwitz, M. A. Teitell, P.-Y. Chiou, *Nat. Methods* **2015**, *12*, 439–444.
[201] C. Yao, F. Rudnitzki, Y. He, Z. Zhang, G. Hüttmann, R. Rahmanzadeh, *J. Biophotonics* **2020**, *13*, e202000017.
[202] J. N. Sloand, T. T. Nguyen, S. A. Zinck, E. C. Cook, T. J. Zimudzi, S. A. Showalter, A. B. Glick, J. C. Simon, S. H. Medina, *ACS Nano* **2020**, *14*, 4061–4073.

1.1.1.2 Chemical methods

The chemical methods have been classified into agents that release their contents into the cell by membrane fusion and agents that form chemical pores in cell membranes.

1.1.1.2.1 Polymers

Some carriers with polymeric nature also have a membrane fusion entry mechanism. For example, the covalent attachment of 2-pyridinecarboxaldehyde polymers to the N-terminal position of proteins such as GFP and RNAse A, resulted in cytosolic protein delivery.[203] The site-selective protein functionalization minimally affects protein structure and function. Moreover, the uptake mechanism was confirmed by using different inhibitors showing that only methyl-β-cyclodextrin was able to inhibit cellular uptake. Provided that methyl-β-cyclodextrin is known to inhibit both endocytosis and fusion mechanisms by removing cholesterol from plasma membranes,[204] the results suggested that the conjugate entry occurs through the fusion mechanism.

Recently, a library of guanidinium functionalized poly(oxanorborneneimide) (PONI) homopolymers were synthesized by the group of Prof. Rotello and collaborators for the delivery of engineered proteins (GFP, Cre recombinase, tdTomato) derivatized with terminal oligoglutamate "E-tags".[205] The proposed mechanism of delivery was by membrane fusion due to a fast cellular internalization (within 40 s) and lack of effect using endocytic inhibitors, with the exception of methyl-β-cyclodextrin which support a dependency related with membrane flexibility.

A special type of polymers are cell penetrating poly(disulfide)s (CPDs) studied by Prof. Matile. Their principal characteristic is the backbone composed by poly(disulfides)s, which exchange with endogenous thiols at the membrane surface in order to induce the cell uptake.[206] In addition, their depolymerization after the uptake strongly reduces their toxicity. This CPDs system was effective for the introduction of streptavidin.[207] Moreover, a system of quantum dots functionalized with CPDs delivered other protein cargos such as GFP or anti-GFP nanobodies.[208] Afterwards, the mechanistic concept of CPDs evolved into benzopolysulfanes (BPs), which increase thiol exchange with membrane components. Protein delivery with BPs was confirmed with streptavidin and anti-GFP.[209] A step further was the development a cell-penetrating streptavidin, which contains BPs attached to lysines for cell penetration, that can carry biotinylated cargos. The system codelivered streptavidin and anti-GFP in a spatiotemporal way.[210]

1.1.1.2.2 CPPs

Cell penetrating peptides (CPPs) are short sequences of amino acids based on natural, artificial or combinations of small fragments, that are able to translocate into cells. The first example of a CPP carrier for supramolecular protein delivery was Pep-1.[71] This peptide is

[203] R. Sangsuwan, P. Tachachartvanich, M. B. Francis, *J. Am. Chem. Soc.* **2019**, *141*, 2376–2383.
[204] S.-T. Yang, A. J. B. Kreutzberger, J. Lee, V. Kiessling, L. K. Tamm, *Chem. Phys. Lipids* **2016**, *199*, 136–143.
[205] Y.-W. Lee, D. C. Luther, R. Goswami, T. Jeon, V. Clark, J. Elia, S. Gopalakrishnan, V. M. Rotello, *J. Am. Chem. Soc.* **2020**, *142*, 4349–4355.
[206] G. Gasparini, E.-K. Bang, G. Molinard, D. V. Tulumello, S. Ward, S. O. Kelley, A. Roux, N. Sakai, S. Matile, *J. Am. Chem. Soc.* **2014**, *136*, 6069–6074.
[207] G. Gasparini, S. Matile, *Chem. Commun.* **2015**, *51*, 17160–17162.
[208] E. Derivery, E. Bartolami, S. Matile, M. Gonzalez-Gaitan, *J. Am. Chem. Soc.* **2017**, *139*, 10172–10175.
[209] Y. Cheng, L. Zong, J. López-Andarias, E. Bartolami, Y. Okamoto, T. R. Ward, N. Sakai, S. Matile, *Angew. Chemie Int. Ed.* **2019**, *58*, 9522–9526.
[210] J. López-Andarias, J. Saarbach, D. Moreau, Y. Cheng, E. Derivery, Q. Laurent, M. González-Gaitán, N. Winssinger, N. Sakai, S. Matile, *J. Am. Chem. Soc.* **2020**, *142*, 4784–4792.
[71] M. C. Morris, J. Depollier, J. Mery, F. Heitz, G. Divita, *Nat. Biotechnol.* **2001**, *19*, 1173–1176.

commercialized as Chariot™ and has three domains, a hydrophilic lysine rich domain derived from the nuclear localization signal (NLS) from SV40 large T antigen, a tryptophan rich hydrophobic domain and a spacer domain. Protein cargos employed to demonstrate the delivery were GFP, β-Galactosidase and two antibodies, anti-β-actin and anti-LAMP-1. In addition, insights into the mechanism of cell internalization suggested that Pep-1 does not suffer any conformational change during complexation with a cargo, whereas after interacting with phospholipids of the cell membrane, changes into a helical folding leading to the formation of a transient transmembrane pore-like structure.[211]

As commented before, disulfide bonds can trigger membrane interactions for the cell uptake, but can also be exploited to link cargos and carriers. A recently reported CPP based on a linear decaarginine, which also contains a thiol, can be used for covalent protein derivatization and direct intracellular delivery of this adduct. The CPP-protein conjugate demonstrated a direct internalization across plasma membrane and cytosolic distribution of proteins, that was improved in the presence of a slight excess of CPP. With this method, it was possible to deliver proteins such as Cre recombinase, nanobodies and antibodies, demonstrating the labelling of intracellular structures.[212]

1.1.1.2.3 Lipids

Lipids, liposomes and cholesterol are also used as carriers and have the ability to enhance membrane interactions. This is the case of cholesterol, an essential component of the plasma membrane that helps maintain fluidity. In the following example, a carrier that has two molecules of cholesterol for membrane fusion and a Coomassie blue (CB) molecule for protein complexation, was employed for protein delivery (Figure 23). The ability of the system to release proteins into the cytosol was directly related to the size of the protein, with a limit for direct transmembrane permeation around 60 kDa. Larger proteins, such as bovine serum albumin (BSA) or immunoglobulin G (IgG) remain trapped in endosomes. The potential therapeutic effect was measured in different cell lines for proteins such as aprotinin, lysozyme, the apoptosis inducer cytochrome C CytC, or the actin marker LifeAct-GFP.[213] Another type of liposome-based carriers are inspired by N-ethylmaleimide-sensitive factor attachment protein receptor (SNARE) proteins because they induce membrane fusion of cellular vesicles through coiled-coil interactions.[188] Liposomes decorated with a helical peptide from a pair of complementary coiled-coil forming peptides mediate membrane fusion with cell membranes that have been previously loaded with its peptide counterpart. This technology demonstrated its applicability in zebra fish *in vivo models*[214] and later, for protein transport. The studied protein was CytC, which was encapsulated in mesoporous silica nanoparticles (MSNs). These particles were coated with a lipid bilayer, and the delivery was mediated by the complementary pair of coiled-coil forming peptides. The system performed an efficient protein cytosolic delivery in HeLa cells.[215]

[211] S. Deshayes, A. Heitz, M. C. Morris, P. Charnet, G. Divita, F. Heitz, *Biochemistry* **2004**, *43*, 1449–1457.
[212] A. F. L. Schneider, M. Kithil, M. C. Cardoso, M. Lehmann, C. P. R. Hackenberger, *Nat. Chem.* **2021**, *13*, 530–539.
[213] W. Tai, P. Zhao, X. Gao, *Sci. Adv.* **2020**, *6*, eabb0310.
[214] H. R. Zope, F. Versluis, A. Ordas, J. Voskuhl, H. P. Spaink, A. Kros, *Angew. Chemie Int. Ed.* **2013**, *52*, 14247–14251.
[215] J. Yang, J. Tu, G. E. M. Lamers, R. C. L. Olsthoorn, A. Kros, *Adv. Healthc. Mater.* **2017**, *6*, 1700759.

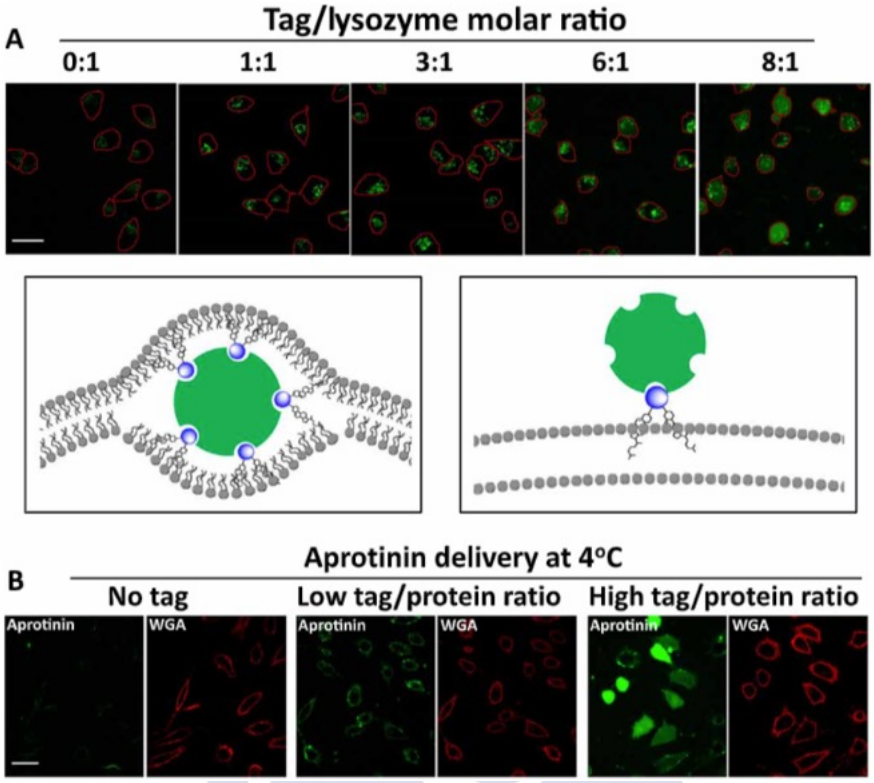

Figure 23. Effect of the cholesterol-CB tag density on delivery. A) Evaluation of the amount of tag necessary to obtain good lysozyme (green) delivery. Cell boundaries were labelled with WGA (red circle). Scale bar, 10 μm. B) Schematic representation of the interaction between membrane and cholesterol-CB tag. C) Cytosolic delivery of AF488 (green) aprotinin. Cell membranes were labelled with WGA (red circle). Scale bar, 10 μm. Reproduced with permission from ref[213] Copyright (2020) American Association for the Advancement of Science.

1.1.1.2.4 Nanoparticles

Inorganic nanoparticles have become novel and versatile nanocarriers for new therapies. Some of their advantages are their high encapsulation efficiency, immobilization of proteins, low toxicity, and potential for systemic delivery or specifical targeting.[39,216] Inorganic nanoparticles that have a hydrophobic surface for membrane interaction can also internalize by membrane fusion mechanisms. Models based on silica nanoparticles were able to deliver proteins/antibodies.

Moreover, in the field of inorganic nanoparticles it is necessary to highlight gold nanoparticles (NP), which have a great impact as biomacromolecule delivery systems. In particular, the research group of Prof. Rotello used these gold nanoparticles for the delivery of proteins by using a novel electrostatic complexation strategy, where anionic proteins interact with cationic peptide tags present in the NP, which are composed by His-Lys-Arg-Lys (HKRK) sequences. However, the tight binding between HKRK-NPs and proteins resulted in an ineffective release of the cargo into the cytosol. For that reason, authors proposed a new formulation with hydrophobic components in order to increase membrane interactions providing direct delivery of the cargo into the cytosol.[217] The new emulsion, which they called nanoparticle stabilized nanocapsules (NPSCs), employed linoleic acid to enhance membrane

[216] M. Ray, Y. W. Lee, F. Scaletti, R. Yu, V. M. Rotello, *Nanomedicine* **2017**, *12*, 941–952.
[217] R. Tang, Z. Jiang, M. Ray, S. Hou, V. M. Rotello, *Nanoscale* **2016**, *8*, 18038–18041.

interactions. The proposed uptake mechanism was of a membrane-fusion type and displayed efficient delivery of the large proteins β-galactosidase and dsRed. In order to apply this strategy to a new formulation, authors proposed a model of membrane-spanning nanoassemblies. Once again, the complexation approach was by electrostatic interactions between cationic nanoparticles (ArgNPs) and anionic proteins tagged with glutamic acid in C-terminus (Figure 24).[218] The transport was confirmed with the nanoassembly of proteins: GFP, Histone 2A, Granzyme A, Cre recombinase and Prothymosin-α.[219] Furthermore, the same technology was also applied for the direct transfer of Cas9 ribonucleoprotein.[220]

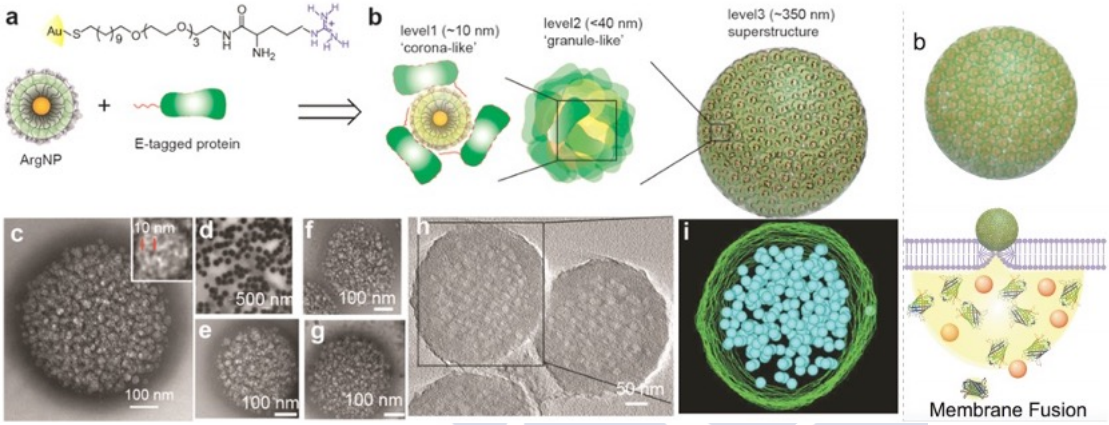

Figure 24. Arginine-functionalized gold nanoparticles. Top: from chemical structure to the formation of protein-nanoparticles. Bottom: TEM images and tilt section of a tomogram (left). Illustration of membrane fusion mechanism of the nanoparticles for protein delivery across plasma membrane (right). Reproduced with permission from refs[218] Copyright (2017) American Chemical Society. Adapted with permission from refs[39,218] Copyright (2018) Royal Society of Chemistry.

1.1.1.2.5 Protein channels

Many channels of multimeric protein units can assemble in membranes in order to allow the transport of macromolecules. Most of these **protein channels** have bacterial origin, for instance, protein injection machines known as types III, IV and VI protein-secretion systems.[221] The type III secretion systems (T3SS) has a needle-like structure, which allow the traffic of antigens, using non-replicating bacterial minicells that express both the antigen and the T3SS, into $CD8^+$ T cells to develop vaccine systems.[222] Other bacterial membrane channels like mechanosenstive channels of E. Coli (MscL) allow the control delivery of peptides like phalloidin.[223] Another type of pore-forming proteins are perforins, which belong to the membrane attack complexes/perforin-like family (MACPF).[224] Perforins (MACPF) facilitate the delivery of cationic cargos such as CytC or positively supercharged GFP, but not of neutral (Bid) or negatively charged (negatively supercharged GFP) proteins.[225] Another example are pore-forming cholesterol dependent cytolysins (CDCs),[224] such as Streptolysin O (SLO, pore

[218] R. Mout, G. Yesilbag Tonga, L. S. Wang, M. Ray, T. Roy, V. M. Rotello, *ACS Nano* **2017**, *11*, 3456–3462.
[219] R. Mout, M. Ray, T. Tay, K. Sasaki, G. Yesilbag Tonga, V. M. Rotello, *ACS Nano* **2017**, *11*, 6416–6421.
[220] R. Mout, M. Ray, G. Yesilbag Tonga, Y.-W. Lee, T. Tay, K. Sasaki, V. M. Rotello, *ACS Nano* **2017**, *11*, 2452–2458.
[221] J. E. Galán, G. Waksman, *Cell* **2018**, *172*, 1306–1318.
[222] H. A. Carleton, M. Lara-Tejero, X. Liu, J. E. Galán, *Nat. Commun.* **2013**, *4*, 1590.
[223] J. F. Doerner, S. Febvay, D. E. Clapham, *Nat. Commun.* **2012**, *3*, 990.
[224] M. A. Dunstone, R. K. Tweten, *Curr. Opin. Struct. Biol.* **2012**, *22*, 342–349.
[225] S. E. Stewart, S. C. Kondos, A. Y. Matthews, M. E. D'Angelo, M. A. Dunstone, J. C. Whisstock, J. A. Trapani, P. I. Bird, *J. Biol. Chem.* **2014**, *289*, 9172–9181.

diameter 30 nm), which can be used for reversible permeabilization of the plasma membrane for the transport proteins or antibodies.[226,227]

1.1.1.2.6 Self-delivery of proteins

An example of membrane fusion by protein modification is the bioreversible esterification proposed by Prof. Raines.[228] The esterification of carboxyl groups of proteins adding a variety of diazo compounds derived from (p-methylphenyl)glycine, were screened for protein GFP delivery (Figure 25). This strategy minimized the Coulombic repulsion between the anionic part of the proteins and the membranes, allowing the diffusion of the proteins across the membrane. Upon entry of the protein, the esters are hydrolyzed by cellular esterases, restoring the original protein in the cytosol.[29]

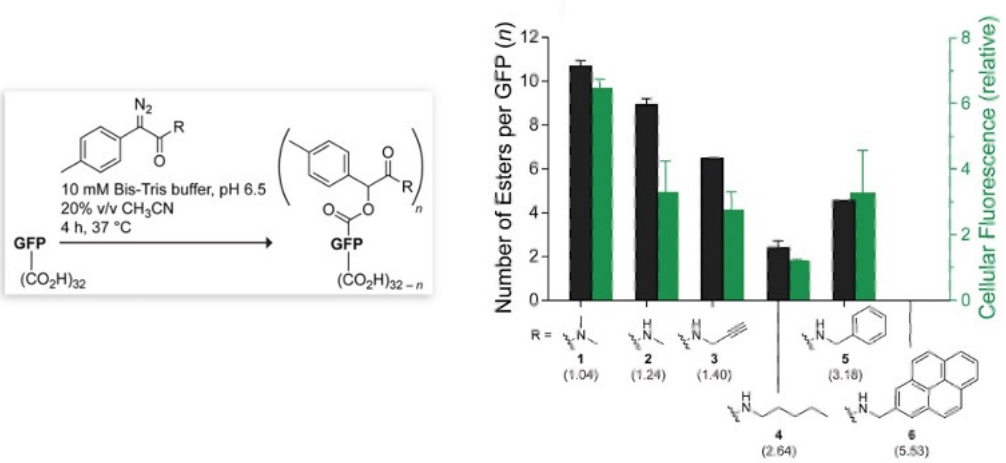

Figure 25. Scheme of GFP sterification reaction (upper) and the different hydrophobic tails incorporated by sterification and the cellular fluorescence. Reproduced with permission from ref[29] Copyright (2017) American Chemical Society.

1.1.2 Endocytic uptake

1.1.2.1 Endosomal routes

Endocytosis is an energy dependent uptake process that consists in the formation of vesicles derived from invaginations of the plasma membrane.[5] Endocytosis can be classified into phagocytosis (used by macrophages or neutrophils in order to acquire large particles, >0.5 μm) or pinocytosis (the uptake of fluid and solutes) (Figure 26). Besides, pinocytosis can be further divided into different types: macropinocytosis, caveolin-dependent endocytosis, clathrin-mediated endocytosis and clathrin and caveolin independent endocytosis. Each pinocytic mechanism might have receptors to trigger the uptake, depending on the target tissue or the cell type.[229]

[5] N. J. Yang, M. J. Hinner, *Methods Mol. Biol.* **2015**, *1266*, 29–53.
[226] K. W. Teng, Y. Ishitsuka, P. Ren, Y. Youn, X. Deng, P. Ge, S. H. Lee, A. S. Belmont, P. R. Selvin, *Elife* **2016**, *5*, e20378.
[227] I. Walev, S. C. Bhakdi, F. Hofmann, N. Djonder, A. Valeva, K. Aktories, S. Bhakdi, *Proc. Natl. Acad. Sci. U. S. A.* **2001**, *98*, 3185–3190.
[228] N. A. McGrath, K. A. Andersen, A. K. F. Davis, J. E. Lomax, R. T. Raines, *Chem. Sci.* **2015**, *6*, 752–755.
[229] S. D. Conner, S. L. Schmid, *Nature* **2003**, *422*, 37–44.

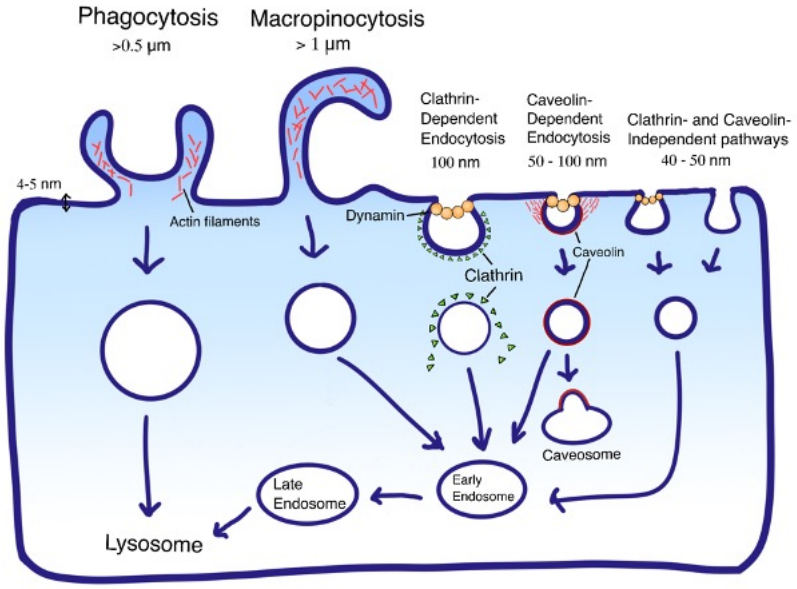

Figure 26. Schematic representation of endocytic routes and representative sizes.

Macropinocytosis forms irregular vesicles called macropinosomes, larger than >1µm, which are mainly dependent by actin ruffles (Figure 26).[230] There are receptors that activate macropinocytosis uptake, such as the chemokine receptor CXCR4, which is a co-receptor for HIV-1 entry. It was observed that this stimulation of macropinocytosis can be triggered by the envelope glycoprotein gp120 from HIV and a dodecaarginine (but not an octaarginine), as well as by its natural ligand, stromal derived factor (SDF-1α).[231] There other receptors that can stimulate macropinocytosis, such as the epidermal growth factor receptor (EGFR).[232]

Clathrin-Dependent endocytosis is the most frequent endocytic pathway in cells. The defining characteristic is that the clathrin protein coats the invaginated vesicles (Figure 26). Membrane binding, internalization and post internalization trafficking involve several proteins such as adaptin, dynamin and numerous *rab* proteins. [233] Adaptin proteins are simultaneously involved in the binding to the cytosolic domain of cell surface receptors as well as to the clathrin heavy chains on the intracellular face allowing the polymerization of clathrin subunits. Then, the scission of vesicles is aided by dynamin, releasing vesicles with a diameter around 100 nm.[229,234] Clathrin-dependent endocytosis can be stimulated by specific receptors such as epidermal growth factor (EGF), transferrin, asialoglycoprotein, chemokine, integrins or cadherin. Examples of ligands to target these receptors are PEGylated albumin nanoparticles loaded with azidothymidine (AZT) with transferrin for internalization through the transferrin receptor and the peptide sequence Arg-Gly-Asp (RGD) that binds to cell adhesion receptors such as integrins.[235]

[230] M. Kirkham, R. G. Parton, *Biochim. Biophys. Acta - Mol. Cell Res.* **2005**, *1745*, 273–286.
[231] G. Tanaka, I. Nakase, Y. Fukuda, R. Masuda, S. Oishi, K. Shimura, Y. Kawaguchi, T. Takatani-Nakase, Ü. Langel, A. Gräslund, et al., *Chem. Biol.* **2012**, *19*, 1437–1446.
[232] I. Nakase, A. Aoki, Y. Sakai, S. Hirase, M. Ishimura, T. Takatani-Nakase, Y. Hattori, M. Kirihata, *ACS Omega* **2020**, *5*, 22731–22738.
[233] J. Mosquera, I. García, L. M. Liz-Marzán, *Acc. Chem. Res.* **2018**, *51*, 2305–2313.
[234] S. Mayor, R. E. Pagano, *Nat. Rev. Mol. Cell Biol.* **2007**, *8*, 603–612.
[235] L. Bareford, P. Swann, *Adv. Drug Deliv. Rev.* **2007**, *59*, 748–758.

Caveolin-Dependent Endocytosis involves caveolae, flask-shaped invaginations coated by caveolin protein and with a vesicular diameter ranging from 50 to 100 nm. Actin filaments held in place these vesicular invaginations (Figure 26). The most common membrane protein in this mechanism is caveolin-1 that coats the cytosolic face. Next, vesicles are scissed by dynamin. Finally, the caveolin-coated vesicles are transferred to complex tubular organelles called caveosomes. Natural ligands that activate caveolar endocytosis are Simian Virus 40 (SV40), folic acid, albumin and cholesterol.[235]

Clathrin and caveolin-independent endocytosis are mechanisms of uptake related to lipid-raft domains.[234] These regions are enriched with cholesterol, phospholipids, glycophospholipids and sphingomyelin. The vesicular scission can be dynamin-dependent or dynamin-independent and vesicle size is close to 40-50 nm (Figure 26).[233] Moreover, lipid-raft-associated ligands have allowed for vesicular trafficking to non-lysosomal compartments. Specific ligands, like cholera toxin B (CTB), bind receptors that are located in these lipids-rich areas.[235]

1.1.2.2 Endosome characteristics

Lipid composition in plasma membrane and early endosomes are pretty similar. However, the maturation of endosomes triggers changes in the lipidic composition and thus, diverse lipids recruit specific proteins from the cytosol and control the vesicle trafficking. For instance, endosomes trigger the enhancement of bis(monoacylglycero) phosphate (BMP) anionic lipids. Then, BMP lipids are involved in fusion processes and sphingolipid hydrolysis.[236] Afterwards, the formation of certain phosphoinositides, mediated by kinases and phosphatases, recruit different subsets of proteins involved in vesicle trafficking and organelle targeting.[237] At the same time, in the maturation process, endosomes also develop acidification changes. The enzyme responsible is H^+-ATPase or vacuolar ATPase (V-ATPase), which differs from others ATPases (like Na^+, K^+ or Ca^{2+}) in the lack of a coupled influx of permeant anions. An acidic environment is needed for the release of ligands from internalized receptors and their redirection to the membrane, to preserve the activity of endo/lysosomal enzymes, and to trigger enzymatic or oxidation.[238] The difference in H^+ concentration, as well as other ions, between early endosomes (about pH 6.5), late endosomes (about pH 5.5) and lysosomes (about pH 4.5) creates a membrane potential. The positive potential is placed towards the lumen of endosomes and the negative charge faces towards the cytosol, with membrane potential values of +134 mV, +46 mV and +100 mV, early endosomes, late endosomes and lysosomes respectively.[239,238]

1.1.2.3 Delivery strategies

There are different delivery strategies to overcome endosomal entrapment. The following examples are ordered according to the chemical nature of the carrier (i.e., lipids, CPPs, polymers, etc). The carriers also follow two complexation approaches (supramolecular or covalent). Moreover, these chemical carriers might overcome endosomal entrapment by four different mechanisms (Figure 27): 1) by membrane fusion (as explained in the previous section 5.1), 2) by endosomal bursting due to osmotic pressure, 3) by pores or channels inserted in the

[236] H. Matsuo, J. Chevallier, N. Mayran, I. Le Blanc, C. Ferguson, J. Fauré, N. S. Blanc, S. Matile, J. Dubochet, R. Sadoul, et al., *Science* **2004**, *303*, 531–534.
[237] G. van Meer, D. R. Voelker, G. W. Feigenson, *Nat. Rev. Mol. Cell Biol.* **2008**, *9*, 112–124.
[238] Y.-B. Hu, E. B. Dammer, R.-J. Ren, G. Wang, *Transl. Neurodegener.* **2015**, *4*, 18.
[239] A. Saminathan, J. Devany, A. T. Veetil, B. Suresh, K. S. Pillai, M. Schwake, Y. Krishnan, *Nat. Nanotechnol.* **2021**, *16*, 96–103.

endosomal membranes, and 4) by other membrane disruptive effects. The mechanism for endosomal escape will be described in each example.

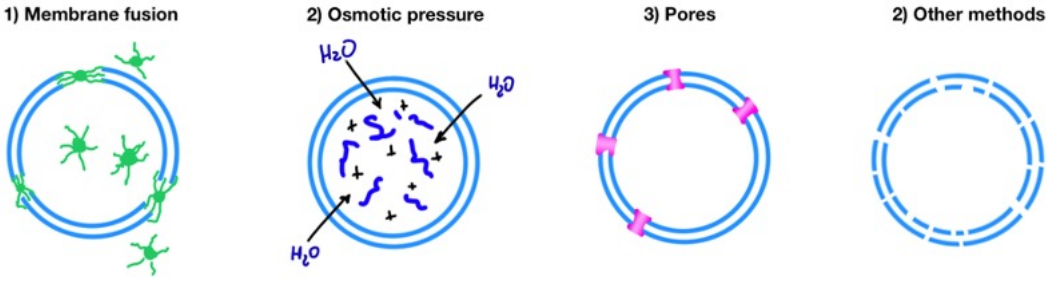

Figure 27. Mechanisms for endosomal escape: 1) hydrophobic interactions between carrier-membrane, which leads to membrane fusion. 2) Osmotic pressure bursting due to the proton sponge effect caused by carrier. 3) Pores inserted in the membrane. 4) Other mechanisms for membrane disruption.

1.1.2.3.1 Polymers

Polymers and dendrimers are excellent protein delivery carriers, as their physical and chemical properties can be easily modified.[240] Moreover, the modulation of polymers has been extensively applied to endosomal escape. One of the most common polymers employed to enhance the endosomal escape is PEI **(**polyethylenimine) branched polymer, which takes advantage of its protonable amines in the endosomal environment and produces a "proton sponge effect", which induce osmotic swelling and the subsequent endosome burst.[241]

PEI polymers have evolved into multiple modifications. The combination of PEI with fluoroalkyls to achieve amphiphiles, taking advantage of the higher hydrophobicity of CF_2 than CH_2, was explored to enhance the cytosolic delivery of proteins. These fluoroamphiphiles have particular properties such as protein encapsulation, limited toxicity and improvement of cellular uptake. The use of fluoroamphiphiles allowed the cytosolic delivery of BSA-FITC and saporin.[242] Other PEI derivatives include guanidinium ligands, because guanidinium residues enhance the cell uptake in protein transduction domains (PTD). Therefore, cationic polymers enriched with guanidinium groups were developed to stablish hydrogen bonds with membranes or with proteins. An association of a biguanide scaffold with PEI polymer led to phenylbiguanide polyethylenimine (bPEI). The activity of this bPEI polymer showed high protein binding affinity and efficient cytosolic delivery of a wide collection of proteins such as R-phycoerythrin, GFP, FITC labeled Cytochrome C (CytC-FITC), lysozyme-RBITC and FITC labeled ribonuclease A (RNaseA-FITC).[243] A new combination of PEI polymer with a benzene-guanidinium scaffold produced a new generation of polymers, the 4-guanidinobenzene (GBA) polymers. The stabilization through paired guanidinium-π interactions between benzene-guanidyl ligands allowed the complexation of GBA polymer with proteins to form stable nanoparticles that are finally transported and released from the endosome (Figure 28). The wide variety of proteins tested included β-galactosidase, horseradish peroxidase, chymotrypsin and trypsin.[244]

[240] J. Lv, Q. Fan, H. Wang, Y. Cheng, *Biomaterials* **2019**, *218*, 119358.
[241] A. El-Sayed, S. Futaki, H. Harashima, *AAPS J.* **2009**, *11*, 13–22.
[242] Z. Zhang, W. Shen, J. Ling, Y. Yan, J. Hu, Y. Cheng, *Nat. Commun.* **2018**, *9*, 1–8.
[243] C. Yu, E. Tan, Y. Xu, J. Lv, Y. Cheng, *Bioconjug. Chem.* **2019**, *30*, 413–417.
[244] J. Lv, E. Tan, Y. Wang, Q. Fan, J. Yu, Y. Cheng, *J. Control. Release* **2020**, *320*, 412–420.

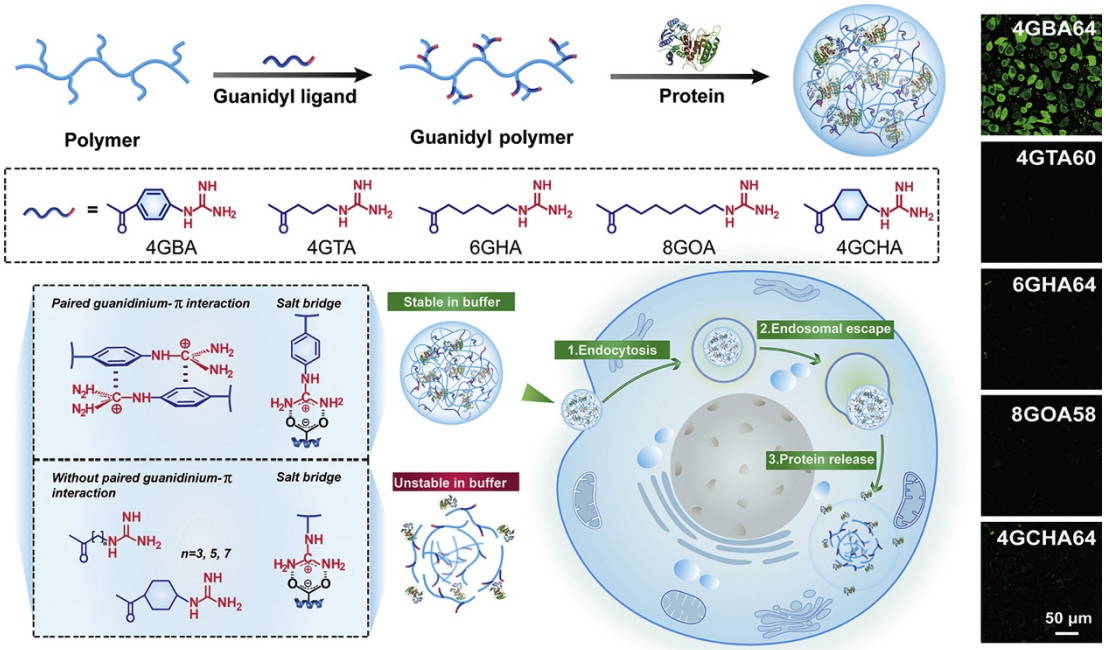

Figure 28. Schematic representation of guanidyl-rich polymers and the synthesis with the different guanidyl components (upper). Illustration of guanidium interactions and cytosolic polymer-protein complex delivery in cells (bottom). Micrographs of BSA-FITC delivery with guanidyl-rich polymers. Barrs 50 μm. Reproduced with permission from ref[244] Copyright (2020) Elsevier.

Another family of guanidinium rich PEI received the name of protein transduction domain mimics (PTDMs).[245] These polymers have an amphiphilic architecture with phenyl, alkyl and guanidinium scaffolds. Then, first insights of PTDMs capabilities for protein-antibody delivery were tested using cargos such as an antibody against the phosphorylated form of pPKCθ for their distribution into the cytosol, interfering with the signalling pathway in human peripheral mononuclear blood cells.[246] Next, the best candidate of PTDMs, the $MePh_{10}$-*b*-dG5 polymer, was also reported to deliver ovalbumin (OVA) into monocytes for vaccination The same polymer was employed for intracellular delivery of other proteins, such as GFP and antibodies as IgG or $F(ab')_2$, in a wide range of cell lines including hard-to-transfect cells such as Jurkat (immune cell line) or MSC (stem cells) among others.[247]

Other polymers include moieties for the incorporation of small peptide sequences. For instance, a nanogel prepared from a random copolymer formed by a hydrophilic oligo (ethylene glycol) methacrylate and a lipophilic methacrylate monomer containing a pyridyldisulfide (PDS) was evaluated for protein delivery. In this example, a fraction of the PDS units were used for the crosslinking reaction, while the remaining subunits were conjugated with Cys-Arg-Arg-Arg peptide sequences to enhance electrostatic interactions. The resulting nanogels obtained after the assembly allowed the encapsulation of β-galactosidase and small dyes simultaneously for delivery in HeLa cells.[248] An improved modification was constructed by replacing the PDS groups for *p*-nitrophenylcarbonate (NPC). NPC, which is connected to the polymer scaffold through a disulfide moiety, can react with proteins to form carbamates and also with a diamine crosslinker to generate a covalent polymer self-assembled network. The supramolecular

[245] B. M. DeRonde, J. A. Torres, L. M. Minter, G. N. Tew, *Biomacromolecules* **2015**, *16*, 3172–3179.
[246] E. I. Ozay, G. Gonzalez-Perez, J. A. Torres, J. Vijayaraghavan, R. Lawlor, H. L. Sherman, D. T. Garrigan, A. S. Burnside, B. A. Osborne, G. N. Tew, et al., *Mol. Ther.* **2016**, *24*, 2118–2130.
[247] C. M. Backlund, C. R. Hango, L. M. Minter, G. N. Tew, *ACS Appl. Bio Mater.* **2020**, *3*, 180–185.
[248] D. C. González-Toro, J.-H. Ryu, R. T. Chacko, J. Zhuang, S. Thayumanavan, *J. Am. Chem. Soc.* **2012**, *134*, 6964–6967.

covalent assembly is internalized in HeLa cells through endosomes where the reduction of the disulfide bonds results in the carbamate cleavage, releasing the original amines of the proteins. The system was used for the delivery of CytC, RNaseA, lysozyme and GFP.[249]

A special type of polymers are **dendrimers,** spherical macromolecules composed by branched building blocks repetitions. There are dendrimers inspired in the design of PEI polymer such as poly(amidoamine) (PAMAM) dendrimers. As illustrated in the previous case of the PEI polymer, PAMAM dendrimers have also been extensively modified to produce a wide variety of polymers. For example, PAMAM in conjugation with fluoroalkyls and fluoroaromatics moieties delivered proteins *in vitro* such as BSA, β-galactosidase, saporin and cyclic hendecapeptide. Furthermore, an *in vivo* assay showed inhibition of tumor growth in a breast cancer model by saporin/dendrimer complex delivery.[250] Another PAMAM modification included boronic acids, useful recognition ligands for polyphenols. Proteins are associated to polyphenols thanks to the natural affinity of these compounds towards proteins, or by attachment of the polyphenols using dynamic covalent bonds. These protein-polyphenol associations are then complexed by boronic dendrimers allowing cytosolic delivery while maintaining the protein bioactivity after intracellular release. The strategy showed good efficiency for the transport of BSA, Rphycoerythrin, and RNSase A, whose bioactivity after intracellular release was maintained in all cases.[251]

New dendrimers based on 2,2'-Dipicolylamine (DPA),[252] which coordinate Zn^{2+} ions, have transport abilities for proteins with different isoelectric point (pI). The metal ion incorporation provides an enhancement of protein coordination, both with carbonyl groups and amine or imidazole residues. After comparison with other ions such as Cu^{2+}, Mn^{2+}, Fe^{2+}, Ni^{2+}, and Co^{2+} the results confirmed Zn^{2+}as the best metal ion for protein binding. At least 13 protein cargos were tested successfully with DPA Zn^{2+} such as β-Galactosidase, saporin, or RNase A, among others (Figure 29).[252]

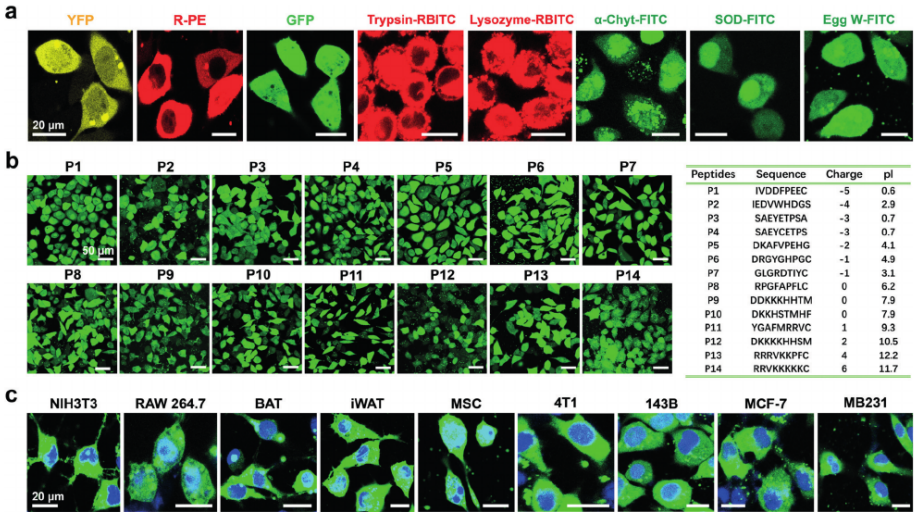

Figure 29. Confocal images of HeLa cells incubated with GD57-Zn^{2+} dendrimer as carrier for cytosolic delivery a) of a collection of proteins b) of a collection of FITC-labelled peptides c) BSA-FITC protein delivery in different cell lines. Scale bars a) 20 μm, b) 50 μm, c) 20 μm. Reproduced with permission from ref[252] Copyright (2020) John Wiley and Sons.

[249] K. Dutta, D. Hu, B. Zhao, A. E. Ribbe, J. Zhuang, S. Thayumanavan, *J. Am. Chem. Soc.* **2017**, *139*, 5676–5679.
[250] J. Lv, B. He, J. Yu, Y. Wang, C. Wang, S. Zhang, H. Wang, J. Hu, Q. Zhang, Y. Cheng, *Biomaterials* **2018**, *182*, 167–175.
[251] C. Liu, W. Shen, B. Li, T. Li, H. Chang, Y. Cheng, *Chem. Mater.* **2019**, *31*, 1956–1965.
[252] L. Ren, J. Lv, H. Wang, Y. Cheng, *Angew. Chemie Int. Ed.* **2020**, *59*, 4711–4719.

1.1.2.3.2 CPPs

Cell penetrating peptides (CPPs) are oligopeptides that stablish multitude of membrane interactions with counterions such lipids phosphates or hydrophobic contacts. Moreover, CPPs can deliver membrane-impermeable bioactive agents.[253,254] For peptide mediated transport of proteins, two strategies have been applied, the covalent attachment or the supramolecular complexation. Regarding covalent functionalization we can find two approaches: the expression of the CPP and the cargo as a fusion protein[255] or the covalent binding between pure proteins and peptides using chemicall reactions. This method allows multiple functionalizations in different positions of the protein.[256]

One of the firsts examples of purified protein cytosolic delivery *in vivo* was in 1999 when Prof. Dowdy fused β-galactosidase protein with TAT CPP[257] and later TAT fused with Cre recombinase enzyme. [258] The fused protein internalized following a macropinocytic pathway, then enzymes escaped from endosomes and showed biological intracellular activity.[257,258] Recent examples of these chimeric macromolecules have been reported, most of them using TAT fragment or octaarginines (R8), for instance: TAT-U1A (RNA binding protein),[259] Dot1l-GFP conjugation,[260] a monoclonal antibody against the Hepatitis B Virus protein HBcAg chemically attached to TAT *in vivo*,[261] fluorescent proteins conjugated with oligoarginines, which are activated for penetration by coiled coils interactions[262] or by click reactions.[263]

In the supramolecular approach multitude of examples have been developed. As previously described, Pep-1 was the first example of supramolecular protein delivery using a CPP. Later methods used modifications of the TAT peptide like dfTAT for the supramolecular delivery of proteins, such as, GFP, Cre recombinase or FITC-Anti-ATP5A antibody (Figure 30A). The structure of the dfTAT peptide is formed by a dimer of two units of tetramethylrhodamine labeled TAT (fTAT), which dimerize by a disulfide bond.[264] The dfTAT peptide enhanced the endosomolytic activity as compared with TAT and its proposed **endosomolytic mechanism** was based on fusion membrane events.[265]

Prof. Futaki has developed new strategies using CPPs for protein delivery by supramolecular complexation. Inspired in the membrane active capabilities of venoms, he proposed variants of venom peptides. [137,24] The modifications consisted in the incorporation of glutamic acids in the hydrophobic face of amphipathic peptide sequences, in order to attenuate

[253] W. L. L. Munyendo, H. Lv, H. Benza-Ingoula, L. D. Baraza, J. Zhou, *Biomolecules* **2012**, *2*, 187–202.
[254] D. W. P. M. Löwik, *ChemBioChem* **2017**, *18*, 2196–2198.
[255] J. Jo, S. Hong, W. Y. Choi, D. R. Lee, *Sci. Rep.* **2014**, *4*, 4378.
[256] M. Zorko, Ü. Langel, *Adv. Drug Deliv. Rev.* **2005**, *57*, 529–545.
[257] S. R. Schwarze, *Science.* **1999**, *285*, 1569–1572.
[258] J. S. Wadia, R. V. Stan, S. F. Dowdy, *Nat. Med.* **2004**, *10*, 310–315.
[259] Y. Miyoshi, M. Kadono, S. Okazaki, A. Nishimura, M. Kitamatsu, K. Watanabe, T. Ohtsuki, *Bioconjug. Chem.* **2020**, *31*, 916–922.
[260] J. Geng, X. Guo, L. Wang, R. Q. Nguyen, F. Wang, C. Liu, H. Wang, *Biomolecules* **2020**, *10*, 217.
[261] Y. Li, Z. Liu, L. Hui, X. Liu, A. Feng, W. Wang, L. Zhang, N. Li, G. Zhou, Q. Wang, et al., *Br. J. Pharmacol.* **2017**, *174*, 2261–2272.
[262] S. A. Bode, I. C. Kruis, H. P. J. H. M. Adams, W. C. Boelens, G. J. M. Pruijn, J. C. M. van Hest, D. W. P. M. Löwik, *ChemBioChem* **2017**, *18*, 185–188.
[263] S. A. Bode, S. B. P. E. Timmermans, S. Eising, S. P. W. van Gemert, K. M. Bonger, D. W. P. M. Löwik, *Chem. Sci.* **2019**, *10*, 701–705.
[264] A. Erazo-Oliveras, K. Najjar, L. Dayani, T.-Y. Wang, G. A. Johnson, J.-P. Pellois, *Nat. Methods* **2014**, *11*, 861–867.
[265] A. Erazo-Oliveras, K. Najjar, D. Truong, T. Y. Wang, D. J. Brock, A. R. Prater, J. P. Pellois, *Cell Chem. Biol.* **2016**, *23*, 598–607.
[137] N. Tamemoto, M. Akishiba, K. Sakamoto, K. Kawano, H. Noguchi, S. Futaki, *Mol. Pharm.* **2020**, *17*, 2175–2185.
[24] M. Akishiba, T. Takeuchi, Y. Kawaguchi, K. Sakamoto, H.-H. Yu, I. Nakase, T. Takatani-Nakase, F. Madani, A. Gräslund, S. Futaki, *Nat. Chem.* **2017**, *9*, 751–761.

the leaky activity of these peptides. At physiological pH, glutamic acid masks the hydrophobicity and decreases membrane interactions. However, when the *en route* acidification of the endosomes reaches an acidic pH of 5, the protonation of Glu reveals the lytic activity of the peptide and the release of bioactive cargos into the cytosol.[137] Following this strategy, M-lycotoxin was modified to afford L17E, where a Leu residue was replaced by a Glu residue. The enhanced amphiphilicity in endosomes leads to the efficient delivery of saporin and Cre recombinase, and antibodies (Figure 30B).[24] Subsequent studies showed that membrane ruffling and transient plasma permeabilization can also contribute as an additional uptake mechanism.[266] The strategy of glutamic mutation for protein delivery was also applied to other peptides such as ponericin, melittin,[137] δ-hemolysin and chrysophsin peptides.[267] Another design based on the transformation of a high cationic peptide into an anionic peptide allowed endosomal disruption for the delivery of a fragment antigen binding (Fab) into the cytosol and nuclei. Mastoparan X peptide (wasp venom) was modified including three glutamic acids in the N-terminus and Ni^{II}-dipicolylamine that enhance the uptake. Therefore, at endosomal pH~5, glutamic acids were protonated unmasking a cationic peptide with leaky membrane interactions for Fab delivery.[268]

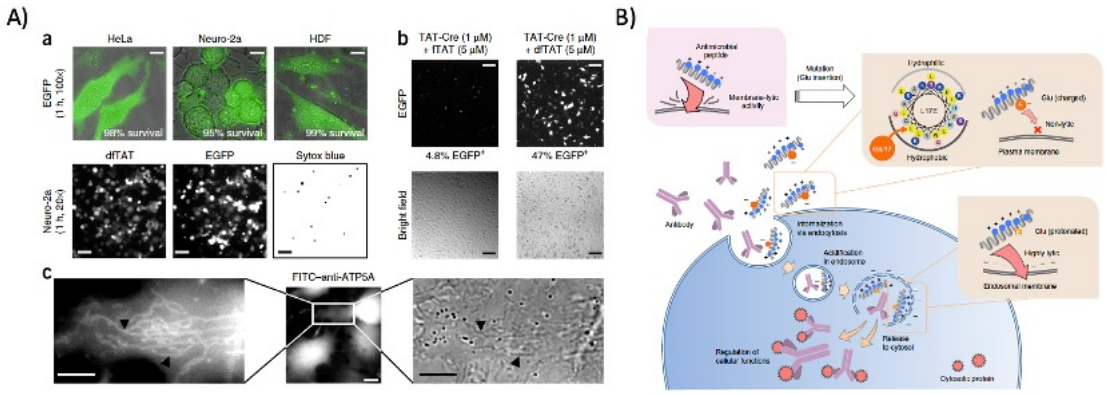

Figure 30. A) (a) EGFP, (b) Cre recombinase and (c) Antibody (FITC-anti-ATP5A) delivery mediated by dfTAT. Reproduced with permission from ref[264] Copyright (2014) Springer Nature. B) Antibody delivery by L17E peptide. Reproduced with permission from ref[24] Copyright (2017) Springer Nature.

To further improve uptake peptide, sequences that promote endocytosis can be used. A new generation of chimeric peptides that include ligands for inducing endosomal uptake were designed. This is the case of SN21 peptide sequence for activation of the CXCR4 macropinocytosis receptor. The combination of SN21 peptide with LK15 endosomolytic peptide sequence leads to the delivery and endosomal release of Cre recombinase enzyme, transcription activator-like effector (TALE) and antibodies.[269]

CPPs containing dynamic bonds such as hydrazones or oximes are promising vectors for the supramolecular delivery of proteins, as they can be formed in fully biocompatible conditions.[123] For instance, the combination of a unique cationic peptide with a wide variety of hydrophobic tails by hydrazone bond formation, has allowed straightforward screening and

[266] M. Akishiba, S. Futaki, *Mol. Pharm.* **2019**, *16*, 2540–2548.
[267] H. Yu, K. Sakamoto, M. Akishiba, N. Tamemoto, H. Hirose, I. Nakase, M. Imanishi, F. Madani, A. Gräslund, S. Futaki, *Pept. Sci.* **2020**, *112*, e24144.
[268] Y. Azuma, H. Imai, Y. Kawaguchi, I. Nakase, H. Kimura, S. Futaki, *Angew. Chemie - Int. Ed.* **2018**, *57*, 12771–12774.
[269] J. V. V. Arafiles, H. Hirose, M. Akishiba, S. Tsuji, M. Imanishi, S. Futaki, *Bioconjug. Chem.* **2020**, *31*, 547–553.
[123] A. Dirksen, S. Dirksen, T. M. Hackeng, P. E. Dawson, *J. Am. Chem. Soc.* **2006**, *128*, 15602–15603.

rapid identification of new formulations for the delivery of the Cas9 RNP enzyme into the cytosol of cells.[78] In a similar strategy, CPPs decorated with hydroxylamines were used for the attachment of protein recognition ligands such as glycans, for the selective recognition and intracellular delivery of lectins.[79] The formation of these hydrazone or oxime bonds is reversible leading to the endosomal escape and subsequent release of the cargo into the cytosol, as they can be hydrolyzed at the endosomal pH. In the supramolecular approach for protein delivery, there are systems based on host-guest interactions such as adamantane and cyclodextrin. For instance, an octaarginine CPP terminated with a cyclodextrin moiety complexed proteins labeled with adamantane for efficient cell uptake and delivery of proteins or antibodies such as GFP, β-galactosidase or IgG. The system transported the cargos by endosomal disruption, although direct translocation was also present as a minor mechanism.[270]

1.1.2.3.3 Lipids

Lipids and liposomes have been applied extensively to the transport of nucleic acids and other cargos. Cationic formulations of liposomes have also been used for the delivery of protein and antibodies. Vesicles composed by the combination of dioleoyl phosphatidylethanolamine (DOPE) and positively charged lipids like bis(guanidinium)-tren-cholesterol (BGTC) lead to the intracellular delivery of β-Galactosidase. The optimized lipid formulation depends on the nature of the protein cargo, as another vesicle system based on aminoglycoside lipid dioleyl succinyl paromomycin (DOSP) associated with an imidazole-based helper lipid (MM27) had to be developed for efficient intracellular transport of anticytokeratin 8 antibody (K8).[271] Liposomes allow synergistic combinations with peptides or glycans to improve cargo delivery. For instance, a vesicle system decorated with peptides, such as octaarginine R8 (for enhancing cell uptake) and GALA (for endosome disruption), was able to get cytosolic distribution of IgG and nuclear membrane labelling with anti-nuclear pore complex (anti-NPC) antibodies.[272] In another example, liposomes decorated with a targeting ligand such as *N*-tosylated glucosamine derivative, are used as specifically recognize Langerhans cells. These liposomes can be loaded with small proteins like BSA and fuse with endosomal membranes in order to deliver BSA into the cytosol.[273]

1.1.2.3.4 Nanoparticles

As described in the previous section, inorganic nanoparticles have been applied as good protein delivery carriers, although there are a few of examples that present endosomal escape abilities. Gold nanoparticles have a great potential as biomacromolecule transport systems. The first designs of Prof. Rotello for protein transport, β-galactosidase, with NPs were mediated by endosomal escape maintaining the biological activity of proteins.[274] Another example, in the delivery of Cas9 enzyme combined with gold nanoparticles and with poly(N-(N-(2-aminoethyl)-2-aminoethyl) aspartamide) (PAsp(DET)), a polymer agent for endosomal disruption.[275] Models based on silica nanoparticles were able to deliver proteins/antibodies such as GFP, RNase A or an antibody anti-phospho-Akt (pAkt). Cargos were adsorbed to

[78] I. Lostalé-Seijo, I. Louzao, M. Juanes, J. Montenegro, *Chem. Sci.* **2017**, *8*, 7923–7931.
[79] M. Juanes, I. Lostalé-Seijo, J. R. Granja, J. Montenegro, *Chem. - A Eur. J.* **2018**, *24*, 10689–10698.
[270] H. Kitagishi, M. Jiromaru, N. Hasegawa, *ACS Appl. Bio Mater.* **2020**, *3*, 4902–4911.
[271] B. Chatin, M. Mével, J. Devallière, L. Dallet, T. Haudebourg, P. Peuziat, T. Colombani, M. Berchel, O. Lambert, A. Edelman, et al., *Mol. Ther. - Nucleic Acids* **2015**, *4*, e244.
[272] Y. Yamada, S. M. V. Perez, M. Tabata, J. Abe, Y. Yasuzaki, H. Harashima, *J. Pharm. Sci.* **2015**, *104*, 2845–2854.
[273] J. Schulze, M. Rentzsch, D. Kim, L. Bellmann, P. Stoitzner, C. Rademacher, *Biochemistry* **2019**, *58*, 2576–2580.
[274] P. Ghosh, X. Yang, R. Arvizo, Z.-J. Zhu, S. S. Agasti, Z. Mo, V. M. Rotello, *J. Am. Chem. Soc.* **2010**, *132*, 2642–2645.
[275] K. Lee, M. Conboy, H. M. Park, F. Jiang, H. J. Kim, M. A. Dewitt, V. A. Mackley, K. Chang, A. Rao, C. Skinner, et al., *Nat. Biomed. Eng.* **2017**, *1*, 889–901.

hydrophobic silica nanoparticles before endosomal escape and cytosolic delivery.[276] Other systems like rough silica nanoparticles (RSN) were able to deliver an antibody against phosphorylated Akt, effectively blocking that protein, which acts as an inhibitor of apoptosis, causing cell death.[277]

1.1.2.3.5 Protein channels

As in the case of direct plasma membrane delivery, there are also natural protein channels operating at the endosomal membrane level. The insertion of protein channels in endosomal bilayers can trigger cytosolic protein delivery. For instance, cytolysins channels as lysteriolysin O (LLO) and perfringolysin O (PFO) form endosomal pores that might be activated by low pH. The transport abilitiy of this pore forming cytolysins was confirmed by the antitumour enhancement when codelivering an immunotoxin consisting on a targeting antibody fused to gelonin with another targeting antibody fused to these proe-formin toxins on *in vivo* xenograft models[23,278]

1.1.2.3.6 Self-delivery methods

There are a few examples of self-delivery and endosomal escape of antibodies. Prof. Y-S Kim and co-workers found an antibody (TMab-4) that was able to escape from endosomes allowing the identification of an endosomal disruptive segment in the variable light chain and its further improvement (YYH to WYW).[186] Then, a second modification of the antibody included the attachment of a RGD10 cyclic peptide that binds to tumor specific integrins, and the substitution of the variable heavy chain for one specific for Ras-GTP binding. The resulting antibody, namely RT11, also showed good *in vivo* anti-tumor activity after intravenous administration.[279] The authors improved the design with new modifications, for instance, in-4 as fusogenic peptide instead of RGD10, and the best endosomal escape sequence previously described (WYW), which improved the *in vivo* activity on this oncogenic Ras antibody (Figure 31A).[279]

Another type of self-delivery methods is based on supercharged proteins, a family of proteins with unusually high net positive or negative charge (Figure 31B).[185] Supercharged proteins are the result of a process of mutagenesis that changes the acidic or basic amino acids on the protein surface. “Supercharged” GFP chimeras have been described with mutations at their surface-exposed residues, resulting in extremely high theoretical net charges ranging from -30 to +48.[185] The super cationic GFP variants are able to penetrate into an array of mammalian cells following an endocytic pathway through the binding to anionic proteoglycans in an energy-dependent manner and clathrin-independent way.[280] Following this strategy, the fusion of supercharged peptide tags to proteins allowed the efficient delivery with low toxicity of different proteins into the nucleus of living cells (Figure 31A).[281] This methodology consists in using K4-tagged (K4 is a supercharged peptide of 120 aa combining A, G, K, P, S, and T with 40 cationic charges) proteins, such as K4-GFP, Cas9-K4, K4-HOXB4 (stimulator of hematopoietic stem cell expansion) or histone 2A-K4 (DNA packaging protein), as it has been shown that K4 increased the cellular uptake thanks to its high-density positive charges.[281]

[276] S. S. Bale, S. J. Kwon, D. A. Shah, A. Banerjee, J. S. Dordick, R. S. Kane, *ACS Nano* **2010**, *4*, 1493–1500.
[277] Y. Niu, M. Yu, J. Zhang, Y. Yang, C. Xu, M. Yeh, E. Taran, J. J. C. Hou, P. P. Gray, C. Yu, *J. Mater. Chem. B* **2015**, *3*, 8477–8485.
[278] C. J. Provoda, E. M. Stier, K.-D. Lee, *J. Biol. Chem.* **2003**, *278*, 35102–35108.
[279] S.-M. Shin, D.-K. Choi, K. Jung, J. Bae, J. Kim, S.-W. Park, K.-H. Song, Y.-S. Kim, *Nat. Commun.* **2017**, *8*, 15090.
[280] J. J. Cronican, D. B. Thompson, K. T. Beier, B. R. McNaughton, C. L. Cepko, D. R. Liu, *ACS Chem. Biol.* **2010**, *5*, 747–752.
[281] J. Yin, Q. Wang, S. Hou, L. Bao, W. Yao, X. Gao, *J. Am. Chem. Soc.* **2018**, *140*, 17234–17240.

Moreover, these supercharged GFP proteins have also been investigated for drug delivery in specific tissues, for instance, for their good penetrating properties in cartilage.[282]

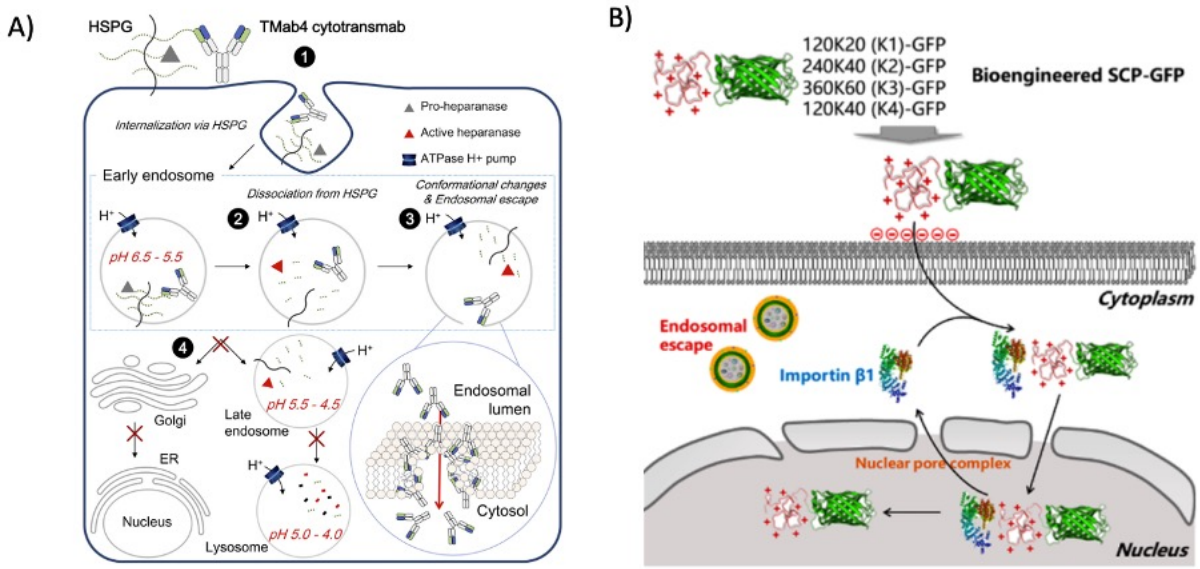

Figure 31. A) Intracellular delivery and endosomal escape of the antibody TMab-4. Reproduced with permission from ref[186]. Copyright (2016), Elsevier. B) Intracellular delivery of GFP using a supercharged polypeptide. Reproduced with permission from ref[281] Copyright (2018) American Chemical Society.

1.2 Intracellular targeting

Fine-tuning of cellular distribution and location at organelle level has been demanding more attention. There are several diseases caused by dysfunctions at the organelle level, like lysosomal or peroxisomal disorders, neurodegenerative, autoimmune and infectious diseases, or even cancer.[138] Intracellular targeting of proteins can be useful for the treatment of this kind of diseases, but it is a challenge, because reaching a specific site inside the cell such as the nucleus or the mitochondria is a difficult task. The identification of particular cell targeting moieties such as small molecules or peptide sequences is key to ensure subcellular delivery of payloads. (*e.g.,* Triphenylphosphonium (TTP), mitochondrial targeting sequence (MTS),[283] mitochondria penetrating peptide (MPP), nuclear localization sequence (NLS), nucleolar localization sequence (NOLS), lysosomal targeting moiety (LTM)).[284,285,138]

There are a high number of lysosomal storage diseases (LSDs) to be treated or corrected by functional proteins, where many of them present an acidic nature, i.e., low isoelectric points (pI). One example of these LSDs is Gaucher disease, a disorder caused by the lack of functionality of β-glucocerebrosidase (GBA).[286] In this example, GBA is fused to an exosome-anchoring protein, the vesicular stomatitis virus glycoprotein (VSVG), and a GFP protein for

[282] Y. Krishnan, H. A. Rees, C. P. Rossitto, S.-E. Kim, H.-H. K. Hung, E. H. Frank, B. D. Olsen, D. R. Liu, P. T. Hammond, A. J. Grodzinsky, *Biomaterials* **2018**, *183*, 218–233.
[138] Ü. Langel, *CPP, Cell-Penetrating Peptides*, Springer Singapore, Singapore, **2019**.
[283] R. Lin, P. Zhang, A. G. Cheetham, J. Walston, P. Abadir, H. Cui, *Bioconjug. Chem.* **2015**, *26*, 71–77.
[284] S. N. Sugiman-Marangos, G. L. Beilhartz, X. Zhao, D. Zhou, R. Hua, P. K. Kim, J. M. Rini, B. A. Minassian, R. A. Melnyk, *Sci. Adv.* **2020**, *6*, eabb0385.
[285] A. Parodi, C. Corbo, A. Cevenini, R. Molinaro, R. Palomba, L. Pandolfi, M. Agostini, F. Salvatore, E. Tasciotti, *Nanomedicine* **2015**, *10*, 1923–1940.
[286] M. A. Do, D. Levy, A. Brown, G. Marriott, B. Lu, *Sci. Rep.* **2019**, *9*, 17274.

fluorescent signaling. The GBA loaded exosomes internalized in cells and remained bound to the exosomal membrane during endosomal maturation until they reached the lysosomes, where they displayed a correct enzymatic activity (Figure 32).[286] Another example of LSD is the Batten disease, which is caused by the malfunction of the enzyme tripeptidyl peptidase-1 (TPP1).[284] This TPP1 fused with a receptor-binding fragment of diphtheria toxin as lysosomal targeting moiety (LTM) reached the lysosome for enzymatic replacement. The chimera TPP1-LTM showed enzymatic activity after cellular uptake on *in vitro* and *in vivo* assays.[284] Fabry's disease (FD) is another example of LSD, whose treatment is based on enzyme replacement using α-galactosidase A (GLA). The vehicle used for the transport of GLA was a cationic cell-penetrating peptide based on polylysine-polyhistidine (K10H16). The peptide vehicle complexated with GLA due to the low pI of the protein, and showed good transport activity and a restorative effect on proliferation on GLA-defficient cells.[287]

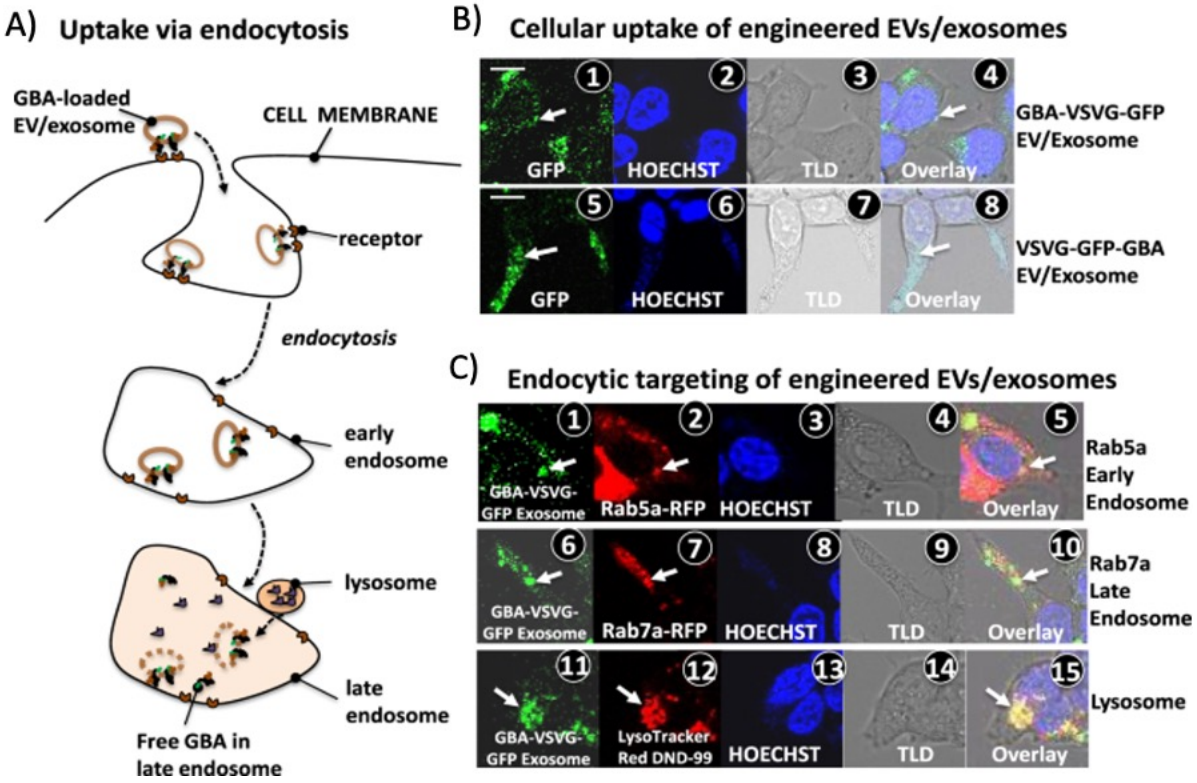

Figure 32. A) Schematic illustration of the delivery of GBA by endocytosis B) Endosomal localization of the exososomes loaded with GBA-VSVG-GFP or VSVG-GFP-GBA in HEK 293 cells C) Colocalization assay between GBA-VSVG-GFP and labeling early endosomes (Rab5a), late endosomes (Rab7a) or lysosomes. Scale bar: 10 μm. Reproduced with permission from ref[286] Copyright (2019) Springer Nature.

Mitochondrial targeting is a challenging task because a multitude of diseases are caused by mitochondrial disfunctions. An example of this is propionic acidemia, which is caused by a deficiency of propionyl coenzyme-A carboxylase (PCC).[288] The fusion of PCC with a CPP, like TAT peptide labeled with a mitochondria-targeting sequence (MTS), is able to restore the correct enzymatic activity in mitochondria.[288] Parkinson's disease (PD) is another well-known mitochondrial dysfunction disorder that can be inhibited with Parkin protein through the

[287] T. Iwasaki, N. Murakami, T. Kawano, *Biochem. Biophys. Res. Commun.* **2020**, *533*, 905–912.
[288] M. Darvish-Damavandi, H. K. Ho, T. S. Kang, *Mol. Genet. Metab. Reports* **2016**, *8*, 51–60.

removal of damaged mitochondria and the removal of α-synuclein and other protein aggregates. A new cell permeable Parkin protein (iCP-Parkin) with enhanced solubility and optimized intracellular delivery, can address Parkinson's disease.[289] This new Parkin protein incorporates a macromolecule transduction domain (MTD) in order to increase the cellular uptake, and a solubilization domain (SD) attached to the native form. The resulting iCP-Parkin protein was called MTD524-Parkin-SDB and showed mitochondrial localization *in vitro*. After systemic administration in mice, the protein was distributed throughout the entire body, including the brain, indicating that the iCP-Parkin protein is able to cross the Blood-Brain Barrier (BBB). The administration of the iCP-Parkin protein drug promoted mitophagy, a beneficial feature that increased mitochondrial biogenesis and removed the accumulation of the harmful α-synuclein.[289]

The synthesis and design of new carriers to target mitochondria is key to treat site-localized dysfunctions. Nanoparticle carriers can be decorated, for example, with triphenylphosphonium (TPP) for targeting mitochondria (Figure 33).[290] In this example, biodegradable silica nanoparticles decorated with a cell-penetrating poly(disulfides) (CPD) and TPP, as a mitochondrial targeting moiety, are used to trigger nanoparticle disassembly at the cytosol by glutathione effect and release of the encapsulated proteins. This nanocarrier displays mitochondria-targeting of native proteins and antibodies, such as BSA, MAO-A, or a CytC oxidase subunit 2 antibody. [290]

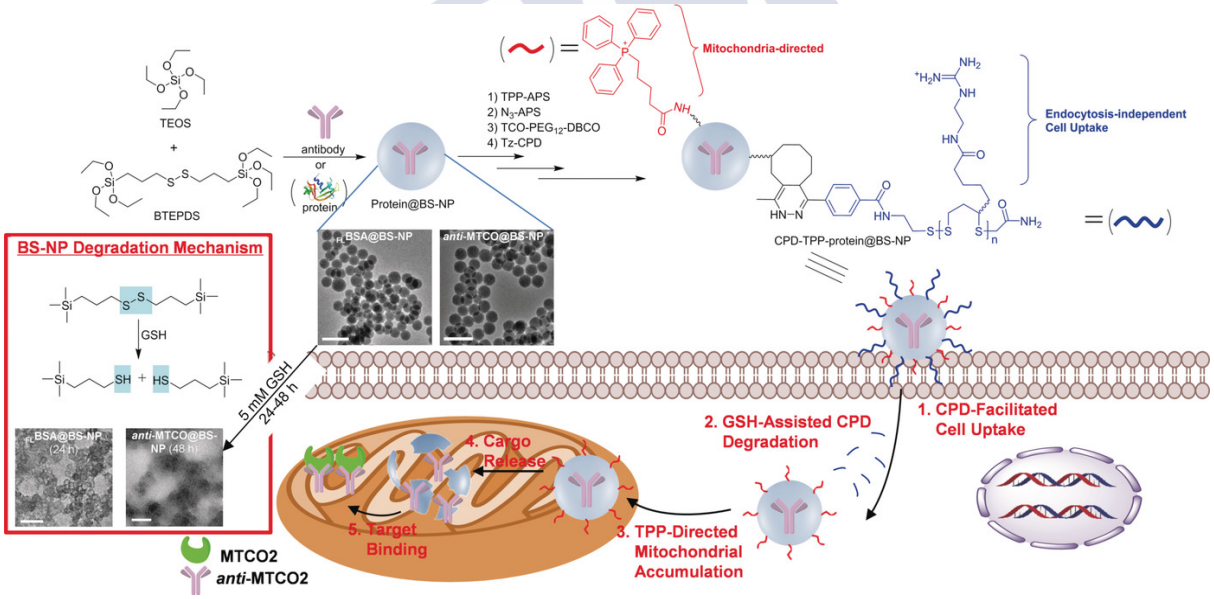

Figure 33. Preparation of cell-permeable CPD-TPP-protein@BS-NPs Cellular uptake, bypassing endocytosis, and mitochondrial targeting. Reproduced with permission from ref[290] Copyright (2019) John Wiley and sons.

Computational methods allow the design of new carriers. An example that demonstrates the utility of this technique was the design of cell-penetrating artificial mitochondria-targeting peptide (CAMP).[291] In addition, the authors confirmed the utility of the designed peptide by *in vitro* and *in vivo* experiments. The result of conjugating CAMP peptide with proteins (i.e. GFP,

[289] E. Chung, Y. Choi, J. Park, W. Nah, J. Park, Y. Jung, J. Lee, H. Lee, S. Park, S. Hwang, et al., *Sci. Adv.* **2020**, *6*, eaba1193.
[290] P. Yuan, X. Mao, X. Wu, S. S. Liew, L. Li, S. Q. Yao, *Angew. Chemie Int. Ed.* **2019**, *58*, 7657–7661.
[291] Y. C. Kang, M. Son, S. Kang, S. Im, Y. Piao, K. S. Lim, M.-Y. Song, K.-S. Park, Y.-H. Kim, Y. K. Pak, *Exp. Mol. Med.* **2018**, *50*, 1–13.

or antioxidant protein human metallothionein 1A, hMT1A) showed colocalization and restoration of mitochondrial activity *in vitro* and therapeutic effect on *in vivo* models of Parkinson's disease. Instead of delivering proteins into the mitochondria for therapeutic purposes, the possibility of organelle replacement to restore enzymatic function has been reported. In this regard, the delivery of exogenous mitochondria was possible by means of Pep-1 carrier. In this example the delivery of healthy donor mitochondria induces recovery of mitochondrial normal functions.[292]

USC UNIVERSIDADE DE SANTIAGO DE COMPOSTELA

[292] J.-C. Chang, F. Hoel, K.-H. Liu, Y.-H. Wei, F.-C. Cheng, S.-J. Kuo, K. J. Tronstad, C.-S. Liu, *Sci. Rep.* **2017**, *7*, 10710.

2. Objectives

USC
UNIVERSIDADE
DE SANTIAGO
DE COMPOSTELA

Biomacromolecular drugs such as proteins and antibodies have showed limited cellular internalization due to endocytic entrapment. If during internalization these drugs are trapped in endosomes, they will be degraded or exocytosed. This situation can be controlled if the drug transport is mediated by an exogenous vehicle. Peptides are a type of carriers with good potential as membrane transporters. By knowing the supramolecular behavior of a peptide vehicle to self-assemble into membranes, the cytosolic release of drugs might be controlled (Figure 34). In this chapter of the thesis we aimed to:

1. Design and synthesize a set of oligoalanines peptides **MP1**, **MP2** and **P3** following the principles proposed in chapter 2.

2. Study the helical folding of the structures in different environments such as aqueous buffer, lipids or TFE.

3. Carry out the physicochemical characterization of **MP1** peptide in presence of artificial membrane systems such as Large Unilamellar Vesicles (LUVs).

4. Test macromolecular delivery abilities of the oligoalanines **MP1**, **MP2** and **P3** and correlate the results with the helical folding.

5. Study the behaviour of **MP1** peptide by computational simulations in order to predict the conditions of the supramolecular assembly and elaborate a hypothesis about the mechanism of action.

6. Evaluate the mechanism of action and the potential formation of a dynamic supramolecular pore by experiments with artificial vesicles LUVs, planar membranes (BLM).

7. Test the potential extension of peptide transport to the macromolecular cytosolic delivery in different cell lines and with different functional assays, employing different cargos (saporin, Cre-recombinase, GST-NLS-GFP, antibodies).

8. Carry out a final evaluation for potential antibody delivery in living tissue (*ex vivo*) such as in murine cornea.

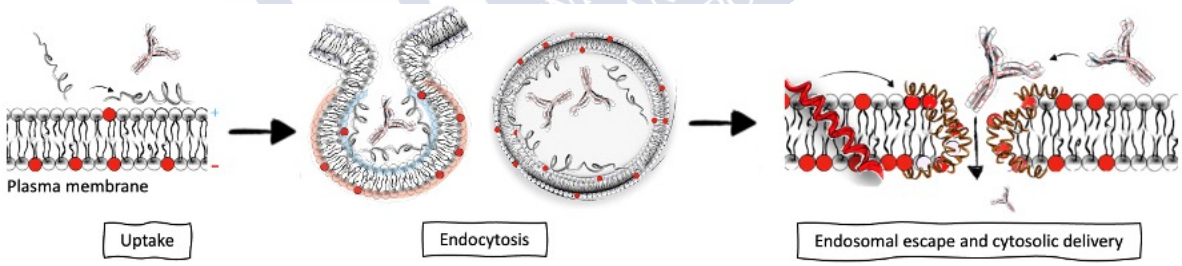

Figure 34. Scheme for antibody and CPP uptake by endocytosis, enchanced peptide folding and membrane permeation for release into the cytosol.

USC
UNIVERSIDADE
DE SANTIAGO
DE COMPOSTELA

3. Results: Short oligoalanine helical peptides for supramolecular nanopore assembly and protein cytosolic delivery

The results of this chapter were originally published 2021 in *RSC Chemical Biology* as:

M. Pazo,[a] G. Salluce,[a] I. Lostalé-Seijo,[a] M. Juanes,[a] F. Gonzalez,[b,c] R. Garcia-Fandiño [a] and J. Montenegro [a] "Short oligoalanine helical peptides for supramolecular nanopore assembly and protein cytosolic delivery" RSC Chem. Biol. **2**, 503–512, 2021, doi: 10.1039/D0CB00103A

https://pubs.rsc.org/en/content/articlelanding/2021/CB/D0CB00103A#!divAbstract

Affiliations:

[a]*Centro Singular de Investigación en Química Biolóxica e Materiais Moleculares (CIQUS), Departamento de Química Orgánica, Universidade de Santiago de Compostela, 15782 Santiago de Compostela, Spain Email: javier.montenegro@usc.es*

[b]*Centro Singular de Investigación en Medicina Molecular y Enfermedades Crónicas (CIMUS), Universidade de Santiago de Compostela, Santiago de Compostela, Spain*

[c]*Instituto de Investigación Sanitaria de Santiago de Compostela (IDIS) and Service of Ophthalmology, Complejo Hospitalario Universitario de Santiago, 15706 Santiago de Compostela*, Spain

Copytights:

This article is licensed under a Creative Commons Attribution-NonCommercial 3.0 Unported Licence. Copyright © 2021, Rights managed by Royal Society of Chemistry. Material from this article can be used in other publications provided that the correct acknowledgement is given with the reproduced material and it is not used for commercial purposes.

Contributions:

Synthesis characterization of the peptides, physicochemical characterization in artificial membrane models. Collaboration in biological assays of dextran transport and cellular toxicity.

USC
UNIVERSIDADE
DE SANTIAGO
DE COMPOSTELA

4. Conclusions

USC
UNIVERSIDADE
DE SANTIAGO
DE COMPOSTELA

In this chapter, we have studied the supramolecular assembly properties of an oligoalanine peptide and its interaction with the membrane of vesicles and living cells. We demonstrated the potential of this peptide for the delivery and release of numerous macromolecules with biological function. We could conclude that the enhancement of peptide helicity in the presence of anionic lipids allowed the assembly of a supramolecular nanopore for the cytosolic release of giant cargos.

1. The **MP1** peptide showed a stronger helical behaviour in lipids than aqueous buffer. The extension of the **MP1** peptide length, with an extra turn in the heptad **P3**, further increased the helicity both in aqueous and lipid media but caused cellular toxicity. While **MP2**, a prototypical peptide with the opposite helical behaviour (lower in lipids than aqueous buffer) did not improve delivery.

2. Initial protein delivery activity of these three peptides **MP1**, **MP2** and **P3,** together with **R8** and **GALA** controls were evaluated with the saporin assay. This study showed that **MP1** had the best delivery efficiency while maintaining a good cellular viability in the control without saporin.

3. The physicochemical characterization of **MP1** peptide also confirmed an enhanced affinity for anionic membranes of LUVs and an increasing helicity of **MP1** peptide in the presence of anionic vesicles.

4. FRET studies using donor and acceptors placed on the peptides or in the peptide and lipids, confirmed the orientation of the leucine residues to the inner side of the membrane leaflet.

5. Efficient release of fluorescent cargoes (fluorophores and polymers) by MP1 was confirmed in vesicle assays.

6. The supramolecular nanopore assembly of **MP1** predicted by molecular dynamics simulations, was confirmed by gating experiments in LUVs⊃ANTS/DPX and dextran release in LUVs⊃Dextran.

7. Planar membrane (BLM) recordings experiments also confirmed the presence of a pore showing activity events, which could remain for several seconds in the opened state.

8. BLM experiments allowed the measurement of the pore size, which corresponded to a diameter around 3.16 nm and 4.4 nm.

9. Cytosolic release of different giant cargos such as dextran of different sizes was confirmed in various cell lines.

10. The cytosolic release of dextran was dependent on an endocytic uptake, as it was reduced by inhibition of macropinocytosis or dynamin-dependent pathways.

11. We also observed that after endosomal release of the cargo, **MP1** remains associated with endosomes. This effect was proved after observation of the colocalization of **MP1** with lysotracker.

12. These results were consistent with an assembly at the endosomal membrane and nanopore transport mechanism. In addition, plasma membrane ruffling could also trigger cytosolic release.

13. Cre recombinase was also efficiently delivered as shown by by the use of cells expressing a Cre reporter, and the efficiency achieved by MP1 was higher compared to state-of-the-art controls **R8**, **GALA**, **L17E**, **Pep-1** and **dfTAT**.

14. We demonstrate the **MP1** potential for antibody delivery using fluorescent Immunoglobulin G (IgG) and a monoclonal antibody against the nuclear pore complex (Mab414). Experiments with Mab414 were carried out in HeLa cells and ARPE-19 cells, and in tissues, as *ex vivo* murine cornea.

USC
UNIVERSIDADE
DE SANTIAGO
DE COMPOSTELA

General discussion

USC
UNIVERSIDADE
DE SANTIAGO
DE COMPOSTELA

This general discussion includes an extension of the experiments presented in the articles and other new experiments, which do not appear in the articles but were performed during the thesis.

Chapter 1

The plasma membrane is the basic barrier for compartmentalizing, protecting the interior of the cell and regulating the entry of exogenous molecules. The molecules that can be internalized into cells follow different routes. Some by a natural cellular process (activation of membrane proteins, channels or endocytosis) or by simple diffusion across the membrane. However, other microorganisms, such as viruses, can penetrate cells and introduce their genetic material inside them. About 30 years ago, the transactivator of transcription domain Tat was discovered for spontaneously tranlocating across the membrane of living cells. The minimal domain, composed of a 12-aa peptide sequence, was isolated, and new area of cell penetrating peptides (CPPs) was initiated. The characterization of these new CPP sequences prompted the development of new techniques, such as artificial membrane models. One of the most widely used models due to their simplicity and robustness are LUVs, which allow the encapsulation of different fluorescent probes. These techniques allowed the measurement of the transport by CPPs or even to detect DNA transport with CPP carriers.

Dynamic chemical bonds can be employed to create new CPP libraries without synthetic effort. These dynamic bonds include hydrazones, oximes or disulfides. These bonds present two essential advantages. On the one hand, the synthetic advantage that leads to the final product in short times, with good yields, without side reactions and they also are compatible with aqueous media. On the other hand, these bonds respond to external stimuli, i.e. they hydrolyze depending on the conditions under which they are during a cell internalization pathway. In our research group, a methodology to include reactive motifs in CPPs during solid-phase peptide synthesis (SPPS) was developed. The strategy consisted in an amide coupling reactions between the amine residue of a lysine and a commercial acid, which contains an alkoxy amine protected by boc (boc aminooxy acetic acid). For this purpose, in SPPS elongation we included a lysine with methyltrityl (Mtt) protecting group that is labile to the soft acid condition. This allowed us an orthogonal deprotection (DCM/HFIP/TFE/TIS; 6.5:2:1:0.5) and a subsequent boc aminooxy amide coupling (Figure 35).

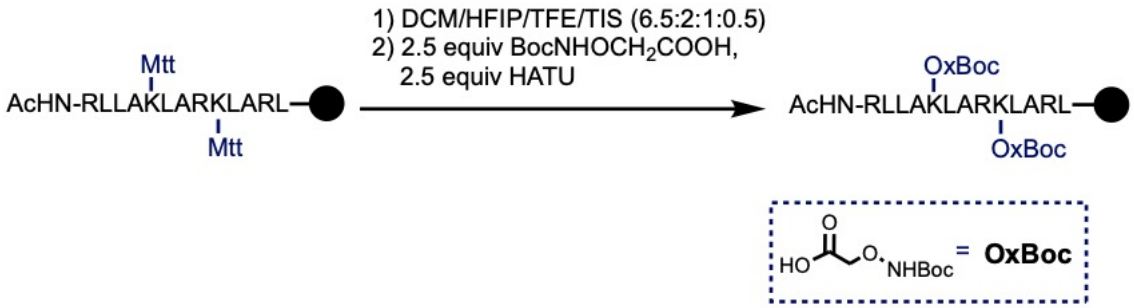

Figure 35. Scheme of orthogonal Mtt deprotection and Boc-alckoxyamione coupling in solid phase.

The possibility of including the dynamic connectors during SPPS allowed us to build a small library of synthetic CPPs from a single peptide design. Our aim was to determine the critical relationships between the structure and activity of these CPPs after modifications of these chemical bonds. To this purpose, an initial peptide sequence was reacted in the presence of different aldehydes to give rise to a small library of peptide amphiphiles. In this first chapter

of the thesis, several proof-of-concept experiments on transport in both vesicles and cells were carried out to compare the transport properties of the different peptide amphiphiles.

For the parent peptide design, we chose an amphiphilic pro-helical initial structure. The amphiphilicity was implemented by the segregation of the hydrophobic and hydrophilic amino acids into two different domains of an α-helix. At the interface of both domains, reactive alkoxyamine motifs were included, which react with aldehydes (hydrophobic and cationic) to give the final amphiphiles. The inclusion of the alkoxyamines at the interface of both domains allows the modulation of the structure without disturbing the amphipathic character (Figure 36B). The sequence was based on two heptads and three helical turns composed by three arginines (providing the cationic charge), two lysines (used to anchor alkoxyamines), five leucines (as stronger hydrophobic moiety for lipid interactions) and three alanines (as soft hydrophobic moiety that stabilizes helicity). To obtain an amphipathic sequence, a distribution pattern is used for the cationic residues, in this case: (i, i+3), (i, i+4) (Figure 36A). The synthetic structure is finished by acetylating the N-terminus (Ac) and purification by reverse phase HPLC. The secondary structure of the parent peptide **AcP(Ox)$_2$** was studied by circular dichroism (CD) experiments showing the two characteristic bands at 208 nm and 222 nm of the α-helix. In addition, it was possible to quantify the helical content in percentage, obtaining 15 % in aqueous buffer and 35 % helical content in TFE solvent measured at 10°C. This helical character was maintained even at high temperatures (Figure 36C).

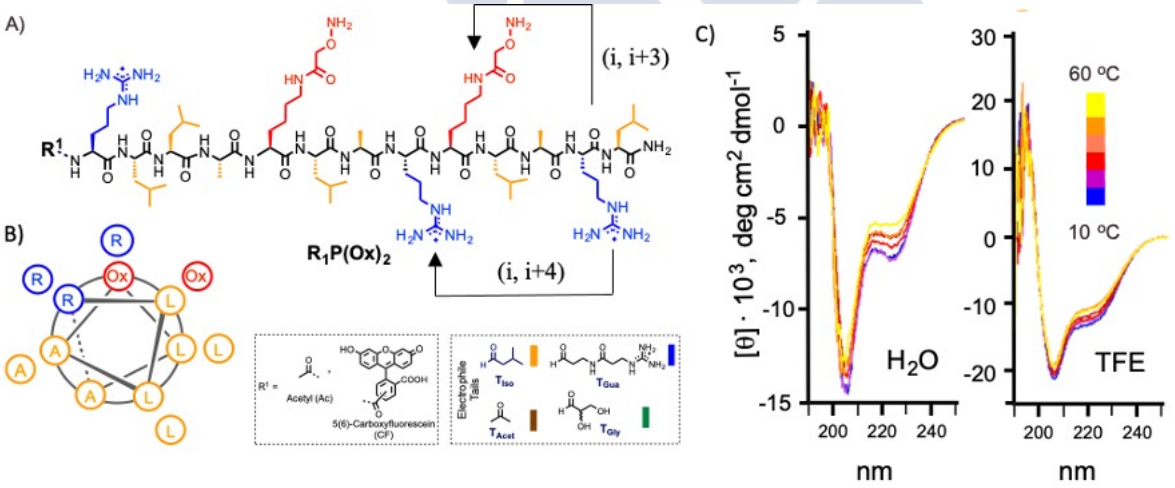

Figure 36. A) Peptide structure with the repetition patterns (i, i+3) and (i, i+4). B) Zenital view of peptide in a heptad representation. C) Circular dichroism spectra at different temperatures. Adapted with permission from *Synlett* **2017**, *28*, 924–928.

We carried out the derivatization of parent peptide **AcP(Ox)$_2$** with different aldehydes. To choose aldehydes that could improve transport. We selected different molecules such as isovaleraldehyde that could mimic a leucine and that showed good transport capacities in vesicles transport assays.[100] We also selected a synthetic guanidinium aldehyde as a suitable cationic tail. Both aldehydes were studied in our research group with excellent results for DNA transport in vesicles and siRNA transfection *in vitro*.[100] T_{Gua} (guanidinium aldehye) and T_{Iso} (isovaleraldehyde) were reacted with the parent peptide **AcP(Ox)$_2$** (under 60°C conditions, to

[100]J. M. Priegue, D. N. Crisan, J. Martínez-Costas, J. R. Granja, F. Fernandez-Trillo, J. Montenegro, *Angew. Chemie Int. Ed.* **2016**, *55*, 7492–7495.

favor unfolding, and in a H_2O/DMSO/AcOH 1:1:0.5 medium) to give rise to the final amphiphiles.

To evaluate the internalization and transport capacity of the new peptide amphiphiles we performed experiments on model membranes such as LUVs. These artificial systems allow us to characterize the transport of a short double-stranded DNA sequence (herring DNA, <50 base pairs). To prepare unilamellar large vesicles LUVs, we used the egg yolk phosphatidylcholine (EYPC) lipids loaded with an anionic fluorophore 8-hydroxy-1,3,6-pyrenetrisulfonate (HPTS) and a cationic quencher p-xylene-bis-pyridinium bromide (DPX). Intravesicular concentrations of the fluorophore and quencher are optimized to set the LUVs⊃HPTS/DPX in a resting state of minimal fluorescent emission. To perform the transport assays, three sequential additions of peptide, DNA and detergent are made to the vesicles while collecting the HPTS fluorescence emission kinetics. The first addition at t = 25s is the peptide amphiphile, which should not alter the fluorescence unless it causes damage to the membrane. Then, at t = 50s, we added the anionic DNA and if the previously added peptide can transport the DNA, an increase in fluorescence will be observed due to the DPX quencher export to extravesicular media (Figure 37A). Finally, at t = 225 s we added a strong detergent such as Triton-X-100 that releases all the vesicular contents and allow the normalization the fluorescence data (Figure 37B). The normalized transport kinetics showed absence of DNA transport for the parent peptide **AcP(Ox)$_2$** and its modification with isovaleraldehyde tail, **AcP(T$_{Iso}$)$_2$**. On the other hand, the cationic **AcP(T$_{Gua}$)$_2$** showed optimal transport activity for DNA in vesicles, as shown by the 50% transport observed at 5nM of the peptide amphiphile. Moreover, this amphiphile did not show any efflux of HPTS/DPX prior to DNA addition, indicating that it maintains membrane integrity (Figure 37).

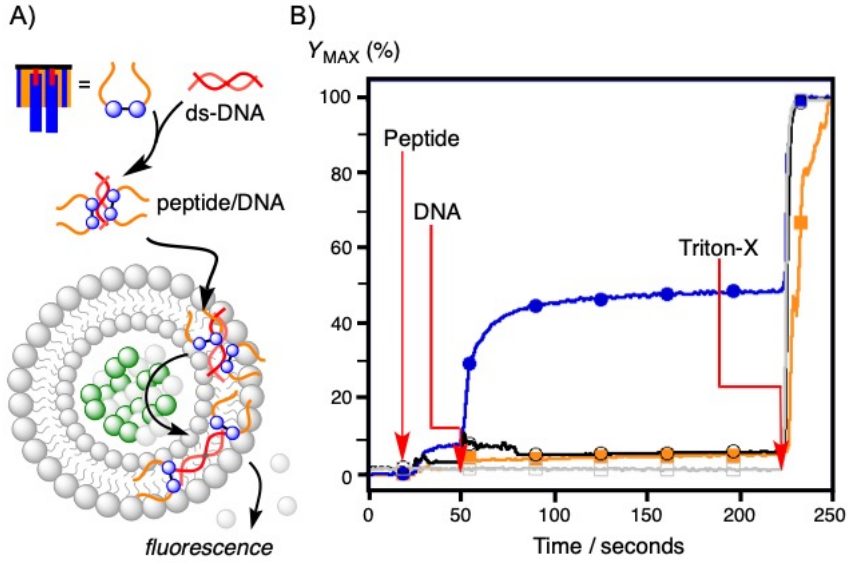

Figure 37. A) Schematic representation of of the LUVs fluorescence assay to detect DNA transport by amphiphiles. B) Normalized HPTS fluorescence in kinetics of DNA (Herring DNA, <50 bp, t= 50 s) transport mediated by amphiphiles (5nM, t=25 s) and Triton-X-100 (7.5 μM, t = 225 s) **AcP(T$_{Gua}$)$_2$** in blue, **AcP(Ox)$_2$** in black, **AcP(T$_{Iso}$)$_2$** in orange and control experiment in gray. Reproduced with permission from *Synlett* **2017**, *28*, 924–928.

Once we concluded with the transport results in artificial membrane models, we decided to test the peptide effect in living cells. In order to visualize the peptide inside the cell and evaluate its capacity to cross the cell membrane, the peptide was labelled with a fluorescent probe, Carboxyfluorescein (CF), by a simple amide coupling. However, this fluorescent parent

peptide was not stable in solution over time and it was necessary to carry out the oxime bond formation with aldehydes immediately after resin cleavage. For this reason, it was not possible to perform cell assays with the **CFP(Ox)$_2$** parent peptide. The aldehyde tails selected were guanidium aldehyde, acetone and glyceraldehyde (**T$_{Gua}$**, **T$_{Acet}$** and **T$_{Gly}$**). Acetone (**T$_{Acet}$**) is hydrophobic as T$_{Iso}$ and would increase the cell penetration and glyceraldehyde (**T$_{Gly}$**) is the simplest glycan like moiety would display uncharged hydrophilic saccharide residue. Finally, we selected octaarginine also labelled with CF (**R$_8$**) as control peptide.

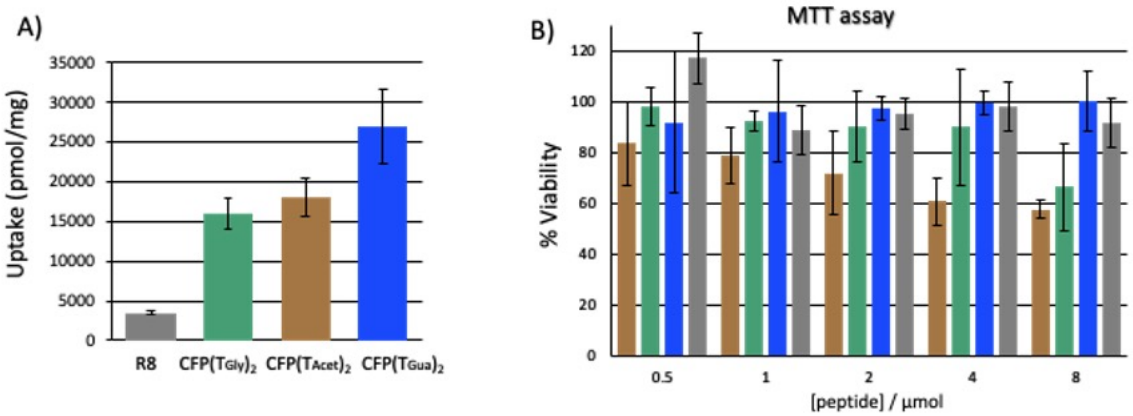

Figure 38. A) Fluorometry quantification of the uptake of the peptides in HeLa cells (amphiphiles incubated for 30 min at 4 µM in HKR buffer). After incubation cells were washed, trypsinized, lysed and the amount of peptide determined by fluorescence measurements comparing with a calibration curve. Values were normalized to protein contents of the cells, quantified by Bradford method. B) Cell viability (MTT assay). Error bars indicate SD of three replicates. Reproduced with permission from *Synlett* **2017**, *28*, 924–928.

After purification of the fluorescent amphiphiles we carried out uptake quantification experiments. Cell incubations revealed that all three compounds were internalized to a higher extent than the control peptide octaarginine **R$_8$** (Figure 38A). Furthermore, we found that the highest internalization of the series was for **CFP(T$_{Gua}$)$_2$**, which is in consonance with DNA transport in LUVs. On the other hand, we also performed cell viability assays following the colorimetric reduction of 3-(4,5-dimethylthiazol-2-yl)-2,5-diphenyltetrazolium bromide to formazan (MTT assay). This assay showed the best viability for the case of **CFP(T$_{Gua}$)$_2$**, confirming that the cationic enhancement improved uptake and viability. However, increasing hydrophobicity with **CFP(T$_{Acet}$)$_2$**, showed a significant reduction in viability (Figure 38B). This result is in agreement with the proposed disruptions of the plasma membrane during uptake of the hydrophobic peptide.

The three fluorescently labelled peptide amphiphiles were also studied in living cells by inverted epifluorescent microscopy. We could visualize the internalization on *in vitro* assays at 4 µM and the micrographs displayed different behavior for each peptide (Figure 39A). The control peptide (**R$_8$**) showed a punctate and cytoplasmic intracellular distribution, typical of the combination of membrane translocation and endocytosis mechanism (Figure 39A). A similar distribution was observed for **CFP(T$_{Gly}$)$_2$** although the punctate aggregates seem to increase in size. Finally, cytoplasmatic distributions were observed for **CFP(T$_{Acet}$)$_2$** and more intense for **CFP(T$_{Gua}$)$_2$**. The punctate pattern is usually indicative of endocytosis (Figure 39A). Therefore, we decided to confirm the endosomal uptake mechanism by colocalization with LysoTracker Deep Red after 3 h incubation. The results displayed peptide-lysosome colocalization for **R$_8$**

and **CFP(T_{Gly})$_2$** (Figure 39B). The signal in the cytoplasm for **CFP(T_{Gua})$_2$** and **CFP(T_{Acet})$_2$** was too intense that it saturated the cell image. Therefore, the concentration was reduced to 2μM and the pattern of **CFP(T_{Gua})$_2$** internalization was similar to the R_8 control, showing lysotracker colocalization and certain cytosolic distribution. This slight change in behavior is understandable because the mechanism of uptake is also concentration dependent. Nevertheless, **CFP(T_{Acet})$_2$** still showed a cytosolic distribution, suggesting a direct translocation mechanism across the membrane for this very hydrophobic and also toxic peptide amphiphile (Figure 39C).

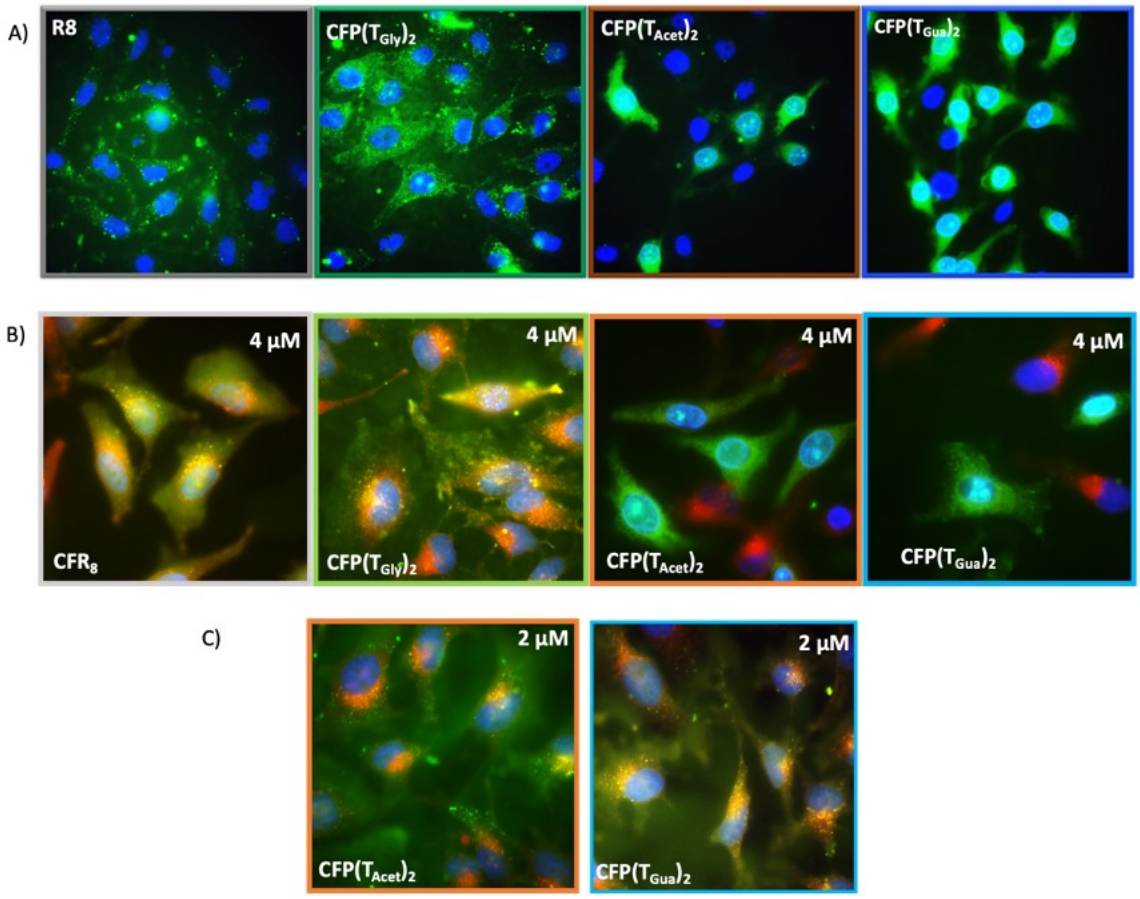

Figure 39. A) Epifluorescence images at 4 μM of petide with the three CF labeled amphiphiles **CFP(T_{Gua}),** (blue border) **CFP(T_{Acet})$_2$** (brown border), **CFP(T_{Gly})$_2$** (green border), and **R8** control (gray border), 30 min incubated over Hela cells. Amphiphiles are shown in green, nuclei in blue B) Epifluorescence pics of a colocalization study between amphiphiles (green) and lysotracker, 3h after peptide incubation) at 4μM for every amphiphile and C) repeated at 2μM for CFP(T_{Acet})$_2$ and CFP(T_{Gua})$_2$. Reproduced with permission from *Synlett* **2017**, *28*, 924–928.

One of the most important conclusions drawn from this work is the importance of the hydrophobic/hydrophilic ratio (5/5 in this particular case) to maintain good viability and uptake. The peptide designs of the following **chapter 2** have this characteristic in common.

Chapter 2

During the progress of chapter 2, we addressed the development of a peptide library, based on oligoalanines peptide scaffold, by the systematic substitution of certain amino acids of the peptide sequence. Penetrating peptides designs have evolved over time to cover and generate new structures with improved functions. In this regard, chemists have employed peptides that adopt secondary structures such as α helices and study them as amphiphilic cell penetrating peptides (CPPs). However, understanding these designs is a challenging task because even short sequences can afford a large number of potential sequences combining natural amino acids. Uncountable permutations are possible between basic and hydrophobic residues, which is a limitation for drawing simple conclusions about the activity of cell penetrating peptides (CPPs).

In this chapter 2, we proposed to use helical sequences of oligoalanines of 16 amino acids including 3 leucines and 3 arginines. A systematic permutation of amino acids allowed us to study the helical folding in different environments, the cellular internalization and the cytotoxicity. We propose that the control of the folding of peptides into membranes could control assembly of this peptide and, at the same time, help us to extract activity conclusions for the transport across membranes. The peptide designs that we proposed in chapter 2 are based on a parent sequence of oligoalanines. The chosen length was taken from Prof. Baldwin's[150] designs (16aa), which are similar in length to the Tat peptide and include two heptad helical turns. Prof. Baldwin's proposed peptides that were based on oligoalanines that stabilized their helicity in water and three hydrophilic motifs to enable solubility in aqueous media. We also selected alanines as the peptide backbone because of the helical stabilizing character (0.77 kcal/mol) of the alanine amino acid. The hydrophobic amino acid selected in our designs was leucine, as we did in the previous chapter. In addition, Leu is also an alpha-helix stabilizer, and can be oriented towards the inner or the surface side of membranes. Finally, we selected arginines as a cationic element because of their full protonation at physiological pH. Moreover, arginine has a helical stabilizing character and a side chain long enough to be embedded in the membrane and facilitate assembly in lipid environments. The number and the position of arginines as well as their orientation were inspired by Prof. Dowdy's work that showed an excellent cell penetrating capacity of shorter TAT analogues with only 3 Arginines.[76]

The synthesis of this small peptide library was carried out by solid-phase peptide synthesis (SPPS) and terminated with a fluorescent probe, 5-carboxytetramethylrhodamine (TAMRA). During the synthesis of all compounds, we observed a solubility/aggregation problem that made us change the resin type (polystyrene-based) during SPPS to PEG-based ChemMatrix resin. In addition, we also had to perform size exclusion chromatography prior to HPLC purification of the peptides to remove the excess of the non-reacted fluorescent probe.

After HPLC purification, we characterized the helical folding properties of the different peptides. For this purpose, we used CD circular dichroism by placing the peptide in three different media: aqueous buffer (HKR, pH = 7.4), liposomes (EYPC) and trifluoroethanol. The CD comparison was done at 40°C because this is the temperature closer to the cell experiments conditions (37.5°C). The folding of these oligoalanine sequences was affected by the location of the Arg and Leu residues. In addition, the helical structure was also influenced by the presence of the fluorophore and the hexane linker between the peptide and the fluorophore (indicated with * in the peptide name). The presence of the linker slightly increased the helical

[150] S. Marqusee, V. H. Robbins, R. L. Baldwin, *Proc. Natl. Acad. Sci. U. S. A.* **1989**, *86*, 5286–5290.
[76] A. Ho, S. R. Schwarze, S. J. Mermelstein, G. Waksman, S. F. Dowdy, *Cancer Res.* **2001**, *61*, 474–7.

folding of the peptide in aqueous conditions and reduced it in liposomes, as shown between peptides **P6*** and **P7** (Figure 40C and D). The synthetic process started with **P1** structure that did not contain any Leu residues; this structure confirmed the poor helical behavior of the peptide (Figure 40A). Furthermore, we observed that **P1** had a rather low cellular internalization in HeLa cell cultures compared to the control peptide **R8** (Figure 40A). We next tested the structure containing two leucines, **P2**, which showed a clear increase in helicity compared to **P1** (Figure 40A). Despite the improvement in folding, **P2** still had negligible uptake on *in vitro* assays (Figure 40B). The incorporation of a third leucine into the peptide sequence, **P3***, demonstrated a transcendent impact on both helicity and cellular internalization (Figure 40A-D). However, the location of these leucines conditioned folding as well as uptake behavior. For example, the proximity of hydrophobic Leu residues to cationic Arg stabilized helicity in buffer (**P3*** and **P5***). Another example of the modulation of the properties of these peptides was the comparison of the radial distribution of leucines, **P7** and **P8**, with an aligned distribution of the leucines as in **P5***. The radial leucine distribution confirmed a more helical arrangement in liposomes (**P7** with 31.6 % and **P8** with 49.2 % helical content). In these two peptides, the difference between liposome and buffer folding was also maximized (**P7** with 16.1% and **P8** 12.8%) (Figure 40). This change of helicity from aqueous to lipidic medium when the Leu was in radial distribution can be explained by a carpet-like arrangement. In this disposition the arginine residues would be accommodated towards the aqueous part of the lipid-buffer interface, while the leucines would be embedded in the lipid bilayer. To confirm the stability of these structures with the leucines in radial arrangement we designed a sequence that radially arranged both Leu and Arg, **P4**. Comparison between **P8** and **P4** shows that the alignment of Arg was beneficial for both folding and cell internalization (**P4** and **P8** 13% vs. 50% helicity in liposomes) (Figure 40E). Finally, we ordered the selection of TAMRA-labeled peptides by their helicity in liposomes from **P1** with a random structure to **P8** with 50% helicity.

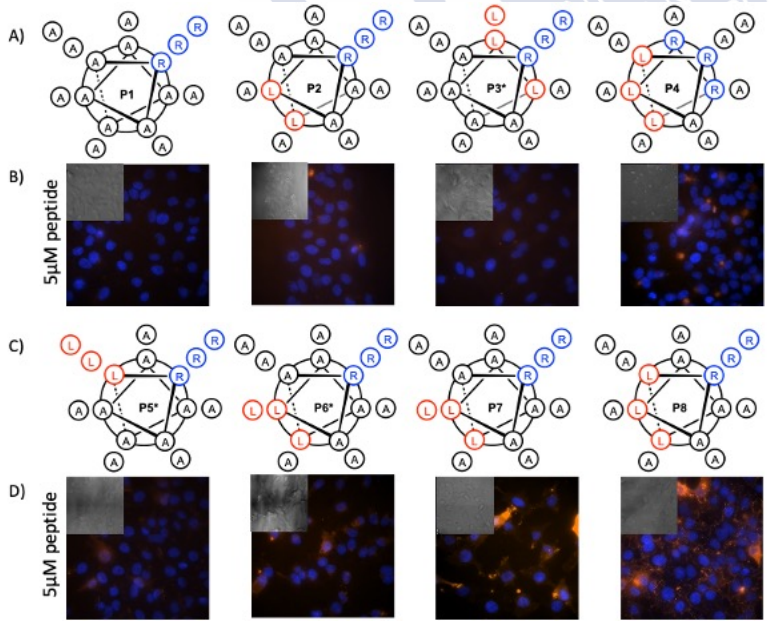

E)

% Helicity Data at 40°C			
Peptide	Liposomes	Buffer	TFE
P1	0.2	9.7	40.7
P2	6.5	12.4	42.8
P3 *	12.7	21.7	45.8
P4	13.3	1.9	42.3
P5 *	29.5	19.3	57.8
P6 *	29.9	35.1	57.8
P7	31.6	16.1	54.8
P8	49.2	12.8	55.7

Figure 40. A) and C) Heptad representation of oligoalanines in increasing order of helicity in liposomes. B) and D) micrographs of epifluorescence of each peptide at 5 μM. E) Percent of Helicity data calculated from 222nm minimum in CD at 40ºC. Images adapted with permission from *Chem. Commun.* **2018**, *54*, 6919–6922.

To characterize the uptake of these oligoalanines in cells we carried out flow cytometry experiments. For this purpose, peptides dissolved in HKR buffer at different concentrations (0.5 to 10 µM) were incubated on cells for one hour at 37°C. Cells were then trypsinized and the level of uptake determined as the median fluorescence of the population by flow cytometry (Figure 41A). Dose response assays for each peptide showed a higher level of cell internalization as the helicity in liposomes increased. In addition, negligible uptake was shown for peptides that had less than 30% helical behavior in liposomes (**P1**, **P2**, **P3*** and **P4**) (Figure 41B). Peptides that had helical folding in lipid (~30%) and aqueous media (between 20% and 30%) such as **P5*** and **P6*** showed higher internalization than less helical structures such as **P1** and **P2**, although the uptake was still below of the control signal of **R8**. However, peptides with higher folding in liposomes and maximum transition difference between buffer and liposomes such as **P7** and **P8** had strong internalization comparable to the octaarginine control. Also remarkable is the comparison between **P6*** and **P7** where the internalization was found to be five fold higher for **P7**, which maximized the difference in helicity between buffer and liposomes (~15% difference in liposome helical content). We also characterized internalization using inverted epifluorescence microscopy. The micrographs of the dose response (0.5 to 5 µM) of each peptide agreed with the results obtained in cytometry, observing the peptide in red inside the cell at 5µM from peptide **P5*** to **P8** (Figure 40B and Figure 40D). Moreover, from the micrographs we could observe a punctate fluorescent pattern of internalization, which would suggests an endocytic uptake.

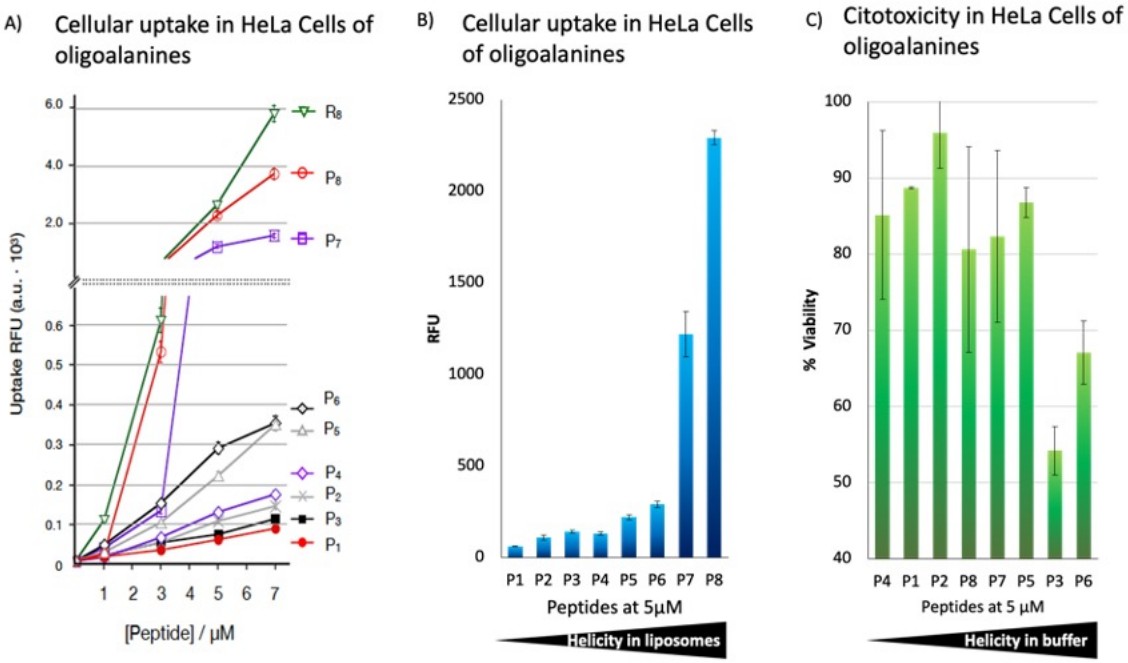

Figure 41. A) Quantification of the uptake of oligoalanines in HeLa cells by flow cytometry. B summary of the uptake at 5 µM in HeLa cells. Peptides were sorted by increasing helicity in liposomes. C) Viability of HeLa cells after incubation with 5 µM of each peptide. Peptides have been ordered by their helicity in HKR buffer. Images reproduced with permission from *Chem. Commun.* **2018**, *54*, 6919–6922.

Afterwards, we performed cell viability studies using the colorimetric MTT assay. As described in the previous chapter, mitochondrial metabolic activity reduces 3-(4,5-dimethylthiazol-2-yl)-2,5-diphenyltetrazolium to purple formazan. Plotting the viability at

5μM for each peptide helped us to compare the behaviors of the peptides. For example, the peptides with the highest toxicity were those with the highest helicity in buffer such as **P3*** and **P6***. In addition, these two compounds showed higher helicity in buffer than in liposomes (especially **P3*** with the lowest viability). In comparison, peptides that show higher helicity in liposomes than in buffer had better viability regardless of the level of cell internalization. This cytotoxicity seemed to correlate with the increased helicity of the peptides in aqueous buffer. (Figure 41C). This association may be due to a detergent or disruptive character, which these amphiphilic peptides possess when they are folded in aqueous medium. It is important to note that the hydrophobic fluorophores can increase cytotoxicity, which is clearly shown by comparing **P8** (IC_{50} 9 μM) with the acetylated structure based on the same sequence depicted in the third chapter **MP1** (IC_{50} 129μM).

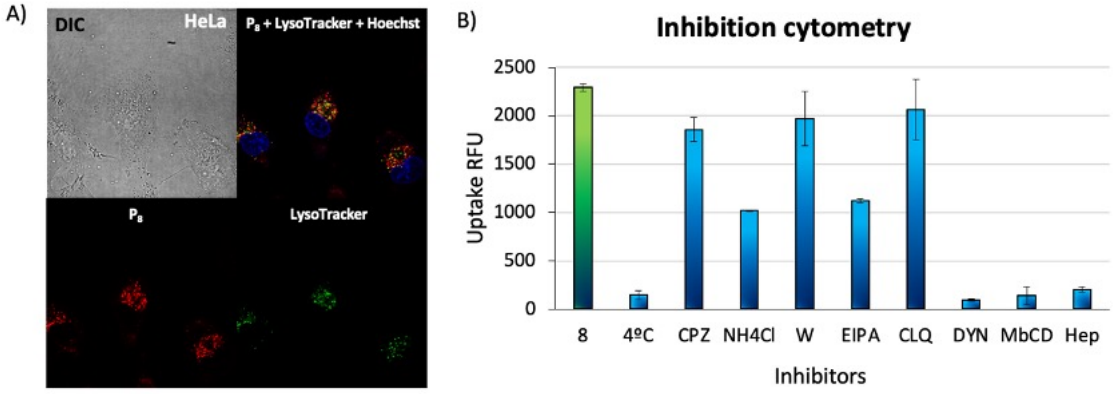

Figure 42. Confocal images of a colocalization study between **P8** (red) and LysoTracker (green), 3 h after incubating for 30 min with 5 uM of peptide. B) Quantification by flow cytometry of the uptake of 5μM **P8** in the presence of endocytosis inhibitors. CPZ (Chlorpromazine), NH_4Cl, W (Wortmannin), EIPA (5-(*N*-Ethyl-N-isopropyl)amiloride), CLQ (Chloroquine), DYN (Dynasore), MbCD (Methyl-β-cyclodextrin), Hep (Heparin). Error bars indicate SD of three replicates. Images reproduced with permission from *Chem. Commun.* **2018**, *54*, 6919–6922.

The punctate fluorescent pattern, observed in the micrographsis usually suggestive of an endocytic uptake. We decided to focus on characterizing the uptake mechanisms for the best peptide candidate **P8**. First, we carried out a colocalization study with LysoTracker. The positive colocalization indicated that the dotted pattern was as a result of endocytic uptake (Figure 42A). In order to study deeply the endosomal uptake route, we also performed endocytosis inhibition studies by flow cytometry, in presence of inhibitors or at low temperature (4ºC), which confirmed an energy-dependent internalization. Some of the inhibitors tested showed reduced uptake for **P8**. Dynasore (DYN), which inhibits dynamin-dependent endocytosis, radically affected internalization. Methyl-β-cyclodextrin (MbCD), which removes cholesterol from membranes and it also inhibits caveolin-mediated mechanisms, also significantly reduced the uptake of the peptide. Therefore, we deduced that the main endocytosis pathway for **P8** was mediated by a caveolin dependent mechanism. This behavior coincides with other CPPs as in the case of helical polyprolines reported by Prof. Giralt.[81] However, other inhibitors showed a partial inhibition of internalization, such as Chlorpromazine (CPZ) or 5-(*N*-Ethyl-*N*-isopropyl) amiloride (EIPA), affecting clathrin and macropinocytosis processes respectively. This partial inhibition indicates that there are several

[81] S. Pujals, E. Giralt, *Adv. Drug Deliv. Rev.* **2008**, *60*, 473–484.

mechanisms operating at the same time during **P8** internalization although the predominant one is caveolin-mediated endocytosis (Figure 42B). Other inhibitors such as ammonium chloride (NH_4Cl) or Heparin (Hep) are general inhibitors for endocytosis because they prevent endosome acidification and glycosaminoglycans interactions respectively.

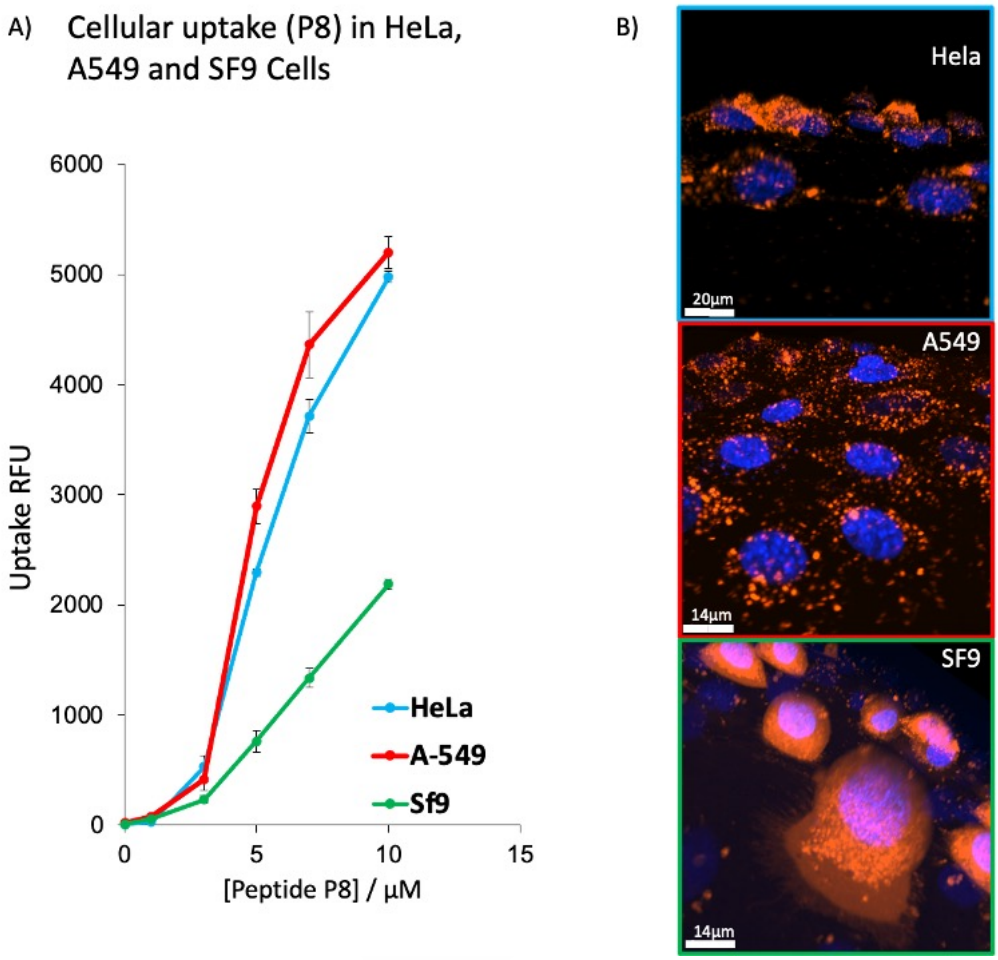

Figure 43. A) Flow cytometry analysis of the uptake of **P8** in three cell lines, HeLa (blue), A549(red) and SF9 (green). Error bars indicate SD of three replicates. B) 3D reconstruction of confocal images of different cell lines after 30 min of incubation with 5 µM **P8**, Hela Hela (blue border), A549 (red border) and SF9 (green border) 5µM (30min of incubation in HKR), the 3D projections were obtained from the different individual confocal planes using the Imaris bitplane © 9.0.0 software. Images reproduced with permission from *Chem. Commun.* **2018**, *54*, 6919–6922.

We decided to investigate the behavior of **P8** in cell lines other than HeLa cells, such as A549 and SF9, both by flow cytometry and microscopy. The level of internalization was comparable to the data obtained in the HeLa cell line (Figure 43A). On the other hand, new colocalization studies with LysoTraker also showed an endocytosis-dependent mechanism for A549 cells. Furthermore, we also found a cytoplasmic staining of the peptide for SF9 cells. The cytoplasmatic distribution of **P8** in SF9 was consistent with a combined internalization mechanism of internalization (Figure 43B). Moreover, it should be taken into account that this type of SF9 cells have a different membrane composition[293] (with lower cholesterol than

[293] K. Marheineke, S. Grünewald, W. Christie, H. Reiländer, *FEBS Lett.* **1998**, *441*, 49–52.

mammalian cells and they are incubated at a lower temperature (28ºC). Therefore, the helical character of the structure will be slightly higher than in the other two cell cultures. The confocal microscopy and the 3D reconstruction micrographs allowed us to observe with greater definition the punctate pattern in the cells.

The presence of a supramolecular aggregation of the peptide that could affect this type of internalization was discussed during the review process. However, a critical micellar concentration (cmc) assay performed with pyrene revealed no pyrene encapsulation. It was also not possible to determine the presence of aggregates by DLS at these low concentrations. (Figure 44A-B) (not included in the article), concluding that there are no aggregates, or particle size analysis by DLS could not be stable enough to be measured. Finally, the degradation time of the peptide in the presence of serum was checked and revealed a half-life of 2.2 hours. (Figure 44C).

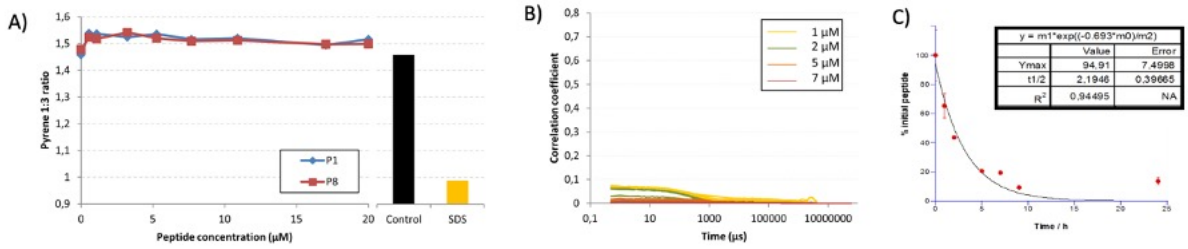

Figure 44. A) Pyrene 1:3 ratio data of peptides **P_1** and **P_8**. A 100 nM pyrene solution was incubated with increasing amounts of the peptides. The ratio between pyrene emission, after excitation at 335 nm, at 373 nm and 383 nm (1:3 ratio) was calculated. No drop of this value, indicating micelle formation, was observed at the maximum concentration tested in this experiment. Black bar indicates ratio of the pyrene solution alone; yellow bar is the ratio of the same sample after adding SDS at a concentration above cmc, as a positive control. B) Correlation curves of peptide **P_8** at the indicated concentrations determined by Dynamic Light Scattering. C) Calculation of the half-life of **P_8** in serum.

The most important conclusion that we drew from the development of this chapter 2 was the ability to control helical folding by rational design. Therefore, by controlling the folding of the CPPs structures we were able to control their cellular activity such as internalization and cytotoxicity.

Chapter 3

Selective disruption of membranes by specific carriers is a challenge in the field of drug delivery. One of the most employed strategies is the use of amphiphiles due to their interaction with the hydrophobic part of the membrane. Some of the specific characteristics of endosomes can help to design carriers targeted to this type of membranes. For example, the maturation process of endosomes (pH 6.5 in early endosomes) leads to a pH transition to obtain the acidic pH in lysosomes (pH 4.5).[238] In addition, the lipid composition of the endosomal membranes includes the incorporation of anionic lipids involved in fusion processes.[236] Finally, there is also a voltage potential of around 150 mV with a positive potential gradient from the endosomes to the cytosol.[239]

Macromolecule-based therapies such as proteins and antibodies with intracellular functions usually require a specific carrier that either introduces the macromolecule across the plasma membrane or release them from endosomes, since the endosomal pathway is the internalization pathway of most of these types of therapeutic agents. The field of protein and antibody transport into the cellular interior has been gaining importance in recent years. The cellular internalization of proteins and antibodies represents a challenge due to the great variety in size, shape, isoelectric points, etc.

Non covalent peptide carriers such as Pep-1, df-Tat and L17E are emerging as a new promising strategy in the field. Pep-1 was the first peptide reported in protein transport by supramolecular complexation and was also the first peptide to be commercialized under the name Chariot®.[71] Pep-1 was characterized as a plasma membrane disruptor for direct transport of proteins into the cytosol.[211] df-TAT is a dimeric peptide including a disulfide bond and two fluorescent monomers. This peptide can transport several proteins at low concentrations.[264] The mechanism proposed by authors was by endosome membrane fusion.[265] Finally, L17E is a venom attenuated peptide by the substitution of a glutamic residue, which is protonated at low pH in endosomes. This peptide was even able to carry functional antibodies loaded in exosomes.[24]

In Chapter 3, we considered whether modulable helical oligoalanine scaffolds would be able to act as efficient carriers for macromolecules. Therefore, we proposed the evaluation of the potential selective assembly of prehelical peptides on endosome membranes to disrupt or perturb the membranes and release biomacromolecules into the cytosol. To this end, we characterized the peptide structure identified in Chapter 2. The potential transport properties of this peptide were characterized in artificial membrane models and in computational simulations.

---

[238] Y.-B. Hu, E. B. Dammer, R.-J. Ren, G. Wang, *Transl. Neurodegener.* **2015**, *4*, 18.

[236] H. Matsuo, J. Chevallier, N. Mayran, I. Le Blanc, C. Ferguson, J. Fauré, N. S. Blanc, S. Matile, J. Dubochet, R. Sadoul, et al., *Science.* **2004**, *303*, 531–534.

[239] A. Saminathan, J. Devany, A. T. Veetil, B. Suresh, K. S. Pillai, M. Schwake, Y. Krishnan, *Nat. Nanotechnol.* **2021**, *16*, 96–103.

[71] M. C. Morris, J. Depollier, J. Mery, F. Heitz, G. Divita, *Nat. Biotechnol.* **2001**, *19*, 1173–1176.

[211] S. Deshayes, A. Heitz, M. C. Morris, P. Charnet, G. Divita, F. Heitz, *Biochemistry* **2004**, *43*, 1449–1457.

[264] A. Erazo-Oliveras, K. Najjar, L. Dayani, T.-Y. Wang, G. A. Johnson, J.-P. Pellois, *Nat. Methods* **2014**, *11*, 861–867.

[265] A. Erazo-Oliveras, K. Najjar, D. Truong, T. Y. Wang, D. J. Brock, A. R. Prater, J. P. Pellois, *Cell Chem. Biol.* **2016**, *23*, 598–607.

[24] M. Akishiba, T. Takeuchi, Y. Kawaguchi, K. Sakamoto, H.-H. Yu, I. Nakase, T. Takatani-Nakase, F. Madani, A. Gräslund, S. Futaki, *Nat. Chem.* **2017**, *9*, 751–761.

In the previous chapter we confirmed that 4 helical turns were sufficient to quantify helicity by CD. We selected the optimal peptide candidates with a length of 16 amino acids combining three leucines and three arginines in a oligoalanines peptide scaffold. We designed and synthesized three new structures: minimal peptide 1 (**MP1**), minimal peptide 2 (**MP2**), as prototypical examples of different peptide helical behaviour, and peptide 3 (**P3**), which has one extra helical turn. **MP1**, **MP2** and **P3** are acetylated in *N*-termini. As control structures, we chose the **GALA** peptide and the octaarginine peptide **R8** (Figure 45A-B). The **GALA** peptide was chosen as a control because it exhibits a transient folding character and it was described as helical peptide in acidic conditions that triggered the formation of membrane pores. Octaarginine **R8** was selected as a control fully cationic penetrating peptide.

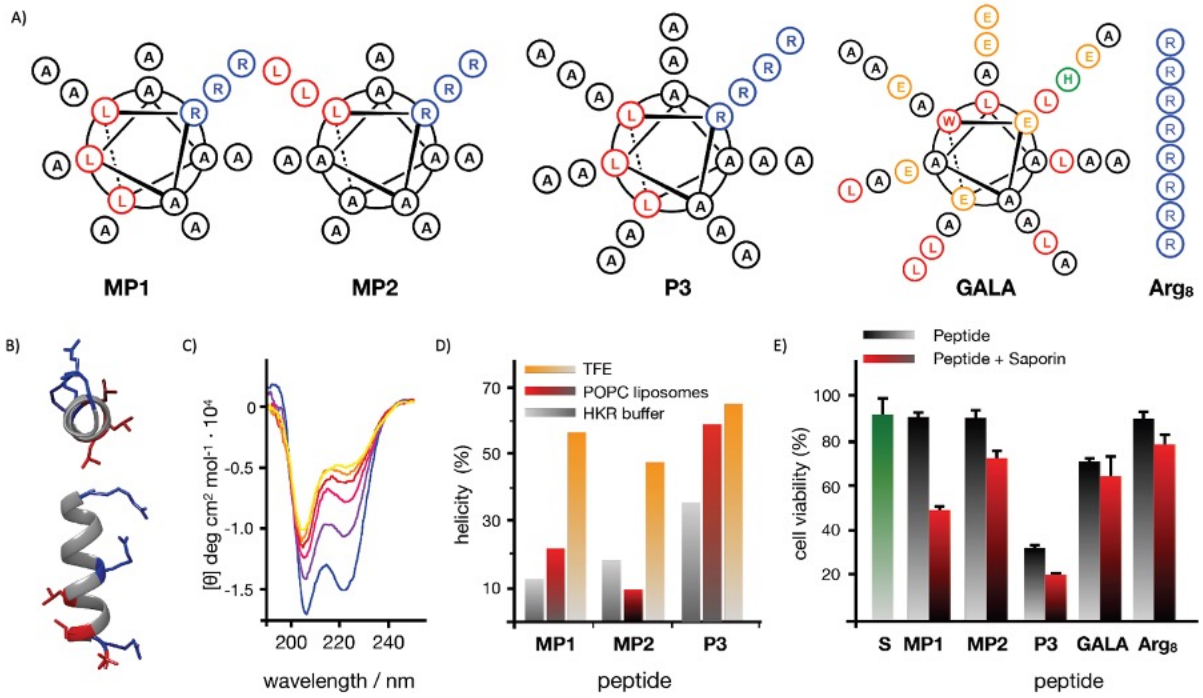

Figure 45. A) Heptad representation of peptides **MP1**, **MP2**, **P3**, **GALA**, and the octaarginine sequence. B) Two perspectives of 3D prediction of **MP1** by PEP-FOLD 3.5.[312] C) CD spectra of MP1 (100μM) in HKR buffer at different temperatures. D) Quantification of % content from 222nm minimum of alpha helical of **MP1**, **MP2** and **P3** (100μM) in three different media HKR buffer, POPC liposomes and TFE at 40ºC E) Cell viability of peptide candidates (30μM) with (red) or without (grey) saporin (10μg). Error bars represent the standard deviation (SD) of 3 replicates. Images reproduced with permission from RSC Chem. Biol. 2021, 2, 503–512.

We started the study with the characterization of the helicity of the different peptides by circular dichroism (CD). The **MP1** peptide showed a helical content of 22% in neutral liposomes (POPC: 1-palmitoyl-2-oleoyl-sn-glycero-3-phosphocholine) and 10% in water. **MP2** was less helical in liposomes (7%) and more helical in buffer (14%) and **P3** showed a much stronger helical folding close to 60% in liposomes and 40% in buffer (Figure 45C-D).

We performed a preliminary study to evaluate the abilities of these peptides as protein carriers. The initial studied protein was saporin (28.4 kDa), which is a ribosome inactivating protein (RIP) and that internalizes by endocytic pathway. Cytosolic release of saporin triggers cell death, and thus the activity of this protein can be measured by MTT cytotoxicity assays. These initial characterization cofirmed **MP1** as the best candidate for both delivery and

viability. **P3** showed high toxicity, as its high helicity in water could be causing membrane lysis. Finally, the control structures, **GALA** and **R8**, showed slightly lower transport efficiency and more toxicity compared to **MP1** (Figure 45E). From the observed saporin release, we assumed that a selective rupture of the endosomal membranes was possible, and we focused on a deeply characterization of the optimal **MP1** in lipid bilayers and cellular assays.

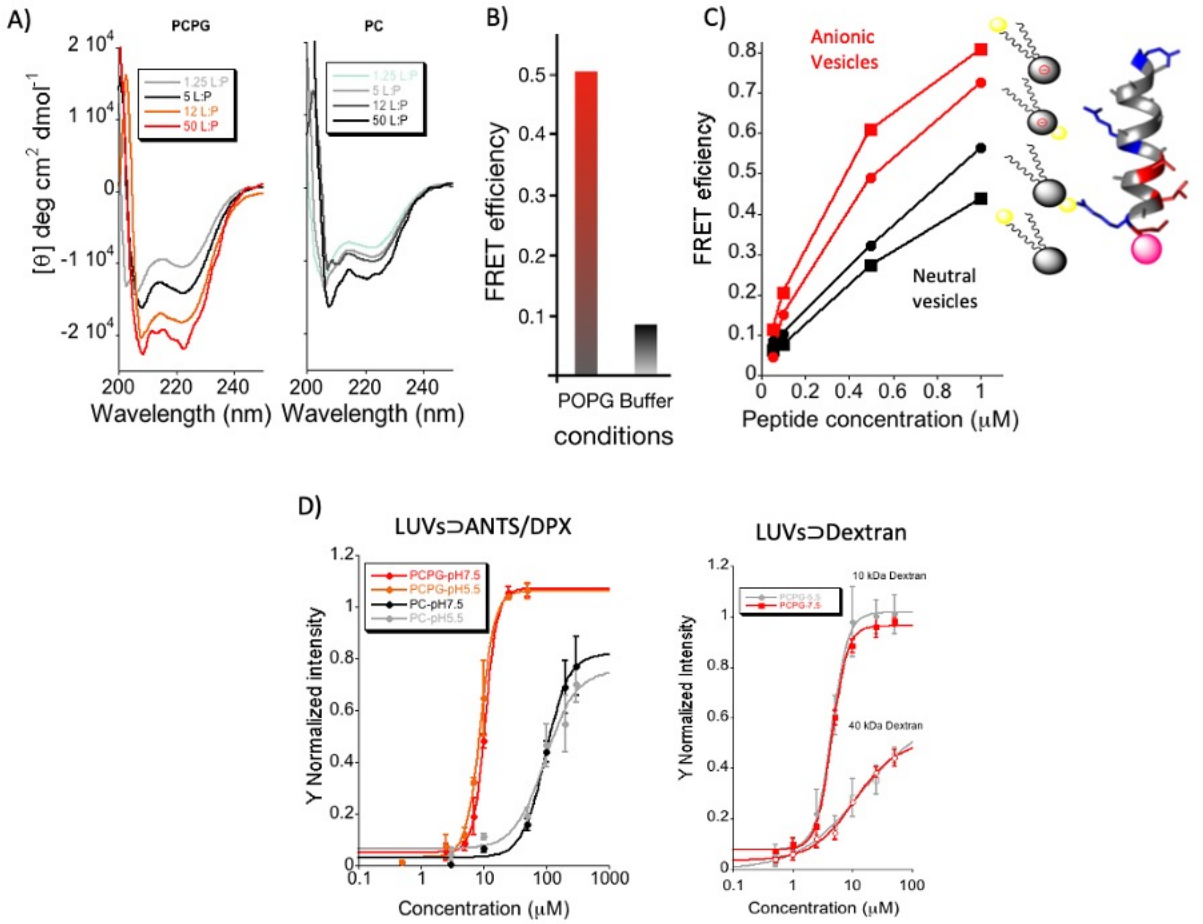

Figure 46. A) CD spectra of **MP1** (100μM) at different lipid:peptide ratios (1.25, 5, 12, 50) with anionic LUVs (POPC:POPG 3:1, left) or neutral LUVs (POPC, right). B) FRET efficiency of **TM-MP1** (acceptor) and CF-MP (donor) in buffer and in presence of anionic LUVs. C) FRET efficiency of **TM-MP1** (acceptor) and LUVS labeled with NBD (donor), squares represents NBD in the tail, circles represents NBD in phospholipid head, anionic LUVs are represented in red and neutral in black lines. D) Dose response curves of normalized ANTS fluorescence (left) with neutral POPC (black and grey lines) or anionic POPC:POPG 3:1 (red and orange lines) LUVs⊃ANTS/DPX at two pH: 7.4 (red and black lines) and 5.5 (orange and gray lines). Dose response of anionic LUVs⊃Dextran (right panel) with FITC-Dextran (10 kDa, filled markers) and TM-Dextran (40 kDa, empty markers) at neutral (red) or acid (gray) pH. Images reproduced with permission from RSC Chem. Biol. 2021, 2, 503–512.

We next characterized the potential transport and release of the **MP1** peptide in artificial membrane systems. For this purpose, we carried out different experiments based on large unilamellar vesicles (LUVs), planar membranes (BLMs) and computational modeling. In the case of LUVs, two sets of vesicles were prepared. Neutral vesicles composed of POPC (1-palmitoyl-2-oleoyl-sn-glycero-3-phosphocholine) and anionic vesicles composed by a 3:1 ratio of POPC:POPG (POPG, 1-palmitoyl-2-oleoyl-sn-glycero-3-phosphoglycerol). We studied the

helical folding and affinity that **MP1** had for these vesicles. We analyzed the CD signal with increasing amounts of vesicles and found a higher α-helix folding with higher amounts of lipids. Moreover, this effect was more intense for anionic vesicles, reaching values from 20% to 65% of the helical content (Figure 46A).

To investigate the peptide assembly on the membrane, we performed fluorescence resonance energy transfer (FRET) experiments that were carried out by labeling the peptide with two probes, carboxyfluorescein (**CF-MP1**, donor) and TAMRA (**TM-MP1**, acceptor) (Figure 46B). The probes were placed close to the leucine. The FRET efficiency shows a clear preference for peptide intercalation in the presence of anionic vesicles compared to aqueous buffer. In solution, a fluorescence shift effect in **TM-MP1** was observed, which indicated that the peptide might be forming labile micellar-like aggregates. To find out the orientation preference of the peptide, a NBD-labeled lipid (donor) and **TM-MP1** (acceptor) were studied. Four types of vesicles were developed, two anionic and two neutral, either with the NBD on the surface or with the NBD on the inner side of the membrane. The results showed a higher FRET efficiency for the anionic LUVs, that was increased in the case of the NBD-tag towards inner bilayer part, suggesting the insertion of the leucines in the bilayer. The FRET efficiency in neutral vesicles showed lower interaction and leucine preference for the surface part (Figure 46C).

The selectivity for anionic membranes was confirmed again in leakage studies by LUVs⊃ANTS/DPX vesicles. These experiments showed a tenfold lower EC_{50} for anionic vesicles POPC:POPG than for neutral vesicles POPC (Figure 46D). However, pH selectivity was not observed. Trying to get more information from this type of release assays, we decided to use vesicles containing fluorescent polymers. We used dextrans of two molecular weights, 10kDa and 40kDa, to make LUVs⊃Dextran, vesicles loaded with model cargos of hydrodynamic radius around 2.3 nm and 4.5 nm respectively. This assay allowed the estimation of the release size threshold of the **MP1** peptide. The results showed the preference of **MP1** to release the 10 kDa dextran with an EC_{50} similar to the LUVs⊃ANTS/DPX system and a 10-fold higher EC_{50} for the 40 kDa dextran (Figure 46D). We also performed DLS measurements of vesicles in the presence of high amounts of peptide. The DLS results confirmed full membrane integrity supporting a non-destructive membrane disruption mechanism.

Computational modeling confirmed the helical folding of **MP1** in buffer and TFE. These computational calculations also attempted to predict how the peptide assembled in membranes and under which conditions. For this purpose, Dr. Rebeca García-Fandiño developed coarse-grained (CG-MD) simulations with membranes of endosomal composition in the presence of peptide. The membrane system and the peptide were subjected to an electric field and two conclusions could be extracted from the simulations. On the one hand, we could observe the orientation of the peptide with the Leu towards the inner side of the membrane, which matched with the FRET results (Figure 47A). On the other hand, simulations displayed a prefibrillar assembly of **MP1** on themembrane dependent on alanine interactions. Moreover, the peptide self-assembly in membranes led to membrane invaginations and transient pore disruptions (Figure 47B). For the simulation were employed 31 units of peptides and 1309 lipids, with a ratio L/P ~ 42, a ratio close to the maximum helical behavior in CD measurements.

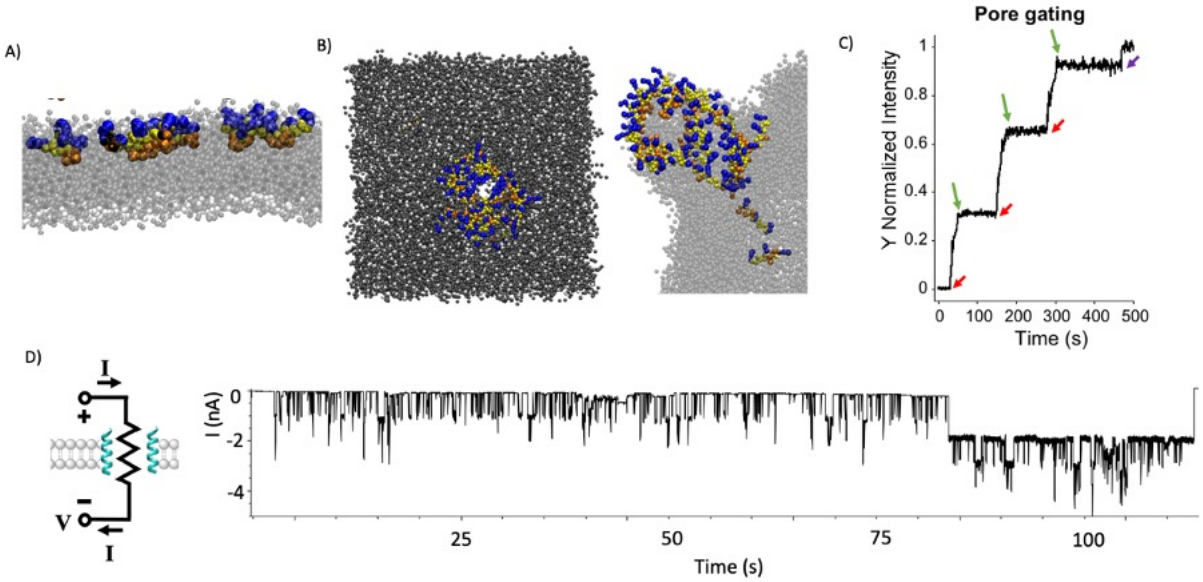

Figure 47. A) Snapshot of CG-simulation (300ns) subject to an external field of 30 mV showing peptide interaction in a DPPC:DPPE:DPPS (3:5:2) membrane, leucines are represented in orange color, arginines in blue and alanines in yellow. B) Detail of the insertion of the peptides in the membrane, showing the orientation of Leu (orange) towards the hydrophobic core of the bilayer, Ala(yeloow) and Arg (blue) cationic residues exposed to the solvent. C) Pore gating of normalized ANTS fluorescence in a kinetic measurement, red arrows are peptide addition (10 μM), green arrows POPG addition (50 μM) and violet arrow Triton-X100 addition. D) Scheme of electrical circuit (left) through a membrane, and BLM recording (right) at 25μM of **MP1** at 200 mV. Conditions: lipid: DPhPC, buffer: 0.5 M KCl 10 mM MOPS and pH 7.4. The current signal was acquired at 1 kHz and sampled at 5kHz, data was filtered using low pass Bessel (8-pole). Images reproduced with permission from RSC Chem. Biol. 2021, 2, 503–512.

From these predictions and the preliminar results in LUVs and cells, we deduced the presence of a pore in the membranes. Therefore, the following experiments were performed to verify the presence of this pore. First, we decided to carry out pore gating experiments in LUVs by blocking and opening the channels by sequential additions of anionic lipid, POPG (to close), and peptide (to open). We used a kinetic measurement of LUVs⊃ANTS/DPX at a peptide concentration where the fluorescence grew progressively (e.g., 10μM). Peptide and lipid were added at different time intervals, to observe perfect pore gating over three cycles of opening and closing events (Figure 47C). Finally, we evaluated the formation of this nanopore by BLM. Experimentally, we can measure the response to voltage differences with planar lipid bilayer or black lipid membrane (BLM) experiments (Figure 47D left). In these studies, the selected lipid was 1,2-diphytanoyl-sn-glycero-3-phosphocholine (DPhPC), which offers electrical resistance to the passage of current. The flat membrane is placed between two buffer chambers, where we add 25 μM of **MP1** in buffer. After applying different voltages, at 200 mV we observed conductivity events. The formation of these stochastic events reached a maximum steady-state current intensity close to 1.1 nA. However, long lasting open states for several seconds were observed with an increase in the current intensity up to 1.9 nA (Figure 47D). We associate this current increase with dynamic peptide assembly. In addition, the BLM technique allowed us to calculate the pore diameter using the Hille equation,[105] which in this case was 3.2

[105] B. Hille, *Ionic Channels of Excitable Membranes*, Sinauer Associates, Sunderland, MA, **1992**.

nm for short events and 4.4 nm for long opening states. The supramolecular assembly of a nanopore that maintains the integrity of the bilayer membrane even at longer recording times has never been observed for this class of peptides.

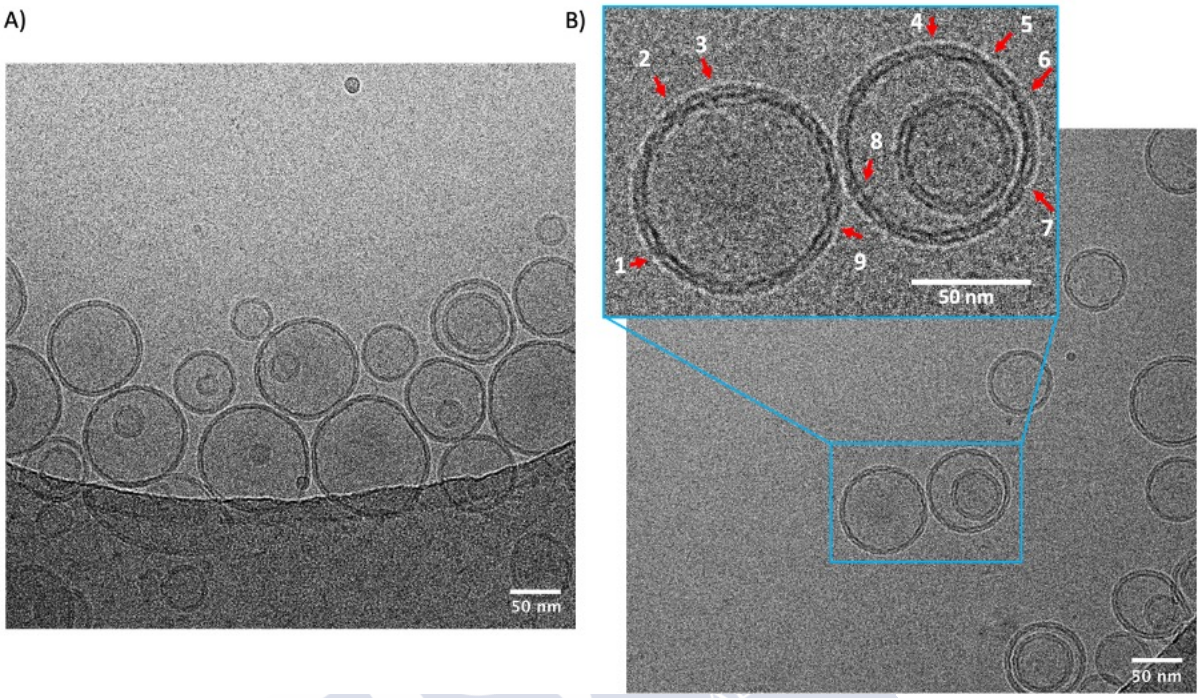

Figure 48. Cryo-TEM images (Talos Artica) of LUVs (POPC:POPG, 3:1) diameter ~ 100 nm vitrified at 25ºC (Leica EM CPC). A) Lipid at 20mM in buffer B) LUVs in presence of **MP1** at 1.6 mM, ratio L/P 12 (right). Red arrows point to pores in vesicles and the diameters measures are in white 1) 4.8 nm, 2) 3.9 nm, 3) 3.7 nm, 4) 2.6 nm, 5) 4.1 nm, 6) 1.7 nm, 7) 2.2 nm and 8) 2.2 nm 9) 5.2 nm. Buffer 10 mM HEPES, 150 mM NaCl, pH 7.4. Scale bars are 50 nm. All measures were performed in Centro Nacional de Biotecnología CNB.

An extra experiment not included in the publication was a Cryo-TEM microscopic characterization of the **MP1** nanopore in LUVs. Comparing the control of untreated LUVs with LUVs in presence of peptide **MP1** in a ratio Lipid:Peptide 12:1, we observed several disruptions maintaining the structural integrity of the vesicle and confirming by a direct visual technique the presence of a pore (Figure 48). The diameters of these pores were measured ranging from 2 to 5 nm. Following preliminary results in model membrane systems, we decided to move to *in vitro* cellular systems. One of the first experiments tested in cell culture, in addition to the transport of the protein saporin previously commented, was the transport of dextran. Dextran is a natural polymer well-known for its internalization by macropinocytosis. The cytosolic delivery of the dextran appeared as a fluorescence diffuse signal inside the cell, while the peptide carrier **TM-MP1** (in red) remained in a punctate pattern (Figure 49A). A variety of dextran sizes by the **MP1** carrier were assayed for release into the cytosol, showing a cytosolic distribution to a greater or lesser extent depending on the size (10, 40 and 70 kDa). The best efficiency was observed after 3 hours of incubation and a size selectivity 10 > 40 > 70 kDa was found in codelivery experiments (Figure 49B and D). We also found that the presence of FBS did not affect to the final delivery of the dextran (45%). Moreover, the cytosolic delivery by MP1 was demonstrated in different cell lines such as Hela, Vero or A549 cells (Figure 49C). A time lapse study of dextran delivery showed peptide-dextran colocalization in a punctate pattern

in the first images (time 0h) and then, a dextran cytosolic staining after three hours of incubation (3h), confirming a time dependency for the endosomal release with peptide still encapsulated and colocalizing with lysotracker. Endocytosis inhibition studies partially limited the cytosolic distribution of dextran when using dynasore (dynamin-dependent endocytosis inhibitor) and EIPA (macropinocytosis inhibitor) (Figure 49E). Therefore, it is suggested that the general mechanism for uptake depended on the polymer dextran cargo.

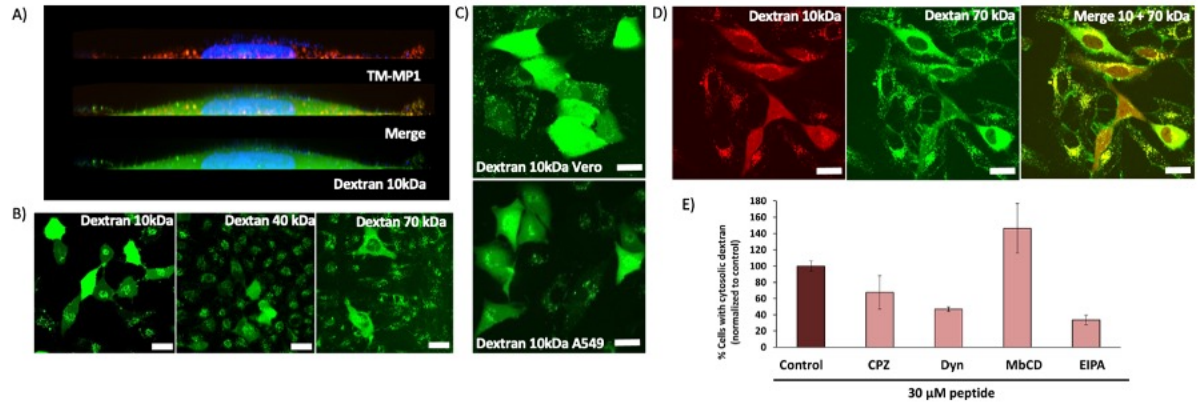

Figure 49. A) 3D projection of a single cell with **TM-MP1** in red in a punctate pattern (top) and cytosolic distribution of Alexa488-Dextran 10kDa (down) and the merge of both (middle). the 3D projections were obtained from the different individual confocal planes using the Imaris bitplane © 9.0.0 software B) Dextran cytosolic distribution of Alexa488-Dextran, 10 kDa (left) Alexa488-Dextran, 40 kDa (middle) and FITC-Dextran, 70 kDa with 30 µM of **MP1** of confocal images taken at 60x in Hela cells. C) Dextran cytosolic distribution (Alexa488-Dextran 10k Da) in Vero Cells (top) **MP1** 20µM and A549 cell (down) **MP1** 50µM. D) Cytosolic Dextran distribution in Hela cells after a codelivery of 10 kDa TM-Dextran and 70kDa FITC-Dextran with **MP1** 30µM. E) Cytosolic delivery of dextran in HeLa cells incubated with 0.25 mg/mL 10 kDa TM-labelled dextran and 30 µM of **MP1** in the presence of the indicated inhibitors for 1 h. After incubation, the number of cells with cytosolic dextran was counted and normalized to the control with 30 µM peptide in the absence of inhibitors (100%). Data is presented as mean of three independent experiments ± SD. Images reproduced with permission from RSC Chem. Biol. 2021, 2, 503–512.

The good transport profile of the **MP1** peptide prompted its further characterization as a vehicle for macromolecular therapeutic drugs such as proteins and antibodies. In the process of selecting target proteins of interest to transport, saporin, Cre recombinase, GST-NLS-GFP, CF labeled IgG, and a monoclonal antibody (Mab414) were chosen. The saporin administration experiments were successful (70% increase in toxicity), as it was discussed previously, with an optimal concentration of **MP1** between 30 and 50 µM. The saporin delivery was confirmed in A549 cell line with a 50% increment of toxicity. Then, we tested Cre recombinase, which is 38.5 kDa tyrosine recombinase enzyme. This enzyme catalyzes the site-specific recombination between two DNA recognition sites (LoxP sites). Cells transfected with a plasmid carrying the Cre reporter system express the DsRED proteins and products of Cre-mediated recombination at LoxP sites are express EGFP (Figure 50A). In the dose-response experiments performed for **MP1**, for **GALA** and **R8** controls, the highest conversion was observed at an optimal concentration of 10 µM **MP1** (40% of conversion) (Figure 50B-C). Likewise, the delivery activity of this protein was compared with other three peptide relevant in the field (Pep-1, dfTAT and L17E) (Figure 50B-C). Competitive activity at a lower concentration was found for **MP1**, showing its potential as a vector transport and endosome disruptor. In addition, we also observed during these experiments the decrease in Cre delivery efficiency at higher **MP1** concentrations. Microscopy images showed the presence of aggregates at high peptide

concentrations. These aggregates are probably peptide precipitated with protein and would explain the decrease in efficiency. Another protein that we successfully transported was GFP tagged with NLS to stain the nucleus.

Cellular viability studies were also carried to compare the delivery efficiency of **MP1** and the different control peptides. The MTT assays showed a lower IC_{50} for **GALA** and octaarginine. **L17E** and **Pep-1** have similar viabilities and **dfTAT** peptide a very low viability compared to **MP1**. The IC_{50} testing concentrations of **MP1** were four and ten times higher than the optimal **MP1** concentrations used in delivery experiments e.g. 30 µM and 10 µM for dextran and Cre recombinase, respectively.

A)

B)

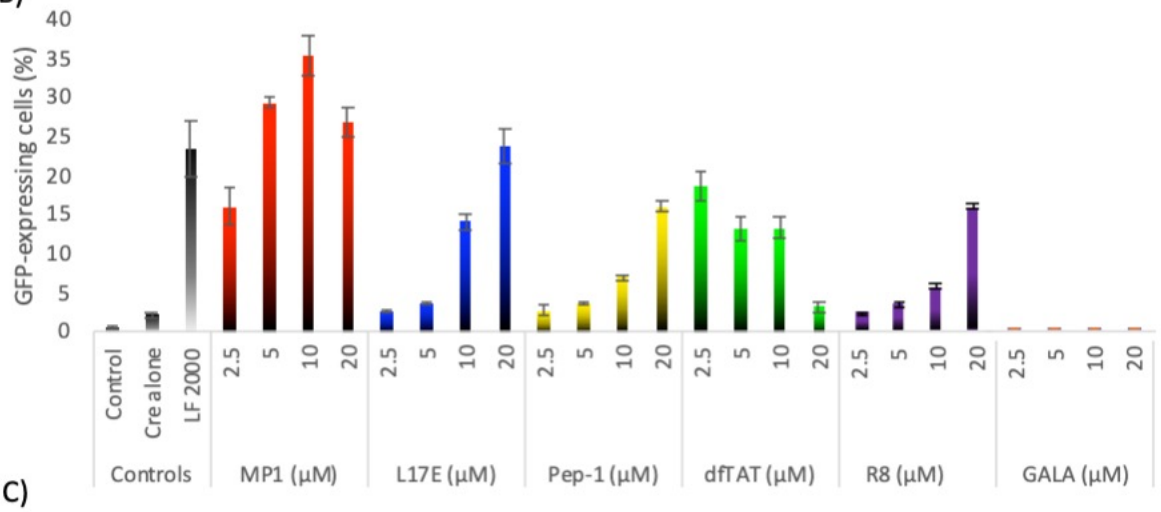

C)

	MP1	L17E	Pep-1	dfTAT	Arg	GALA
2.5 µM	16.0 ± 2.4	2.6 ± 0.2	2.7 ± 0.7	18.6 ± 1.9	2.4 ± 0.1	0.4 ± 0.1
5 µM	29.2 ± 0.7	3.6 ± 0.2	3.6 ± 0.1	13.2 ± 1.4	3.4 ± 0.2	0.4 ± 0.1
10 µM	35.3 ± 2.6	14.1 ± 1.0	6.9 ± 0.4	13.3 ± 1.5	5.8 ± 0.3	0.3 ± 0.0
20 µM	26.7 ± 1.7	23.6 ± 2.1	16.0 ± 0.7	3.1 ± 0.8	16.0 ± 0.4	0.2 ± 0.1

Figure 50. A) Schematic representation of the Cre reporter assay. Before Cre recombinase treatment, cells express a red fluorescent protein. LoxP site recombination by delivery of Cre recombinase with 10 µM of **MP1** activates the expression of a green fluorescent protein, that can be detected after 3 days.. B) Flow cytometry quantification of GFP expression after Cre recombinase delivery (after three days) with **MP1** and the control peptides: **L17E**, **Pep-1**, **dfTAT**, **R8** and **GALA**. C) Table summarizing the percentages of GFP expressing cells in each condition. (Error bars indicate SD of four replicates). Images reproduced with permission from RSC Chem. Biol. 2021, 2, 503–512.

The excellent biomacromolecular transport results with proteins made us think about testing the transport of antibodies. Antibodies have a larger hydrodynamic radius of 5.4 nm,

thus endosomal release is hindered. The first antibody that we tested in vitro was a fluorescent IgG (150 kDa). Experiments showed a distribution in the cytosol of IgG-CF when incubated in cells in the presence of 30 µM of **MP1**. Next, we tested a mouse monoclonal antibody, Mab414, which binds to the nuclear pore complex. The administration of Mab414 with 40 µM **MP1** showed 70% labeled nuclei in Hela cells (Figure 51A) and 57% in ARPE-19 cells (human retinal pigment epithelium cells at 50 µM **MP1** (Figure 51B). Finally, the last experiment we performed the transport of the Mab414 antibody in animal tissue, specifically, in murine cornea. After confocal microscopy analysis, labeled nuclei were observed when the antibody was transported by **MP1** at the highest concentration, 150 µM. At the same time, the integrity of the tissue was preserved showing excellent viability very similar to the untreated cornea control (Figure 51C). Administration of these antibodies without **MP1** carrier (control experiments) resulted in a punctate fluorescence inside the cell.

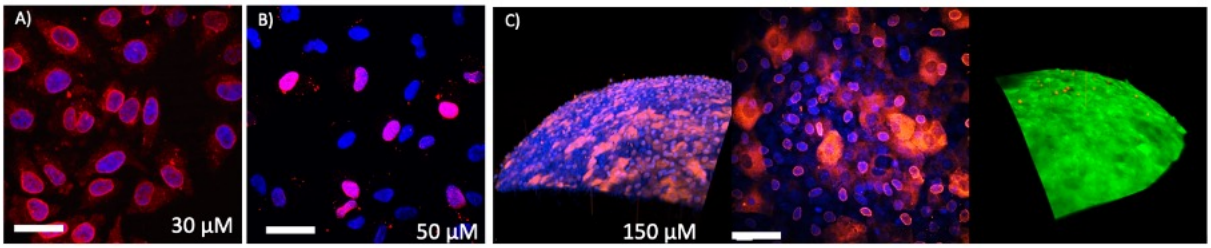

Figure 51. A) HeLa cells (**MP1** at 30µM) and B) ARPE-19 cells (**MP1** at 50µM) showed perinuclear antibody stainning. Images were taken after 1h of incubation with compounds, 2h of incubation in serum 10% supplemented media and fixation for immunofluorescence with Mab414 detection using a secondary antibody (red). Nuclei were stained blue with DAPI C) Cornea of murine (**MP1** at 150µM) with perinuclear antibody stained in red (left panel), maximum intensity projection (middle panel), and fluorescein diacetate/propidium iodide viability stain (right panel) (green: live cells, red: dead cells) [Mab414] = 0.3 mg/mL in (A, and C) and 0.15 mg mL^{-1} in (B). Scale bars are all 50 mm. Images reproduced with permission from RSC Chem. Biol. 2021, 2, 503–512.

The results obtained in biological experiments confirmed that **MP1** works as an efficient agent to deliver functional proteins *in vitro* as well as *ex vivo* tissues. In addition, during this **chapter 3** of the thesis we elaborated a collection of experiments that allowed us to evaluate the capabilities of **MP1**. Many of these experiments were based on artificial vesicles (LUVs), for example, peptide folding and supramolecular assembly, assessment of charge size in transport or vesicular integrity. In addition, the membrane models helped us to hypothesize the presence of a pore that after being evaluated by computational calculations, could be characterized by indirect methods such as BLM and by direct methods such as Cryo-TEM. With all these data we can assert that **MP1** is an optimal candidate to assist the endosomal escape of potentially therapeutic cargoes with cellular functional properties. More , this research demonstrated that the progressive helical folding of short peptides can be applied as a general rule for the controlled delivery of biomacromolecules.

General Conclusions

USC UNIVERSIDADE DE SANTIAGO DE COMPOSTELA

USC
UNIVERSIDADE
DE SANTIAGO
DE COMPOSTELA

General Conclusions

Chapter 1: We have prepared a small peptide library using a "clickable" reaction that modulate the behavior of a parent peptide **AcP(Ox)$_2$**. Moreover, the importance of peptide hydrophilicity/hydrophobicity balance for cell uptake and cytotoxicity has been studied.

Chapter 2: We have studied the folding properties of a simple peptide structures with helical folding capacity. We have observed how amino acid substitutions along an oligoalanine peptide scaffold can modulate the biological properties such as uptake and toxicity.

Chapter 3: We have studied the supramolecular assembly properties of an oligoalanine peptide and its interaction with the membrane of vesicles and living cells. We demonstrated the potential of this peptide for the delivery and release of numerous macromolecules with biological function. We could conclude that the enhancement of peptide helicity in the presence of anionic lipids allowed the assembly of a supramolecular nanopore for the cytosolic release of giant cargos.

USC UNIVERSIDADE DE SANTIAGO DE COMPOSTELA

USC
UNIVERSIDADE
DE SANTIAGO
DE COMPOSTELA

SUPPORTING INFORMATION

USC
UNIVERSIDADE
DE SANTIAGO
DE COMPOSTELA

1. Tuning the Properties of Penetrating Peptides by Oxime Conjugation

USC UNIVERSIDADE DE SANTIAGO DE COMPOSTELA

USC
UNIVERSIDADE
DE SANTIAGO
DE COMPOSTELA

Tuning the Properties of Penetrating Peptides by Oxime Conjugation

Marta Pazo[a], Héctor Fernández-Caro[a], Juan M. Priegue[a], Irene Lostalé-Seijo and Javier Montenegro[a]*

Singular Research Centre in Chemical Biology and Molecular Materials, (CIQUS), Organic Chemistry Department, University of Santiago de Compostela (USC), Santiago de Compostela, Spain[a]

Supporting Information

Table of Contents

1. Supporting methods
   - 1.1. Materials and methods S2
   - 1.2. Abbreviations S3
   - 1.3. Synthesis S4
     - 1.3.1. General protocol for the solid phase synthesis S4
     - 1.3.2. Synthesis of $AcP(Ox)_2$ S5
     - 1.3.3. Synthesis of the fluorophore labelled peptide S5
     - 1.3.4. Preparation of $AcP(T_{Iso})_2$ and $AcP(T_{Gua})_2$ S6
     - 1.3.5. Preparation of $CFP(T_{Acet})_2$, $CFP(T_{Gly})_2$ and $CFP(T_{Gua})_2$ S6
   - 1.4. Circular dichroism S7
   - 1.5. General procedures for vesicle experiments S7
     - 1.5.1. Vesicle preparation S7
     - 1.5.2. DNA transport experiments in vesicles S8
   - 1.6. Cell assays S8
     - 1.6.1. Cell culture and live cell-imaging S8
     - 1.6.2. Uptake quantification by fluorometry S9
     - 1.6.3. Cell viability: MTT assay S10
2. Supporting figures S11

1. Supporting methods

1.1. Materials and methods

Briefly, reagents for synthesis were purchased from Fluka, GL Biochem and Aldrich, amino acid derivatives from Iris Biotech and GL Biochem, Trizma buffer (99.9 %) was from Aldrich, salts of the best grade available were from Scharlau, Panreac and Fischer used as received. 8-Hydroxypyrene-1,3,6-trisulfonic acid trisodium salt (HPTS) was from Sigma and *p*-xylene-bis-pyridinium bromide (DPX) was from Invitrogen. The aldehyde tested (Tgua) was synthesized following reported protocols.[1a] The CFR_8 peptide was prepared as reported elsewhere.[1b] Egg yolk L-α-phosphatidylcholine (EYPC) was from Avanti Polar Lipids. Deoxyribonucleic acid from herring sperm (Herring DNA) was from Aldrich. All reactions were performed under N_2 atmosphere. Unless stated otherwise, column chromatography was carried out on silica gel 60 (Fluka, 40-63 μm). Analytical thin layer chromatography (TLC) was performed in silica gel 60 (Merck, 0.2 mm, F254).

Ultra-high-performance liquid chromatography coupled with mass spectrometry (UHPLC-MS) analyses were carried out on Agilent Technologies 1260 Infinity II associated with a 6120 Quadrupole LC-MS using an Agilent SB-C18 column with *Solvent A: Solvent B* gradients between 5:95, 95:5 (*Solvent A*: H_2O with 0.1 % TFA; *Solvent B*: CH_3CN with 0.1 % TFA). High-performance liquid chromatography (HPLC) preparative purification was carried out on Waters 1525 composed by a binary pump with a dual Waters 2489 detector with a Phenomenex Luna C18(2) 100A column. An Agilent 1200 with an Agilent Luna C18(2) 100A column were used for semi-preparative purifications, with gradients between 95:5 and 5:95 (*Solvent A*: H_2O with 0.1 % TFA; *Solvent B*: CH_3CN with 0.1 % TFA). All the HPLC spectra reported show the absorbance at 222 nm in ordinates axis and the time in minutes in abscises axis.

Nuclear Magnetic Resonance (NMR) spectra were recorded on a Bruker 500 MHz spectrometer. Chemical shifts are reported in ppm (δ units) referenced to the following solvent signals: D_2O δH 4.79. Accurate mass determinations (HR-MS) using ESI-MS were

[1] a) Priegue, J. M.; Crisan, D. N.; Martínez-Costas, J.; Granja, J. R.; Fernandez-Trillo, F.; Montenegro, J. *Angew. Chem. Int. Ed.* **2016**, *55*, 7492–7495. b) Rothbard, J. B.; Kreider, E.; VanDeusen, C. L.; Wright, L.; Wylie, B. L.; Wender, P. A. *J. Med. Chem.* **2002**, *45* (17), 3612-3618.

performed on a Sciex QSTAR Pulsar mass spectrometer and are reported as mass-per-charge ratio *m/z*.

Recalculations of concentrations of the labelled peptide (CF extinction coefficient = 81500 M^{-1} cm^{-1}) were carried out by ultraviolet-visible (UV-VIS) spectra, which were recorded on a Dynamica HALO XB-10 UV-VIS Single Beam Spectrophotometer. Circular Dichroism (CD) measurements were performed with a Jasco J-1100 CD Spectrometer equipped with a Jasco MCB-100 Mini Circulation Bath.

Vesicles were prepared with a Mini-Extruder from Avanti Polar Lipids (pore size 100 nm). Peptide/aldehyde incubation for oxime bond formation was performed in 500 µl eppendorf vials in a Thermo-shaker TS-100C Biosan. Fluorescence measurements were performed with a FluoroMax-2 spectrofluorometer (Jobin-Yvon Spex) equipped with a stirrer and a temperature controller.

Cell fluorescent images were acquired with an Andor Zyla 4.2 digital camera mounted on a Nikon Eclipse Ti-E fluorescence microscope. Absorbance and fluorescence of cellular extracts were measured using a microplate reader Tecan Infinite F200Pro. $[\alpha]_D^{22}$ values were recorded on a Jasco P-1030 Polarimeter (reported for concentrations c in g / 100 ml solvent). IR spectra were recorded on a Perkin Elmer Spectrum One FT-IR spectrometer (ATR, Golden Gate, unless stated otherwise) and are reported as wavenumbers ν in cm^{-1} with band intensities indicated as s (strong), m (medium), w (weak), b (broad).

1.2. Abbreviations

Aa: Amino acid; Arg: Arginine; Boc: tert-Butoxycarbonyl; Calcd: Calculated; Cbz: (Benzyloxy)carbonyl; CF: 5(6)-Carboxyfluorescein; DCM: Dichloromethane; DIEA: *N*,*N*-Diisopropylethylamine; DMF: *N*,*N*-Dimethylformamide; DMSO: Dimethylsulfoxide; DPX: p-Xylene-bispyridinium bromide; EYPC: Egg yolk phosphatidylcholine; HFIP: 1,1,1,3,3,3-Hexafluoro-2-propanol; HPTS: 8-Hydroxypyrene-1,3,6-trisulfonic acid trisodium salt; HR-MS (ESI): High resolution mass spectrometry (electrospray ionization); LUVs: Large unilamellar vesicles; Lys: Lysine; Tris: Tris(hydroxymethyl)aminomethane; Mtt: 4-Methyltrytil; *N*-HATU: *N*-[(Dimethylamino)-1*H*-1,2,3-triazolo[4,5-*b*]pyridine-1-

ylmethylene]-*N*-methylmethanaminium-hexafluorophosphate *N*-oxide; *N*-HBTU: *N*-[(1*H*-Benzotriazol-1-yl)-(dimethylamino)methylene]-*N*-methylmethanaminium hexafluorophosphate *N*-oxide; Ox: Oxime; Pbf: 2,2,4,6,7-Pentamethyldihydrobenzofuran-5-sulfonyl; SPPS: solid phase peptide synthesis; TFE: Trifluoroethanol; TIS: Triisopropylsilane; TNBS: 2,4,6-Trinitrobenzenesulfonic acid.

1.3 Synthesis

1.3.1. General protocol for the solid phase synthesis

The peptide was synthesized by manual Fmoc solid-phase peptide synthesis (SPPS)[2] using Rink amide solid support (140 mg, load: 0.71 mg/mmol) previously swelled in DMF (peptide synthesis grade) for 30 min and then filtered and washed with DMF (3 x 4 ml, 3 min). Coupling cycle consisted of Fmoc group deprotection with a solution of piperidine in DMF (20%, 2 x 5 ml, 15 min) and DMF wash (3 x 3 ml, 1 min) followed by coupling with α-amino acids (4 equiv), *N*-HBTU (4 equiv) and DIEA (4 equiv, 0.195 M solution in DMF) for 30 min. Finally the resin was washed with DMF (3 x 3 ml, 1 min). Each peptide coupling and deprotection was monitored employing the TNBS test.[3] Once the lineal peptide was finished the acetylation capping of N-terminal group was performed by standard Fmoc deprotection conditions (20% piperidine in DMF (2 x 5 ml, 15 min)) followed by treatment with a solution of 2,6-lutidine/acetic anhydride (1:1, 3 ml). The resin suspension was mechanically shaken for 40 min and washed with DMF (3 x 3 ml, 1 min) and DCM (3 x 3 ml, 5 min). The Mtt protective group was selectively removed by mechanically stirring the resin in a mixture of DCM/HFIP/TFE/TIS (6.5:2:1:0.5, 2 x 3 ml, 3 h). After Mtt deprotection, the resin was washed with DCM (3 x 3 ml, 1 min) and DMF (3 x 3 ml, 10 min). A solution of (Boc-aminooxy)acetic acid (2.5 equiv per free Lysine) and *N*-HATU (2.5 equiv per free Lysine) in DMF (1 ml) was added to resin followed by the dropwise addition of a solution of a DIEA (2.5 equiv per free Lysine) in DMF (1 ml). The resin was then mechanically stirred for 45 min and finally washed with DMF (3 x 3 ml, 5 min) and DCM (3 x 3 ml, 5 min). The peptides were deprotected and cleaved from the resin

[2] Behrendt, R.; White, P.; Offer, J. *J. Pept. Sci.* **2016**, *22*, 4-27.
[3] Kay, C.; Lorthioir, O.E.; Parr N.J.; Congreve, M.; McKeown, S.C.; Scicinski, J.J.; Ley, S.V. *Biotechnol. Bioeng.* **2000**, *71*, 110-8.

by standard TFA cleavage at room temperature (TFA/DCM/H_2O/TIS, 90:5:2.5:2.5, 2 h) as shown in the scheme in fig. S1. Then, the mixture was filtered and the peptides were precipitated in ice-cold Et_2O and filtered. The precipitate was centrifuged and washed with Et_2O (2 x 10 mL). Crude peptides were dissolved in CH_3CN/H_2O (1:1, 1 mL) and purified using a C18 reverse-phase HPLC [Nucleosil 100-7 C18, H_2O (0.1% TFA)/CH_3CN (0.1% TFA) with a binary gradient of *Solvent A* and *Solvent B*, the collected fractions were lyophilized and stored at -20 °C. Purity and characterization were confirmed by analytical HPLC, ^{1}H NMR and mass spectrometry.

1.3.2. Synthesis of AcP(Ox)$_2$

Following the general protocol for the solid phase synthesis, the AcP(Ox)$_2$ was obtained after HPLC purification with an overall yield of 12 %. R_t = 16.7 min. RP-HPLC [Nucleosil 100-7 C18, H_2O (0.1% TFA)/CH_3CN (0.1% TFA) 95:5→5:95 (5→35 min), 0:100 (>35 min)]. $[\alpha]_D^{22}$: -6.3 (c = 0.0525 in H_2O/CH_3CN, 1:1). IR (neat): 3292 (m), 3250 (m), 2957 (m), 2805 (w), 1542 (m), 1451 (w), 1340 (w), 1224(w), 1200 (w), 1178 (m), 1136 (m), 1096 (w), 1012 (w), 836 (w), 725 (w). ^{1}H-NMR (500 MHz, D_2O): 4.4-4.1 (m, 17H), 3.3-3.2 (m, 10H), 2.1 (s, 3H), 1.9-1.5 (m, 40H), 1.5-1.4 (m, 11H), 1.0-0.85 (m, 32H). MS (ESI, H_2O): 1709 (10, $[M+H]^+$), 855 (50, $[M+2H]^{2+}$), 571 (100, $[M+3H]^{3+}$), 428 (10, $[M+4H]^{4+}$) (Fig. S2). HR-MS (ESI) Calcd for: $C_{71}H_{135}N_{25}O_{14}$ 1709.1026 found: 1709.1021.

1.3.3. Synthesis of the fluorophore labelled peptide

Following the general protocol for the solid phase synthesis, CFP(Ox)$_2$ was obtained after the last Fmoc group deprotection with a solution of piperidine in DMF (20%, 2 x 5 ml, 15 min) and DMF wash (3 x 3 ml, 1 min) followed by coupling with 5(6)-carboxyfluorescein (2 equiv), *N*-HBTU (2 equiv) and DIEA (0.25 equiv) for 4 hours (Fig. S5). The CFP(Ox)$_2$ was directly reacted with the corresponding aldehydes and the resulting oximes were purified by HPLC.

1.3.4. Preparation of $AcP(T_{Iso})_2$ and $AcP(T_{Gua})_2$

5 µL of $AcP(Ox)_2$ (50 mM) in H_2O/DMSO/AcOH (1:1:0.05) were mixed with 2 equivalents of the different aldehyde for each aminooxyacetate of the peptide (e.g., 10 µl of 100 mM hydrophobic aldehyde in DMSO and adjusted to a total volume to 100 µl with H_2O/DMSO/AcOH (1:1:0.05). The mixture was stirred at 60°C for 1 hour and the resulting O-alkyloximes (upon corresponding dilution) were then used for DNA activation experiments. Oxime-bond formation was confirmed by HPLC-MS. RP-HPLC [Nucleosil 100-7 C18, H_2O (0.1% TFA)/CH_3CN (0.1% TFA) 95:5→5:95 (5→35 min), 0:100 (>35 min)]. $AcP(T_{Gua})_2$: R_t: 20.5 min; MS (ESI, H_2O/CH_3CN): 1194 (90, $[M+3TFA+2H]^{2+}$), 720 (20, $[M+TFA+3H]^{3+}$), 512 (100, $[M+4H]^{4+}$) (Fig. S4). $AcP(T_{iso})_2$: R_t: 22.5 min; MS (ESI, H_2O): 1846 (65, $[M+H]^{+}$), 924 (100, $[M+2H]^{2+}$), 616 (80, $[M+3H]^{3+}$) (Fig. S3).

1.3.5 Preparation of $CFP(T_{Gly})_2$, $CFP(T_{Gua})_2$ and $CFP(T_{Acet})$

Reactive peptides of $CFP(Ox)_2$ in H_2O (5 mM) were mixed with 2 equivalents of T_{Gly} (60 mM), T_{Gua} (60 mM) and T_{Acet} (60 mM) and adjusted the total volume to 500 µl with H_2O/DMSO/AcOH (1:1:0.05). The mixture was stirred at 60°C for 1 hour and the resulting O-alkyloximes were then directly used, after dilution in HKR buffer, in HeLa cells experiments. Oxime-bond formation was confirmed HPLC-MS. RP-UHPLC [SB-C18, H_2O (0.1% TFA)/CH_3CN (0.1% TFA) 95:5→5:95 (5→15 min), 0:100 (>15 min)]. $CFP(T_{Gly})_2$: R_t: 11.1 min; MS (ESI, H_2O/CH_3CN): 724 (100, $[M+3H]^{3+}$) (Fig S6). $CFP(T_{Gua})_2$: R_t: 10.5 min; MS (ESI, H_2O/CH_3CN): 788 (100, $[M+3H]^{3+}$)], 592 (15, $[M+4H]^{4+}$), 473 (10, $[M+5H]^{5+}$) (Fig S7). $CFP(T_{Acet})_2$: R_t: 12 min; MS (ESI, H_2O/CH_3CN): 703 (100, $[M+3H]^{3+}$)], 528 (10, $[M+4H]^{4+}$) (Fig. S8).

1.4. Circular Dichroism

Circular dichroism measurements were carried out with the following settings: acquisition range: 300-190 nm; band width: 1.0 nm; accumulation: 3 scans; data pitch: 1 nm; CD scale 200 mdeg/1.0 dOD; D.I.T. (Data Integration Time): 1 s; scanning mode: continuous; scanning speed: 200 nm/min. Measurements were done from 10 ºC to 60 ºC (data interval: 10 ºC; temp. gradient 5 ºC/min) in a quartz cell of 0.2 cm path length at a final volume of 0.5 mL (H_2O or TFE) with a final peptide concentration of 200 μM. The results are expressed as the mean residue molar ellipticity $[\theta]_{MRt}$ with units of degrees·cm^2·dmol^{-1} and calculated using the following equation S1.

$$[\Theta]_{MRt} = \frac{0.1\ x\ \Theta}{C \cdot l \cdot \text{number of residues}} \quad (\text{deg} \cdot \text{cm}^2 \cdot \text{dmol}^{-1}) \qquad \text{(S1)}$$

Equation S1: Formula to calculate the ellipticity. Θ is the ellipticity (mdeg), C is the peptide concentration (M) and l is the cell path length (cm).

1.5. General procedures for vesicle experiments

1.5.1. Vesicle preparation

A thin lipid film was prepared by evaporating a solution of EYPC (25 mg) in a mixture of MeOH and $CHCl_3$ (1:1, 1 ml) on a rotary evaporator (room temperature) and then *in vacuo* overnight. The resulting film was hydrated with 1.0 ml buffer (5 mM HPTS, 16.5 mM DPX, 10 mM Tris, 72 mM NaCl, pH 7.4) for more than 30 min, subjected to freeze-thaw cycles (7 times) and extrusions (15 times) through a polycarbonate membrane (pore size 100 nm). Extravesicular components were removed by gel filtration (Sephadex G-50) with 10 mM Tris, 107 mM NaCl, pH 7.4. Final conditions: ~5 mM EYPC; inside: 5 mM HPTS, 16.5 mM DPX, 10 mM Tris, 72 mM NaCl, pH 7.4; outside: 10 mM Tris, 107 mM NaCl, pH 7.4.

1.5.2. DNA transport experiments in vesicles

EYPC-LUV stock solutions (5 µl) were diluted with a buffer (10 mM Tris, 107 mM NaCl, pH 7.4) and placed in a thermostated fluorescence cuvette (25 °C) and gently stirred (total volume 2000 µl; final lipid concentration 13 µM). HPTS efflux was monitored at λ 511 nm (λ_{ex} 413 nm) as a function of time after addition of oxime-peptide [(20 µl in DMSO) at variable concentrations 0.1-5 µM] at t = 25 s, DNA (20 µl stock solution in buffer, at fixed concentration 70 µM) at t = 50 s and aqueous Triton X-100 (1.2%, 40 µl, 370 µM final concentration) at t = 225 s. Fluorescence intensities were normalized to fractional emission intensity I(t) using equation S2.

$$I(t) = \frac{(It - I_0)}{(I\infty - I_0)} \qquad \text{(S2)}$$

Equation S2: Formula to normalize transport kinetics. I_0 = It at DNA addition, I_∞ = It at saturation after lysis.

1.6. Cell assays

1.6.1. Cell culture and live cell imaging

HeLa cells were grown at 37 ºC, 5 % CO_2, in Dulbecco's Modified Eagle's Medium (4500 mg/l glucose, L-glutamine, sodium pyruvate and sodium bicarbonate; Sigma-Aldrich), supplemented with 10 % fetal bovine serum (Sigma-Aldrich) and 1 % of Penicillin-Streptomycin-Glutamine Mix (Fischer).

For live cell imaging, HeLa cells grown on glass bottom dishes were washed with HEPES-Krebs-Ringer (HKR) buffer (5 mM HEPES, 137 mM NaCl, 2.68 mM KCl, 2.05 mM $MgCl_2$, 1.8 mM $CaCl_2$, pH 7.4) and incubated for 30 min with 1 µM Hoechst 33342 (ThermoFisher) in HKR to stain the nucleus. This solution was removed and cells were incubated for another 30 min with 4 µM of each ($CFP(T)_2$) diluted in HKR buffer, washed twice with HKR and examined on an epifluorescence microscope (Nikon Eclipse Ti-E).

For co-localization studies with lysosomes, cells were washed and then incubated with the different peptides in HKR for 30 min. After three HKR washes, pre-warmed complete culture media was added to the cells and they were incubated for 3 h at 37 ºC. For

lysosomal staining, the cells were washed again and incubated with 100 nM LysoTracker Deep Red (ThermoFisher) in HKR buffer for 10 min, followed by three washes and immediately imaged.

1.6.2. Uptake quantification by fluorometry

Cellular uptake of the $CFP(T)_2$ was determined by fluorometry following the procedure described by Holm *et al*.[4] with minor modifications. HeLa cells seeded the day before in 12-well plates were washed with HKR and incubated with 4 μM of each $CFP(T)_2$ diluted in HKR buffer for 30 min at 37 ºC. After incubation, cells were washed twice with HKR buffer, trypsinized and 1 ml of HKR buffer was added before pelleting cells by centrifugation at 500 g for 5 min. The supernatant was removed and the cell pellet was lysed by incubation with 300 μl of 0.1 M NaOH at 4 ºC for 1h.

The fluorescence of the $CFP(T)_2$ in the lysates was measured in a Infinite F200Pro microplate reader (Tecan) using λ_{ex} 485 nm and λ_{em} 535 nm and the concentration of the $CFP(T)_2$ was calculated by comparison with a calibration curve. Protein concentration was determined after neutralization of the NaOH in the lysates with a volume of 0.1 M HCl using a Coomassie (Bradford) assay kit (ThermoFisher) and measuring the absorbance at 570 nm (Infinite F200Pro, Tecan). Cellular uptake of the peptide was expressed as pmoles of peptide per mg of total protein.

To compare the uptake of the different $CFP(T)_2$, the distribution of each $CFP(T)_2$ in live cells was studied by microscopy and the amount of peptide internalized quantified by fluorometry as described in materials and methods. Cells incubated with the $CFP(T_{Gly})_2$ showed a punctate cytoplasmic fluorescence, suggesting the presence of the peptide inside vesicles. Although the punctate pattern is similar to the one observed for octaarginine, the number of fluorescent vesicles seemed higher in the case of the $CFP(T_{Gly})_2$. This was confirmed by quantification of the uptake by fluorometry, where it was observed a much higher uptake for the $CFP(T_{Gly})_2$ than for octaarginine.

---

[4] Holm, T.; Johansson, H.; Lundberg, P.; Pooga, M.; Lindgren, M.; Langel, U. *Nat. Protoc.* **2006**, *1*, 1001-1005.

1.6.3. Cell viability: MTT assay

Cell viability was established by a standard MTT assay. One day before the assay, a suspension of HeLa cells was plated in 96-well tissue culture plates (Costar 96 Flat Bottom Transparent Polystyrol) by adding 100 µl (~10.000 cells) per well. The next day, the medium was aspirated and cells were incubated in the presence of $CFP(T)_2$ (50 µl/well) in HKR buffer at different concentrations. After 30 min of incubation at 37 ºC, the HKR buffer was changed to DMEM containing 10% Fetal Bovine Serum (FBS) and the viability was measured by quantifying the cellular ability to reduce the water-soluble tetrazolium dye (3-(4,5-dimethylthiazol-2-yl)-2,5-diphenyltetrazolium bromide) (MTT) to its insoluble formazan salt as follows. MTT (5 mg/ml in PBS, 10 µl/well) was added to the wells and the cells were further incubated for 4 h. The supernatant was carefully removed and the water-insoluble formazan salt was dissolved in DMSO (100 µl/well). The absorbance at 560 nm was measured. Data points were collected in triplicate and expressed as normalized values for untreated control cells (100%).

USC UNIVERSIDADE DE SANTIAGO DE COMPOSTELA

2. Supporting Figures

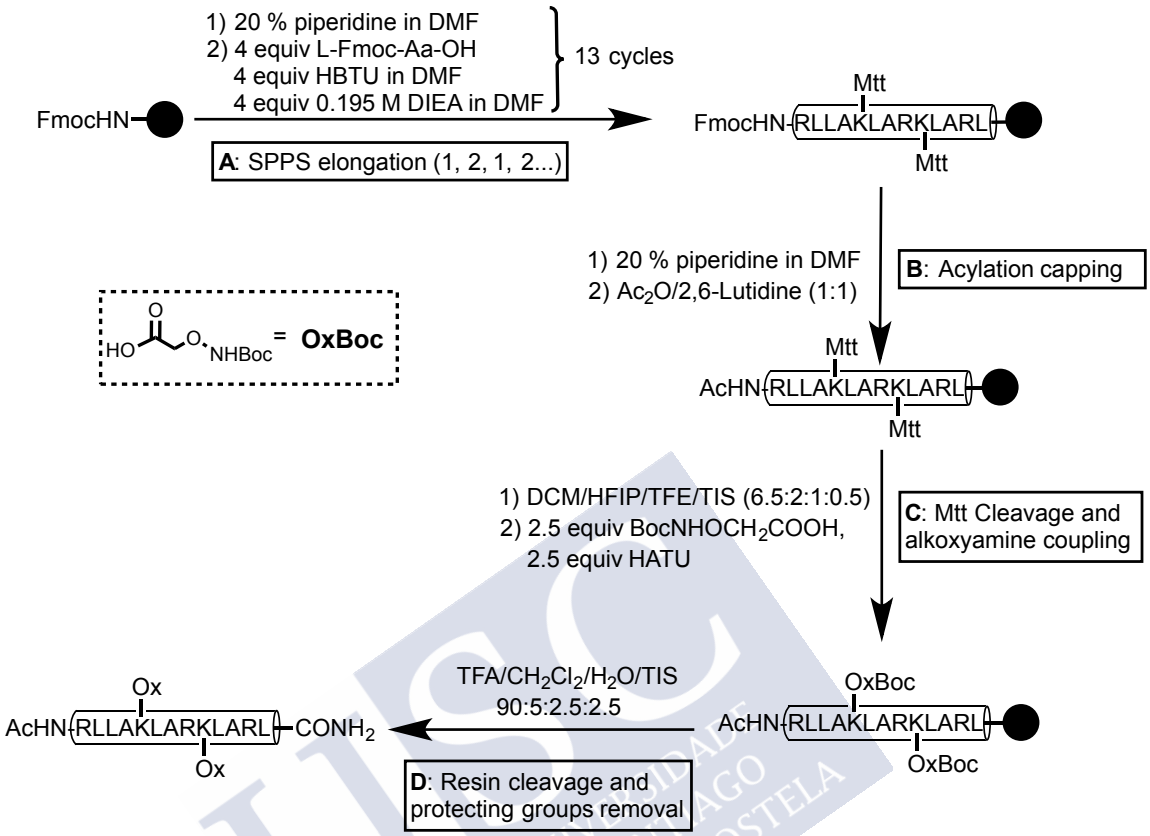

Fig. S1: General synthetic scheme for the acetylated reactive peptide.

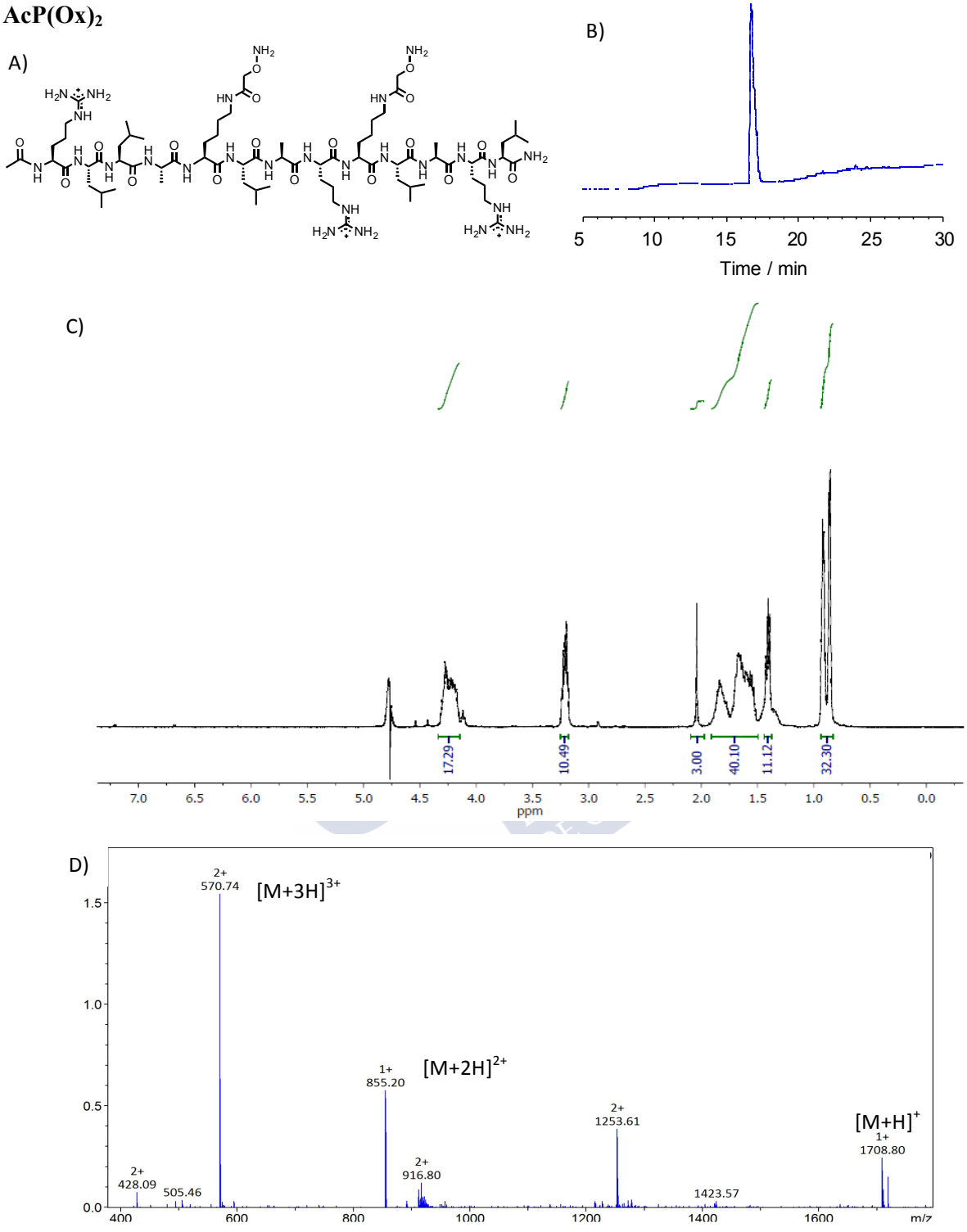

Fig. S2: A) Structure of $AcP(Ox)_2$; B) RP-HPLC [Nucleosil 100-7 C18, H_2O (0.1% TFA)/CH_3CN (0.1% TFA) 95:5→5:95 (5→35 min), 0:100 (>35 min)]. R_t 16.7 min; C) ^{1}H-NMR in D_2O; D) ESI-MS.

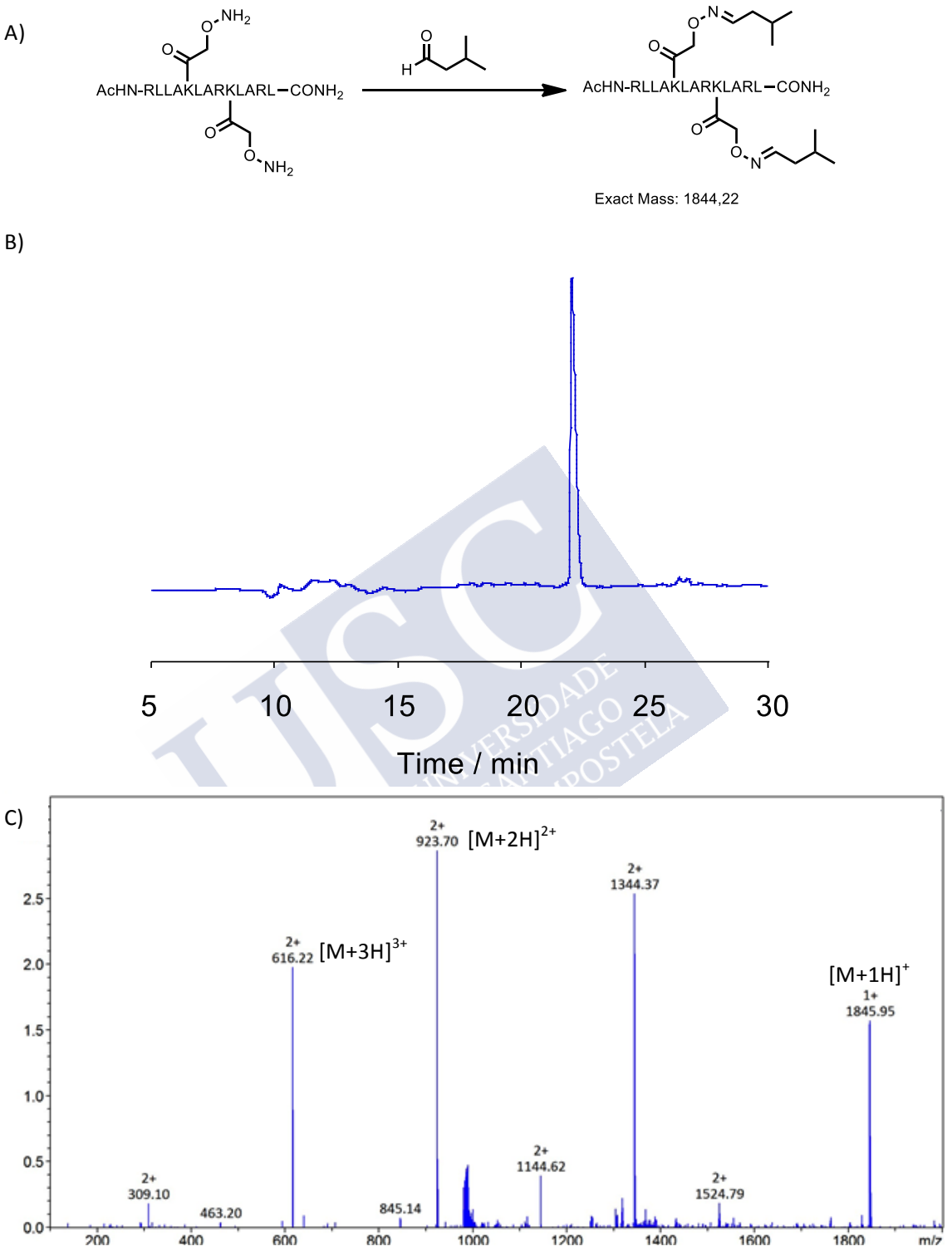

Fig. S3: A) Contracted structure of AcP(T_{iso})$_2$; B) RP-HPLC [Nucleosil 100-7 C18, H_2O (0.1% TFA)/CH_3CN (0.1% TFA) 95:5→5:95 (5→35 min), 0:100 (>35 min)]. R_t 22.5 min; C) ESI-MS.

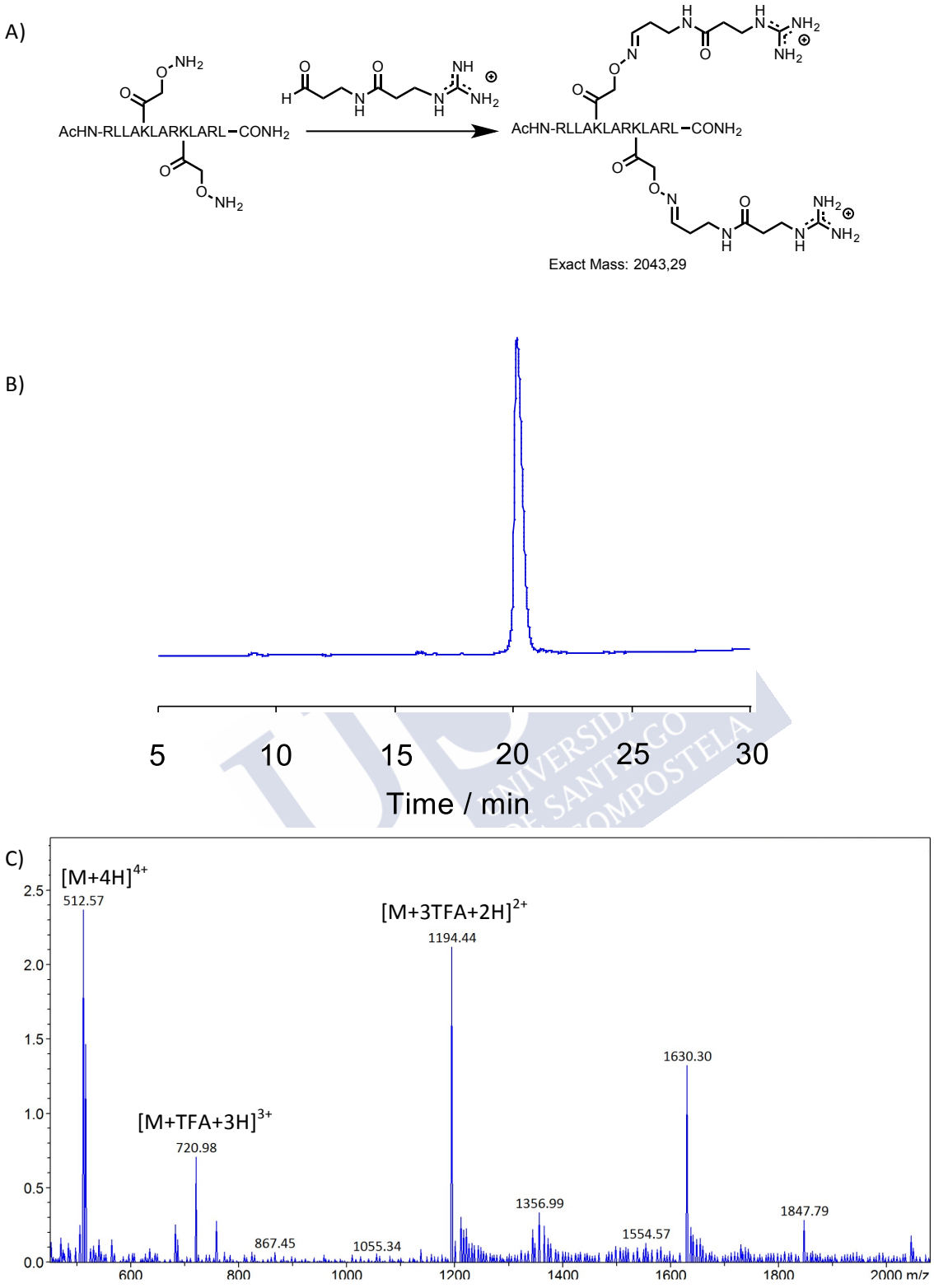

Fig. S4: A) Contracted structure of AcP(T_{Gua})$_2$; B) RP-HPLC [Nucleosil 100-7 C18, H_2O (0.1% TFA)/CH_3CN (0.1% TFA) 95:5→5:95 (5→35 min), 0:100 (>35 min)]. R_t 20.5 min; C) ESI-MS.

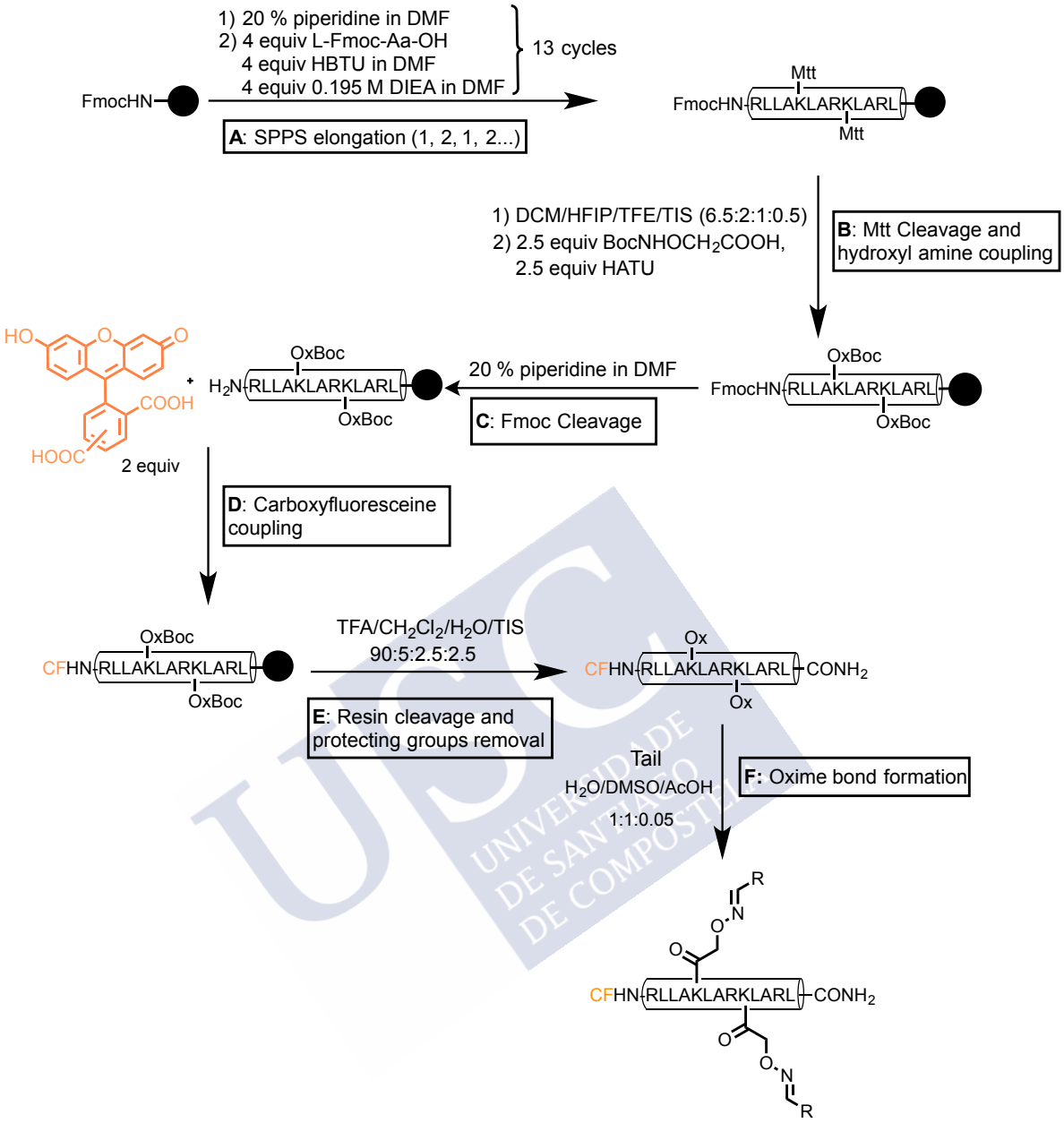

Fig. S5: General synthetic scheme for the reactive peptide labeled with fluorophore.

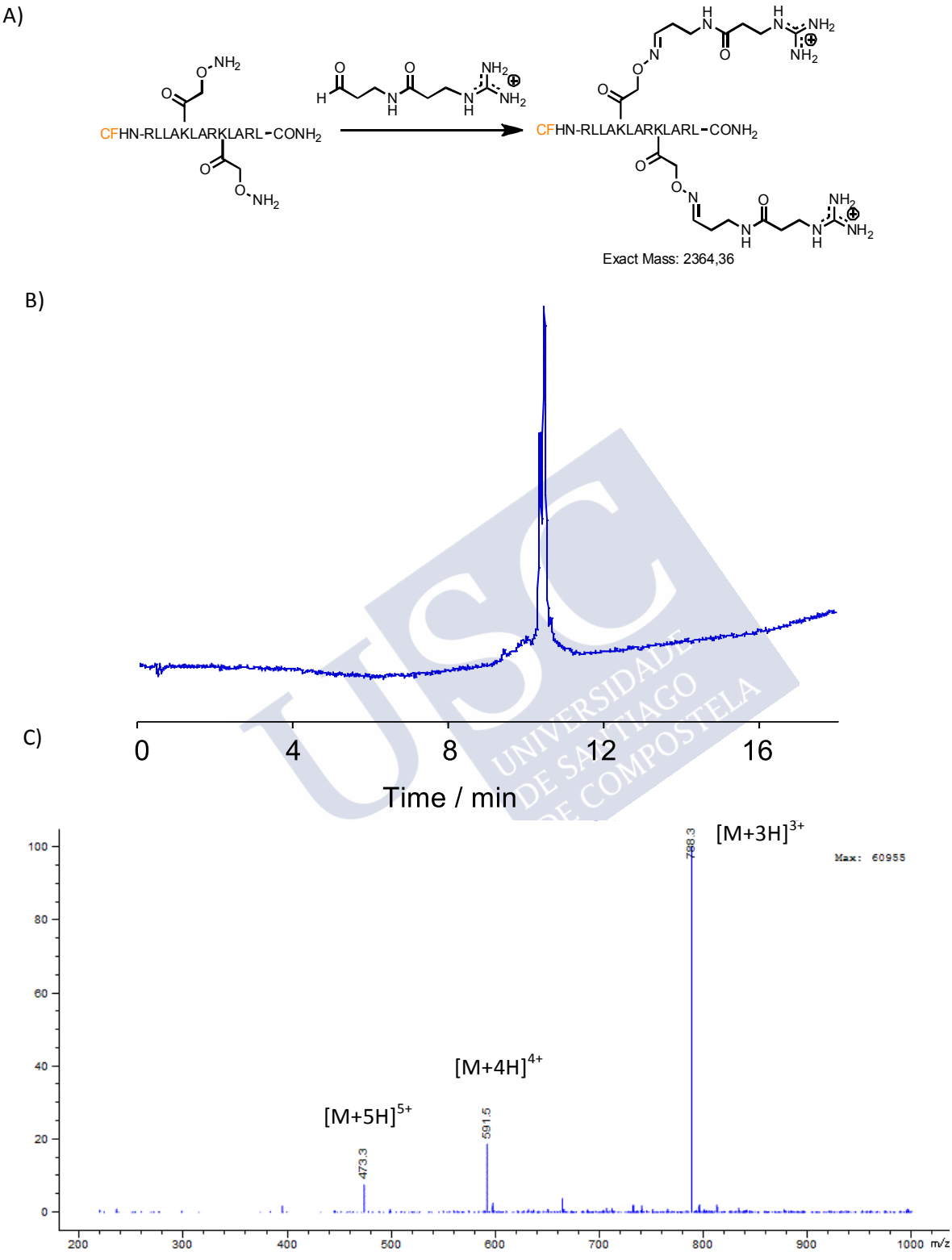

Fig. S7: A) Contracted structure of CFP(T_{Gua})$_2$; B) RP-UHPLC [SB-C18, H_2O (0.1% TFA)/CH_3CN (0.1% TFA) 95:5→5:95 (5→15 min), 0:100 (>15 min)]. R_t 10.5 min. The double peak (both with equal mass) could be due to CF regioisomers; C) ESI-MS.

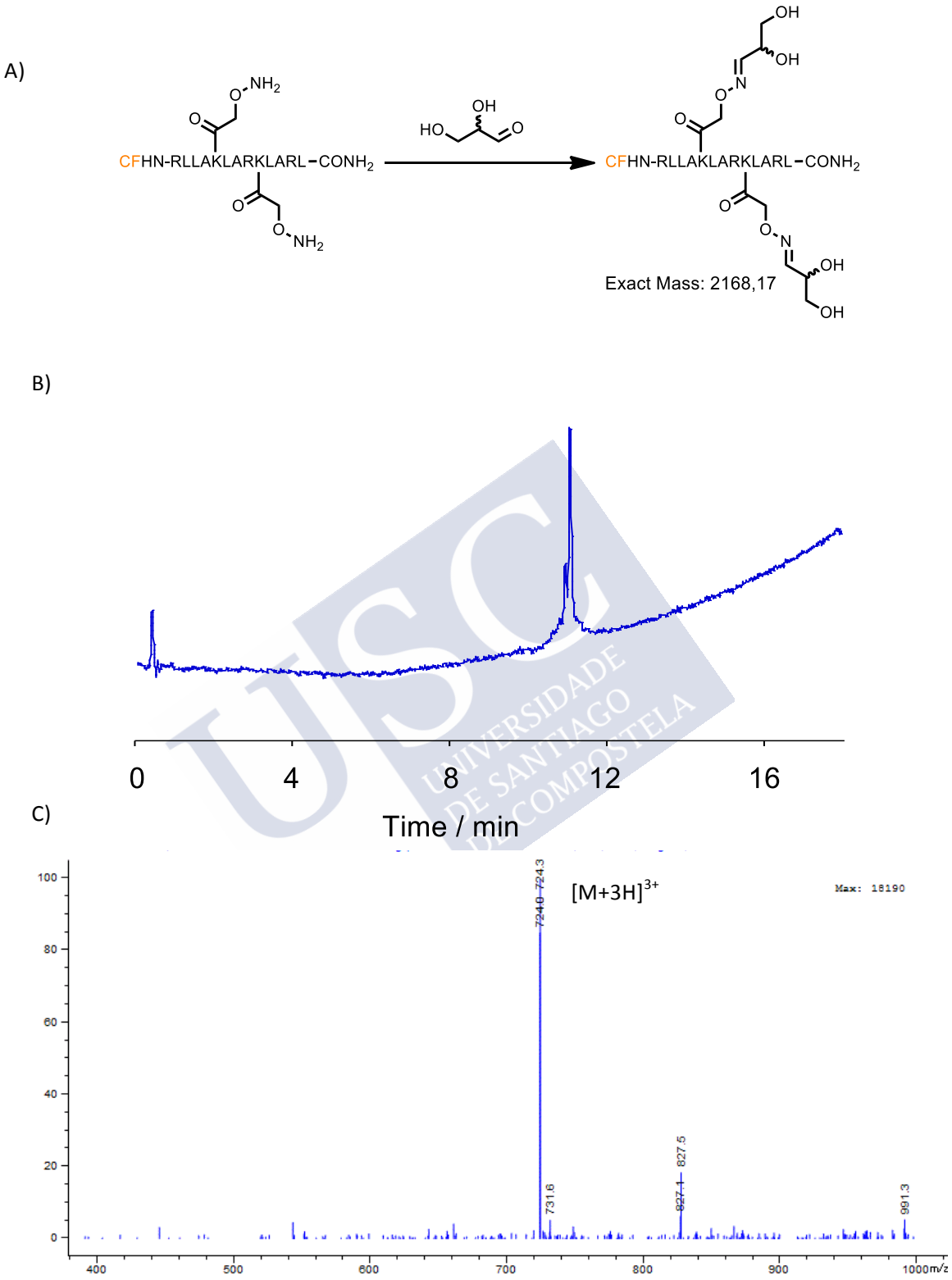

Fig. S6: A) Contracted structure of CFP(T_{Gly})$_2$; B) RP-UHPLC [SB-C18, H_2O (0.1% TFA)/CH_3CN (0.1% TFA) 95:5→5:95 (5→15 min), 0:100 (>15 min)]. R_t 11.1 min. The double peak (both with equal mass) could be due to CF regioisomers; C) ESI-MS.

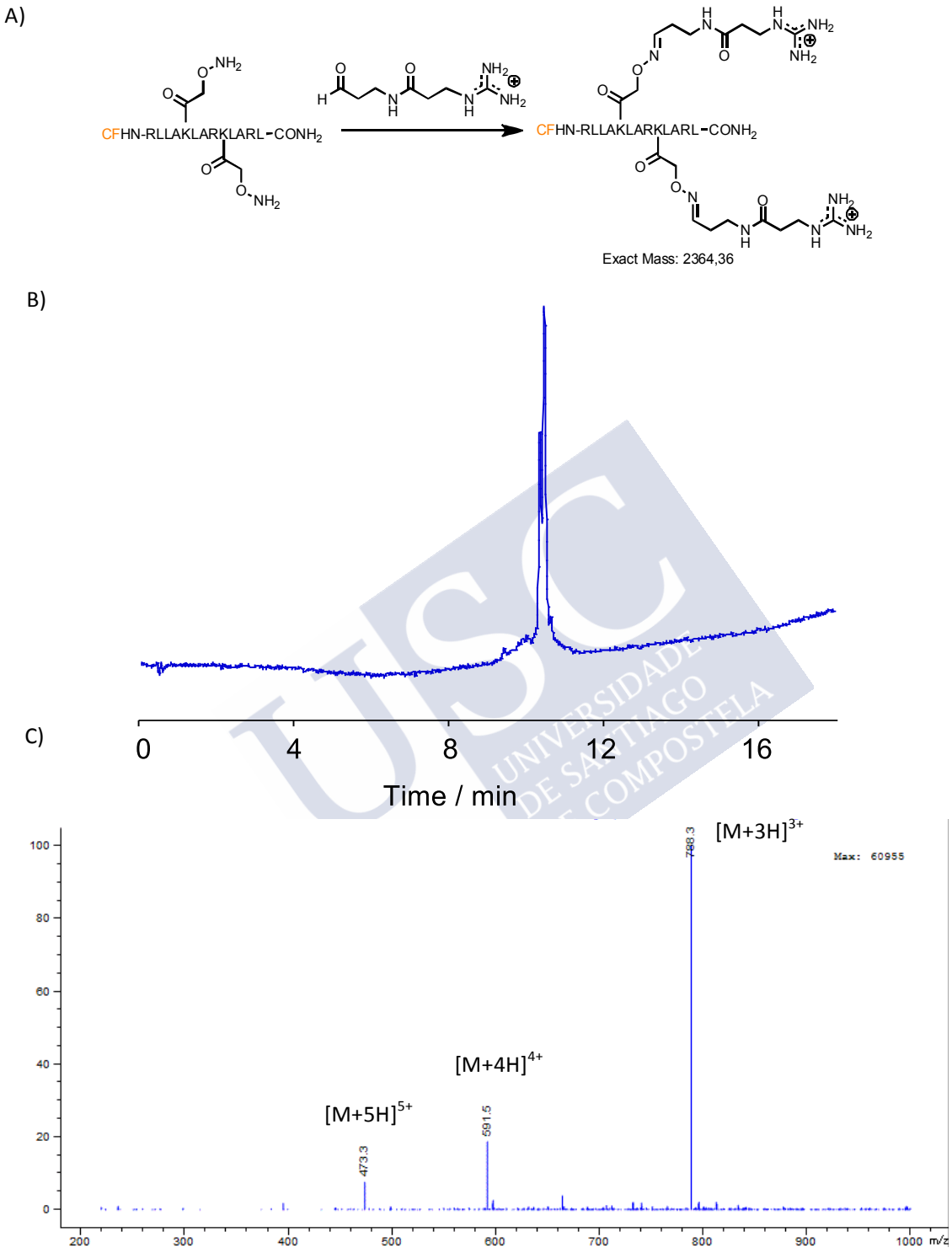

Fig. S7: A) Contracted structure of CFP(T_{Gua})$_2$; B) RP-UHPLC [SB-C18, H_2O (0.1% TFA)/CH_3CN (0.1% TFA) 95:5→5:95 (5→15 min), 0:100 (>15 min)]. R_t 10.5 min. The double peak (both with equal mass) could be due to CF regioisomers; C) ESI-MS.

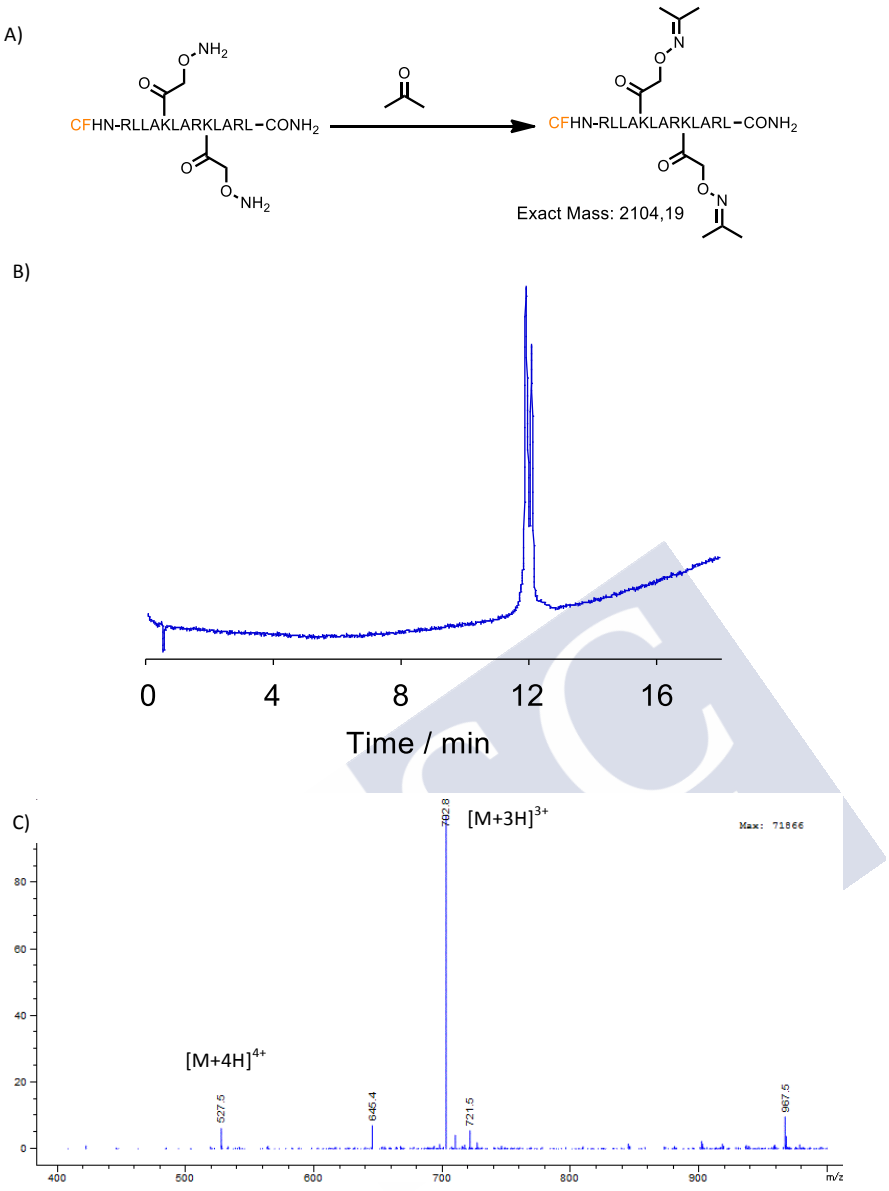

Fig. S8:A) Contracted structure of CFP(T_{Acet})$_2$; B) RP-UHPLC [SB-C18, H_2O (0.1% TFA)/CH_3CN (0.1% TFA) 95:5→5:95 (5→15 min), 0:100 (>15 min)]. R_t 12 min; The double peak (both with equal mass) could be due to CF regioisomers; C) ESI-MS.

USC
UNIVERSIDADE
DE SANTIAGO
DE COMPOSTELA

2. Oligoalanine Helical Callipers for Cell Penetration

USC UNIVERSIDADE DE SANTIAGO DE COMPOSTELA

USC
UNIVERSIDADE
DE SANTIAGO
DE COMPOSTELA

Oligoalanine Helical Callipers for Cell Penetration

*Marta Pazo,[a] Marisa Juanes,[a] Irene Lostalé-Seijo[a] & Javier Montenegro[a]**

[a] *Centro Singular de Investigación en Química Biolóxica e Materiais Moleculares (CIQUS), Departamento de Química Orgánica, Universidade de Santiago de Compostela, 15782 Santiago de Compostela, Spain.*

**e-mail: javier.montenegro@usc.es*

Supporting information

Table of contents:

Materials and methods S2
Abbreviations S3
General protocols S3
General protocol for the SPPS S3
General protocol for peptide cleavage and purification S4
Synthesis of peptide **P_1** S4
Synthesis of peptide **P_2** S4
Synthesis of peptide **P_{3*}** S5
Synthesis of peptide **P_4** S5
Synthesis of peptide **P_{5*}** S5
Synthesis of peptide **P_{6*}** a) and **P_7** b) S5
Synthesis of peptide **P_8** S6
Synthesis of peptide **R_8** S6
General protocol to measure Circular Dichroism S6
Cell assays S7
Cell culture and live cell imaging S7
Quantification of the uptake by flow cytometry S7
Quantification of inhibition of the uptake by flow cytometry S8
Cell viability S8
Peptide stability in serum S9
Supporting figures S10
Supporting figures of Characterization S20
Supporting references S26

Materials and methods

Commercially available Rink Amide-resin ChemMatrix, Fmoc-*L*-Ala-OH, Fmoc-*L*-Leu-OH, Fmoc-*L*-Arg(pbf)-OH, triisopropylsilane (TIS), Disopropylethyl amine (DIEA), diisopropylcarbodiimide (DIC) were obtained from Sigma-Aldrich. Trifluoroethanol, 1,1,1,3,3,3-Hexafluoroisopropanol (HFIP) was purchased from TCI. Egg yolk L-α-phosphatidylcholine was purchased from Avanti Polar Lipids. Ethyl(hydroxyimino)cyanoacetate (Oxyma) and 5-carboxytetramethyl rhodamine (TAMRA) were available from Carbosynth. *N*-HATU by Glentham life sciences. *N*-HBTU was obtained from Iris. Peptide synthesis grade *N,N*-dimethylformamide was purchased from Scharlau. Deuterated solvent (D_2O) was from EMD Millipore Corporation. All the other solvents were HPLC grade, purchased from Sigma-Aldrich® or Fisher Scientific®, and used without further purification.

Chlorpromazine was purchased from TCI Chemicals. Ammonium chloride, Chloroquine, Heparin sodium salt and 5-(N-Ethyl-N-isopropyl)amiloride were purchased from Sigma-Aldrich. Methyl-β-cyclodextrin was purchased from Carbosynth. Hoechst 33342 Trihydrochloride Trihydrate, and LysoTracker Deep Red were purchased in ThermoFisher. Wortmannin was obtained from Fluorochem. Dulbecco's Modified Eagle's Medium (4500 mg/L glucose, L-glutamine, sodium pyruvate and sodium bicarbonate) was purchased from Gibco.

A microwave assisted peptide synthesiser (Liberty Lite, CEM) was used to prepare the peptide according to standard methods developed by the manufacturers involving diisopropylcarbodiimide (DIC) 0.5 M in DMF as activator and ethyl(hydroxyimino)cyanoacetate (Oxyma) 1 M in DMF as activator base. Previous to HPLC, a quick size exclusion chromatography in sephadex G-25 eluted with Milli-Q water was carried out to remove the excess of fluorophore. High-performance liquid chromatography coupled with mass spectrometry (HPLC-MS) analyses were carried out on Agilent Technologies 1260 Infinity II associated with a 6120 Quadrupole LC-MS using an Agilent SB-C18 column or on DIONEX Ultimate 3000 U-HPLC$^+$ (Thermo Scientific) with an Acclaim RSLC 120-C18 column with *Solvent A:Solvent B* gradients between 5:95 (*Solvent A*: H_2O with 0.1% TFA; *Solvent B*: CH_3CN with 0.1% TFA). High-performance liquid chromatography (HPLC) semi-preparative purification was carried out on Jasco LC-4000 with an Agilent Eclipse XDB-C18 column.

Nuclear Magnetic Resonance (NMR) spectra were recorded on a Varian Mercury 300 MHz. Chemical shifts are reported in ppm referenced to the following solvent signals: HOD δ H 4.79 ppm. Spin multiplicities are reported as a singlet (s), doublet (d), triplet (t) with coupling constants (*J*) given in Hz, or multiplet (m). Accurate mass determinations (HR-MS) using ESI-MS were performed on a Bruker MicroTof mass spectrometer.

Circular Dichroism (CD) measurements were performed with a Jasco J-1100 CD Spectrometer equipped with a Jasco MCB-100 Mini Circulation Bath for temperature control.

For the acquisition of cell microscopy images an Andor Zyla 4.2 digital camera mounted on a Nikon Eclipse Ti-E epifluorescence microscope was used, and to do the images in 3D a Dragonfly confocal spinning-disk on a Nikon Eclipse Ti-E equipped with a Andor Zyla 4.2 PLUS sCMOS digital camera. The

3D projection was obtained from the different individual confocal planes with Imaris bitplane © 9.0.0 software.

A Tecan Infinite F200Pro microplate reader was used to measure directly in Costar cell culture 96-well plates UV-Vis absorbance for the MTT viability assays.

Flow cytometry was performed on a Guava easyCyteTM cytometer. Data analysis was performed with InCyte software included in GuavaSoft 3.2 (Millipore).

Abbreviations

Aa: Amino acid; Arg: Arginine; Calcd: Calculated; CLQ: Chloroquine; CPZ: Chlorpromazine; DCM: Dichloromethane; DIC: diisopropylcarbodiimide; DIEA: *N*,*N*-Diisopropylethylamine; DMF: *N*,*N*-Dimethylformamide; DYN: Dynasore; EIPA: 5-(*N*-Ethyl-*N*-isopropyl)amiloride; EYPC: Egg yolk phosphatidylcholine; Hep: Heparin sodium salt; HFIP: 1,1,1,3,3,3-Hexafluoro-2-propanol; HRMS (ESI): High resolution mass spectrometry (electrospray ionization); Leu: Leucine; Lys: Lysine; MbCD: Methyl-beta-Cyclodextrin; Mtt: 4-Methyltrytil; *N*-HATU:*N*-[(Dimethylamino)-1H-1,2,3-triazolo[4,5-b]pyridine-1ylmethylene]-*N*-methylmethanaminium-hexafluorophosphate *N*-oxide; *N*-HBTU: *N*-[(1HBenzotriazol-1-yl)-(dimethylamino)methylene]-*N*-methylmethanaminium hexafluorophosphate *N*-oxide; Pbf: 2,2,4,6,7-Pentamethyldihydrobenzofuran-5-sulfonyl; SPC: spacer; SPPS: solid phase peptide synthesis; TAMRA: 5-carboxytetramethyl rhodamine; TFE: Trifluoroethanol; TNBS: 2,4,6-Trinitrobenzenesulfonic acid; TIS: Triisopropylsilane; W: Wortmannin; 6Ahx: 6-aminohexanoic acid.

General protocols

General protocol for the SPPS

All peptides were synthesized by automated or manual Fmoc solid-phase peptide synthesis[S1] using Rink Amide ChemMatrix resin (loading 0.5 mmol/g). For manual synthesis, the resin (0.5 mmol) was swelled in DMF (peptide synthesis grade, 2 mL) for 20 min in a peptide synthesis vessel prior synthesis. Coupling cycle consisted of the removal of Fmoc protecting group with a solution of piperidine in DMF (20%, 2 mL) for 10 min and then the mixture was filtered and the resin was washed with DMF (3 x 2 mL, 1 min). The amino acid coupling was carried out by treatment with a solution of α-amino acids (4 equiv.), *N*-HBTU (3.95 equiv.) in DMF (2 mL), which was mixed with DIEA (0.195 M solution in DMF, 1.2 equiv.) 1 min before the addition and the resulting mixture was shaken by bubbling Ar for 15 min. Finally, the resin was washed with DMF (3 x 2 mL, 1 min). The efficiency of each amino acid coupling and deprotection was monitored employing the TNBS test.[S2]

For automated synthesis, a variant of the previous protocol was used instead, according to manufacturer's recommendations. 0.05 mmol of Rink Amide resin was placed into the peptide synthesiser reaction vessel, swollen in DMF, followed by cycles of Fmoc cleavage with piperidine 20% in DMF, washings (3 x 5 mL), then amino acid (5 equiv. 2M amino acid solution in DMF), DIC (10 equiv.) and Oxyma (10 equiv.) were

added into the reaction vessel and microwaved for 5 min under temperature control followed by washings (3 x 5 mL). All steps were performed under nitrogen atmosphere. After the linear peptide was finished the resin was transferred to a different reaction vessel to perform the peptide modification manually.

A) Linker coupling: after Fmoc cleavage with piperidine/DMF (20%, 2 mL), the linear peptide was treated with a solution of N-Fmoc-6-aminohexanoic acid (4 equiv.), *N*-HBTU (3.95 equiv.) and DIEA (0.195 M solution in DMF, 1.2 equiv.) in DMF.

B) Fluorophore coupling: the Fmoc-protecting group of the lineal final peptide (or the previously attached linker) was removed by using a solution of piperidine in DMF (20%, 4 mL) for 15 min and the resin was washed with DMF (3 x 3 mL). The coupling was carried out by the addition of a solution of 5-Carboxytetramethylrhodamine (1 equiv.), HATU (1 equiv.), and DIEA (0.195 M, 1 equiv.) in DMF (2 mL) and the mixture was stirred by bubbling Ar for 4 hours. Finally, the resin was washed with DMF (3 x 3 mL) and DCM (3 x 3 mL).

General protocol for peptide cleavage and purification

Finally, peptides were deprotected and cleaved from the resin by standard TFA cleavage procedure at rt by using the TFA/DCM/H_2O/TIS (90:5:2.5:2.5, 3 mL per 70 mg of resin) for 2 h. Then, the mixture was filtered, washed with TFA (1 mL) and the peptide was precipitated with ice-cold Et_2O (50 mL). The precipitate was centrifuged and dissolved in H_2O (5 mL).

Peptides were purified first with sephadex size exclusion chromatography (G-25, Milli-Q water) and then by semi-preparative high-performance liquid chromatography (HPLC) as previously described. Finally, the corresponding fractions were lyophilised to afford the pure peptide as pink solids.

Synthesis of peptide P_1

Following the general protocol of the SPPS followed by fluorophore coupling, **P_1** was obtained after RP-HPLC purification [Phenomenex Luna C18(2) 100A column, H_2O (0.1% TFA)/ CH_3CN (0.1% TFA) 95:5→5:95 (0→5 min), 95:5→5:95 (5→35 min)] with an overall yield of 12%. R_t 13.0 min [RP-HPLC Agilent SB-C18 column, H_2O (0.1% TFA)/ CH_3CN (0.1% TFA) 95:5→5:95 (0→20 min)] (Fig. S12). **MS** (ESI, H_2O): 911.9 (35, $[M+2H]^{2+}$), 608.3 (100, $[M+3H]^{3+}$), 456.5 (35, $[M+4H]^{4+}$). **HRMS** (ESI): Calcd for $C_{82}H_{126}N_{28}O_{20}$ $[M+2H]^{2+}$: 911.4846; found: 911.4839.

Synthesis of peptide P_2

Following the general protocol of the SPPS followed by fluorophore coupling, **P_2** was obtained after RP-HPLC purification [Phenomenex Luna C18(2) 100A column, H_2O (0.1% TFA)/ CH_3CN (0.1% TFA) 95:5→5:95 (0→5 min), 95:5→5:95 (5→35 min)] with an overall yield of 10.7%. R_t 14.6 min [RP-HPLC Agilent SB-C18 column, H_2O (0.1% TFA)/ CH_3CN (0.1% TFA) 95:5→5:95 (0→20 min)] (Fig. S13). **MS** (ESI, H_2O): 953.9 (40, $[M+2H]^{2+}$), 636.3 (100, $[M+3H]^{3+}$), 477.6 (35, $[M+4H]^{4+}$). **HRMS** (ESI): Calcd for $C_{88}H_{138}N_{28}O_{20}$ $[M+2H]^{2+}$: 953.5317; found: 953.5316.

Synthesis of peptide P_{3*}

Following the general protocol of the SPPS followed by linker and fluorophore coupling, **P_{3*}** was obtained after RP-HPLC purification [Phenomenex Luna C18(2) 100A column, H_2O (0.1% TFA)/ CH_3CN (0.1% TFA) 95:5→5:95 (0→5 min), 95:5→5:95 (5→35 min)] with an overall yield of 8.7%. R_t 14.2 min. [RP-HPLC Agilent SB-C18 column, H_2O (0.1% TFA)/ CH_3CN (0.1% TFA) 95:5→5:95 (0→20 min)] (Fig. S14). **MS** (ESI, H_2O): 1088.8 (5, $[M+2H+TFA]^{2+}$), 1031.4 (35, $[M+2H]^{2+}$), 688.0 (100, $[M+3H]^{3+}$), 516.3 (40, $[M+4H]^{4+}$). **HRMS** (ESI): Calcd for $C_{97}H_{155}N_{29}O_{21}$ $[M+2H]^{2+}$: 1031.0976; found: 1031.0971.

Synthesis of peptide P_4

Following the general protocol of the SPPS followed by fluorophore coupling, **P_4** was obtained after RP-HPLC purification [Phenomenex Luna C18(2) 100A column, H_2O (0.1% TFA)/ CH_3CN (0.1% TFA) 95:5→5:95 (0→5 min), 95:5→5:95 (5→35 min)] with an overall yield of 6.5%. R_t 14.9 min [RP-HPLC Agilent SB-C18 column, H_2O (0.1% TFA)/ CH_3CN (0.1% TFA) 95:5→5:95 (0→20 min)] (Fig. S15). **MS** (ESI, H_2O): 975.0 (70, $[M+2H]^{2+}$), 650.3 (100, $[M+3H]^{3+}$), 488.0 (15, $[M+4H]^{4+}$). **HRMS** (ESI): Calcd for $C_{91}H_{144}N_{28}O_{20}$ $[M+2H]^{2+}$: 974.5551; found: 974.5550.

Synthesis of peptide P_{5*}

Following the general protocol of the SPPS followed by linker and fluorophore coupling, **P_{5*}** was obtained after RP-HPLC purification [Phenomenex Luna C18(2) 100A column, H_2O (0.1% TFA)/ CH_3CN (0.1% TFA) 95:5→5:95 (0→5 min), 95:5→5:95 (5→35 min)] with an overall yield of 2.9%. R_t 15.2 min [RP-HPLC Agilent SB-C18 column, H_2O (0.1% TFA)/ CH_3CN (0.1% TFA) 95:5→5:95 (0→20 min)] (Fig. S16). **MS** (ESI, H_2O): 1031.4 (38, $[M+2H]^{2+}$), 688.0 (100, $[M+3H]^{3+}$), 516.3 (55, $[M+4H]^{4+}$). **HRMS** (ESI): Calcd for $C_{97}H_{155}N_{29}O_{21}$ $[M+2H]^{2+}$: 1031.0976; found: 1031.0886.

Synthesis of peptide P_{6*} a) and P_7 b)

a) Following the general protocol of the SPPS followed by linker and fluorophore coupling, **P_{6*}** was obtained after RP-HPLC purification [Phenomenex Luna C18(2) 100A column, H_2O (0.1% TFA)/ CH_3CN (0.1% TFA) 95:5→5:95 (0→5 min), 95:5→5:95 (5→35 min)] with an overall yield of 6.4%. R_t 15.2 min [RP-HPLC Agilent SB-C18 column, H_2O (0.1% TFA)/ CH_3CN (0.1% TFA) 95:5→5:95 (0→20 min)] (Fig. S17). **MS** (ESI, H_2O): 1031.4 (40, $[M+2H]^{2+}$), 688.0 (100, $[M+3H]^{3+}$), 516.3 (50, $[M+4H]^{4+}$). **HRMS** (ESI): Calcd for $C_{97}H_{155}N_{29}O_2$ $[M+2H]^{2+}$: 1031.0976; found: 1031.097.

b) Following the general protocol of the SPPS followed by fluorophore coupling, **P_7** was obtained after RP-HPLC purification [Phenomenex Luna C18(2) 100A column, H_2O (0.1% TFA)/ CH_3CN (0.1% TFA) 95:5→5:95 (0→5 min), 95:5→5:95 (5→35 min)] with an overall yield of 5.3%. R_t 15.5 min [RP-HPLC Agilent SB-C18 column, H_2O (0.1% TFA)/ CH_3CN (0.1% TFA) 95:5→5:95 (0→20 min)] (Fig. S18). **MS** (ESI, H_2O): 974.8 (50, $[M+2H]^{2+}$), 650.3 (100, $[M+3H]^{3+}$), 488.1 (30, $[M+4H]^{4+}$). **HRMS** (ESI): Calcd for $C_{91}H_{144}N_{28}O_{20}$ $[M+2H]^{2+}$: 974.5544; found: 974.5550.

Synthesis of peptide P_8

Following the general protocol of the SPPS followed by fluorophore coupling, **P_8** was obtained after RP-HPLC purification [Phenomenex Luna C18(2) 100A column, H_2O (0.1% TFA)/ CH_3CN (0.1% TFA) 95:5→5:95 (0→5 min), 95:5→5:95 (5→35 min)] with an overall yield of 1.7%. R_t 15.2 min [RP-HPLC Agilent SB-C18 column, H_2O (0.1% TFA)/ CH_3CN (0.1% TFA) 95:5→5:95 (0→20 min)] (Fig. S19). **MS** (ESI, H_2O): 974.8 (40, $[M+2H]^{2+}$), 650.3 (100, $[M+3H]^{3+}$), 488.1 (23, $[M+4H]^{4+}$). **^{1}H NMR** (300 MHz, D_2O) δ 8.53-8.45 (m, 1H), 8.18-8.10 (m, 1H), 7.57-7.47 (m, 1H), 7.21-7.10 (m, 2H), 6.96-6.86 (m, 2H), 6.68 (s, 2H), 4.38-4.15 (m, 16H), 3.30-3.10 (m, 18H), 1.94-1.59 (m, 22H), 1.55-1.35 (m, 30H), 1.05-0.84 (m, 18H). **HRMS** (ESI): Calcd for $C_{91}H_{144}N_{28}O_{20}$ $[M+2H]^{2+}$: 974.5555; found: 974.5550.

Synthesis of peptide R_8

Following the general protocol of the SPPS followed by fluorophore coupling, **R8** was obtained after RP-HPLC purification [Phenomenex Luna C18(2) 100A column, H_2O (0.1% TFA)/ CH_3CN (0.1% TFA) 100:0→100:0 (0→5 min), 50:50→50:50 (5→35 min)] with an overall yield of 1.7%. R_t 11.4 min (Fig. S20) [RP-HPLC Agilent SB-C18 column, H_2O (0.1% TFA)/ CH_3CN (0.1% TFA) 95:5→5:95 (0→20min). **MS** (ESI, H_2O): 1067.7 (19, $[M+2H+3TFA]^{2+}$), 1010.8 (10, $[M+2H+2TFA]^{2+}$), 712.2 (45, $[M+3H+3TFA]^{3+}$), 674.2 (100, $[M+3H+2TFA]^{3+}$), 636.5 (75, $[M+3H+TFA]^{3+}$), 598.2 (20, $[M+3H]^{3+}$), 477.5 (40, $[M+4H+TFA]^{4+}$), 448.9 (30, $[M+4H]^{4+}$), 359.4 (27, $[M+5H]^{5+}$). **HRMS** (ESI): Calcd for $C_{79}H_{131}N_{36}O_{13}$ $[M+H]^+$: 1792.0679; found: 1792.0691.

General protocol to measure Circular Dichroism

Circular dichroism measurements were carried out with the following settings: acquisition range: 300-190 nm; band width: 1.0 nm; accumulation: 3 scans; data pitch: 1 nm; CD scale 200 mdeg/1.0 dOD; D.I.T. (Data Integration Time): 1 s; scanning mode: continuous; scanning speed: 200 nm/min. Measurements were done from 10 ºC to 60 ºC (data interval: 10 ºC; temp. gradient 5 ºC/min) in a quartz cell of 0.2 cm path length at a final volume of 0.5 mL (H_2O or TFE) with a final peptide concentration of 100 µM. The results are expressed as the mean residue molar ellipticity $[\theta]_{MRt}$ with units of degrees·cm^2·dmol^{-1} and calculated using the equation S1. The percentage of helicity was calculated using the equation S2. For the measurements in liposomes, samples were prepared by drying under reduced pressure L-α-phosphatidylcholine (16.7 µL, 25 mg/mL solution in $CHCl_3$) and peptide (300 µL, 100µM) in TFE to obtain a ratio lipid/peptide of 18:1 in a 10 mL round bottomed flask. The mixture was concentrated in a rotary evaporator to dryness, forming a film. The lipid/peptide mixture were suspended in HKR buffer (300 µL) to a final peptide concentration 100 µM and sonicated for 45 min until a clear solution was obtained. Spectra were recorded in a 0.2 cm path length quartz cell.[S3]

$$[\Theta]_{MRt} = \frac{0.1\,x\,\Theta}{C \cdot l \cdot \text{number of residues}} \quad (\text{deg} \cdot \text{cm}^2 \cdot \text{dmol}^{-1}) \qquad \text{(S1)}$$

Equation S1: Formula to calculate the ellipticity. Θ is the ellipticity (mdeg), C is the peptide concentration (M) and l is the cell path length (cm).

$$[\Theta]\% = \frac{\theta MRt_{222} - 2340}{30300}\ x\ 100 \qquad \text{(S2)}$$

Equation S2: Formula to calculate the percent of helicity in where the molar ellipticity at 222 nm is an absolute value.

Cell assays

Cell culture and live cell imaging

HeLa cells were grown at 37 ºC, 5% CO_2, in Dulbecco's Modified Eagle's Medium (4500 mg/L glucose, L-glutamine, sodium pyruvate and sodium bicarbonate; SigmaAldrich), supplemented with 10% fetal bovine serum (Sigma-Aldrich) and 1% of Penicillin-Streptomycin-Glutamine Mix.

SF9 Cells were grown at 28 ºC, in mechanical stirring, in Gibco Sf-900-II medium, complemented with 10% fetal bovine serum (Sigma-Aldrich) and 1% of Penicillin-Streptomycin-Glutamine Mix.

A-549 cells were grown at 37 ºC, 5% CO_2, in Dulbecco's Modified Eagle's Medium (4500 mg/L glucose, L-glutamine, sodium pyruvate and sodium bicarbonate; SigmaAldrich), supplemented with 10% fetal bovine serum (Sigma-Aldrich) and 1% of Penicillin-Streptomycin-Glutamine Mix.

For live cell imaging, HeLa cells grown on glass bottom dishes were washed with HEPES-Krebs-Ringer (HKR) buffer (5 mM HEPES, 137 mM NaCl, 2.68 mM KCl, 2.05 mM $MgCl_2$, 1.8 mM $CaCl_2$, pH 7,4) and incubated for 30 min with 1 µM Hoechst 33342 (ThermoFisher) in HKR to stain the nucleus. This solution was removed and cells were incubated for another 30 min with 0.5; 1; 3; 5 µM of each peptide diluted in HKR buffer, washed twice with HKR and examined on an epifluorescence microscope (Nikon Eclipse Ti-E).

For live cell imaging, SF9 cell grown on glass bottom dishes were washed with Sf-900-II medium incubated for 30 min with 1 µM Hoechst 33342 (ThermoFisher) in Sf-900-II to stain the nucleus. This solution was removed and cells were incubated for another 30 min with 1; 3; 5; 7 µM of each (Peptides) diluted in Sf-900-II medium, washed twice with Sf-900-II and examined on an epifluorescence microscope (Nikon Eclipse Ti-E).

For live cell imaging, A-549 cells grown on glass bottom dishes were washed with HEPES-Krebs-Ringer (HKR) buffer (5 mM HEPES, 137 mM NaCl, 2.68 mM KCl, 2.05 mM $MgCl_2$, 1.8 mM $CaCl_2$, pH 7.4) and incubated for 30 min with 1 µM Hoechst 33342 (ThermoFisher) in HKR to stain the nucleus. This solution was removed and cells were incubated for another 30 min with 0.5; 1; 3; 5 µM of each peptide diluted in HKR buffer, washed twice with HKR and examined on an epifluorescence microscope (Nikon Eclipse Ti-E).

Quantification of the uptake by flow cytometry

For internalization standard assays, we measured the amount of peptide by flow cytometry. Briefly, semiconfluent monolayers of HeLa cells seeded the day before were washed twice with HKR before incubation with different concentrations (1, 3, 5, 7, 10 µM) of TAMRA labelled peptides for 1 hour at 37

ºC. Then, cells were trypsinized to remove membrane bound peptides[S4,S5] and to prepare the samples for flow cytometry using 100 µL of Trypsin-EDTA (Gibco) for 10 min at 37 ºC, and trypsin neutralized with 100 µL of 2% FBS in PBS with 5 mM EDTA. Pipetting broke cell clumps and the analysis was done in a Guava easyCyte™ cytometer. TAMRA levels were determined by excitation at 532 nm and detection at 575/25 nm. For the analysis, cells with typical FSC and SSC parameters were selected, and median fluorescence intensity was calculated for each sample. Data analysis was performed with InCyte software included in GuavaSoft 3.2 (Millipore).

Quantification of inhibition of the uptake by flow cytometry

To study the cellular uptake mechanisms, HeLa cells growing in a 96 well plate (100.000 cells per well seeded) were treated for 30 min with the following compounds diluted in DMEM without serum or antibiotics: Dynasore (80 µM), chlorpromazine (30 µM), methyl-β-cyclodextrin (5 mM), Wortmannin (200 nM), EIPA (50 µM), heparin (5 µg/mL), chloroquine (100 µM) or ammonium chloride (50 mM). For the incubation at low temperature, another plate was incubated on ice and ice-cold solutions were used for the washes and incubations. Cells were then incubated with the TAMRA-labelled peptides in the presence of the same amount of inhibitors in DMEM for 30 min at 37 ºC. Cells were washed twice with HKR and 0.1 mg/mL of heparin in HKR and trypsinized. Trypsin was neutralized with 2% FBS in PBS with 5 mM EDTA and cell fluorescence was measured on a Guava EasyCyte™ cytometer using a green laser (532 nm) and collecting the emission at 575/25 nm. Cells with typical FSC and SSC parameters were selected and the median fluorescence intensity calculated for each sample (MFI). Each condition was done in triplicate. In the study of the uptake inhibition at different concentrations of the peptide, fluorescence values were normalized to the uptake of each untreated control (100%) after blank subtraction. In all cases, data analysis was performed with InCyte software included in GuavaSoft 3.2 (Millipore).

Cell viability

Cell viability was established by a standard MTT assay. One day before the assay, a suspension of HeLa cells was plated in 96-well tissue culture plates (Costar 96 Flat Bottom Transparent Polystyrol) by adding 100 µl (~10.000 cells) per well. The next day, the medium was aspirated and cells were incubated in DMEM containing 10% Fetal Bovine Serum (FBS) in the presence of the different peptides (50 µl/well) at different concentrations (1, 3, 4, 5, 7, 10 µM). After 1 h of incubation at 37 ºC, the viability was measured by quantifying the cellular ability to reduce the water-soluble tetrazolium dye 3-4,5-dimethylthiazole-2,5-diphenyl tetrazolium bromide (MTT) to its insoluble formazan salt as follows. MTT (5 mg/ml in PBS, 10 µl/well) was added to the wells and the cells were further incubated for 4 h. The supernatant was carefully removed and the water-insoluble formazan salt was dissolved in DMSO (100 µl/well). The absorbance at 570 nm was measured. Data points were collected in triplicate and expressed as normalized values for untreated as control cells (100%) after blank subtraction.

Peptide stability in serum

To determine the half-life of $\mathbf{P_8}$ in serum, the peptide was dissolved in FBS at a final concentration of 100 μM and incubated at 37 ºC. At different time points, 40 μL aliquots were taken. Samples were mixed with an equal volume of acetonitrile and centrifuged for 5 min at 10000 rpm to remove most serum proteins. Supernatants were freeze-dried and resuspended in 50 μL Milli-Q water, before quantitation by HPLC, measuring TAMRA absorbance at 555 nm [RP-HPLC Agilent SB-C18 column, H_2O (0.1% TFA)/ CH_3CN (0.1% TFA) 95:5→5:95 (0→20min)].

USC UNIVERSIDADE DE SANTIAGO DE COMPOSTELA

Supporting figures

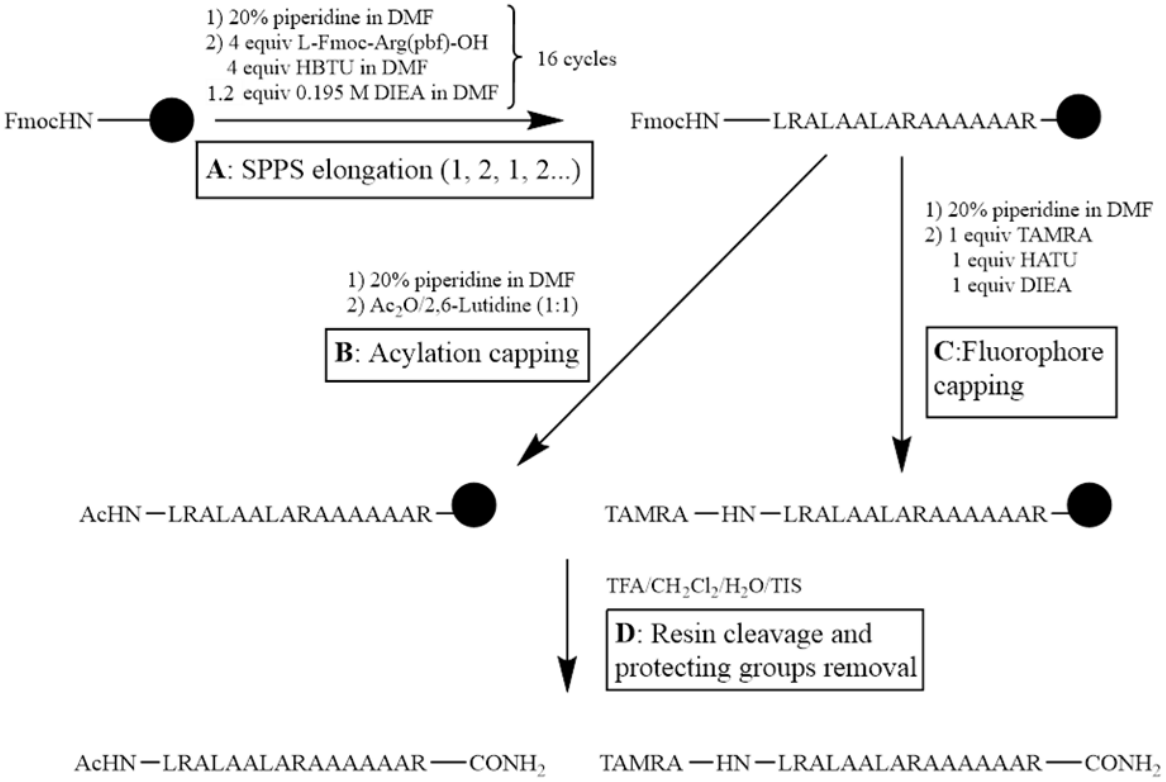

Figure S1: General synthetic scheme for the solid phase peptide synthesis (SPPS).

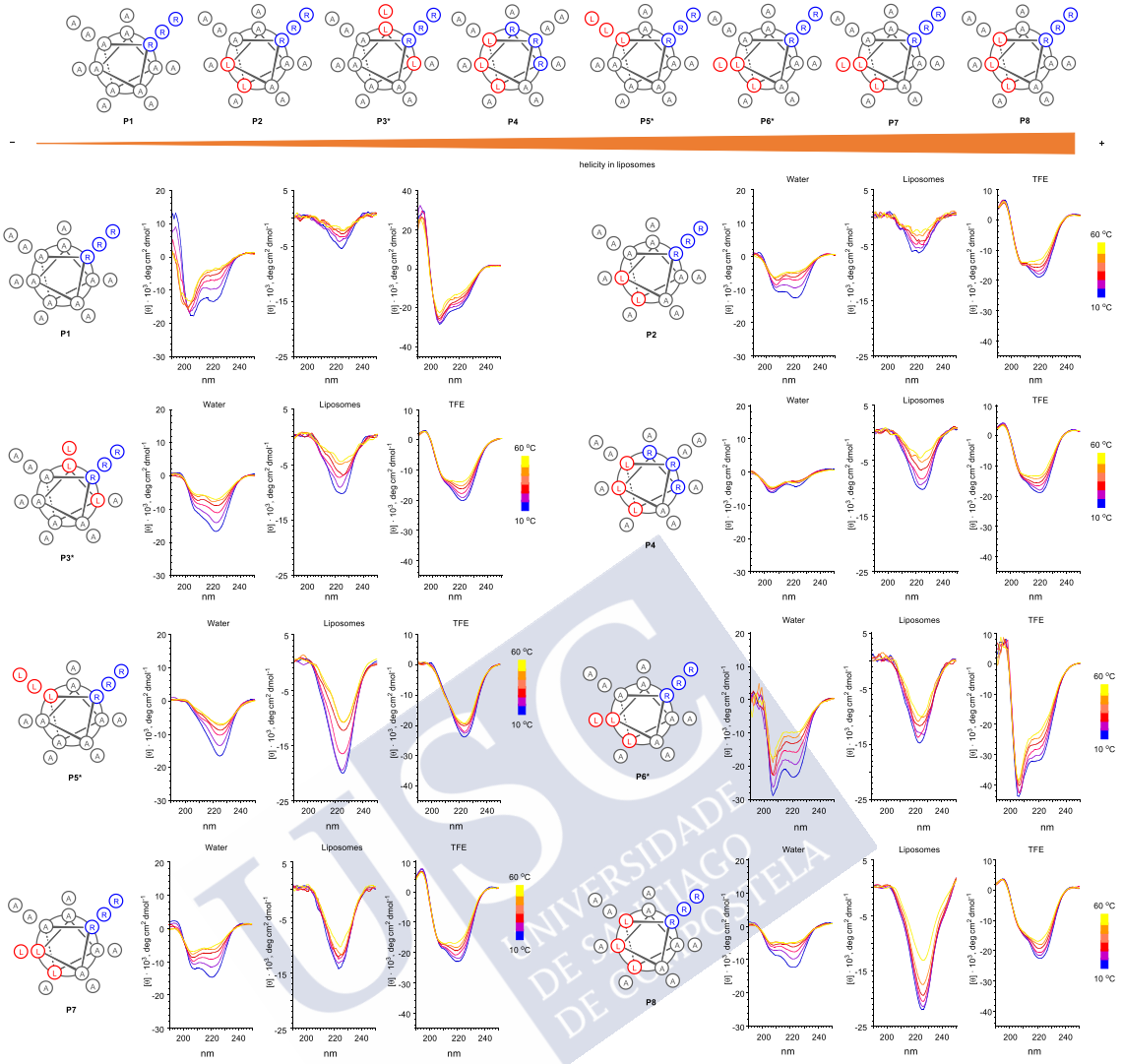

Figure S2: A) Heptad structures of the peptides ordered by increased helicity in liposomes. B) Circular dichroism in HKR buffer, liposomes and TFE (from left to right) of all peptides. The measurements were taken at different temperatures (10-60 ^{o}C). All samples were at 100 µM peptide final concentration.

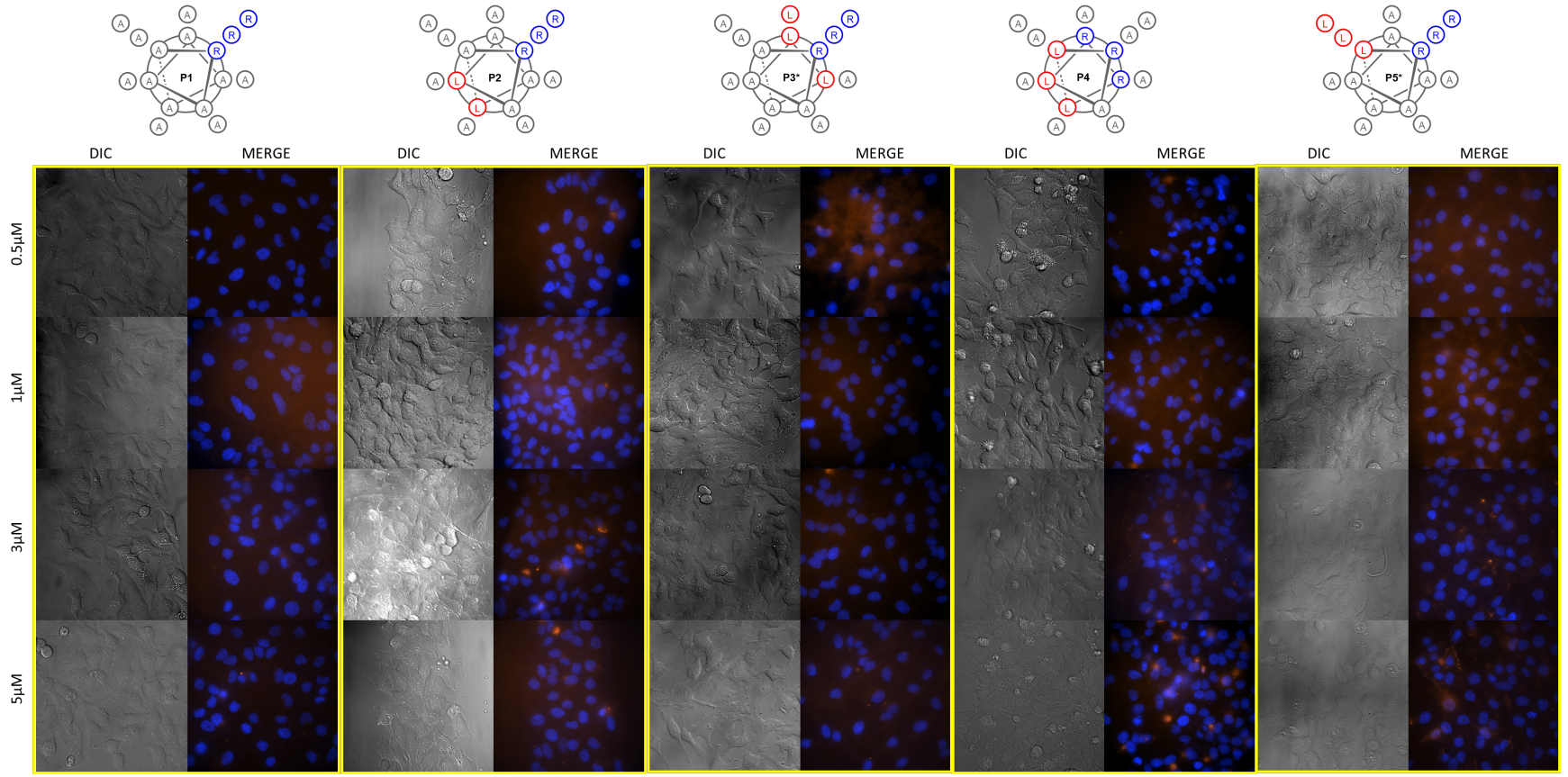

Figure S3: Epifluorescence image of peptides in HeLa cells. **P_1**, **P_2**, **P_{3*}**, **P_4** and **P_{5*}**. DIC on the left and merge channels (peptide and nuclei) on the right. HeLa cells were treated first with Hoechst 33342 for 30 min, washed (HKR buffer, 1x) and then incubated with the peptides (0.5, 1, 3 and 5 µM) in HKR buffer for 30 min. The cells were finally washed (HKR buffer, 3x) and then observed with the epifluorescence microscope.

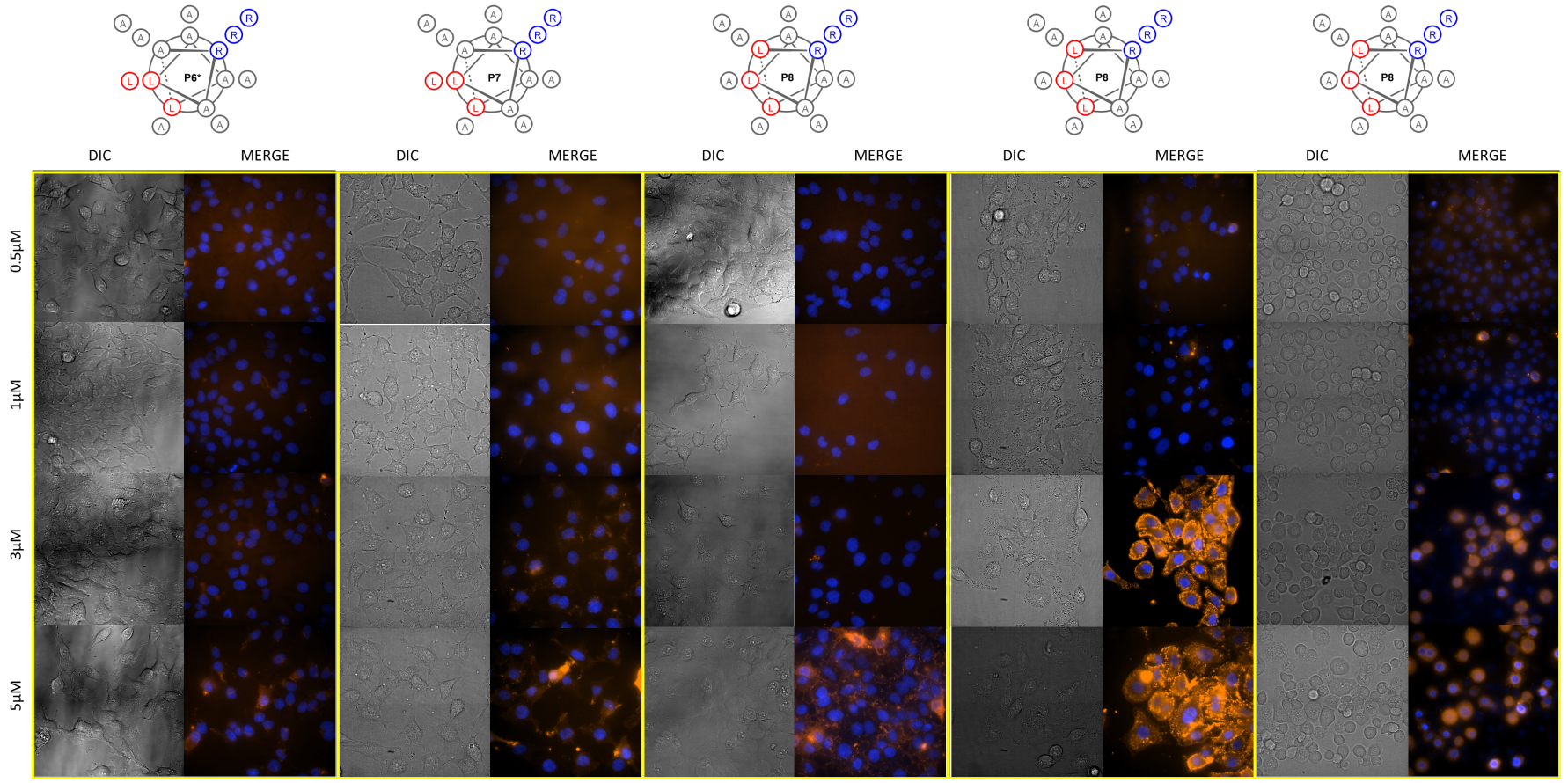

Figure S4: Epifluorescence image of peptides in HeLa cells. $\mathbf{P_6}$ in HeLa cells; $\mathbf{P_7}$ in HeLa cells; $\mathbf{P_8}$ in HeLa cells; $\mathbf{P_8}$ in A-549 cells; $\mathbf{P_8}$ in SF9 cells. DIC on the left and merge channels (peptide and nuclei) on the right. HeLa cells were treated first with Hoechst 33342 for 30 min, washed (HKR buffer, 1x) and then incubated with the peptides (0.5, 1, 3 and 5 µM) in HKR buffer for 30 min. The cells were finally washed (HKR buffer, 3x) and then observed with the epifluorescence microscope. In the case of SF9 the buffer used was Sf-900-II.

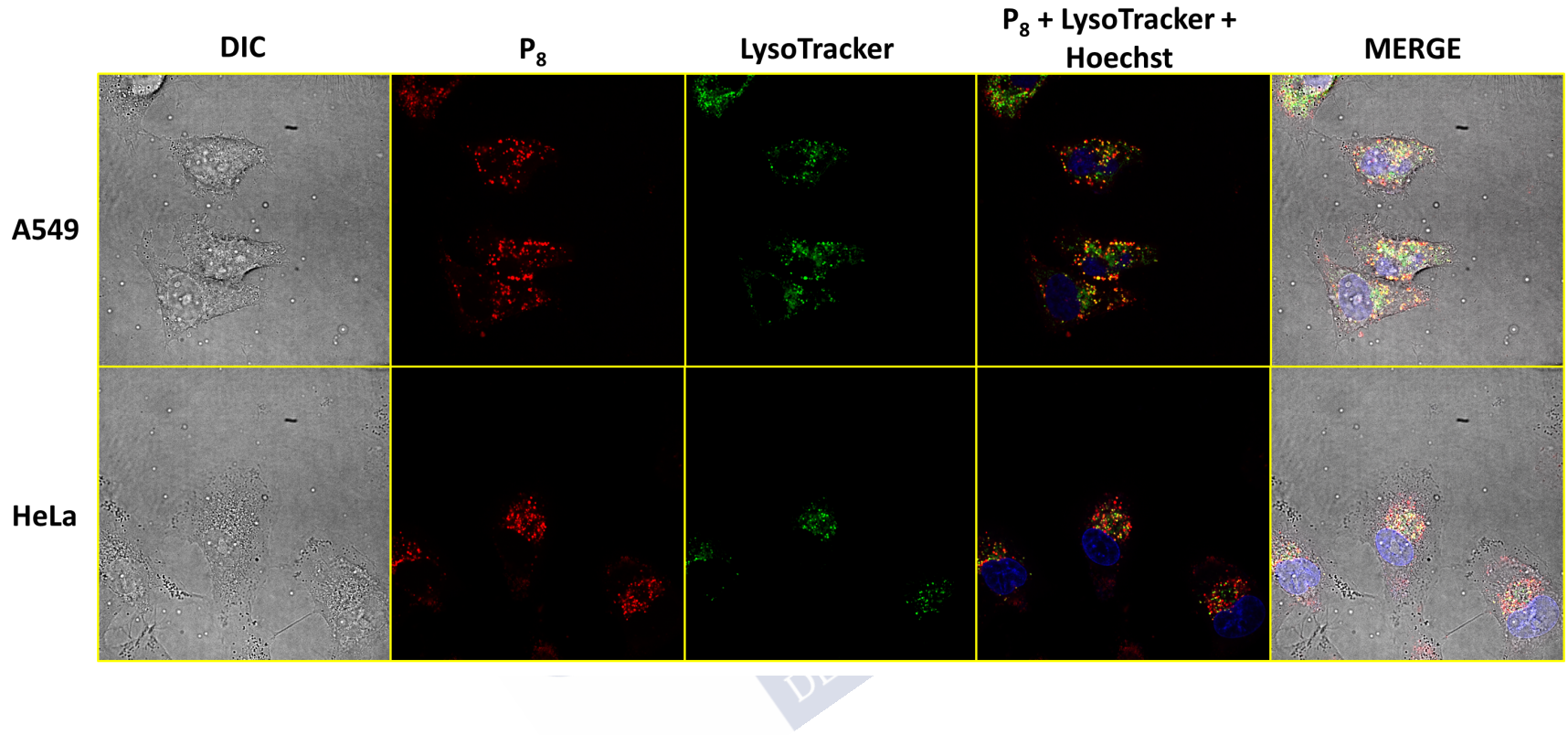

Figure S5: LysoTracker colocalization studies. HeLa cells and A549 cells were incubated with 5 μM **P₈** peptide for 30 min in HKR, washed and incubated with DMEM with 10 % serum for 3 h. Lysosomes were stained with 50 nM LysoTracker Deep Red the last 30 min of incubation before imaging in a confocal microscope. **P₈** is shown in red, LysoTracker is shown in green. Nuclei were counterstained blue with Hoechst.

A)

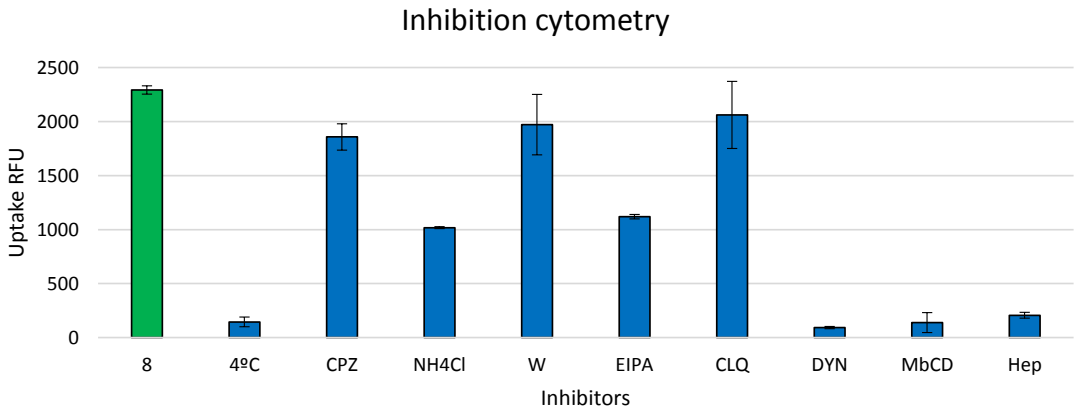

B)

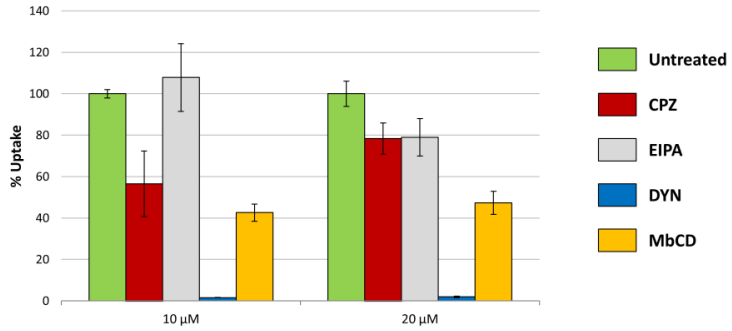

Figure S6: A) Histogram of the uptake in relative fluorescence units (RFU) for $\mathbf{P_8}$ (5 µM) in the presence of different endocytic inhibitors. In the histogram, the green column is the peptide alone, and the blue columns are the uptake in the presence of the inhibitors: 4ºC, CPZ: chlorpromazine; NH4Cl: Ammonium Chloride; W: Wortmannin; EIPA: 5-(*N*-Ethyl-*N*-isopropyl)amiloride; CLQ: chloroquine; DYN: Dynasore; MβCD: methyl-β-cyclodextrin; Hep: heparin. Error bars indicate SD of three replicates. Hela cells were treated in DMEM (-) for 30 min prior to trypsinization and cytometry quantification. B) Study of the endocytic mechanism at different peptide concentrations. HeLa cells were treated with the indicated inhibitors for 30 min in DMEM (-) before incubating with the peptide $\mathbf{P_8}$ at different concentrations for 30 min. Cells were then trypsinized and analyzed by flow cytometry. Error bars indicate SD of three replicates.

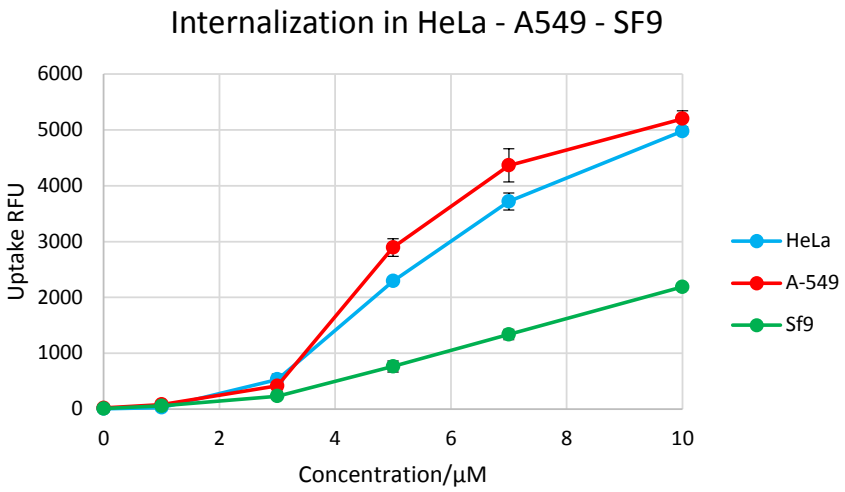

Figure S7: Uptake quantification by flow cytometry of the peptide $\mathbf{P_8}$ in three different cell lines: HeLa cells in blue, A-549 cells in red and SF9 cells in green. The points were collected at six different concentrations (0, 1, 3, 5, 7, 10 µM). Cells were treated in DMEM (-) or Sf-900-II in the case of Sf9 cells for 1 hour prior to trypsinization and cytometry quantification. Error bars indicate SD of three replicates.

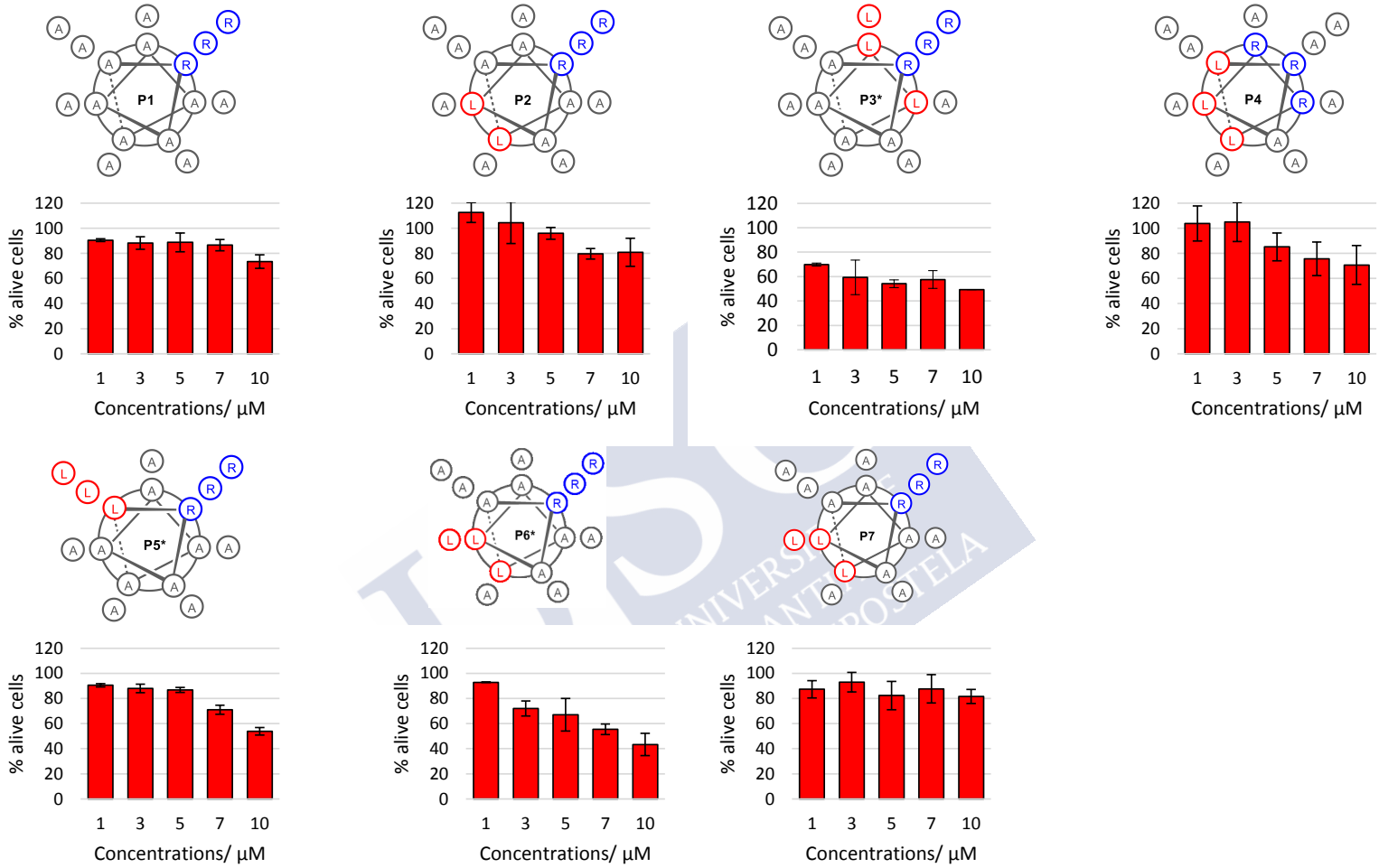

Figure S8: MTT assay at different concentrations of peptides: $\mathbf{P_1}$, $\mathbf{P_2}$, $\mathbf{P_{3*}}$, $\mathbf{P_4}$, $\mathbf{P_{5*}}$, $\mathbf{P_{6*}}$, $\mathbf{P_7}$ in HeLa cells. Hela cells were treated in DMEM (-) for 1 hour prior to MTT-assay.

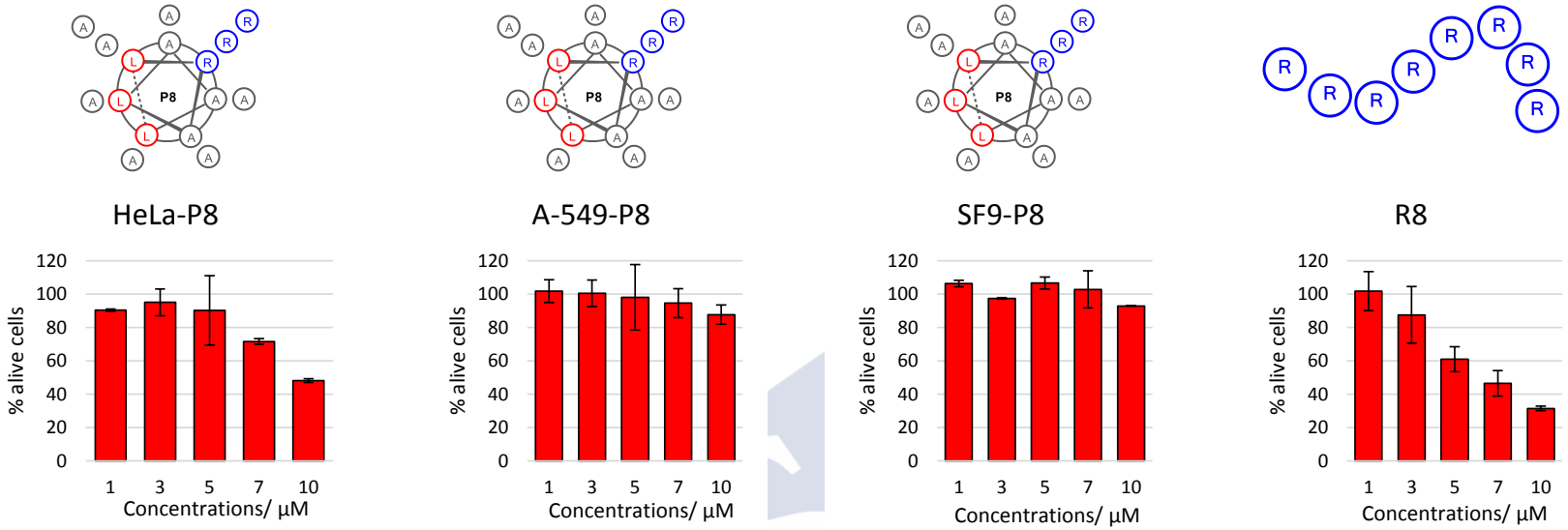

gure S9: MTT assay at different concentrations of peptide $\mathbf{P_8}$ in three different cell lines: HeLa, A-549, SF9 and $\mathbf{R_8}$ in HeLa cells. Hela cells were treated in DMEM for 1 hour prior to MTT-assay.

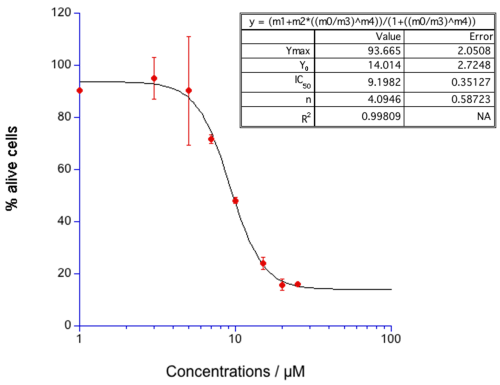

Figure S10: MTT assay at increasing concentrations of $\mathbf{P_8}$ in HeLa cells. Cells were incubated for 1 h with the peptide in DMEM (-) before MTT assay. Curve fitting was done with KaleidaGraph software, using a 4-parameters logistic model. $\mathbf{IC_{50}}$ = 9.2 µM.

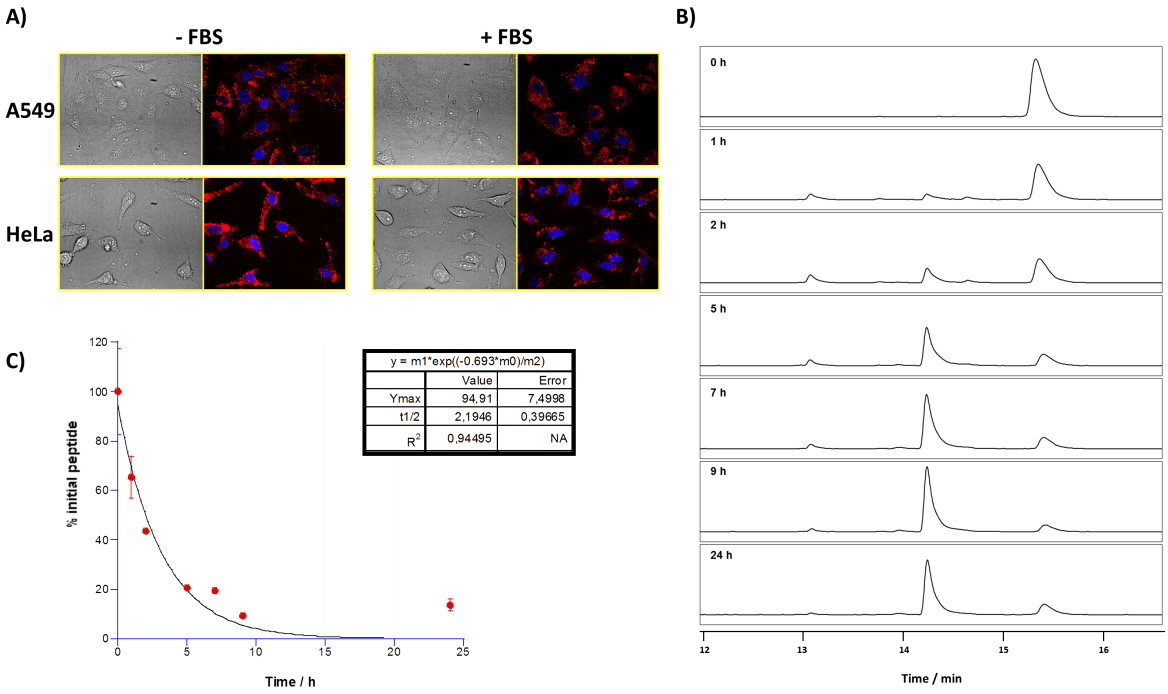

Figure S11: Stability in the presence of serum. A) A-549 and HeLa cells were incubated for 30 min with 5 µM disolved in DMEM (-) or DMEM supplemented with 10 % FBS. Cells were then washed three times with DMEM (-) and imaged in a confocal microscope. B) RP-HPLC of $\mathbf{P_8}$ after different incubation times with FBS (555 nm absorbance) C) Calculation of $\mathbf{P_8}$ half-life in serum. Area of the peak corresponding to the intact peptide was measured for all the time points and normalized to time 0 h (100 %). Data was adjusted to an exponential decay curve using KaleidaGraph. $\mathbf{P_8}$ half-life ~ 2.2 h.

Supporting figures of Characterization

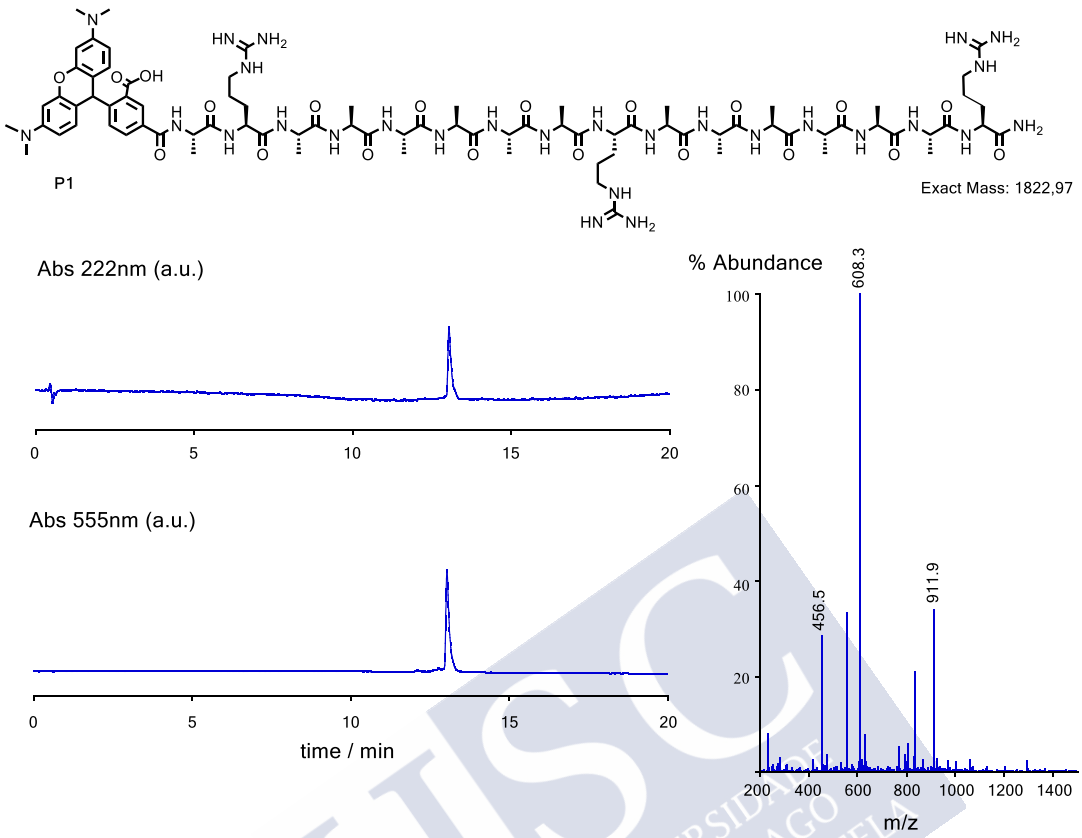

Figure S12: RP-HPLC [Agilent SB-C18 column, H_2O (0.1% TFA)/ CH_3CN (0.1% TFA) 95:5→5:95 (0→20 min)] (R_t 13 min) absorbance at 222 nm and 555 nm and ESI-MS for Peptide $\mathbf{P_1}$.

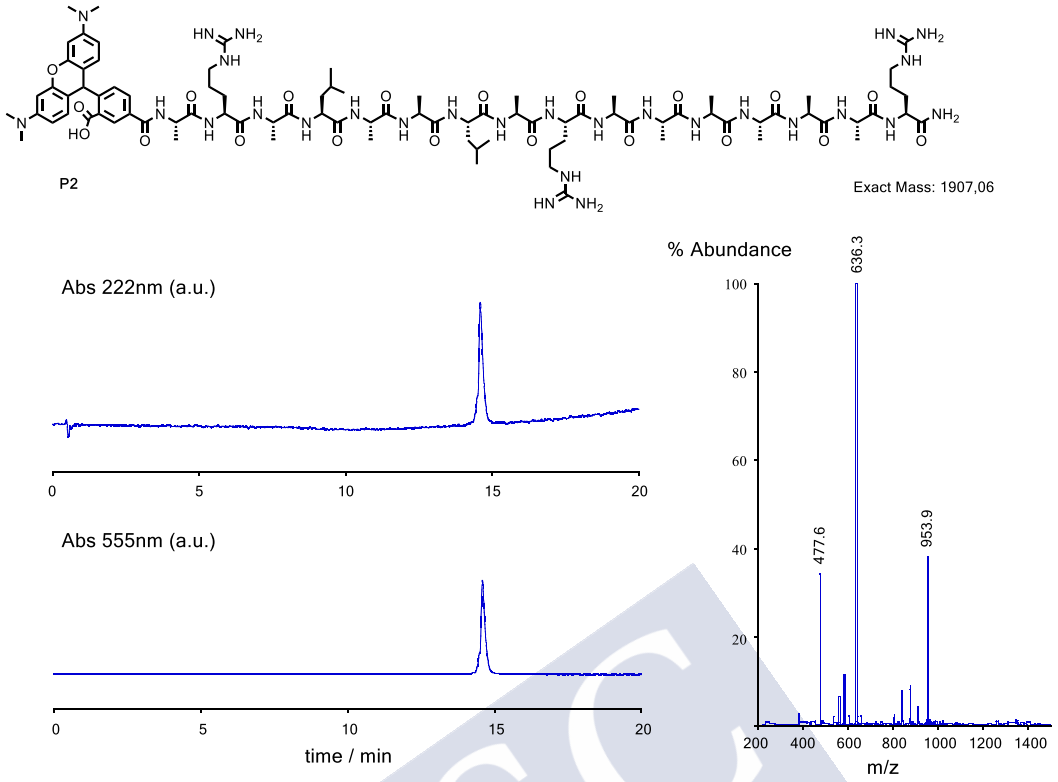

Figure S13: RP-HPLC [Agilent SB-C18 column, H_2O (0.1% TFA)/ CH_3CN (0.1% TFA) 95:5→5:95 (0→20 min)] (R_t 14.6 min) absorbance at 222 nm and 555 nm and ESI-MS for Peptide $\mathbf{P_2}$.

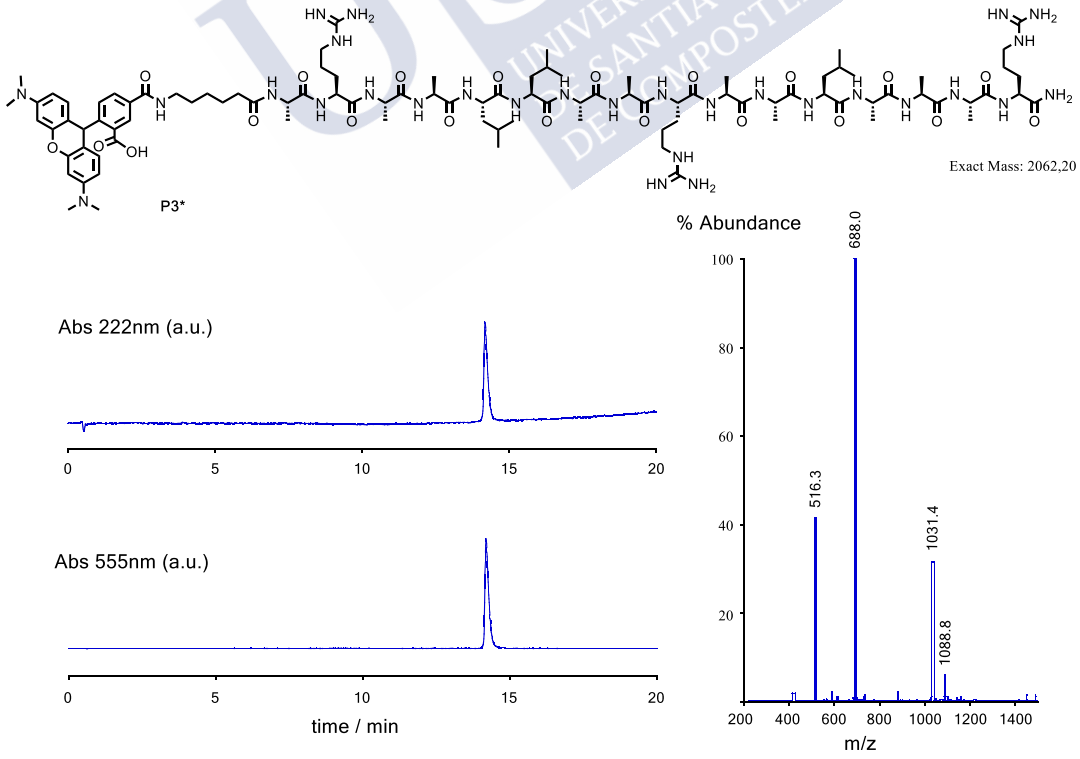

Figure S14: RP-HPLC [Agilent SB-C18 column, H_2O (0.1% TFA)/ CH_3CN (0.1% TFA) 95:5→5:95 (0→20 min)] (R_t 14.2 min) absorbance at 222 nm and 555 nm and ESI-MS for Peptide $\mathbf{P_{3*}}$.

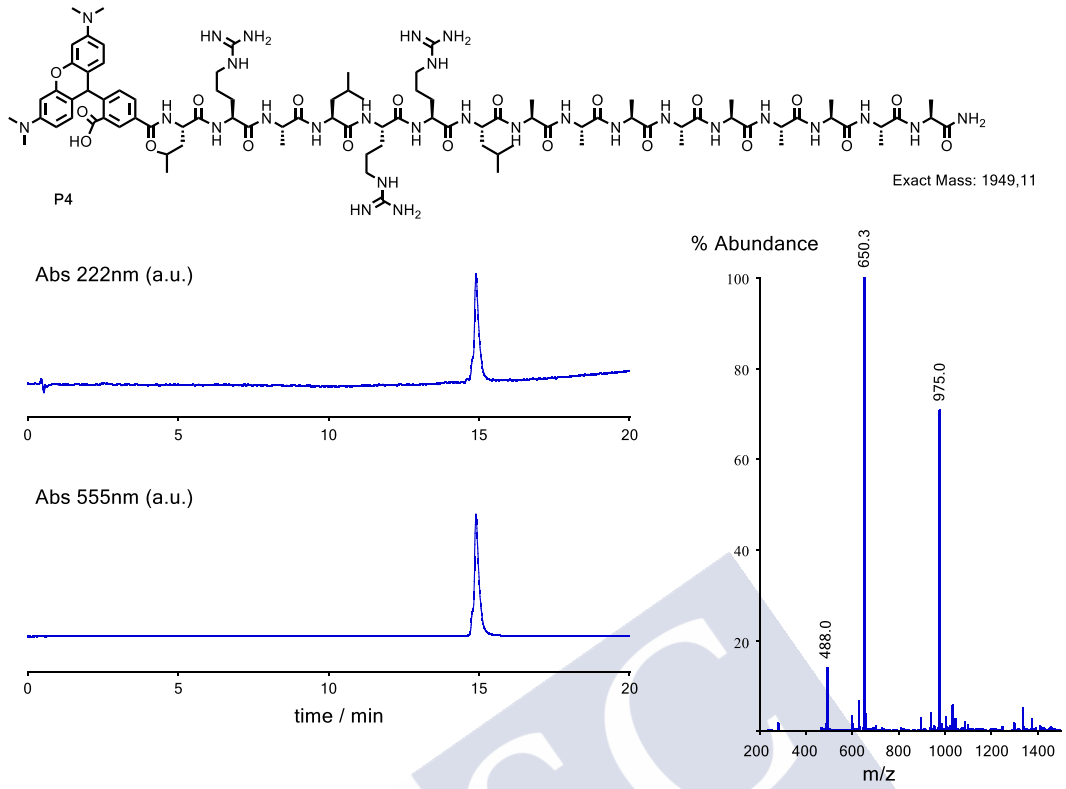

Figure S15: RP-HPLC [Agilent SB-C18 column, H_2O (0.1% TFA)/ CH_3CN (0.1% TFA) 95:5→5:95 (0→20 min)] (R_t 14.9 min) absorbance at 222 nm and 555 nm and ESI-MS for Peptide $\mathbf{P_4}$.

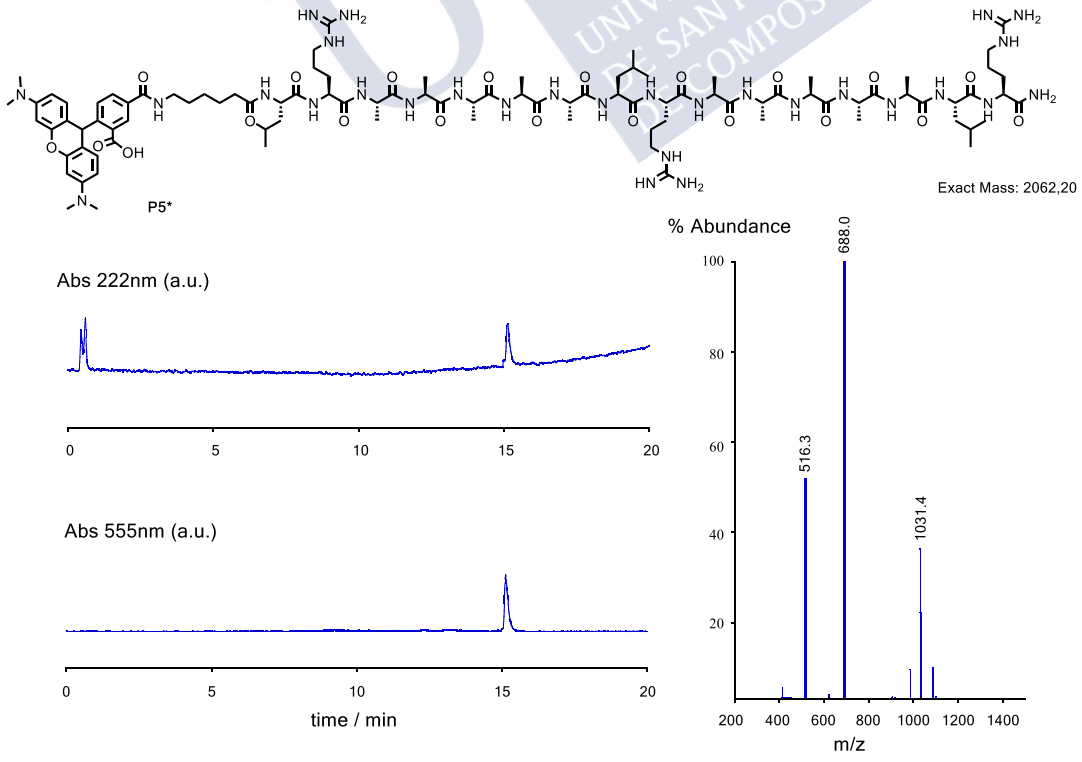

Figure S16: RP-HPLC [Agilent SB-C18 column, H_2O (0.1% TFA)/ CH_3CN (0.1% TFA) 95:5→5:95 (0→20 min)] (R_t 15.2 min) absorbance at 222 nm and 555 nm and ESI-MS for Peptide $\mathbf{P_{5*}}$.

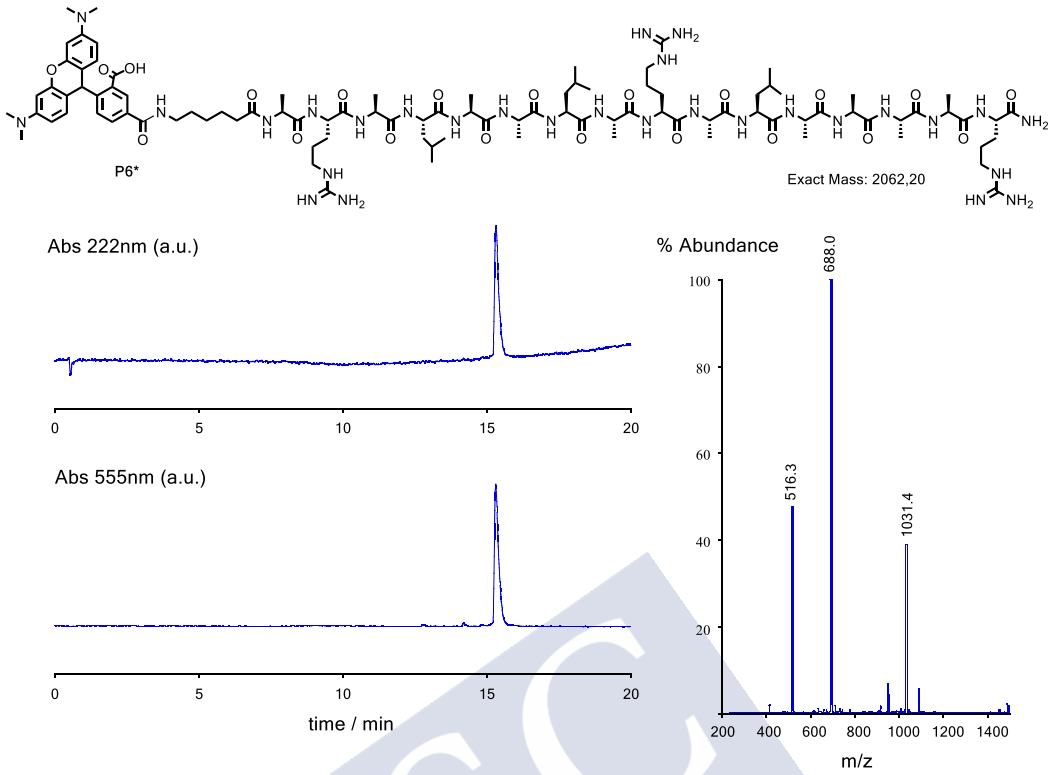

Figure S17: RP-HPLC [Agilent SB-C18 column, H_2O (0.1% TFA)/ CH_3CN (0.1% TFA) 95:5→5:95 (0→20 min)] (R_t 15.3 min) absorbance at 222 nm and 555 nm and ESI-MS for Peptide $\mathbf{P_{6*}}$.

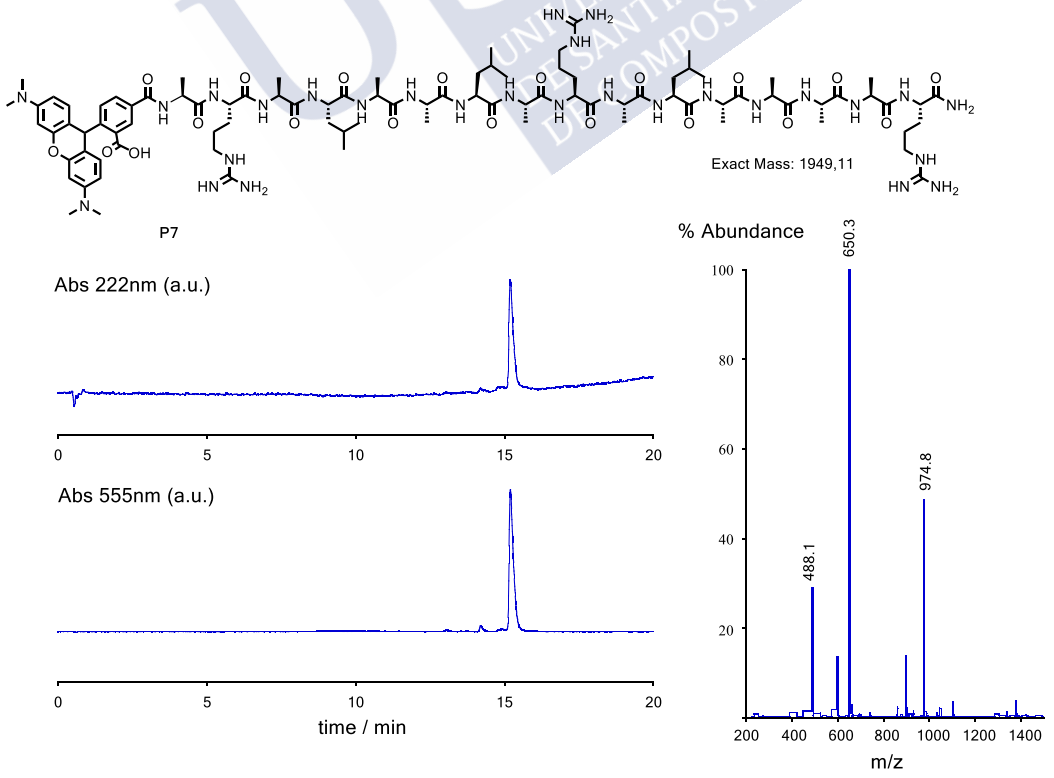

Figure S18: RP-HPLC [Agilent SB-C18 column, H_2O (0.1% TFA)/ CH_3CN (0.1% TFA) 95:5→5:95 (0→20 min)] (R_t 15.5 min) absorbance at 222 nm and 555 nm and ESI-MS for Peptide $\mathbf{P_7}$.

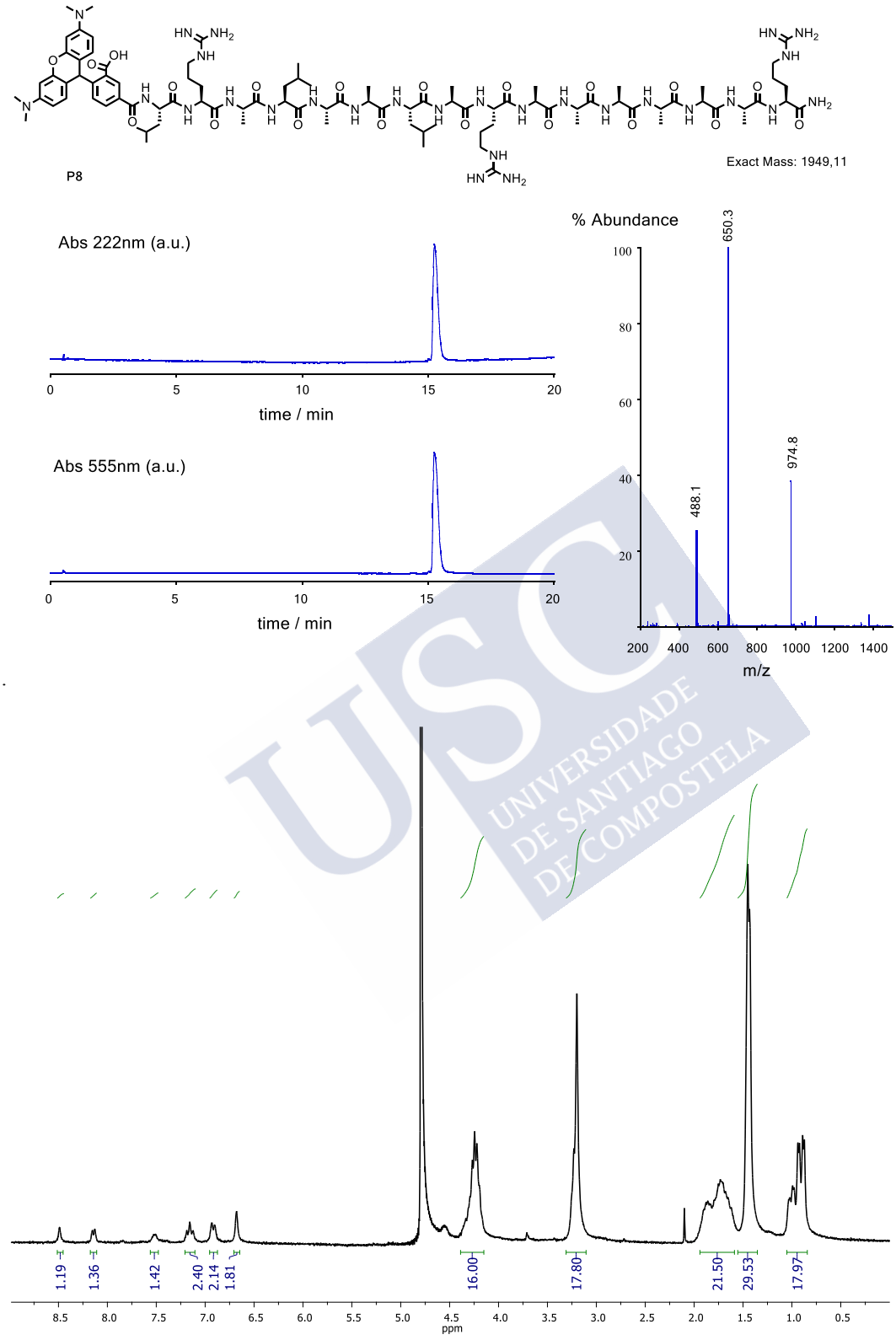

Figure S19: RP-HPLC [Agilent SB-C18 column, H_2O (0.1% TFA)/ CH_3CN (0.1% TFA) 95:5→5:95 (0→20 min)] (R_t 15.2 min) absorbance at 222 nm and 555 nm and ESI-MS and NMR in D_2O for Peptide **P_8**.

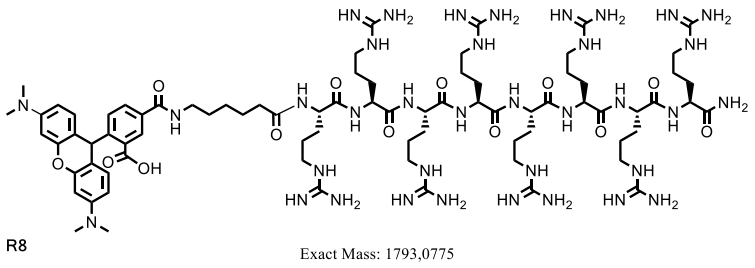

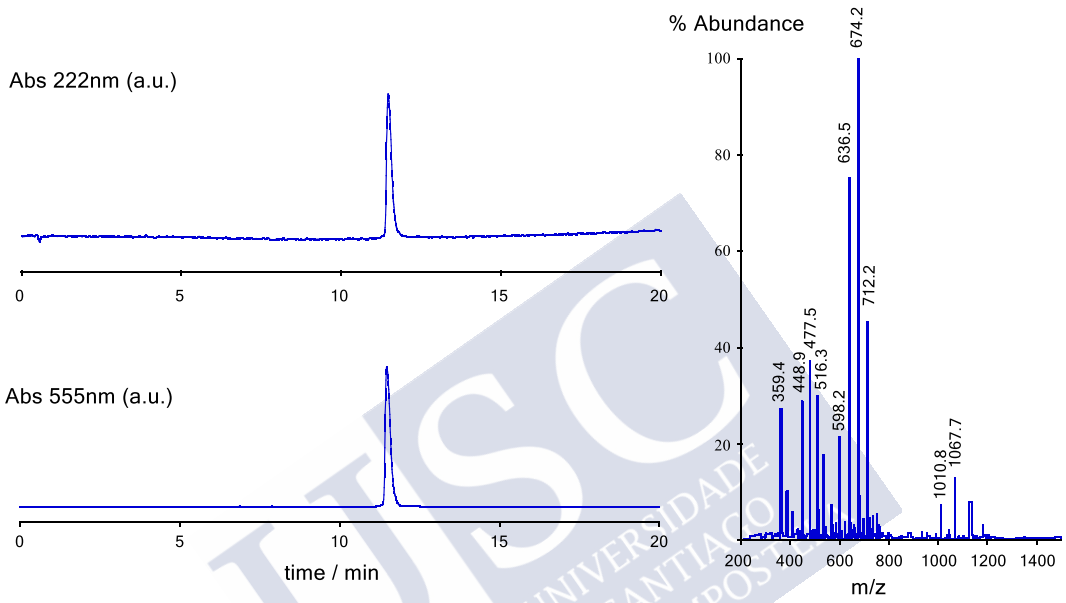

Figure S20: RP-HPLC [Agilent SB-C18 column, H_2O (0.1% TFA)/ CH_3CN (0.1% TFA) 95:5→5:95 (0→20 min)] (R_t 11.4 min) absorbance at 222 nm and 555 nm and ESI-MS for Peptide $\mathbf{R_8}$.

Supporting references

(S1) R. Behrendt, P. White, J. Offer, *J. Pept. Sci.* **2016**, *22*, 4–27.

(S2) C. Kay, O. E. Lorthioir, N. J. Parr, M. Congreve, S. C. McKeown, J. J. Scicinski, S. V. Ley, *Biotechnol. Bioeng.* **2000**, *71*, 110–118.

(S3) I. Louzao, R. García-Fandiño, J. Montenegro, *J. Mater. Chem. B* **2017**, *5*, 4426–4434.

(S4) T. Holm, H. Johansson, P. Lundberg, M. Pooga, M. Lindgren, U. Langel, *Nat. Protoc.* **2006**, *1*, 1001–1005.

(S5) J. P. Richard, K. Melikov, E. Vives, C. Ramos, B. Verbeure, M. J. Gait, L. V Chernomordik, B. Lebleu, *J. Biol. Chem*. **2003**, *278*, 585–90.

USC UNIVERSIDADE DE SANTIAGO DE COMPOSTELA

3. Short oligoalanines helical peptides for supramolecular nanopore assembly and protein cytosolic delivery

USC UNIVERSIDADE DE SANTIAGO DE COMPOSTELA

USC
UNIVERSIDADE
DE SANTIAGO
DE COMPOSTELA

Short Oligoalanine Helical Peptides for Supramolecular Nanopore Assembly and Protein Cytosolic Delivery

Marta Pazo, Giulia Salluce, Irene Lostalé-Seijo, Marisa Juanes, Francisco Gonzalez, Rebeca Garcia-Fandiño and Javier Montenegro*

e-mail to: javier.montenegro@usc.es

Supporting Information

Table of contents

1. Supporting Figures 2

2. Experimental Procedures 17

2.1. Materials 17

2.2. Abbreviations 18

2.3. General protocol for the SPPS 18

2.3.1. Synthesis of peptide **MP1** 19
2.3.2. Synthesis of peptide **CF-MP1** 19
2.3.3. Synthesis of peptide **TM-MP1** 19
2.3.4. Synthesis of peptide **MP2** 19
2.3.5. Synthesis of peptide **P3** 19
2.3.6. Synthesis of peptide **Arg$_8$** 19
2.3.7. Synthesis of peptide **GALA** 20
2.3.8. Synthesis of peptide **L17E** 20
2.3.9. Synthesis of **Pep-1** 20
2.3.10. Synthesis of **dfTAT** 20

2.4. Liposome preparation 20

2.5. ANTS/DPX assay 21

2.6. Dextran release in vesicles 21

2.7. Circular Dichroism 22

2.8. DLS experiments 22

2.9. FRET and fluoresence experiments 22

2.10. Computational methods 23

2.11. Planar lipid bilayer recordings 23

2.12. Cell culture experiments 24

2.12.1. Cell lines and culture 24
2.12.2. Cellular uptake and endosomal release of dextran 24
2.12.3. Cell viability assay (MTT) 25
2.12.4. Saporin experiments 25
2.12.5. Cre recombinase expression and purification 25
2.12.6. Cre recombinase delivery experiments 25
2.12.7. Antibody delivery in cell culture 26
2.12.8. CF-labelling and delivery of IgG 26
2.12.9. Purification and delivery of GST-NLS-GFP 26

2.13. *Ex vivo* cornea experiments 27

2.13.1. Murine corneas culture 27
2.13.2. Antibody delivery in cornea 27
2.13.3. Live/Dead Staining 27

2.14. Sources for Figure 6 table 27

3. Supporting References 28

1. Supporting Figures

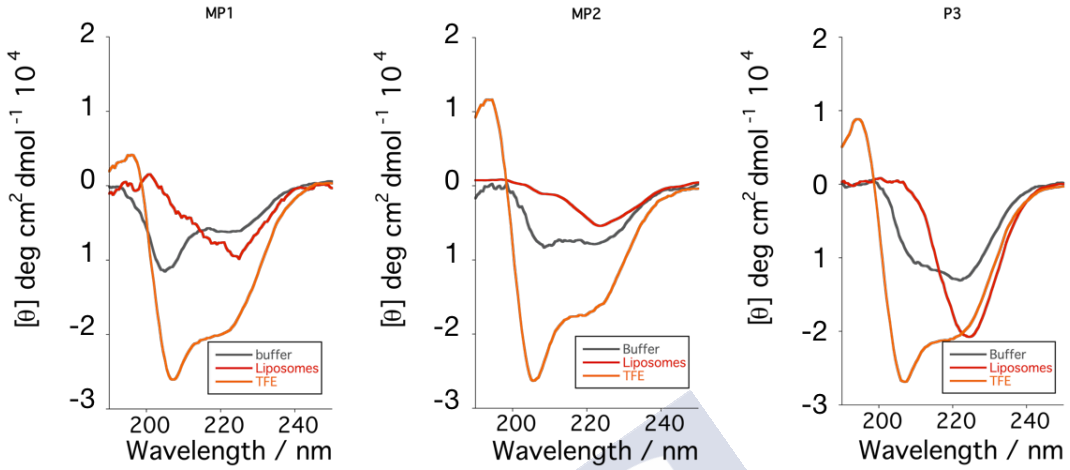

Figure S1. Circular dichroism spectra of MP1, MP2 and P3 in HKR buffer (gray), Liposomes (red) (L/P ratio: 12) and TFE (orange). Measurements were done at 40 °C. See also Fig. 1d.

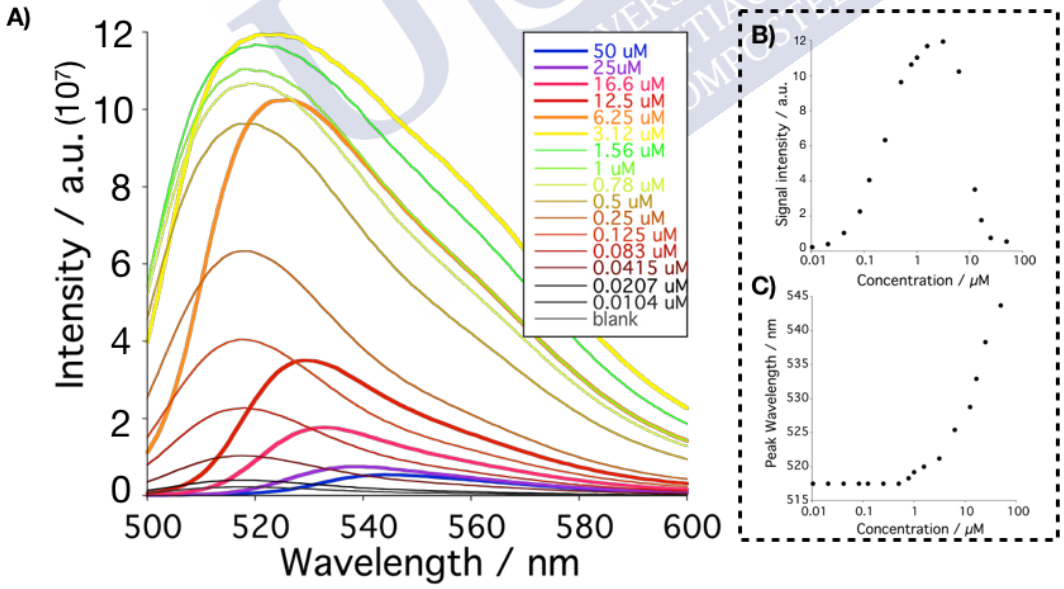

Figure S2. CF-MP1 aggregates in solution. A) Emission spectra of **CF-MP1** (λ_{ex} = 494 nm) in aqueous solution at different concentrations. B) Maximum fluorescence intensity at different concentrations C) Wavelength of the peak of maximum fluorescence at different concentrations.

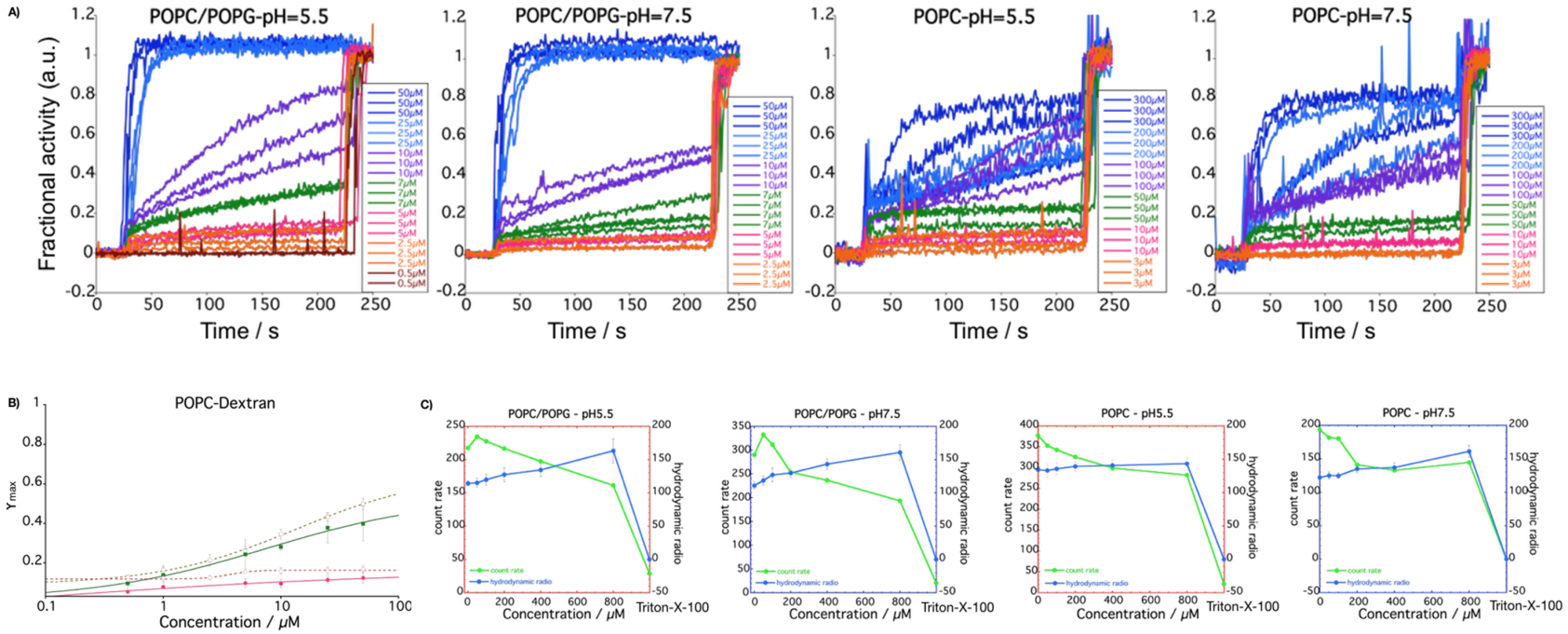

Figure S3. Vesicle release experiments. A) Kinetic fluorescent traces of LUVs⊂ANTS/DPX after addition of **MP1** (at t = 25 s). Triton X-100 was added at 225 s for complete vesicle lysis and normalization. B) Dose response curves for dextran release in neutral POPC vesicles (LUVs⊂Dextran) at different **MP1** concentrations. The 10 kDa FITC-Dex (green) and 40 kDa TM-Dex (pink) are shown with empty squares (pH = 7.5) and filled circles (pH = 5.5) respectively. C) DLS measurements of vesicles in the presence of **MP1**. Representation of photon count rate (an indicator of measurement quality) and size (hydrodynamic radius, indicative of vesicle size and stability). Error bars indicate the standard deviation of three replicates calculated by equation S5 for DLS experiments. In all cases the buffer was MES 10 mM with NaCl 150 mM. Experiments were done with neutral POPC or anionic POPC/POPG vesicles at either pH 7.5 or pH 5.5 as indicated at the top of the charts.

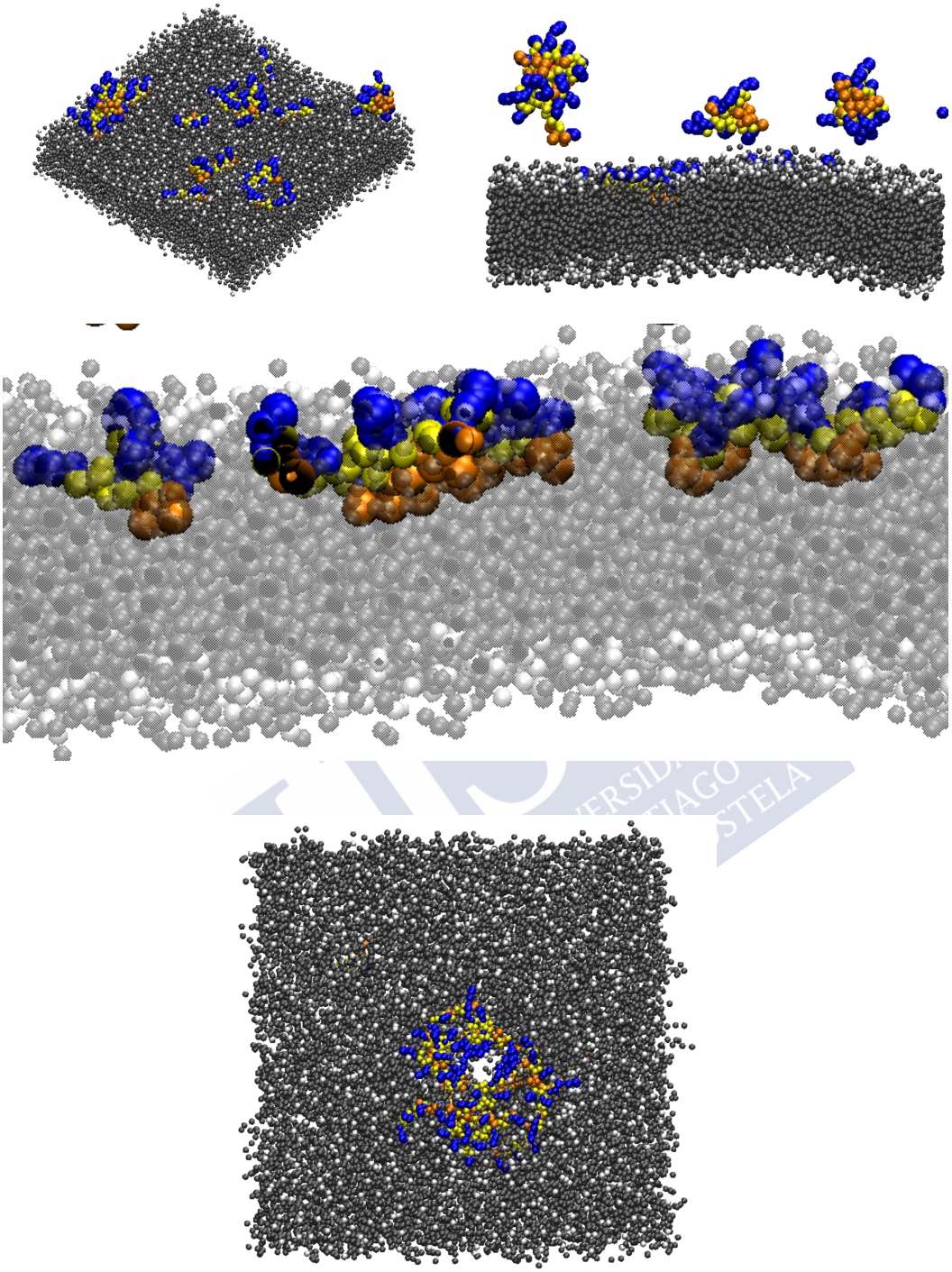

Figure S4. Molecular dynamics simulation. Top: Snapshot at t = 70 ns of the CG-MD simulation of 31 units of peptide **MP1** interacting with a membrane composed by DPPC:DPPE (9:1) and DPPC:DPPE:DPPS (3:5:2), in absence of electric field. Middle: Detail of the insertion of the peptides in the membrane by anchoring and orienting the Leu (orange) enriched hydrophobic N-terminus of peptide **MP1** towards the hydrophobic core of the lipid bilayer, and the arginine (blue) cationic residues exposed to the solvent. Down: Detail of the top view of the ensemble of MP1 interacting with the membrane, under an external electric field of 0.03 V/nm applied across the membrane (t = 300 ns, from Figure 5). An initial poration of the membrane can be inferred.

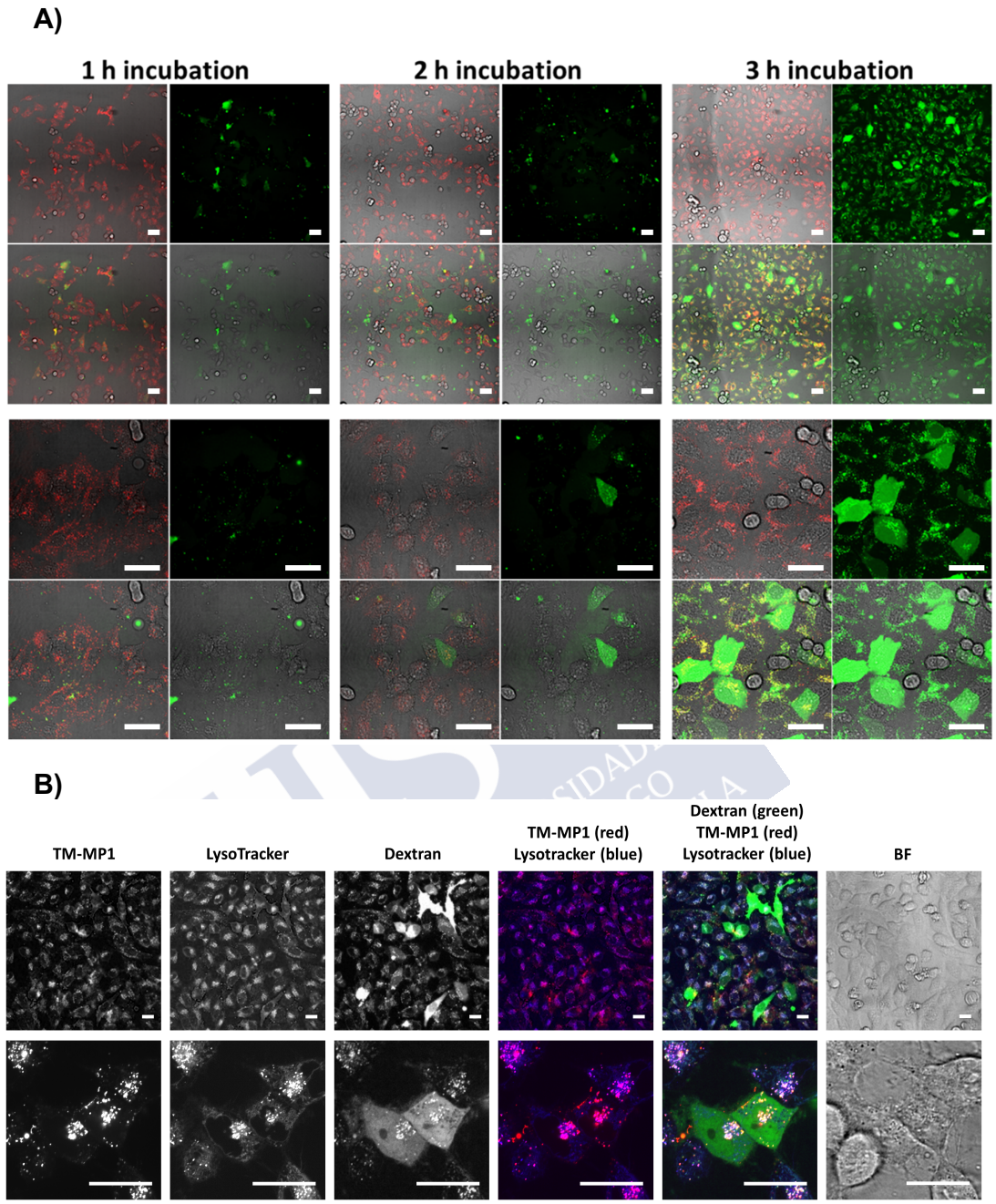

Figure S5. Time lapse of dextran cytosolic release in HeLa cells. A) HeLa cells were incubated with 0.25 mg/mL of Alexa$_{488}$-Dextran (10 kDa, green) in the presence of 5 μM of **TM-MP1** (red) for 1 h in DMEM without FBS. Cells were washed and incubated in DMEM with FBS for 1 hour, 2 hours or 3 hours before imaging. Top rows: 20x magnification; bottom rows: 60x magnification. Each set of images shows: merge of brightfield and **TM-MP1** (red; upper left), dextran fluorescence (green; upper right), merge of brightfield and dextran (lower right), merge of **TM-MP1**, dextran, and brightfield (lower left). Scale bars = 50 μm. B) HeLa cells were incubated with 0.25 mg/mL of FITC-Dextran (10 kDa, green), in the presence of 5 μM **TM-MP1** (red) for 1 h in DMEM without FBS. Cells were washed and incubated in DMEM with FBS for 3 h and then stained with LysoTracker Deep Red (100 nM, 30 min, shown in blue), washed and observed at the microscope. Scale bars = 25 μm.

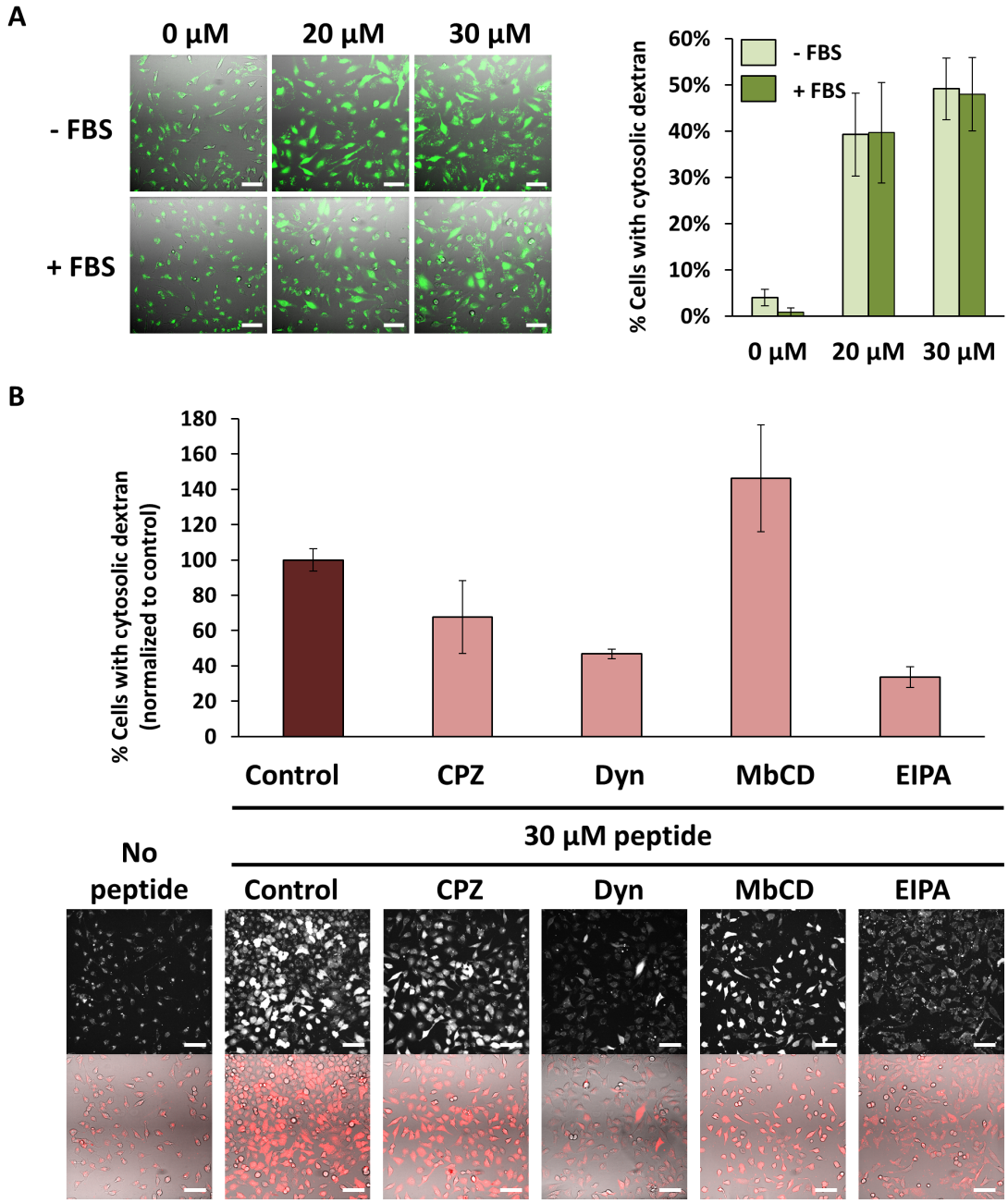

Figure S6. Dextran release in the presence of serum or endocytosis inhibitors. A) HeLa cells were incubated for 1 h with a solution of 0.25 mg/mL 10 kDa Alexa$_{488}$-Dextran (green) and the indicated concentrations of **MP1** in DMEM stock (top row) or in DMEM supplemented with 10% FBS (bottom row). Cells were then washed and incubated for 3 hours with DMEM supplemented with 10% FBS before confocal imaging. Cells with diffuse signal were counted and expressed as percentage. Graph shows mean of three experiments ± SD. B) HeLa cells were incubated with 0.25 mg/mL 10 kDa TM-labelled dextran and 30 µM peptide **MP1** in the presence of the indicated inhibitors for 1 h. After incubation, the number of cells with cytosolic dextran was counted and normalized to the control with 30 µM peptide in the absence of inhibitors (100%). Data is presented as mean of three independent experiments ± SD. Representative micrographs for each condition are shown at the bottom of the image (top row: dextran fluorescence; bottom row: merge of dextran fluorescence (red) with brightfield). Scale bars = 100 µm.

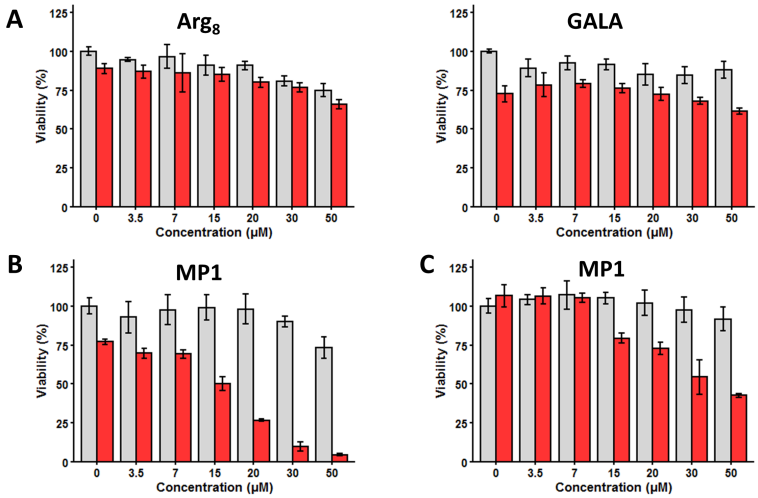

Figure S7. Functional Protein Cytosolic Delivery. A) HeLa cells were incubated with 0 (grey bars) or 10 μg/mL (red bars) saporin in the presence of increasing concentrations of peptides **Arg$_8$** or **GALA** for 1 h; medium was then replaced and cells further incubated for 6 h before measuring viability by MTT assay. B, C) Analogous experiment in HeLa (B) and A549 (C) cells by incubation with **MP1** (1 h) and further incubation for 24 h before viability quantification by MTT assay.

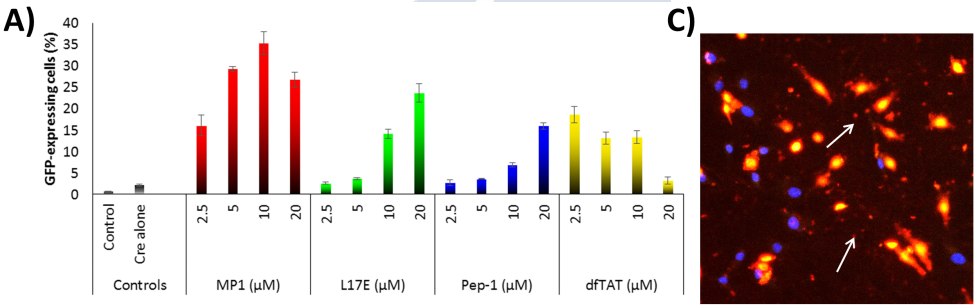

B)

	MP1	Arg$_8$	GALA	L17E	Pep-1	dfTAT
2.5 μM	16.0 ± 2.4	2.4 ± 0.1	0.4 ± 0.1	2.6 ± 0.2	2.7 ± 0.7	18.6 ± 1.9
5 μM	29.2 ± 0.7	3.4 ± 0.2	0.4 ± 0.1	3.6 ± 0.2	3.6 ± 0.1	13.2 ± 1.4
10 μM	35.3 ± 2.6	5.8 ± 0.3	0.3 ± 0.0	14.1 ± 1.0	6.9 ± 0.4	13.3 ± 1.5
20 μM	26.7 ± 1.7	16.0 ± 0.4	0.2 ± 0.1	23.6 ± 2.1	16.0 ± 0.7	3.1 ± 0.8

Figure S8. Cre recombinase delivery efficiency by different peptides. A) and B) Cre-reporter HeLa cells were treated with 1 μM Cre recombinase and 2.5, 5, 10, 20 μM of the indicated peptides for 4 h, and the number of cells that switched from red to green (GFP) fluorescence due to the recombinase activity quantified by flow cytometry 3 days after incubation. The table indicates the percent of GFP-expressing cells ± SD (n = 3) for each peptide and concentration. C) **TM-MP1** and Cre form aggregates. HeLa-Cre reporter cells were incubated with 1 μM Cre recombinase and 20 μM TAMRA-labelled **MP1** (**TM-MP1**) for 4 h, and cells imaged 3 days later. Both TAMRA (peptide) and dsRED (expressed by cells) are shown in red, GFP in green and Hoechst-stained nuclei in blue. Arrows indicate fluorescent peptide aggregates as detected by the TAMRA fluorescence, which may be responsible of the lower uptake at high concentrations.

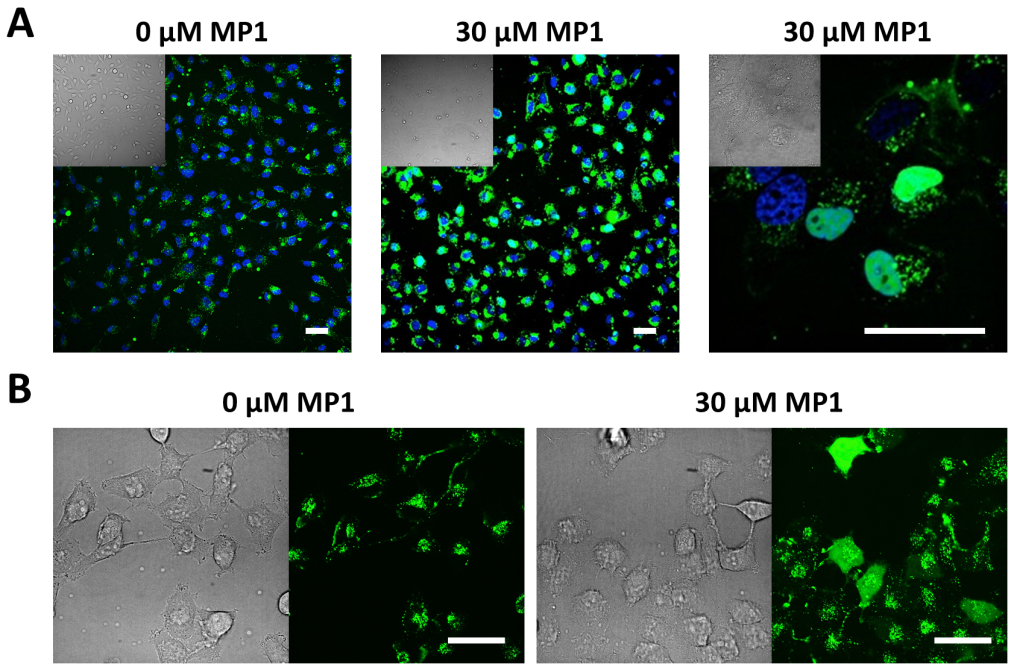

Figure S9. Delivery of GST-NLS-GFP and IgG-CF into HeLa cells. A) HeLa cells were incubated in DMEM with GST-NLS-GFP (10 µM; shown in green) in the absence or presence of 30 µM **MP1** for 1 h, washed and further incubated for 90 min in DMEM supplemented with 10% FBS before confocal imaging. Nuclei were stained with Hoechst (blue). Around 15% of the cells showed nuclear distribution of GST-NLS-GFP. B) HeLa cells were incubated with IgG-CF (1 mg/mL, green) in the presence or absence of 30 µM **MP1** for 1 h, in the same conditions as in A. Scale bars = 50 µm.

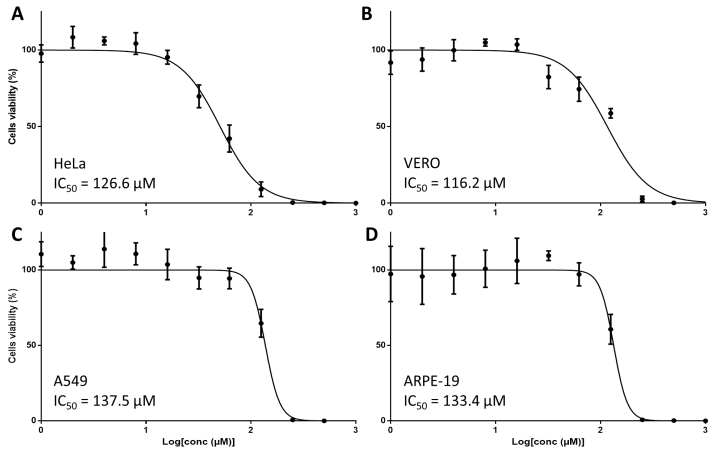

IC_{50}	HeLa	VERO	A549	ARPE-19
MP1	126.6 µM	116.2 µM	137.5 µM	133.4 µM

Figure S10 MTT viability assays. Viability was determined in HeLa (A), Vero (B), A549 (C) and ARPE-19 (D) cells. Cells were incubated with different concentrations of **MP1** (0, 1, 2, 4, 8, 16, 32, 62.5, 125, 250, 500, 1000 µM) in DMEM for 1 h, then the solutions were removed and replaced with complete medium. After 24 hours, cells were incubated for 3 hours with medium supplemented with 0.5 mg/mL MTT tetrazolium salt, and the medium was removed before solubilizing the formazan salt with DMSO. Cells viability was then quantified by absorbance. Data was normalized to the untreated control (100 %). Data is shown as mean of five replicates ± SD.

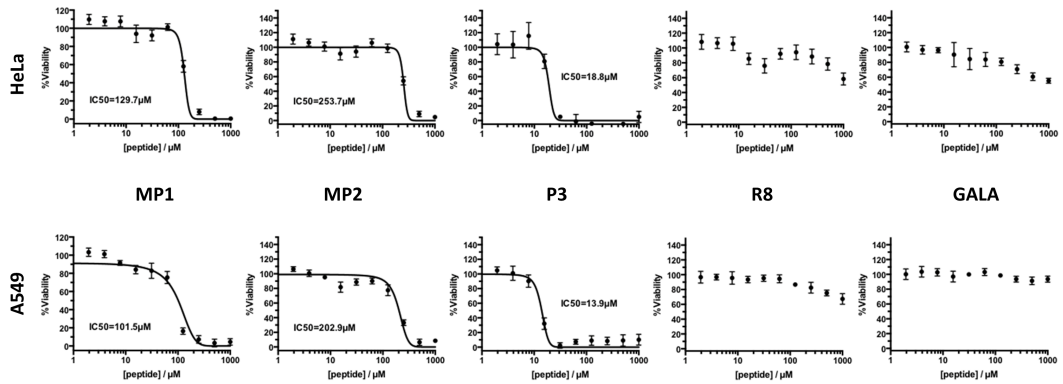

IC_{50}	MP1	MP2	P3	Arg_8	GALA
HeLa	129.7 µM	253.7 µM	18.8 µM	> 1 mM	> 1 mM
A549	101.5 µM	202.9 µM	13.9 µM	> 1 mM	> 1 mM

Figure S11. MTT viability assays at 1 h of incubation. HeLa (top row) or A549 (bottom row) were incubated with increasing concentrations of the indicated peptides in DMEM for 1 h, and then the solutions were removed and replaced by medium supplemented with 0.5 mg/mL MTT, incubated for 1 h, and, after medium removal, formazan salt was solubilized with DMSO and viability measured by absorbance. Data was normalized to untreated control (100%) and represented as mean ± SD (n = 5).

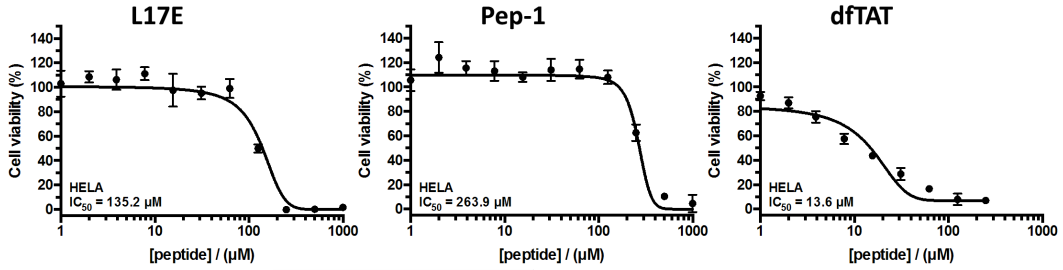

IC_{50}	L17E	Pep-1	dfTAT
HeLa	135.2 µM	263.9 µM	13.6 µM

Figure S12. MTT assay of control protein delivery peptides. Viability was determined in HeLa cells, after 1 h of incubation with different concentrations of the indicated peptides in DMEM, followed by 1 h incubation with medium supplemented with 0.5 mg/mL MTT tetrazolium salt. Formazan salt was solubilized with DMSO after medium removal and the absorbance at 570 nm measured. Data were normalized to the untreated control (100% viability) and shown as the mean of five replicates ± SD. As indicated in Fig. S11, **MP1** IC_{50} = 129.7 µM.

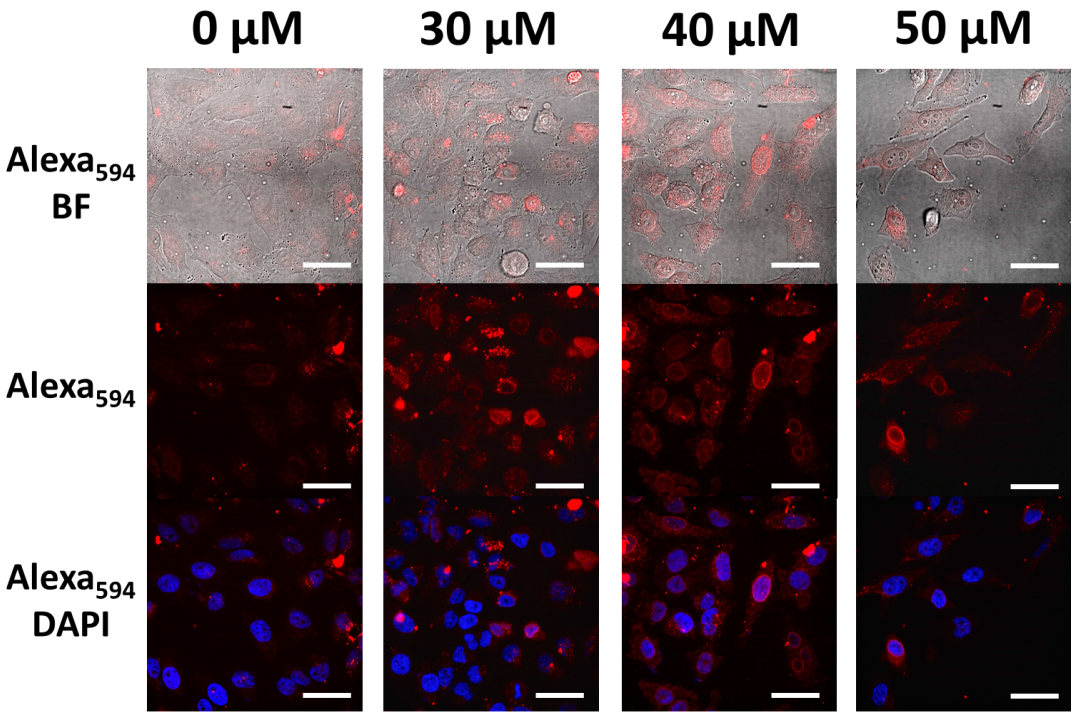

Figure S13. Cytosolic delivery of antibodies in HeLa cells. HeLa cells were incubated with 0.3 mg/mL of Mab414 and increasing amounts of **MP1** for 1 h. Cells were thoroughly washed and incubated for 3 h before fixation and immunofluorescence with Alexa Fluor 594 conjugated secondary antibody ($Alexa_{594}$, red). Nuclei were stained with DAPI (blue). Scale bars = 50 µm.

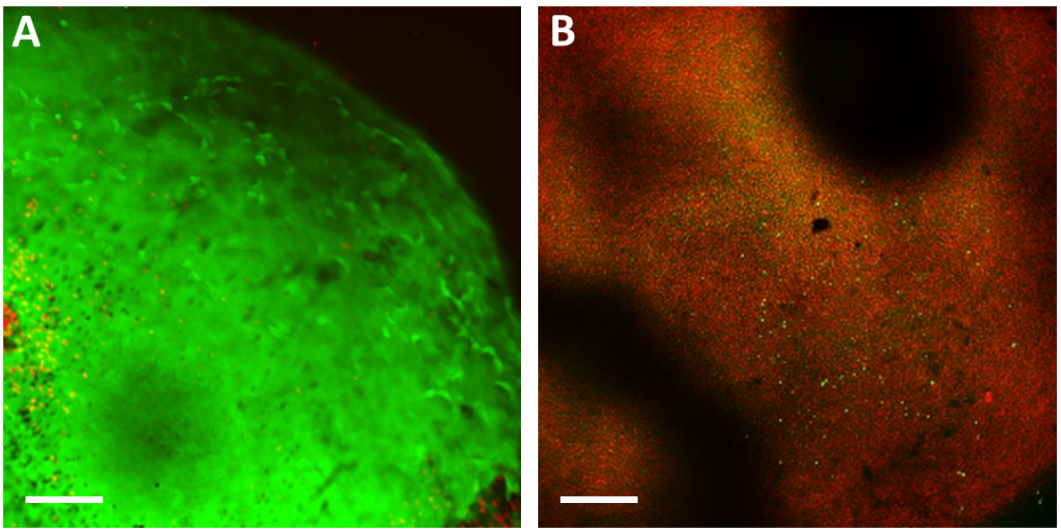

Figure S14. Delivery of antibodies in *ex vivo* corneas. Maximum projections of live/dead staining of murine corneas with propidium iodide (PI)/fluorescein diacetate (FDA). FDA (green) stains live cells' cytosol and PI (red) stains dead cells' nuclei. A) live cornea control. B) dead control. Live control was incubated in Ames' for 1 h, while dead control was incubated with 0.5% Triton X-100 for 1 h. Both were further incubated with Ames's + 10% FBS for 2 h before staining. Scale bars = 200 µm.

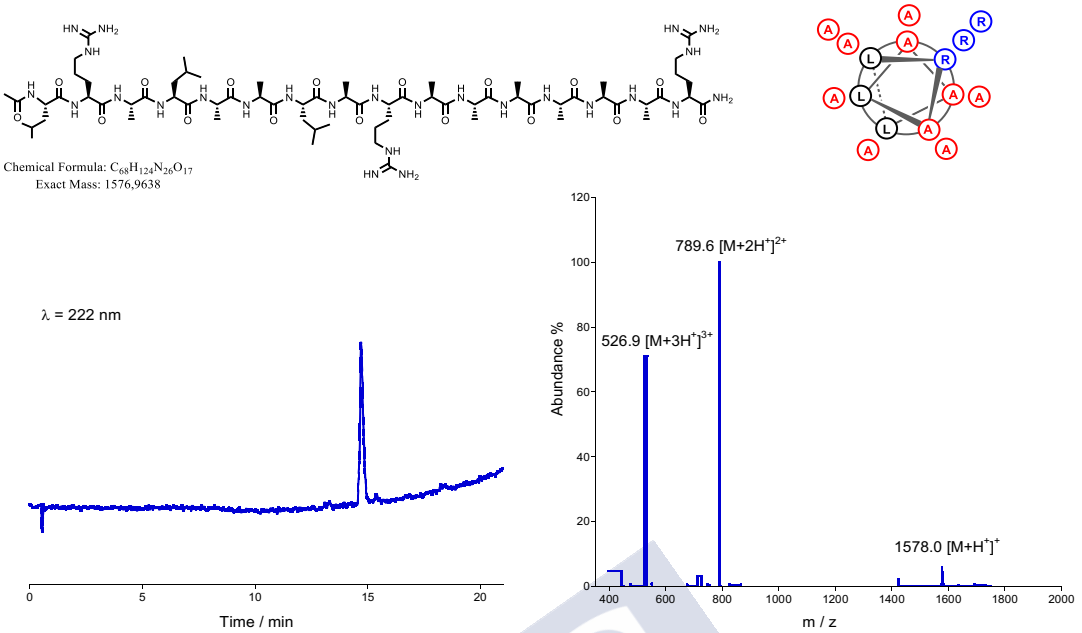

Figure S15. MP1 characterization. RP-HPLC [Agilent SB-C18 column, H_2O (0.1% TFA)/ CH_3CN (0.1% TFA) 95:5→5:95 (0→20 min)] (R_t 14.7 min) absorbance at 222 nm and ESI-MS for Peptide **MP1**.

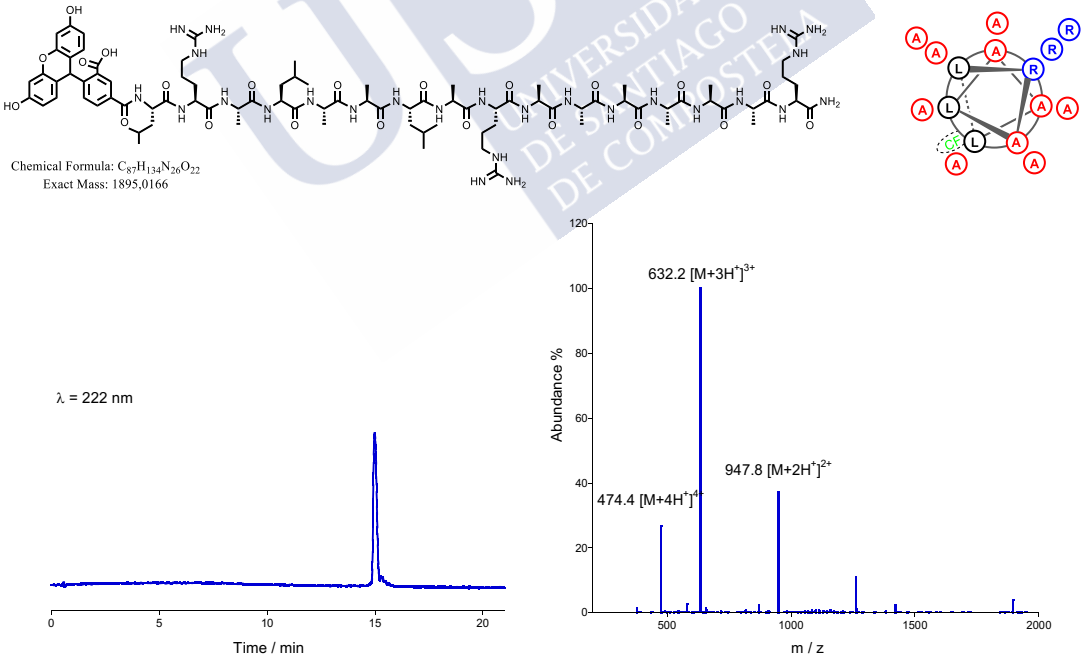

Figure S16. CF-MP1 characterization. RP-HPLC [Agilent SB-C18 column, H_2O (0.1% TFA)/ CH_3CN (0.1% TFA) 95:5→5:95 (0→20 min)] (R_t 14.9 min) absorbance at 222 nm and ESI-MS for Peptide **CF-MP1**.

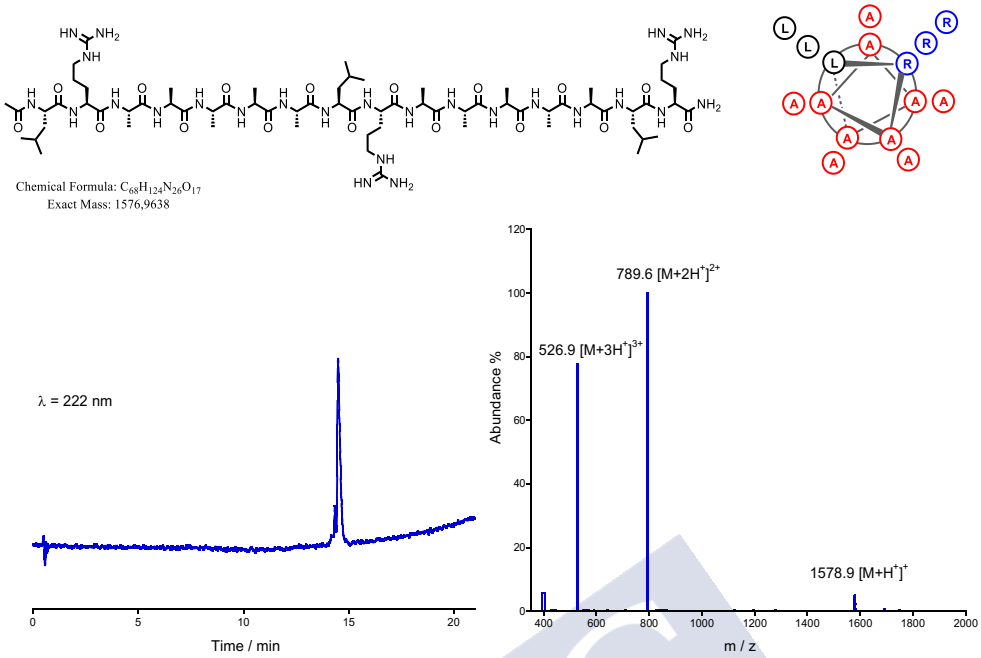

Figure S17. MP2 characterization. RP-HPLC [Agilent SB-C18 column, H_2O (0.1% TFA)/ CH_3CN (0.1% TFA) 95:5→5:95 (0→20 min)] (R_t 14.4 min) absorbance at 222 nm and ESI-MS for Peptide **MP2**.

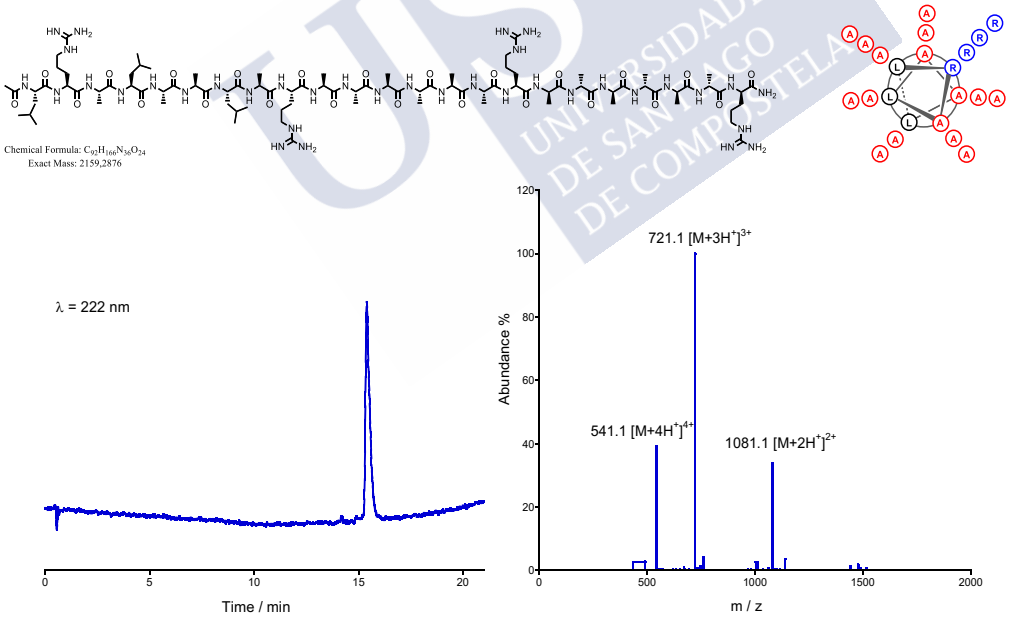

Figure S18. P3 characterization. RP-HPLC [Agilent SB-C18 column, H_2O (0.1% TFA)/ CH_3CN (0.1% TFA) 95:5→5:95 (0→20 min)] (R_t 15.4 min) absorbance at 222 nm and ESI-MS for Peptide **P3**.

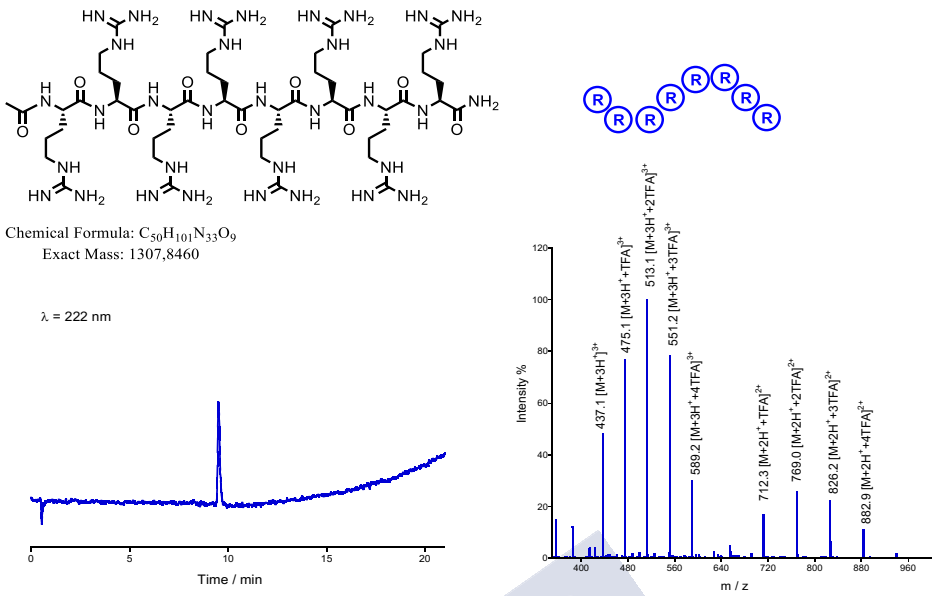

Figure S19. Arg$_8$ characterization. RP-HPLC [Agilent SB-C18 column, H_2O (0.1% TFA)/ CH_3CN (0.1% TFA) 95:5→5:95 (0→20 min)] (R_t 9.5 min) absorbance at 222 nm and ESI-MS for Peptide **Arg$_8$**.

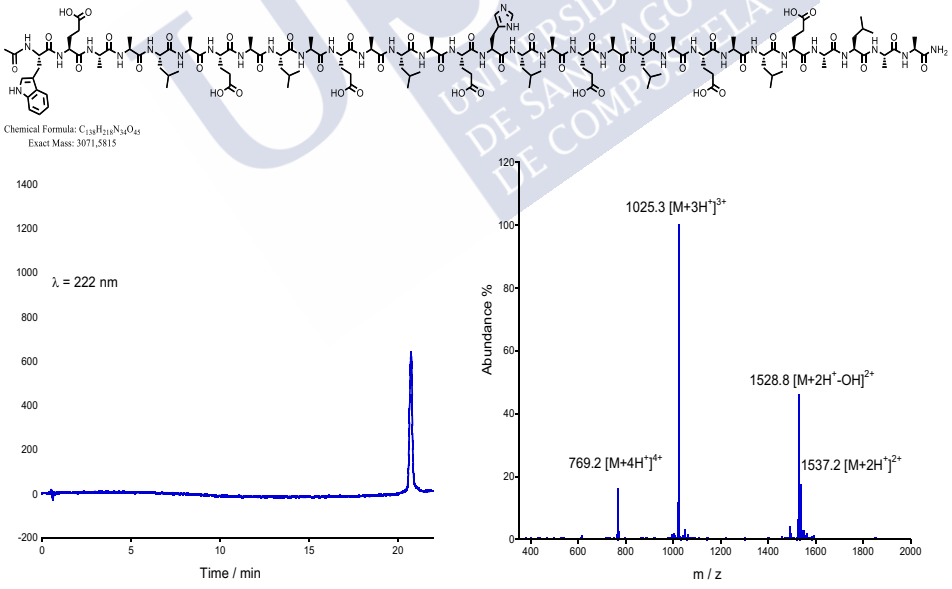

Figure S20. GALA characterization. RP-HPLC [Agilent SB-C18 column, H_2O (0.1% TFA)/ CH_3CN (0.1% TFA) 95:5→5:95 (0→21 min)] (R_t 20.6 min) absorbance at 222 nm and ESI-MS for Peptide **GALA**.

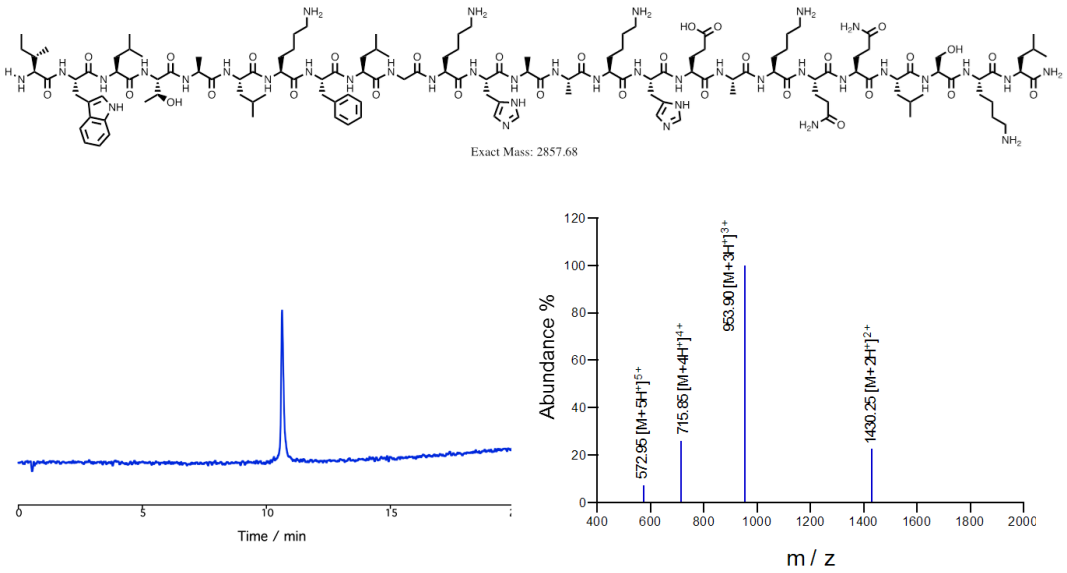

Figure S21. L17E characterization. RP-HPLC [Agilent SB-C18 column, H_2O (0.1% TFA)/ CH_3CN (0.1% TFA) 95:5→5:95 (0→20 min)] (R_t 10.6 min) absorbance at 222 nm and ESI-MS for Peptide **L17E**.

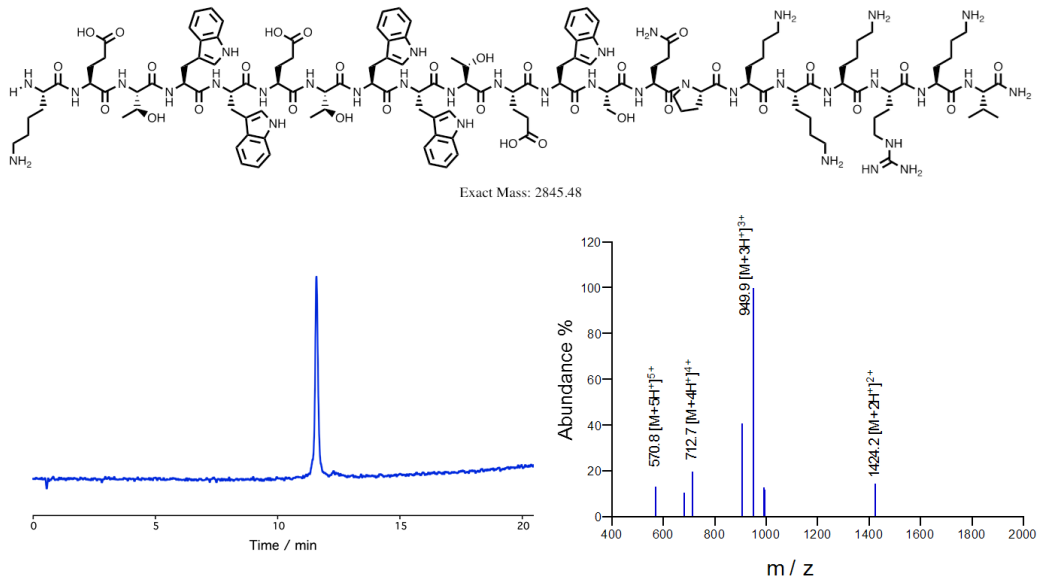

Figure S22. Pep-1 characterization. RP-HPLC [Agilent SB-C18 column, H_2O (0.1% TFA)/ CH_3CN (0.1% TFA) 95:5→5:95 (0→20 min)] (R_t 11.6 min) absorbance at 222 nm and ESI-MS for **Pep-1.**

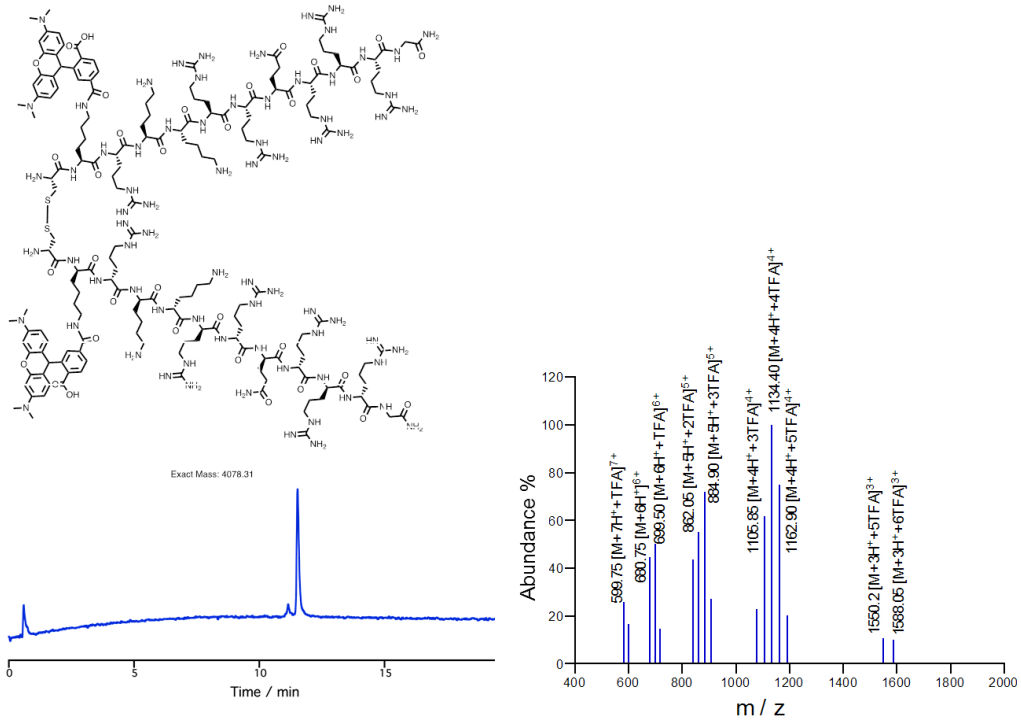

Figure S23. dfTAT characterization. RP-HPLC [Agilent SB-C18 column, H_2O (0.1% TFA)/ CH_3CN (0.1% TFA) 95:5→5:95 (0→20 min)] (R_t 11.5 min) absorbance at 222 nm and ESI-MS for **dfTAT**.

Video S1. Detail of a CG-MD simulations trajectory (5 ns in total) highlighting the initial interaction of **MP1** with a lipid bilayer composed by DPPC:DPPE (9:1) and DPPC:DPPE:DPPS (3:5:2). As it can be noticed, although the preliminary interaction of **MP1** with the membrane is led by electrostatic interactions between the Arg residues and the polar heads of the lipids, the peptide quickly orients the Leu enriched hydrophobic N-terminus of **MP1** towards the hydrophobic core of the lipid bilayer, and the arginine cationic residues remain exposed to the solvent. CG residues are represented in yellow (Ala), orange (Leu) and blue (Arg).

USC UNIVERSIDADE DE SANTIAGO DE COMPOSTELA

2. Experimental Procedures

2.1. Materials

Commercially available Rink Amide-resin ChemMatrix, Fmoc-*L*-Ala-OH, Fmoc-*L*-Leu-OH, Fmoc-*L*-Arg(pbf)-OH, triisopropylsilane (TIS), Diisopropylethyl amine (DIEA), diisopropylcarbodiimide (DIC), and 5-(N-Ethyl-N-isopropyl)amiloride (EIPA) were obtained from Sigma-Aldrich. Trifluoroethanol, 1,1,1,3,3,3-Hexafluoroisopropanol (HFIP) and chlorpromazine were purchased from TCI. Egg yolk L-α-phosphatidylcholine, 1-palmitoyl-2-oleoyl-*sn*-glycero-3-phosphocholine in chloroform (POPC), 1-palmitoyl-2-oleoyl-*sn*-glycero-3-phosphoglycerol sodium salt in chloroform (POPG), 16:0-12:0 1-palmitoyl-2-{12-[(7-nitro-2-1,3-benzoxadiazol-4-yl)amino]dodecanoyl}-*sn*-glycero-3-phosphoethanolamine (NBD-PE), 1,2-dipalmitoyl-*sn*-glycero-3-phosphoethanolamine-N-(7-nitro-2-1,3-benzoxadiazol-4-yl) (PE-NBD) and 1,2-diphytanoyl-*sn*-glycero-3-phosphocholine (DPhPC) were purchased from Avanti Polar Lipids. Ethyl(hydroxyimino)cyanoacetate (Oxyma), methyl-β-cyclodextrin, and 5-carboxytetramethyl rhodamine (TAMRA) were available from Carbosynth. *N*-HATU was provided by Glentham life sciences. *N*-HBTU was obtained from Iris. Peptide synthesis grade *N,N*-dimethylformamide was purchased from Scharlau. Dynasore was from EMD Millipore Corporation. All the other solvents were HPLC grade, purchased from Sigma-Aldrich® or Fisher Scientific®, and used without further purification.

Dulbecco's Modified Eagle's Medium (4500 mg/L glucose, L-glutamine, sodium pyruvate and sodium bicarbonate) was obtained from Gibco. Puromycin was purchased from Enzo Life Sciences. Ames' medium, Alexa Fluor 488 – Dextran (10 kDa), Tetramethylrhodamine – Dextran (10 kDa), fluorescein – Dextran (70 kDa), and LysoTracker Deep Red were acquired from Thermo Fisher. FITC – Dextran (40 kDa), Saporin, Dulbecco's Modified Eagle's Medium/Nutrient F-12 Ham (4500 mg/L glucose, L-glutamine, sodium pyruvate and sodium bicarbonate), human IgG (#I4506) and anti-nuclear pore complex proteins antibody Mab414 (Mouse monoclonal, clone 414, #N8786) were purchased from Sigma-Aldrich.

A microwave assisted peptide synthesiser (Liberty Lite, CEM) was used to prepare the peptide according to standard methods developed by the manufacturers involving diisopropylcarbodiimide (DIC) 0.5 M in DMF as activator and ethyl(hydroxyimino)cyanoacetate (Oxyma) 1 M in DMF as activator base. High-performance liquid chromatography coupled with mass spectrometry (HPLC-MS) analyses were carried out on Agilent Technologies 1260 Infinity II associated with a 6120 Quadrupole LC-MS using an Agilent SB-C18 column or on DIONEX Ultimate 3000 U-HPLC^{+} (Thermo Scientific) with an Acclaim RSLC 120-C18 column with *Solvent A:Solvent B* gradients between 5:95 (*Solvent A*: H_2O with 0.1% TFA; *Solvent B*: CH_3CN with 0.1% TFA). High-performance liquid chromatography (HPLC) semi-preparative purification was carried out on Jasco LC-4000 with an Agilent Eclipse XDB-C18 column.

Accurate mass determinations (HR-MS) using ESI-MS were performed on a Bruker MicroTof mass spectrometer.

Circular Dichroism (CD) measurements were performed with a Jasco J-1100 CD Spectrometer equipped with a Jasco MCB-100 Mini Circulation Bath for temperature control.

Vesicles were prepared with a Mini-Extruder from Avanti Polar Lipids (pore size 100 nm). Sample incubation was performed in 500 µL eppendorf vials. Fluorescence measurements were performed with a FluoroMax-2 spectrofluorometer (Jobin-Yvon Spex) equipped with a stirrer and a temperature controller.

DLS measurements were performed in a Malvern Zetasizer Nano ZSP using standard disposable cuvettes.

For the acquisition of cell microscopy images a Nikon Eclipse Ti-E epifluorescence microscope with an Andor Zyla 4.2 digital camera, or a Dragonfly confocal spinning-disk on a Nikon Eclipse Ti-E equipped with a Andor Zyla 4.2 PLUS sCMOS digital camera were used. Images were processed with FIJI.[S1] 3D images were reconstructed from the different individual confocal planes with Imaris 9.0.0 software (Oxford instruments).

A Tecan Infinite F200Pro microplate reader was used to directly measure in Costar cell culture 96-well plates UV-Vis absorbance for the MTT viability assays. Flow cytometry was performed on a Guava easyCyte™ cytometer and data analysed with InCyte software included in GuavaSoft 3.2 (Millipore).

2.2. Abbreviations

Aa: Amino acid; Arg: Arginine; BSA: bovine serum albumin; Calcd: Calculated; CF: Carboxyfluorescein; CF-MP1: oligoalanine MP1 labelled with carboxyfluorescein at *N*-terminus; CPZ: Chlorpromazine; DCM: Dichloromethane; Dex: dextran; DIC: diisopropylcarbodiimide; DIEA: *N*,*N*-Diisopropylethylamine; DMF: *N*,*N*-Dimethylformamide; DMEM: Dulbecco's Modified Eagle's Medium; DPPC: dipalmitoyl phosphatidylcholine; DPhPC: 1,2-diphytanoyl-*sn*-glycero-3-phosphocholine; DPPE: dipalmitoyl phosphatidylethanolamine; DPPS: dipalmitoyl phosphatidylserine; Dyn: Dynasore; EGFP: enhanced green fluorescent protein; EIPA: 5-(*N*-Ethyl-*N*-isopropyl)amiloride; FDA: fluorescein diacetate; GST: glutathione-S-transferase; HFIP: 1,1,1,3,3,3-Hexafluoro-2-propanol; HRMS (ESI): High resolution mass spectrometry (electrospray ionization); IPTG: Isopropyl β-D-1-thiogalactopyranoside; LB: Lysogeny broth; Leu: Leucine; Lys: Lysine; LUV: large unilamellar vesicles; MbCD: methyl-β-cyclodextrin; MES: 4-Morpholineethanesulfonic acid; Leu: Leucine; Lys: Lysine; MP1: minimal peptide 1; MP2: peptide 2 with aligned leucines; MOPS: 3-(N-Morpholino)propanesulfonic acid; Mtt: 4-Methyltrytil; MTT: 3-(4,5-dimethyl-2- thiazolyl)-2,5-diphenyl tetrazolium bromide; NBD-PE: 16:0-12:0 1-palmitoyl-2-{12-[(7-nitro-2-1,3-benzoxadiazol-4-yl)amino]dodecanoyl}-sn-glycero-3-phosphoethanolamine; *N*-HATU: *N*-[(Dimethylamino)-1H-1,2,3-triazolo[4,5-b]pyridine-1ylmethylene]-*N*-methylmethanaminium-hexafluorophosphate *N*-oxide; *N*-HBTU: *N*-[(1HBenzotriazol-1-yl)-(dimethylamino)methylene]-*N*-methylmethanaminium hexafluorophosphate *N*-oxide; NLS: Nuclear Localization Signal; P3: longer oligoalanine peptide; PE-NBD: 1,2-dipalmitoyl-sn-glycero-3-phosphoethanolamine-N-(7-nitro-2-1,3-benzoxadiazol-4-yl); Pbf: 2,2,4,6,7-Pentamethyldihydrobenzofuran-5-sulfonyl; PBS: Phosphate-Buffered Saline; POPC: 1-palmitoyl-2-oleoyl-*sn*-glycero-3-phosphocholine; PI: propidium iodide; POPG: 1-palmitoyl-2-oleoyl-*sn*-glycero-3-phosphoglycerol; SPPS: solid phase peptide synthesis; SV40: Simian Virus 40; TAMRA: 5-carboxytetramethyl rhodamine; TFE: Trifluoroethanol; TIS: Triisopropylsilane; TM-MP1: oligoalanine 1 labelled with TAMRA at *N*-terminus; TNBS: 2,4,6-Trinitrobenzenesulfonic acid;.

2.3. General protocol for the SPPS

All peptides were synthesized by automated or manual Fmoc solid-phase peptide synthesis[S2] using Rink Amide ChemMatrix resin (loading 0.5 mmol/g). For manual synthesis, the resin (0.5 mmol) was swelled in DMF (peptide synthesis grade, 2 mL) for 20 min in a peptide synthesis vessel prior synthesis. Coupling cycle consisted of the removal of Fmoc protecting group with a solution of piperidine in DMF (20%, 2 mL) for 10 min and then the mixture was filtered and the resin was washed with DMF (3 x 2 mL, 1 min). The amino acid coupling was carried out by treatment with a solution of α-amino acids (4 equiv), *N*-HBTU (3.95 equiv) in DMF (2 mL), which was mixed with DIEA (0.195 M solution in DMF, 1.2 equiv) 1 min before the addition and the resulting mixture was shaken by bubbling Ar for 15 min. Finally, the resin was washed with DMF (3 x 2 mL, 1 min). The efficiency of each amino acid coupling and deprotection was monitored employing the TNBS test.[S3]

For automated synthesis, a variant of the previous protocol was used instead, according to manufacturer's recommendations. 0.05 mmol of Rink Amide resin was placed into the peptide synthesiser reaction vessel, swollen in DMF, followed by cycles of Fmoc cleavage with piperidine 20% in DMF, washings (3 x 5 mL), then amino acid (5 equiv 2 M amino acid solution in DMF), DIC (10 equiv) and Oxyma (10 equiv) were added into the reaction vessel and microwaved for 5 min under temperature control followed by washings (3 x 5 mL). All steps were performed under nitrogen atmosphere. After the linear peptide was finished the resin was transferred to a different reaction vessel to perform the peptide modification manually.

Fluorophore coupling: the Fmoc-protecting group of the initial amino acid was removed by using a solution of piperidine in DMF (20%, 4 mL) for 15 min and the resin was washed with DMF (3 x 3 mL). The coupling was carried out by the addition of a solution of 5-carboxytetramethylrhodamine or 5,6-carboxyfluorescein (1 equiv), HATU (1 equiv), and DIEA (0.195 M, 1 equiv) in DMF (2 mL) and the mixture was stirred by bubbling Ar for 4 hours. Finally, the resin was washed with DMF (3 x 3 mL) and DCM (3 x 3 mL).

Acetylation in the N-terminus: Once the lineal peptide was finished the acetylation capping of N-terminal group was performed by standard Fmoc deprotection conditions (20% piperidine in DMF (2 x 5 mL, 15 min) followed by treatment with a solution of 2,6-lutidine/acetic anhydride (1:1, 3 mL). The resin suspension was mechanically shaken for 40 min and washed with DMF (3 x 3 mL, 1 min) and DCM (3 x 3 mL, 5 min).

General protocol for peptide cleavage and purification: Finally, peptides were deprotected and cleaved from the resin by standard TFA cleavage procedure at rt by using the TFA/DCM/H_2O/TIS (90:5:2.5:2.5, 3 mL per 70 mg of resin) for 2 h. Then, the mixture was filtered, washed with TFA (1 mL) and the peptide was precipitated with ice-cold Et_2O (50 mL). The precipitate was centrifuged and dissolved in H_2O (5 mL) and purified by RP-HPLC. Finally, the corresponding fractions were lyophilised to afford the pure solid peptides.

2.3.1. Synthesis of peptide MP1

Following the general protocol of the SPPS, **MP1** was obtained after RP-HPLC purification [Phenomenex Luna C18(2) 100A column, H_2O (0.1% TFA)/ CH_3CN (0.1% TFA) 95:5→5:95 (0→5 min), 95:5→5:95 (5→35 min)] with an overall yield of 30%. R_t 14.7 min [RP-HPLC Agilent SB-C18 column, H_2O (0.1% TFA)/ CH_3CN (0.1% TFA) 95:5→5:95 (0→21 min)]. **MS** (ESI, H_2O): 1578.0 (6, $[M+H]^+$), 789.6 (100, $[M+2H]^{2+}$), 526.9 (71, $[M+3H]^{3+}$). **HRMS** (ESI): Calcd for $C_{68}H_{125}N_{26}O_{17}$ $[M+H]^+$: 1577.9702; found: 1577.9711. See Figure S15.

2.3.2. Synthesis of peptide CF-MP1

Following the general protocol of the SPPS followed by fluorophore coupling, **CF-MP1** was obtained after RP-HPLC purification [Phenomenex Luna C18(2) 100A column, H_2O (0.1% TFA)/ CH_3CN (0.1% TFA) 95:5→5:95 (0→5 min), 95:5→5:95 (5→35 min)] with an overall yield of 9%. R_t 14.9 min [RP-HPLC Agilent SB-C18 column, H_2O (0.1% TFA)/ CH_3CN (0.1% TFA) 95:5→5:95 (0→20 min)]. **MS** (ESI, H_2O): 947.8 (37, $[M+2H]^{2+}$), 632.2 (100, $[M+3H]^{3+}$), 474.4 (27, $[M+4H]^{4+}$). **HRMS** (ESI): Calcd for $C_{87}H_{134}N_{22}O_{22}$ $[M+2H]^{2+}$: 947.5100; found: 947.5078. See Figure S16.

2.3.3. Synthesis of peptide TM-MP1

Following the general protocol of the SPPS followed by fluorophore coupling, **TM-MP1** was obtained after RP-HPLC purification [Phenomenex Luna C18(2) 100A column, H_2O (0.1% TFA)/ CH_3CN (0.1% TFA) 95:5→5:95 (0→5 min), 95:5→5:95 (5→35 min)] with an overall yield of 12%. R_t 15.2 min [RP-HPLC Agilent SB-C18 column, H_2O (0.1% TFA)/ CH_3CN (0.1% TFA) 95:5→5:95 (0→20 min)]. Synthesis and characterization had been previously described as **P_8** in Pazo *et al*.[S4]

2.3.4. Synthesis of peptide MP2

Following the general protocol of the SPPS, **MP2** was obtained after RP-HPLC purification [Phenomenex Luna C18(2) 100A column, H_2O (0.1% TFA)/ CH_3CN (0.1% TFA) 95:5→5:95 (0→5 min), 95:5→5:95 (5→35 min)] with an overall yield of 10%. R_t 14.4 min [RP-HPLC Agilent SB-C18 column, H_2O (0.1% TFA)/ CH_3CN (0.1% TFA) 95:5→5:95 (0→20 min)]. **MS** (ESI, H_2O): 1578.9 (5, $[M+H]^+$), 789.6 (100, $[M+2H]^{2+}$), 526.9 (77, $[M+3H]^{3+}$). **HRMS** (ESI): Calcd for $C_{68}H_{124}N_{26}O_{17}$ $[M+2H]^{2+}$: 1577.9716; found: 1577.9711. See Figure S17.

2.3.5. Synthesis of peptide P3

Following the general protocol of the SPPS, **P3** was obtained after RP-HPLC purification [Phenomenex Luna C18(2) 100A column, H_2O (0.1% TFA)/ CH_3CN (0.1% TFA) 95:5→5:95 (0→5 min), 95:5→5:95 (5→35 min)] with an overall yield of 16%. R_t 15.4 min [RP-HPLC Agilent SB-C18 column, H_2O (0.1% TFA)/ CH_3CN (0.1% TFA) 95:5→5:95 (0→20 min)]. **MS** (ESI, H_2O): 1081.1 (33, $[M+2H]^{2+}$), 721.1 (100, $[M+3H]^{3+}$), 541.1 (39, $[M+4H]^{4+}$). **HRMS** (ESI): Calcd for $C_{92}H_{168}N_{36}O_{24}$ $[M+2H]^{2+}$: 1080.6515; found: 1080.6511. See Figure S18.

2.3.6. Synthesis of peptide Arg_8

Following the general protocol of the SPPS, **Arg_8** was obtained after RP-HPLC purification [Phenomenex Luna C18(2) 100A column, H_2O (0.1% TFA)/ CH_3CN (0.1% TFA) 95:5→5:95 (0→5 min), 95:5→5:95 (5→35 min)] with an overall yield of 58%. R_t 9.5 min [RP-HPLC Agilent SB-C18 column, H_2O (0.1% TFA)/ CH_3CN (0.1% TFA) 95:5→5:95 (0→20 min)]. **MS** (ESI, H_2O): 882.9 (11, $[M+2H+4TFA]^{2+}$), 826.2 (22, $[M+2H+3TFA]^{2+}$), 769.0 (26, $[M+2H+2TFA]^{2+}$), 712.3 (17, $[M+2H+TFA]^{2+}$), 589.2 (30.3, $[M+3H+4TFA]^{3+}$), 551.2 (78, $[M+3H+3TFA]^{3+}$), 513.1 (100,

$[M+3H+2TFA]^{3+}$), 475.1 (77, $[M+3H+TFA]^{3+}$), 437.1 (48, $[M+3H+TFA]^{3+}$). **HRMS** (ESI): Calcd for $C_{50}H_{103}N_{33}O_9$ $[M+2H]^{2+}$: 654.9304; found: 654.9303. See Figure S19.

2.3.7. Synthesis of peptide GALA

Following the general protocol of the SPPS, **GALA** was obtained after RP-HPLC purification [Phenomenex Luna C18(2) 100A column, H_2O (0.1% TFA)/ CH_3CN (0.1% TFA) 95:5→5:95 (0→5 min), 95:5→5:95 (5→35 min)] with an overall yield of 0.5%. R_t 20.6 min [RP-HPLC Agilent SB-C18 column, H_2O (0.1% TFA)/ CH_3CN (0.1% TFA) 95:5→5:95 (0→20 min)]. **MS** (ESI, H_2O): 1528.8 (46, $[M+2H-OH]^{2+}$), 1537.2 (17, $[M+2H]^{2+}$), 1025.3 (100, $[M+3H]^{3+}$), 769.2 (16, $[M+4H]^{4+}$). **HRMS** (ESI): Calcd for $C_{138}H_{220}N_{34}O_{45}$ $[M+2H]^{2+}$: 1536.7981; found: 1536.7980. See Figure S20.

2.3.8. Synthesis of peptide L17E

L17E was synthesized and purified as previously described,[S5] with an overall yield of 23.3%. R_t 10.6 min [RP-HPLC Agilent SB-C18 column, H_2O (0.1% TFA)/ CH_3CN (0.1% TFA) 95:5→5:95 (0→20 min)]. **MS** (ESI, H_2O): 1430.2 (23, $[M+2H]^{2+}$), 953.9 (100, $[M+3H]^{3+}$), 715.8 (26, $[M+4H]^{4+}$), 572.95 (7, $[M+5H]^{5+}$). See Figure S21.

2.3.9. Synthesis of Pep-1

Pep-1 was synthesized and purified as previously described,[S6] with an overall yield of 3.5%. R_t 11.6 min [RP-HPLC Agilent SB-C18 column, H_2O (0.1% TFA)/ CH_3CN (0.1% TFA) 95:5→5:95 (0→20 min)]. **MS** (ESI, H_2O): 1424.2 (15, $[M+2H]^{2+}$), 949.9 (100, $[M+3H]^{3+}$), 712.7 (20, $[M+4H]^{4+}$), 570.8 (13, $[M+5H]^{5+}$). See Figure S22.

2.3.10. Synthesis of dfTAT

dfTAT was synthesized and purified as previously described,[S7] with an overall yield of 8%. R_t 11.5 min [RP-HPLC Agilent SB-C18 column, H_2O (0.1% TFA)/ CH_3CN (0.1% TFA) 95:5→5:95 (0→20 min)]. **MS** (ESI, H_2O): 1588.0 (10, $[M+3H+6TFA]^{3+}$) 1550.2 (10, $[M+3H+5TFA]^{3+}$), 1162.9 (75, $[M+4H+5TFA]^{4+}$), 1134.4 (100, $[M+4H+4TFA]^{4+}$), 1105.8 (61, $[M+4H+3TFA]^{4+}$) 884.9 (72, $[M+5H+3TFA]^{5+}$), 862.1 (55, $[M+5H+2TFA]^{5+}$), 699.5 (50, $[M+6H+TFA]^{6+}$), 680.75 (45, $[M+6H]^{6+}$), 599.75 (16, $[M+7H+TFA]^{7+}$). See Figure S23.

2.4. Liposome preparation

The procedure for liposome preparation has been previously reported.[S8] Briefly, a thin lipid film was prepared using 1 mL of 25 mg/mL of lipid in chloroform and evaporating the chloroform on a rotary evaporator and then *in vacuo* overnight. The lipids were resuspended with one of the intravesicular solutions described below for 45 min. The resulting vesicles were extruded 11 times through a 0.1 µm Nucleopore polycarbonate filter. Extravesicular components were removed by desalting column (Sephadex G-50) pre-equilibrated with extravesicular buffer. The final concentration of vesicles is 5 mM.

In the case of ANTS/DPX – encapsulated LUVs (LUVs⊂ANTS/DPX) the extravesicular buffer is composed by 10 mM MES and 150 mM NaCl, at pH 7.4 or 5.5, and the intravesicular buffer is composed by 10 mM MES, 70 mM NaCl, 12.5mM ANTS and 45 mM DPX at pH 7.5 or 5.5 respectively. The lipid composition is 100% POPC or POPC/POPG at 3:1 molar ratio.

In order to make NBD-labelled lipid vesicles, lipids labelled in the polar head (PE-NBD) or in the hydrophobic tail (NBD-PE) are added to the lipid mixture as 0.5%. The remaining lipid composition is 99.5% POPC or POPC/POPG molar ratio 3:1. The intra and extravesicular buffer are the same (10 mM MES and 150 mM NaCl, at pH 7.5 or 5.5). In this case, the desalting column (Sephadex G-50) step is not necessary.[S9]

In the case of non-fluorescent LUVs, the intra and extravesicular buffers are composed by 10 mM MES and 150 mM NaCl, at pH 7.5 or 5.5 respectively, and the lipid composition is 100% POPC or POPC/POPG molar ratio 3:1. In this case, the desalting column (Sephadex G-50) step is omitted.

Dextran loaded liposomes (LUVs⊂Dextran) were prepared following the protocol described by Sani *et al.*[S10] First, the film lipid was formed with POPC or POPC/POPG 3:1 by rotary evaporation and then *in vacuo* overnight. Thus, the lipid was rehydrated with a solution of 20 mM of 10 kDa FITC-dextran and 20 mM of 40 kDa TM-Dextran, 10 mM MES, 5 mM NaCl at two different pH (7.5 and 5.5). After that, the resulting mixture was extruded 11 times through a 0.2 µm Nucleopore polycarbonate filter. In order to remove the extravesicular components, the samples were centrifuged three times for 40 min, 1500 rpm at 10 °C. After each centrifugation the supernatant was removed and replaced by fresh extravesicular buffer (10 mM MES, 7 mM NaCl) at the corresponding pH.

2.5. ANTS/DPX assay

LUVs⊂ANTS/DPX stock solutions (50 µL) were diluted with a buffer (10 mM MES and 150 mM NaCl, at pH 7.4 and 5.5), placed in a thermostated fluorescence cuvette (25 ºC) and gently stirred (total volume ~2000 µL; final lipid concentration ~125 µM). ANTS efflux was monitored at λ_{em} 510 nm (λ_{ex} 353 nm) as a function of time after addition of **MP1** at t = 50 s and aqueous Triton X-100 (1.2%, 20 µL, 185 µM final concentration) at t = 225 s; each measurement was made in triplicate. Fluorescence intensities were normalized to fractional emission intensity I(t) using equation (S1).

$$I(t) = (I_t - I_0) / (I_\infty - I_0) \quad \text{(S1)}$$

where I_0 is the initial intensity of the vesicles alone, $I_\infty = I_t$ at saturation after lysis. Effective concentration for peptides (EC_{50}) and Hill coefficient (n) were determined by plotting the fractional activity Y (= I(t) at saturation just before lysis, t = ~200 s) as a function of **MP1** $c_{Peptide}$ and fitting them to the Hill equation (S2).

$$Y = Y_0 + (Y_{MAX} - Y_0) / \{1 + (EC_{50} / c_{Peptide})^n\} \quad \text{(S2)}$$

where Y_0 is Y before the addition of the peptide, Y_{MAX} is Y with an excess of peptide at saturation.

For reversible pore gating experiments, LUVs⊂ANTS/DPX (3:1 molar ratio POPC:POPG) stock solutions (50 µL) were diluted with a buffer (10 mM MES and 150 mM NaCl, at pH 7.4 and 5.5) and placed in a thermostated fluorescence cuvette (25 ˚C) and gently stirred (total volume ~2000 µL; final lipid concentration ~125 µM). ANTS efflux was monitored at λ_{em} 510 nm (λ_{ex} 353 nm) as a function of time after addition of **MP1** (10 µM) at t = 25 s peptide addition, t = 50 s lipid addition (POPG, 50 µM), t = 150 s peptide addition, t = 175 s lipid addition, t = 275 s peptide addition, t = 300 s lipid addition. Finally, an aqueous Triton X-100 solution (1.2%, 20 µL, 185 µM final concentration) was added at t = 475 s.

2.6. Dextran release in vesicles

LUVs⊂Dextran stock solutions (25 µL) were diluted with a buffer (10 mM MES and 7 mM NaCl, at either pH 7.4 or 5.5) and placed in an eppendorf. Then the minimal peptide **MP1** was added at different concentrations and stirred for 30 min (total volume ~1000 µL; final lipid concentration ~125 µM). The mixture was centrifuged for 35 min at 10 ºC and 1500 rpm. The supernatant was collected and measured by spectrofluorometry: FITC-dextran (10 kDa) was monitored at λ_{em} 500 - 650 nm (λ_{ex} 492 nm), TM-dextran (40 kDa) was monitored at λ_{em} 560 - 700 nm (λ_{ex} 555 nm). Fluorescence intensities were normalized to fractional emission intensity I(t) using equation (S1)

$$I(t) = (I_t - I_0) / (I_\infty - I_0) \quad \text{(S1)}$$

where I_0 is I_t of vesicles alone, $I_\infty = I_t$ at saturation after lysis. Effective concentration for peptides (EC_{50}) and Hill coefficient (*n)* were determined by plotting the fractional activity Y (= I(t) at saturation just before lysis) as a function of peptide concentration $c_{Peptide}$ and fitting them to the Hill equation (S2).

$$Y = Y_0 + (Y_{MAX} - Y_0) / \{1 + (EC_{50} / c_{Peptide})^n\} \quad \text{(S2)}$$

where Y_0 is Y without peptide, Y_{MAX} is Y with an excess of **MP1** at saturation.

2.7. Circular Dichroism

Circular dichroism measurements were carried out with the following settings: acquisition range: 300-190 nm; bandwidth: 1.0 nm; accumulation: 3 scans; data pitch: 1 nm; CD scale 200 mdeg/1.0 dOD; D.I.T. (Data Integration Time): 1 s; scanning mode: continuous; scanning speed: 200 nm/min. Measurements were done at 10 ºC and 40 ºC in a quartz cell of 0.2 cm path length at a final volume of 0.5 mL (buffer 10 mM MES, 150 mM NaCl at two pH: 7.4 and 5.5) with a final peptide concentration of 100 µM. The results are expressed as the mean residue molar ellipticity $[\theta]_{MRt}$ with units of degrees·cm^2·dmol^{-1} and calculated using the equation S3. The percentage of helicity was calculated using the equation S4.[S11] As this value is used for comparisons among similar peptides in different environments, no correction for the number of aromatic aminoacids is required. For the measurements in presence of non-fluorescent LUVs (100% POPC or POPC/POPG at molar ratio 3:1), samples were prepared by mixing the peptides at 100 µM and different amounts of liposomes at different lipid:peptide ratios (1.25, 5, 12, 50). For each sample, a blank measurement was done prior addition of the peptide, and subtracted to the other measurements before analysis.

$$[\Theta]_{MRt} = \frac{0.1 \text{ x } \Theta}{C \cdot l \cdot \text{number of residues}} \quad (\text{deg} \cdot \text{cm}^2 \cdot \text{dmol}^{-1}) \quad \text{(S3)}$$

Equation S3: Formula to calculate the ellipticity. Θ is the ellipticity (mdeg), C is the peptide concentration (M) and l is the cell path length (cm).

$$[\Theta]\% = \frac{|\Theta MRt_{222}| - 2340}{30300} \text{ x } 100 \quad \text{(S4)}$$

Equation S4: Formula to calculate the percent of helicity in which the molar ellipticity at 222 nm is an absolute value.[S11]

2.8. DLS experiments

Non-fluorescent LUVs (50 µL, 125 µM) (POPC or POPC/POPG 3:1) were added to a buffer solution (10 mM MES and 150 mM NaCl, at pH 7.5 and 5.5) to a final volume of 200 µL (20 ^{0}C, duration = 70 s). The best parameters were found using the automatic mode, after which the attenuator index was fixed at 6. Measurements were done after the addition of increasing amounts of the peptide (50, 100, 200, 400, 800 µM) to the sample, and ended after vesicle lysis with Triton X-100, when the equipment could not measure, as the counted photons are 0. The standard deviation is given by equation S5.[S12]

$$\text{PdI} = \left(\frac{\text{SD}}{\text{Mean}}\right)^2 \quad \text{(S5)}$$

Equation S5: Formula to calculate the standard deviation using the mean and polydispersity index (PdI).

2.9. FRET and fluoresence experiments

The minimal peptide **MP1** was modified at the N-terminus with either 5-TAMRA or 5-carboxyfluorescein, which constitute a FRET pair, to achieve the peptides **TM-MP1** and **CF-MP1** respectively. The emission of the donor carboxyfluorescein (at λ_{ex} = 494 nm, λ_{em} = 518 nm) was measured in a final volume of 2 mL containing a mixture of 50 µL, 125 µM vesicles and 2.5 µM **CF-MP1**. The peptide FRET partner **TM-MP1** 2.5 µM (5µM final concentration of both **CF-MP1** and **TM-**

MP1) was added at t = 25 s and the fluorescence monitored until t = 200 s. **CF-MP1** emission was determined at t = 10 s and t = 150 s and FRET efficiency calculated according equation S6.

$$E = 1 - (F_{DA}/F_D) \quad \text{(S6)}$$

Equation S6: Formula to calculate the Efficiency (E), F_{DA} is the fluorescence of the donor in the presence of the acceptor; F_D fluorescence of the donor alone.

The second FRET experiment was performed using the same peptide labelled at the N-terminus with TAMRA (**TM-MP1**). Anionic and neutral vesicles containing 0.5% NBD-PE or PE-NBD were diluted (50 µL in 2 mL) in MES buffer at two different pH (7.5 and 5.5). The emission of the donor NBD (λ_{ex} = 470 nm , λ_{em} = 531 nm) was measured at t = 0 s and after the addition of peptide acceptor pair (0.05, 0.1, 0.5, 1 µM) from t = 25 s until t = 200 s. NBD emission values at t = 10 s and t = 150 s were used for FRET efficiency calculation using equation S6.

Emission fluorescence spectra was also measured at different concentrations of **CF-MP1** (λ_{ex} = 494 nm) in aqueous solution (MES buffer, pH 7.5). Quenching effect at increasing concentrations suggests a micelle-like aggregation at concentrations over 1.5µM.[S13] The shift of the peak of maximum fluorescence intensity indicates a complete aqueous solvating effect in peptide molecules at concentration lower than 1.5µM.[S14]

2.10. Computational methods

Since it is generally believed that early endosomes share the same overall lipid composition as the plasma membrane, as they are both part of the same recycling territory,[S15] this study used an asymmetric human erythrocyte membrane model, following the study of Tian *et al.*[S16], which involves three lipid types, including dipalmitoyl phosphatidylcholine (DPPC), dipalmitoyl phosphatidylethanolamine (DPPE), and dipalmitoyl phosphatidylserine (DPPS). In the outer leaflet of the membrane, the lipid ratio is 9:1 for DPPC and DPPE; in the inner membrane leaflet, the lipid ratio is 3:5:2 for DPPC, DPPE, and DPPS. Mapping of lipid molecules was based on the Martini CG force field (Martini_v2.2).[S11,S12] Choline groups of lipids are represented by the CG beads Qo, Qd, and P5 for DPPC, DPPE, and DPPS, respectively. The phosphate groups of all lipids are represented by Qa. The glycerol groups and carbon tails of all lipids are represented by Na and C1, respectively.

The peptide **MP1** model was built following the extended Martini force field for proteins using the martine.py script.[S11,S13] Peptide **MP1** contains 3 Leu residues, 3 Arg residues and 10 Ala residues, so that the total charge of each unit is +3. The terminal edges of the peptides were not charged.

A random distribution of 31 units of peptide **MP1** interaction of an asymmetric membrane composed by 1309 CG lipids was investigated, with an initial size of the box of 20 x 20 x 15 nm. After a short equilibration, long MD simulations of 1000 ns for each case were performed in absence and presence of an external electric field of 0.03 V/nm applied across the bilayer. The system temperature was kept at 310 K using a V-rescale thermostat,[S20] and periodic boundary conditions were used in all simulations. The Parrinello-Rahman barostat[S21] with semisotropic pressure was applied. The van der Waals interaction cutoff was 1.1 nm. In the case of atomistic resolution, AT-MD simulations were carried out using the Gromos54a7 force field.[S22] The edges of peptide **MP1** were modelized as ACE and NH2, respectively. The box was solvated with water or TFE, respectively. The system temperature was kept at 310 K using a V-rescale thermostat,[S20] and periodic boundary conditions were used in all simulations. The Parrinello-Rahman barostat[S21] with isotropic pressure was applied. The van der Waals interaction cutoff was 1.0 nm. Particle mesh Ewald summation (PME) method[S23] was used to determine electrostatic interactions. All simulations were performed by the GROMACS 4.5.4 package[S24] and results were represented by Visual Molecular Dynamics (VMD) 1.9 software.[S25]

2.11. Planar lipid bilayer recordings

Experiments were performed in planar lipid bilayer membranes (BLMs) formed by the Montal and Rudin technique.[S26] The recordings were carried out by using bilayers of 1,2-diphytanoyl-*sn*-glycero-3-phosphocholine (DPhPC) across a 80-100 µm diameter hole of a 25 µm thick PTFE (Goodfellow Corporation, Malvern, PA, USA). Bilayers were formed by first pretreating the aperture with a drop of 1% (v/v) hexadecane in n-pentane. The buffer solution (0.5 M of KCl and 10 mM of MOPS) was added to both 1 mL chambers, then, DPhPC in n-pentane (5 µL, 5 mg/mL) was added to both wells; after that, the solvent evaporated. A bilayer was formed when the electrolyte was lowered and raised, bringing the

two lipid surface monolayers together at the aperture. The capacitance of the bilayer was checked and the stability of the bilayer was monitored for 5 min at +200 mV, observing no fluctuations in the current. After planar membrane formation the peptide dissolved in MQ water was added to both chambers at 25 µM. The whole BLM conductance was measured at voltage-clamp-mode-holding potential from trans to cis chamber. Raw ion current recording was acquired at 1 kHz at a sampling frequence of 5 kHz. The current was amplified by using an Axopatch 200B amplifier (Molecular Devices), digitized with a Digidata 1440 A (Molecular Devices) converter, while data collection was done by the Clampex 10.7 software (Molecular Devices). Data processing and analysis was carried out with Clampfit 10.7 (the resulting current was filtered using Low pass Bessel (8-pole)). All Axons instruments and software are products of Molecular Devices (Sunnyvale, CA). According to the pore conductance, the peptide pore size was calculated following the Hille equation (S7).[S27] The conductivity of 0.5 M KCl 10 mM MOPS at 25 ℃ is 5.1 $S \cdot m^{-1}$, r the radius and l the length of the pore (4.7 nm) (theoretical thickness of DPhPC membrane). From the single channel electrical recordings, the current of the open state is around 1,100 pA and the estimated diameter is around 3.16 nm; for long opened states is around 1,900 pA and the diameter around 4.4 nm.

$$\frac{1}{g} = \left(l + \frac{\pi r}{2}\right) \cdot \left(\frac{\rho}{\pi r^2}\right) \quad \text{(S7)}$$

Equation S7. Hille equation. g is the pore conductance; l the length of the pore, ρ the resistivity of the recording solution and r the inner radius of the pore.

2.12. Cell culture experiments

2.12.1. Cell lines and culture

HeLa, Vero, and A549 cells were grown in the same conditions: at 37 ºC, 5% CO_2, in Dulbecco's Modified Eagle's Medium (DMEM; 4500 mg/L glucose, L-glutamine, sodium pyruvate and sodium bicarbonate), supplemented with 10% fetal bovine serum and 1% of Penicillin-Streptomycin-Glutamine Mix.

Human retinal pigmentary epithelium ARPE-19 cell line was maintained on Dulbecco's Modified Eagle's Medium/Nutrient F-12 Ham (4500 mg/L glucose, L-glutamine, sodium pyruvate and sodium bicarbonate) supplemented with 10% FBS and 1% Penicillin-Streptomycin-Glutamine Mix (Fisher) at 37 ºC, 5% CO_2 in an INCO 108 incubator (Memmert).

To generate a Cre Reporter-expressing HeLa cell line, HeLa cells were transfected with the plasmid Cre Reporter (a gift from Niels Geijsen; Addgene plasmid # 62732).[S28] In this plasmid, the gene for dsRED is flanked by two *loxP* sites and followed by EGFP gene. In the absence of recombination, the stop codon from dsRED prevents EGFP translation, while Cre-mediated recombination removes the dsRED gene, switching the expression from the red fluorescent protein to the green fluorescent protein. Stable transfectants were selected by maintaining the cell culture in presence of 0.5 µg/mL puromycin (Enzo Life Sciences).

2.12.2. Cellular uptake and endosomal release of dextran

For live cell imaging, cells grown on glass bottom dishes were washed with DMEM stock and incubated for 1 h with a solution of peptide and dextran, using different concentrations of **MP1** and 0.25 mg/mL 10 kDa $Alexa_{488}$-Dextran, 0.25 mg/mL 10 kDa TM-Dextran, 1 mg/mL of 40 kDa FITC-Dextran, or 0.25 mg/mL of 70 kDa FITC-Dextran. In co-incubation experiments, 0.25 mg/mL 10 kDa TM-Dextran and 1.25 mg/mL 70 kDa FITC-Dextran were used. After that, cells were washed with DMEM twice and incubated for 3 h with DMEM supplemented with 10% FBS. Finally, cells were washed with DMEM without phenol red and observed with a spinning disk confocal microscope. For lysosomal labelling, cells were incubated for 30 min with 100 nM of LysoTracker Deep Red after the 3 h incubation, and washed before imaging.

For the experiments in the presence of endocytosis inhibitors, HeLa cells were seeded the day before in 8-well micro-slides (ibiTreat, Ibidi) at 30000 cells per well, washed and treated with chlorpromazine (30 µM), dynasore (80 µM), methyl-β-cyclodextrin (5 mM) or EIPA (50 µM) diluted in DMEM without

serum. Hoechst 33342 (1 µM) was added to stain nuclei. After 30 min of incubation, this solution was replaced by 250 µL of DMEM without serum containing 30 µM of **MP1**, 0.25 mg/mL 10 kDa TM-Dextran and the same amount of the corresponding inhibitor. After incubation for 1 h at 37 ºC, cells were washed twice with DMEM without phenol red and imaged at the confocal microscope. The number of cells with cytosolic dextran was counted for more than 300 cells for each condition, and experiments were done three times. Data were normalized to untreated control (100%).

For the comparison of dextran endosomal release in the presence and in the absence of serum, HeLa cells were incubated for 1 h with a solution of 0.25 mg/mL 10 kDa Alexa$_{488}$-Dextran and various concentrations of **MP1** in DMEM stock or in DMEM supplemented with 10% FBS. After that, cells nuclei were stained with 1 µM Hoechst 33342 in DMEM without phenol red for 30 min, then cells were washed with DMEM without phenol red and incubated for 2.5 hours with DMEM without phenol red provided with 10% FBS. Finally, cells were observed with a Dragonfly confocal spinning-disk microscope.

2.12.3. Cell viability assay (MTT)

HeLa, Vero, A549 and ARPE-19 cells were incubated with different concentrations of **MP1** (0, 1, 2, 4, 8, 16, 32, 62.5, 125, 250, 500, 1000 µM) in DMEM for 1 h, then the solutions were removed and replaced with complete medium. After 24 hours, cells were incubated for 3 hours with 0.5 mg/mL MTT (tetrazolium salt), then the medium was removed and the formazan salt formed solubilized with DMSO. Another set of cells was directly incubated with medium containing MTT for 1 h immediately after the initial 1 h incubation, to study the viability in the absence of recovery. Cells viability was then quantified by absorbance at 570 nm with an Infinite 200 PRO microplate reader (Tecan). This viability test measures the reduction of MTT to formazan by mitochondrial activity. Data was normalized to untreated cells (100% viability), after blank subtraction (Triton X-100 treated cells).

2.12.4. Saporin experiments

For the saporin experiments, HeLa cells were incubated in a 96-well plate with 0 or 10 µg/mL of saporin and increasing concentrations of the **MP1**, **Arg$_8$**, and **GALA** acetylated peptides. Cells were co-incubated with protein and peptide for 1 h in culture medium without serum or antibiotics, and then the compounds were removed, cells were washed and complete medium was added. Cells were further incubated for 6 h or 24 h before the addition of MTT tetrazolium salt at a final concentration of 0.5 mg/mL. For the more resistant A549 cells, this incubation was 24 h before adding MTT. Cells were further incubated for 3 h, and the medium removed before solubilizing the formazan salt with DMSO. Cells viability was then quantified by absorbance. Data was normalized to untreated cells (100% viability), after blank subtraction (Triton X-100 treated cells).

2.12.5. Cre recombinase expression and purification

Escherichia coli BL21(DE3)-Codon Plus cells (Stratagene) were transformed with the plasmid pET-Cre recombinase (a gift from Niels Geijsen; Addgene plasmid #62730).[S28] A bacterial preculture grown overnight at 37 ºC was diluted 1:250 in LB medium supplemented with 100 µg/mL Ampicillin. Cultures were incubated at 37 ºC until OD600 ~ 0.8 and induced with 1 mM IPTG for 16 h at 16 ºC. Cells were harvested by centrifugation, pellets were resuspended in 1:50 volume of lysis buffer (600 mM NaCl, 20 mM Tris pH 7.5, 20 mM imidazole, 1 mg/mL lysozyme supplemented with protease inhibitors without EDTA) and sonicated on ice 15 x 10 s (Cycle 0.5, Amplitude 70%) with a UP200S ultrasonic processor (Hielscher). Cellular debris was removed by centrifugation at 16000 g 15 min and the supernatant was incubated with HisPur Ni-NTA resin (ThermoFisher) for 1 h at 4 ºC, washed 3 times with 3 volumes of binding buffer (500 mM NaCl, 20 mM Tris pH 7.5, 5 mM imidazole) and then 2 times with wash buffer (500 mM NaCl, 20 mM Tris pH 7.5, 60 mM imidazole). The protein was eluted with several incubations of elution buffer (500 mM NaCl, 20 mM Tris pH 7.5, 500 mM imidazole). Imidazole from the fractions containing the protein of interest was removed by several washes on an Amicon UFC (Millipore) and finally, protein was concentrated in storage buffer (20 mM HEPES pH 7.5, 500 mM NaCl, 20% glycerol). Aliquots were snap-frozen and stored at -80 ºC.

2.12.6. Cre recombinase delivery experiments

Cells were seeded on round coverslips (12 mm diameter) in 24-well plate at a density of 75000 cells/well the day prior the experiment. Cre recombinase and peptide complexes were prepared as 5X

solutions in DMEM and added to the cells to the final working concentration (1 μM Cre, and 2.5, 5, 10 and 20 μM peptide). Cells were incubated with the complexes for 4 h, and then the complexes were removed and substituted with complete culture medium. After 72 h, cells were processed for epifluorescence microscopy. After incubation with 1 μM Hoechst 33 342 in complete medium for 30 min, cells were washed twice with PBS, incubated 30 min with 4% paraformaldehyde (PFA) in PBS and washed again with PBS, then the coverslips were removed from the 24-well plate, placed onto a glass slide and mounted with Mowiol 4-88 mounting medium (Calbiochem).

For quantification by flow cytometry, cells were seeded in a 24-well plate, and incubated as stated for the microscopy experiment. After 72 h, cells were trypsinized, trypsin was neutralized with PBS supplemented with 2% FBS and 0.5 mM EDTA, and the cell suspension was transferred to a 96-well plate. Cells were analysed by flow cytometry with a Guava EasyCyte BG HT, and the results were processed with InCyte software (GuavaSoft 3.2, Millipore). Cre recombinase delivery was assessed by calculating the percentage of EGFP expressing cells over the total of dsRED- and EGFP-expressing cells, after gating for cells with typical FSC and SSC parameters.

2.12.7. Antibody delivery in cell culture

HeLa or ARPE-19 cells were seeded in glass-bottom black 96-well plates (CellVis). Cells were incubated with mouse monoclonal anti-nuclear pore complex proteins antibody (Mab414), using 0.3 mg/mL for HeLa cells and 0.15 mg/mL for ARPE-19 cells, and several concentrations of peptide **MP1**, diluted in cell culture medium without FBS. After 1 h of incubation, cells were extensively washed and cell culture medium supplemented with 10% FBS was added for a further 2 h incubation. Cells were again washed with PBS and fixed with 4% paraformaldehyde in PBS for 30 min, washed twice with PBS permeabilized with 0.5% Triton X-100 in PBS for 3 min. Cells were incubated in blocking solution (2% BSA in PBS) for 30 min, and then incubated for another 30 min with 1:1000 dilution of goat anti-mouse IgG conjugated with Alexa Fluor 594 (Invitrogen, #A11012) and 0.5 μg/mL DAPI. Finally, cells were washed with PBS and observed with a confocal microscope.

2.12.8. CF-labelling and delivery of IgG

IgG-CF was prepared by the reaction of human IgG (4 mg in 200 μL of PBS pH 7.2) with Carboxyfluorescein-NHS (50 equiv) in $NaHCO_3$ buffer (pH 9) at room temperature for 2 h. The resulting solution was dialysed overnight in PBS buffer with 20% $NaHCO_3$ at 4ºC. To quantify the number of carboxyfluorescein per IgG antibody the absorbance of the mixture was measured using a NanoDrop UV-Vis Spectrophotometer. Absorbance values at 280 nm (maximum absorbance for antibody) and 492 nm (maximum absorbance for the carboxyfluorescein) were measured for various dilutions of the dialysed IgG-CF. Concentrations of antibody and carboxyfluorescein were calculated and the relation between both concentrations gave a value of around 8 CF per antibody. IgG-CF was diluted at 1 mg/mL in DMEM without FBS in the absence or presence of 30 μM **MP1**, and this mixture was added to HeLa cells. After 1 h of incubation, cells were washed and further incubated for 90 min with DMEM supplemented with 10% FBS, before confocal imaging.

2.12.9. Purification and delivery of GST-NLS-GFP

Escherichia coli BL21(DE3)-Codon Plus cells (Stratagene) were transformed with the plasmid pGEX-SV40NLS-GFP[S29] and grown in LB containing ampicillin (100 μg/mL) until OD600 ~ 1. Protein expression was induced with 0.5 mM IPTG at 20 ºC for 16 h. Cells were harvested and resuspended in PBS containing 1% Triton X-100 and protease inhibitors and sonicated on ice with a UP200S ultrasonic processor (Hielscher). After centrifugation (12000 g, 15 min, 4 ºC), the supernatant was filtered and incubated for 40 min with Glutathione Sepharose 4B resin (GE Healthcare). After 3 washes with PBS, protein was eluted from the resin with 10 mM glutathione in 50 mM Tris-HCl (pH 8), concentrated to 80 μM and stored at -80 ºC. The protein obtained is a fusion protein with the glutathione-S-transferase tag followed by SV40 large T-antigen NLS sequence (PKKKRKVEDP) and EGFP, with a theoretical molecular weight of 55 kDa and an isoelectric point of ~ 6. Delivery assays were performed by incubation of HeLa cells with 10 μM GST-NLS-GFP alone or in combination with 30 μM **MP1** for 1 h in DMEM without FBS. Cells were washed and incubated for 90 min in DMEM supplemented with 10% FBS and observed with a confocal microscope.

2.13. *Ex vivo* cornea experiments

2.13.1. Murine corneas culture

Mice (Sfl-Cre, The Jackson Laboratory) were treated and sacrificed according to the guidelines for the good use of laboratory animals in effect at the animal facility of the Center for Research in Molecular Medicine and Chronic Diseases (CiMUS). Mice were sacrificed by an intraperitoneal injection of a fatal dose of ketamine/xylazine. Eviscerated murine eyes were maintained in warm Hank's Balanced Salt Solution (HBSS) (Sigma-Aldrich) while the corneas were removed from the eye bulbs and separated from the iris using surgical forceps and scissors. The corneas were maintained in warm HBSS and immediately used for the experiments. From each mouse, one cornea was used for the immunofluorescence and one to assess the toxicity of the complexes.

2.13.2. Antibody delivery in cornea

The intracellular delivery of anti-nuclear pore complex proteins antibody Mab414 in murine corneas was assessed preparing solutions 2X of antibody (where the final concentration 1X was 0.3 mg/mL) and **MP1** peptide in Ames' medium. 25 µL of antibody solution were placed in a 96-well glass bottom black plate (CellVis) and corneas were placed in this solution, then the peptide solutions were added to the wells and the plate was incubated for 1 h at 37 ºC, 5% CO_2, 95% humidity. After that, the corneas were washed with Ames' medium and incubated with Ames' medium supplemented with 10% FBS at 37 ºC, 5% CO_2, 95% humidity. After 2 h the corneas were washed twice with PBS, incubated 30 min with 4% paraformaldehyde (PFA) in PBS, washed twice again and permeabilized with 0.5% Triton X-100 in PBS for 3 min. To prevent non-specific binding of the secondary antibody, blocking was performed by incubating the corneas in 2% BSA in PBS for 40 min, and then they were incubated for 40 min with a solution of 2% BSA, goat anti-mouse IgG conjugated with Alexa Fluor 594 (Invitrogen, #A11012), diluted 1:1000, and 0.5 µg/mL DAPI. Finally, the corneas were washed twice with PBS and covered with PBS for imaging with a Dragonfly confocal spinning-disk microscope.

2.13.3. Live/Dead Staining

To assess corneas viability after the delivery of Mab414 antibody, corneas were incubated with 3.75 µg/mL fluorescein diacetate (Sigma-Aldrich), and 4 µg/mL propidium iodide (Sigma-Aldrich) in Ames' medium for 4 min in the dark, while gently shaking, then washed twice with PBS and immediately imaged with a confocal spinning-disk microscope.

2.14. Sources for Figure 6 table

Dextran properties were extracted from the manufacturer's specification sheets (Sigma-Aldrich and Fisher Scientific).

Protein structures for saporin (1QI7),[S30] Cre recombinase (1CRX),[S31] and antibody (1HZH),[S32] were retrieved from pdb (rcsb.org)[S33] and processed with Chimera.[S34] Dimensions were calculated using Chimera from the diameters of the inertia ellipsoid of each protein.

Hydrodynamic radius for Cre recombinase[S35] and antibody[S36] were obtained from the indicated references.

pI/MW were calculated from the aminoacid sequences using Compute pI/MW tool from ExPASy.[S37]

3. Supporting References

(S1) J. Schindelin, I. Arganda-Carreras, E. Frise, V. Kaynig, M. Longair, T. Pietzsch, S. Preibisch, C. Rueden, S. Saalfeld, B. Schmid, J.-Y. Tinevez, D. J. White, V. Hartenstein, K. Eliceiri, P. Tomancak and A. Cardona, *Nat. Methods*, 2012, **9**, 676–682.

(S2) R. Behrendt, P. White and J. Offer, *J. Pept. Sci.*, 2016, **22**, 4–27.

(S3) C. Kay, O. E. Lorthioir, N. J. Parr, M. Congreve, S. C. McKeown, J. J. Scicinski and S. V Ley, *Biotechnol. Bioeng.*, 2000, **71**, 110–8.

(S4) M. Pazo, M. Juanes, I. Lostalé-Seijo and J. Montenegro, *Chem. Commun.* 2018, **54**, 6919–6922.

(S5) M. Akishiba, T. Takeuchi, Y. Kawaguchi, K. Sakamoto, H.-H. Yu, I. Nakase, T. Takatani-Nakase, F. Madani, A. Gräslund and S. Futaki, *Nat. Chem.*, 2017, **9**, 751–761.

(S6) M. C. Morris, J. Depollier, J. Mery, F. Heitz and G. Divita, *Nat. Biotechnol.*, 2001, **19**, 1173–1176.

(S7) A. Erazo-Oliveras, K. Najjar, L. Dayani, T.-Y. Wang, G. A. Johnson and J.-P. Pellois, *Nat. Methods*, 2014, **11**, 861–867.

(S8) J. M. Priegue, J. Montenegro and J. R. Granja, *Small*, 2014, **10**, 3613–3618.

(S9) A. Kashiwada, M. Tsuboi, N. Takamura, E. Brandenburg, K. Matsuda and B. Koksch, *Chem. - A Eur. J.*, 2011, **17**, 6179–6186.

(S10) M. A. Sani, T. C. Whitwell, J. D. Gehman, R. M. Robins-Browne, N. Pantarat, T. J. Attard, E. C. Reynolds, N. M. O'Brien-Simpson and F. Separovic, *Antimicrob. Agents Chemother.*, 2013, **57**, 3593–3600.

(S11) Y.-H. Chen and J. T. Yang, *Biochem. Biophys. Res. Commun.*, 1971, **44**, 1285–1291

(S12) Malvern Instruments Limited. Application of Dynamic Light Scattering (DLS) to Protein Therapeutic Formulations: Principles, Measurements and Analysis - 3. DLS Deconvolution Algorithms.Whitepaper, 2014.

(S13) N. O. Mchedlov-Petrossyan, T. A. Cheipesh, A. D. Roshal, A. O. Doroshenko and N. A. Vodolazkaya, *Methods Appl. Fluoresc.*, 2016, **4**, 034002.

(S14) F. M. Zehentbauer, C. Moretto, R. Stephen, T. Thevar, J. R. Gilchrist, D. Pokrajac, K. L. Richard and J. Kiefer, *Spectrochim. Acta Part A Mol. Biomol. Spectrosc.*, 2014, **121**, 147–151.

(S15) C. Bissig and J. Gruenberg, *Cold Spring Harb. Perspect. Biol.*, 2013, **5**, a016816.

(S16) W. Tian and Y. Ma, *Soft Matter*, 2012, **8**, 6378.

(S17) D. H. de Jong, G. Singh, W. F. D. Bennett, C. Arnarez, T. A. Wassenaar, L. V. Schäfer, X. Periole, D. P. Tieleman and S. J. Marrink, *J. Chem. Theory Comput.*, 2013, **9**, 687–697.

(S18) S. O. Yesylevskyy, L. V. Schäfer, D. Sengupta and S. J. Marrink, *PLoS Comput. Biol.*, 2010, **6**, e1000810.

(S19) L. Monticelli, S. K. Kandasamy, X. Periole, R. G. Larson, D. P. Tieleman and S.-J. Marrink, *J. Chem. Theory Comput.*, 2008, **4**, 819–834.

(S20) G. Bussi, T. Zykova-Timan and M. Parrinello, *J. Chem. Phys.*, 2009, **130**, 074101.

(S21) M. Parrinello and A. Rahman, *J. Appl. Phys.*, 1981, **52**, 7182–7190.

(S22) N. Schmid, A. P. Eichenberger, A. Choutko, S. Riniker, M. Winger, A. E. Mark and W. F. van Gunsteren, *Eur. Biophys. J.*, 2011, **40**, 843–856.

(S23) U. Essmann, L. Perera, M. L. Berkowitz, T. Darden, H. Lee and L. G. Pedersen, *J. Chem. Phys.*, 1995, **103**, 8577–8593

(S24) D. Van Der Spoel, E. Lindahl, B. Hess, G. Groenhof, A. E. Mark and H. J. C. Berendsen, *J.*

Comput. Chem., 2005, **26**, 1701–1718.

(S25) W. Humphrey, A. Dalke and K. Schulten, *J. Mol. Graph.*, 1996, **14**, 33–38.

(S26) M. Montal and P. Mueller, *Proc. Natl. Acad. Sci. U. S. A.*, 1972, **69**, 3561–3566.

(S27) B. Hille, *Ionic channels of excitable membranes*, Sinauer Associates, Sunderland, MA, 1992.

(S28) D. S. D'Astolfo, R. J. Pagliero, A. Pras, W. R. Karthaus, H. Clevers, V. Prasad, R. J. Lebbink, H. Rehmann and N. Geijsen, *Cell*, 2015, **161**, 674–690.

(S29) F. Yokoya, N. Imamoto, T. Tachibana and Y. Yoneda, *Mol. Biol. Cell*, 1999, **10**, 1119–31.

(S30) C. Savino, L. Federici, R. Ippoliti, E. Lendaro and D. Tsernoglou, *FEBS Lett.*, 2000, **470**, 239–243.

(S31) F. Guo, D. N. Gopaul and G. D. van Duyne, *Nature*, 1997, **389**, 40–46.

(S32) E. O. Saphire, P. W. Parren, R. Pantophlet, M. B. Zwick, G. M. Morris, P. M. Rudd, R. A. Dwek, R. L. Stanfield, D. R. Burton and I. A. Wilson, *Science*, 2001, **293**, 1155–1159.

(S33) H. M. Berman, J. Westbrook, Z. Feng, G. Gilliland, T. N. Bhat, H. Weissig, I. N. Shindyalov and P. E. Bourne, *Nucleic Acids Res.*, 2000, **28**, 235–242.

(S34) E. F. Pettersen, T. D. Goddard, C. C. Huang, G. S. Couch, D. M. Greenblatt, E. C. Meng and T. E. Ferrin, *J. Comput. Chem.*, 2004, **25**, 1605–1612.

(S35) P. Capasso, M. Aliprandi, G. Ossolengo, F. Edenhofer and A. de Marco, *BMC Biotechnol.*, 2009, **9**, 80.

(S36) J. K. Armstrong, R. B. Wenby, H. J. Meiselman and T. C. Fisher, *Biophys. J.*, 2004, **87**, 4259–4270.

(S37) B. Bjellqvist, G. J. Hughes, C. Pasquali, N. Paquet, F. Ravier, J. C. Sanchez, S. Frutiger and D. Hochstrasser, *Electrophoresis*, 1993, **14**, 1023–1031.

USC UNIVERSIDADE DE SANTIAGO DE COMPOSTELA

USC
UNIVERSIDADE
DE SANTIAGO
DE COMPOSTELA